



LEVEL II

APPROVED FOR PUBLIC RELEASE, DISTRIBUTION UNLIMITED

ALEX(01)-TR-78-00

(12)

AD A0 66714

SECTION PERFORMANCE OF TIME VARYING ADAPTIVE RATE ADAPTIVE BEAMFORMER

TECHNICAL REPORT NO. 18

VELA NETWORK EVALUATION AND AUTOMATIC PROCESSING RESEARCH

Prepared by
Wen-Wu Shen

TEXAS INSTRUMENTS INCORPORATED

Equipment Group
Post Office Box 6015
Dallas, Texas 75222

D D C
Research
APR 2 1978
C
C

Prepared for

AIR FORCE TECHNICAL APPLICATIONS CENTER
Alexandria, Virginia 22314

Sponsored by

ADVANCED RESEARCH PROJECTS AGENCY
Nuclear Monitoring Research Office
ARPA Program Code No. 7F10
ARPA Order No. 2551

15 September 1978

Author/Affiliation: This document was prepared by the Advanced Research Projects Agency Nuclear Monitoring Research Office, under contract to the Air Force Technical Applications Center.

70 04 02 137

DDC FILE COPY



APPROVED FOR PUBLIC RELEASE. DISTRIBUTION UNLIMITED

ALEX(01)-TR-78-06

DETECTION PERFORMANCE OF TIME VARYING ADAPTATION RATE ADAPTIVE BEAMFORMER

TECHNICAL REPORT NO. 18

VELA NETWORK EVALUATION AND AUTOMATIC PROCESSING RESEARCH

Prepared by
Wen-Wu Shen

TEXAS INSTRUMENTS INCORPORATED
Equipment Group
Post Office Box 6015
Dallas, Texas 75222

D D C
R P A P I U R D
APR 2 1979
R E U G I T T L D
C

Prepared for
AIR FORCE TECHNICAL APPLICATIONS CENTER
Alexandria, Virginia 22314

Sponsored by
ADVANCED RESEARCH PROJECTS AGENCY
Nuclear Monitoring Research Office
ARPA Program Code No. 7F10
ARPA Order No. 2551

15 September 1978

Acknowledgment: This research was supported by the Advanced Research Projects Agency, Nuclear Monitoring Research Office, under Project VELA-UNIFORM, and accomplished under the technical direction of the Air Force Technical Applications Center under Contract Number F08606-77-C-0004.

79 04 02 135 Equipment Group

UNCLASSIFIED

SECURITY CLASSIFICATION OF THIS PAGE (When Data Entered)

REPORT DOCUMENTATION PAGE		READ INSTRUCTIONS BEFORE COMPLETING FORM								
1. REPORT NUMBER	2. GOVT ACCESSION NO.	3. RECIPIENT'S CATALOG NUMBER								
6. TITLE (and Subtitle) DETECTION PERFORMANCE OF TIME-VARYING ADAPTION RATE ADAPTIVE BEAMFORMER		5. TYPE OF REPORT & PERIOD COVERED 9 Technical rept. no. 18,								
7. AUTHOR(S) Wen-Wu Shen		8. PERFORMING ORG. REPORT NUMBER 17 ALEX(01)-TR-78-06								
9. PERFORMING ORGANIZATION NAME AND ADDRESS Texas Instruments Incorporated Equipment Group Dallas, Texas 75222		10. PROGRAM ELEMENT, PROJECT, TASK AREA & WORK UNIT NUMBERS 15 F08606-77-C-0004, ARPA Order - 2551								
11. CONTROLLING OFFICE NAME AND ADDRESS Advanced Research Projects Agency Nuclear Monitoring Research Office Arlington, Virginia 22209		12. REPORT DATE 11 15 September 1978								
14. MONITORING AGENCY NAME & ADDRESS (if different from Controlling Office) Air Force Technical Applications Center VELA Seismological Center Alexandria, Virginia 22314		13. NUMBER OF PAGES 180 12 182P.								
16. DISTRIBUTION STATEMENT (of this Report) APPROVED FOR PUBLIC RELEASE, DISTRIBUTION UNLIMITED										
17. DISTRIBUTION STATEMENT (of the abstract entered in Block 20, if different from Report)										
18. SUPPLEMENTARY NOTES ARPA Order No. 2551										
19. KEY WORDS (Continue on reverse side if necessary and identify by block number) <table style="width: 100%; border-collapse: collapse;"> <tr> <td style="width: 50%;">Seismology</td> <td style="width: 50%;">Detection probability</td> </tr> <tr> <td>L₁ Norm ABF</td> <td>Bodywave magnitude measurement</td> </tr> <tr> <td>Detection performance</td> <td>Korean Seismic Research Station Short-</td> </tr> <tr> <td>Coda suppression</td> <td>Period Array</td> </tr> </table>			Seismology	Detection probability	L ₁ Norm ABF	Bodywave magnitude measurement	Detection performance	Korean Seismic Research Station Short-	Coda suppression	Period Array
Seismology	Detection probability									
L ₁ Norm ABF	Bodywave magnitude measurement									
Detection performance	Korean Seismic Research Station Short-									
Coda suppression	Period Array									
20. ABSTRACT (Continue on reverse side if necessary and identify by block number) <p>The previously developed time-varying adaptation rate adaptive beamformer (ABF) was modified for the purpose of using a fixed set of design parameters in different levels of noise and signals. The ABF performance was evaluated in terms of its capability to suppress seismic coda wavetrains of strong earthquakes, accuracy of its bodywave magnitude (m_b) measurements and detection capability, as compared with those of single sites and the conventional beamsteer using recorded data from the Korean</p>										

405076

50B

UNCLASSIFIED

SECURITY CLASSIFICATION OF THIS PAGE(When Data Entered)

20. continued

Seismic Research Station (KSRS) short-period array. A total of 129 events recorded in winter were processed.

m sub b

On the average, the ABF yielded the same magnitude difference (0.1 m_b units smaller) as the beamsteer, when compared with the NEIS and NORSAR bulletin m_b . However, preliminary results indicated that the ABF may have improved the array detection capability by 0.5 m_b units from the conventional beamsteer based on subjective analyst/interpretation of the detection status of processed events. More data with automatic detection criteria applied are needed to more accurately estimate the detection gains which are possible by applying the ABF as a field operating front-end detector.

ACCESSION for	
NTIS	White Section <input checked="" type="checkbox"/>
DOC	Buff Section <input type="checkbox"/>
UNANNOUNCED	<input type="checkbox"/>
JUSTIFICATION	<input type="checkbox"/>
BY	
DISTRIBUTION/AVAILABILITY CODES	
Dist	AVAIL. and / or SPECIAL
A	

UNCLASSIFIED

SECURITY CLASSIFICATION OF THIS PAGE(When Data Entered)

ABSTRACT

The previously developed time-varying adaptation rate adaptive beamformer (ABF) was modified for the purpose of using a fixed set of design parameters in different levels of noise and signals. The ABF performance was evaluated in terms of its capability to suppress seismic coda wavetrains of strong earthquakes, accuracy of its bodywave magnitude (m_b) measurements and detection capability, as compared with those of single sites and the conventional beamsteer using recorded data from the Korean Seismic Research Station (KSRS) short-period array. A total of 129 events recorded in winter were processed.

On the average, the ABF yielded the same magnitude difference (0.1 m_b units smaller) as the beamsteer, when compared with the NEIS and NORSAR bulletin m_b . However, preliminary results indicated that the ABF may have improved the array detection capability by 0.5 m_b units from the conventional beamsteer based on subjective analyst interpretation of the detection status of processed events. More data with automatic detection criteria applied are needed to more accurately estimate the detection gains which are possible by applying the ABF as a field operating front-end detector.

Neither the Advanced Research Projects Agency nor the Air Force Technical Applications Center will be responsible for information contained herein which has been supplied by other organizations or contractors, and this document is subject to later revision as may be necessary. The views and conclusions presented are those of the authors and should not be interpreted as necessarily representing the official policies, either expressed or implied, of the Advanced Research Projects Agency, the Air Force Technical Applications Center, or the US Government.

TABLE OF CONTENTS

SECTION	TITLE	PAGE
	ABSTRACT	iii
I.	INTRODUCTION	I-1
II.	THE ADAPTIVE BEAMFORMER	II-1
III.	DETECTION PERFORMANCE	III-1
	A. CODA REJECTION	III-1
	B. DETECTION PROBABILITY MEASURE-	
	MENT	III-7
	C. SUMMARY	III-27
IV.	CONCLUSION AND SUGGESTIONS	IV-1
	A. CONCLUSION	IV-1
	B. SUGGESTIONS FOR FURTHER STUDY	IV-1
V.	REFERENCES	V-1
Appendix A	PROCESSED DATA PLOTS FROM NEIS BULLETIN	A-1
Appendix B	PROCESSED DATA PLOTS FROM NORSAR BULLETIN	B-1

LIST OF FIGURES

FIGURE	TITLE	PAGE
III-1	BEAMFORMING OUTPUTS FOR A STRONG EVENT FROM THE CERAM SEA (0.5-3.5 Hz)	III-2
III-2	BEAMFORMING OUTPUTS FOR A STRONG EVENT FROM THE CERAM SEA (0.5-1.5 Hz)	III-4
III-3	MEASURED BEAMSTEER AND ABF BEAM PATTERN (0.5-3.5 Hz) FOR THE INITIAL SIGNAL PULSE IN FIGURE III-1	III-5
III-4	MEASURED BEAMSTEER AND ABF BEAM PATTERN (0.5-3.5 Hz) FOR THE SECONDARY SIGNAL PULSE IN FIGURE III-1	III-6
III-5	NEIS OR NORSAR m_b VERSUS MEASURED m_b BY SITE 1 OF THE KSRS	III-16
III-6	NEIS OR NORSAR m_b VERSUS KSRS BEAMSTEER m_b	III-17
III-7	NEIS OR NORSAR m_b VERSUS ABF m_b	III-18
III-8	KSRS SITE 1 DETECTION AND NON-DETECTION HISTOGRAM, AND DETECTION PROBABILITY	III-20
III-9	KSRS BEAMSTEER DETECTION AND NON-DETECTION HISTOGRAM AND DETECTION PROBABILITY	III-21
III-10	KSRS ABF DETECTION AND NON-DETECTION HISTOGRAM AND DETECTION PROBABILITY	III-22
III-11	KSRS SITE 1 DETECTION HISTOGRAM AND PROBABILITY BY ADJUSTING m_b AT 50° DELTA	III-24
III-12	KSRS BEAMSTEER DETECTION HISTOGRAM AND PROBABILITY BY ADJUSTING m_b AT 50° DELTA	III-25
III-13	KSRS ABF DETECTION HISTOGRAM AND PROBABILITY BY ADJUSTING m_b AT 50° DELTA	III-27

LIST OF FIGURES
(continued)

FIGURE	TITLE	PAGE
A-1	PROCESSED TRACES FOR EVENT A-1	A-2
A-2	PROCESSED TRACES FOR EVENT A-2	A-3
A-3	PROCESSED TRACES FOR EVENT A-3	A-4
A-4	PROCESSED TRACES FOR EVENT A-4	A-5
A-5	PROCESSED TRACES FOR EVENT A-5	A-6
A-6	PROCESSED TRACES FOR EVENT A-6	A-7
A-7	PROCESSED TRACES FOR EVENT A-7	A-8
A-8	PROCESSED TRACES FOR EVENT A-8	A-9
A-9	PROCESSED TRACES FOR EVENT A-9	A-10
A-10	PROCESSED TRACES FOR EVENT A-10	A-11
A-11	PROCESSED TRACES FOR EVENT A-11	A-12
A-12	PROCESSED TRACES FOR EVENT A-12	A-13
A-13	PROCESSED TRACES FOR EVENT A-13	A-14
A-14	PROCESSED TRACES FOR EVENT A-14	A-15
A-15	PROCESSED TRACES FOR EVENT A-15	A-16
A-16	PROCESSED TRACES FOR EVENT A-16	A-17
A-17	PROCESSED TRACES FOR EVENT A-17	A-18
A-18	PROCESSED TRACES FOR EVENT A-18	A-19
A-19	PROCESSED TRACES FOR EVENT A-19	A-20
A-20	PROCESSED TRACES FOR EVENT A-20	A-21
A-21	PROCESSED TRACES FOR EVENT A-21	A-22
A-22	PROCESSED TRACES FOR EVENT A-22	A-23
A-23	PROCESSED TRACES FOR EVENT A-23	A-24
A-24	PROCESSED TRACES FOR EVENT A-24	A-25
A-25	PROCESSED TRACES FOR EVENT A-25	A-26
A-26	PROCESSED TRACES FOR EVENT A-26	A-27

LIST OF FIGURES
(continued)

FIGURE	TITLE	PAGE
A-27	PROCESSED TRACES FOR EVENT A-27	A-28
A-28	PROCESSED TRACES FOR EVENT A-28	A-29
A-29	PROCESSED TRACES FOR EVENT A-29	A-30
A-30	PROCESSED TRACES FOR EVENT A-30	A-31
A-31	PROCESSED TRACES FOR EVENT A-31	A-32
A-32	PROCESSED TRACES FOR EVENT A-32	A-33
A-33	PROCESSED TRACES FOR EVENT A-33	A-34
A-34	PROCESSED TRACES FOR EVENT A-34	A-35
A-35	PROCESSED TRACES FOR EVENT A-35	A-36
A-36	PROCESSED TRACES FOR EVENT A-36	A-37
A-37	PROCESSED TRACES FOR EVENT A-37	A-38
A-38	PROCESSED TRACES FOR EVENT A-38	A-39
A-39	PROCESSED TRACES FOR EVENT A-39	A-40
A-40	PROCESSED TRACES FOR EVENT A-40	A-41
A-41	PROCESSED TRACES FOR EVENT A-41	A-42
A-42	PROCESSED TRACES FOR EVENT A-42	A-43
A-43	PROCESSED TRACES FOR EVENT A-43	A-44
A-44	PROCESSED TRACES FOR EVENT A-44	A-45
A-45	PROCESSED TRACES FOR EVENT A-45	A-46
A-46	PROCESSED TRACES FOR EVENT A-46	A-47
A-47	PROCESSED TRACES FOR EVENT A-47	A-48
A-48	PROCESSED TRACES FOR EVENT A-48	A-49
A-49	PROCESSED TRACES FOR EVENT A-49	A-50
A-50	PROCESSED TRACES FOR EVENT A-50	A-51
A-51	PROCESSED TRACES FOR EVENT A-51	A-52
A-52	PROCESSED TRACES FOR EVENT A-52	A-53

LIST OF FIGURES
(continued)

FIGURE	TITLE	PAGE
A-53	PROCESSED TRACES FOR EVENT A-53	A-54
A-54	PROCESSED TRACES FOR EVENT A-54	A-55
A-55	PROCESSED TRACES FOR EVENT A-55	A-56
A-56	PROCESSED TRACES FOR EVENT A-56	A-57
A-57	PROCESSED TRACES FOR EVENT A-57	A-58
A-58	PROCESSED TRACES FOR EVENT A-58	A-59
A-59	PROCESSED TRACES FOR EVENT A-59	A-60
A-60	PROCESSED TRACES FOR EVENT A-60	A-61
A-61	PROCESSED TRACES FOR EVENT A-61	A-62
A-62	PROCESSED TRACES FOR EVENT A-62	A-63
A-63	PROCESSED TRACES FOR EVENT A-63	A-64
A-64	PROCESSED TRACES FOR EVENT A-64	A-65
A-65	PROCESSED TRACES FOR EVENT A-65	A-66
A-66	PROCESSED TRACES FOR EVENT A-66	A-67
A-67	PROCESSED TRACES FOR EVENT A-67	A-68
A-68	PROCESSED TRACES FOR EVENT A-68	A-69
A-69	PROCESSED TRACES FOR EVENT A-69	A-70
A-70	PROCESSED TRACES FOR EVENT A-70	A-71
A-71	PROCESSED TRACES FOR EVENT A-71	A-72
A-72	PROCESSED TRACES FOR EVENT A-72	A-73
A-73	PROCESSED TRACES FOR EVENT A-73	A-74
A-74	PROCESSED TRACES FOR EVENT A-74	A-75
A-75	PROCESSED TRACES FOR EVENT A-75	A-76
A-76	PROCESSED TRACES FOR EVENT A-76	A-77
A-77	PROCESSED TRACES FOR EVENT A-77	A-78
A-78	PROCESSED TRACES FOR EVENT A-78	A-79

LIST OF FIGURES
(continued)

FIGURE	TITLE	PAGE
A-79	PROCESSED TRACES FOR EVENT A-79	A-80
A-80	PROCESSED TRACES FOR EVENT A-80	A-81
A-81	PROCESSED TRACES FOR EVENT A-81	A-82
A-82	PROCESSED TRACES FOR EVENT A-82	A-83
A-83	PROCESSED TRACES FOR EVENT A-83	A-84
A-84	PROCESSED TRACES FOR EVENT A-84	A-85
A-85	PROCESSED TRACES FOR EVENT A-85	A-86
A-86	PROCESSED TRACES FOR EVENT A-86	A-87
A-87	PROCESSED TRACES FOR EVENT A-87	A-88
A-88	PROCESSED TRACES FOR EVENT A-88	A-89
A-89	PROCESSED TRACES FOR EVENT A-89	A-90
A-90	PROCESSED TRACES FOR EVENT A-90	A-91
A-91	PROCESSED TRACES FOR EVENT A-91	A-92
A-92	PROCESSED TRACES FOR EVENT A-92	A-93
A-93	PROCESSED TRACES FOR EVENT A-93	A-94
A-94	PROCESSED TRACES FOR EVENT A-94	A-95
A-95	PROCESSED TRACES FOR EVENT A-95	A-96
B-1	PROCESSED TRACES FOR EVENT B-1	B-2
B-2	PROCESSED TRACES FOR EVENT B-2	B-3
B-3	PROCESSED TRACES FOR EVENT B-3	B-4
B-4	PROCESSED TRACES FOR EVENT B-4	B-5
B-5	PROCESSED TRACES FOR EVENT B-5	B-6
B-6	PROCESSED TRACES FOR EVENT B-6	B-7
B-7	PROCESSED TRACES FOR EVENT B-7	B-8
B-8	PROCESSED TRACES FOR EVENT B-8	B-9
B-9	PROCESSED TRACES FOR EVENT B-9	B-10

LIST OF FIGURES
(continued)

FIGURE	TITLE	PAGE
B-10	PROCESSED TRACES FOR EVENT B-10	B-11
B-11	PROCESSED TRACES FOR EVENT B-11	B-12
B-12	PROCESSED TRACES FOR EVENT B-12	B-13
B-13	PROCESSED TRACES FOR EVENT B-13	B-14
B-14	PROCESSED TRACES FOR EVENT B-14	B-15
B-15	PROCESSED TRACES FOR EVENT B-15	B-16
B-16	PROCESSED TRACES FOR EVENT B-16	B-17
B-17	PROCESSED TRACES FOR EVENT B-17	B-18
B-18	PROCESSED TRACES FOR EVENT B-18	B-19
B-19	PROCESSED TRACES FOR EVENT B-19	B-20
B-20	PROCESSED TRACES FOR EVENT B-20	B-21
B-21	PROCESSED TRACES FOR EVENT B-21	B-22
B-22	PROCESSED TRACES FOR EVENT B-22	B-23
B-23	PROCESSED TRACES FOR EVENT B-23	B-24
B-24	PROCESSED TRACES FOR EVENT B-24	B-25
B-25	PROCESSED TRACES FOR EVENT B-25	B-26
B-26	PROCESSED TRACES FOR EVENT B-26	B-27
B-27	PROCESSED TRACES FOR EVENT B-27	B-28
B-28	PROCESSED TRACES FOR EVENT B-28	B-29
B-29	PROCESSED TRACES FOR EVENT B-29	B-30
B-30	PROCESSED TRACES FOR EVENT B-30	B-31
B-31	PROCESSED TRACES FOR EVENT B-31	B-32
B-32	PROCESSED TRACES FOR EVENT B-32	B-33
B-33	PROCESSED TRACES FOR EVENT B-33	B-34
B-34	PROCESSED TRACES FOR EVENT B-34	B-35

LIST OF TABLES

TABLE	TITLE	PAGE
III-1	PROCESSED EVENT LIST FROM NEIS BULLETIN (01/01/77 TO 01/15/77)	III-8
III-2	PROCESSED WEAK EVENT LIST FROM NOSRAR BULLETIN (01/01/78 TO 01/31/78)	III-13
III-3	SUMMARY OF DETECTION PROBABILITIES AND IMPROVEMENTS FOR ABF, BEAMSTEER, AND SINGLE SITE	III-29

SECTION I INTRODUCTION

This report presents an evaluation of the detection performance for the time-varying adaptation minimum power adaptive beamformer (ABF). The ABF is essentially based on the L_1 Norm Least-Square Formulation. The ABF algorithm described by Shen (1977) was modified in this report to adapt to various levels of noise in the operating environment. The detection performance study is based on the modified algorithm in which the design parameters are kept constant to demonstrate the algorithm's ability to be implemented for operational purposes.

Another element discussed in this report is the problem of coda rejection. The ABF capabilities for coda rejection can be automatically applied in a front-end detection system (Shen, 1978a,b). The coda of seismic signals from strong earthquakes consists of substantial high amplitude and long duration wavetrains. These could be due to the complex nature of source functions and/or the scatterings of waves caused by the complex structure in the media along the propagation paths. Under these circumstances, an automatic signal detector is jammed, or continuously yields false alarms and loses its functions for a certain period of time before returning to normal operation.

Section II briefly describes the new ABF algorithm. Evaluation procedures and results are presented in Section III. The data base, analysis, and a statistical estimate of the detection probability curves are described in detail with a summary in Subsection III-C. Conclusions and suggestions are presented in Section IV. Section V lists the references cited in the text of this report. Finally, Appendices A and B present the processed data displays.

SECTION II THE ADAPTIVE BEAMFORMER

A time-domain linear adaptive beamformer (ABF) was developed to be used in an operational front-end detection system. The objective is to increase the detection capability of a seismic array and to extract the low-magnitude signals of unknown waveform from noise. The algorithm minimizes the squared filter output subject to the constraints which pass energy from steered location. Mathematically, let $y(t)$ be the adaptive filter output at time t for an array of N sensors (channels) with a $2J+1$ points, or tap-pings of filter length per channel. Then, we write

$$y(t) = \sum_{i=1}^N \sum_{j=-J}^J a_i(j) X_i(t - j\Delta t) \quad (\text{II-1})$$

where X_i is time-aligned data input for the i^{th} channel, Δt is the sampling interval, and $a_i(j)$ is the adaptive filter coefficient for the i^{th} channel and the j^{th} point of the channel data. In the algorithm, $a_i(j)$ is updated each data point in the time-domain by the expression

$$a_i^{t+\Delta t}(j) = a_i^t(j) + \bar{\mu} \lambda(t) y(t) \left[\bar{X}(t-j\Delta t) - X_i(t-j\Delta t) \right] \quad (\text{II-2})$$

where $a_i(j)$ is initialized to satisfy the Levin's constraints (Levin, 1964)

$$\sum_{i=1}^N a_i(j) = \delta_{j_0} \quad (\text{II-3})$$

for the center point output described in equation (II-1) and where

$$\bar{X}(t-j\Delta t) = \frac{1}{N} \sum_{i=1}^N X_i(t-j\Delta t). \quad (\text{II-4})$$

\bar{X} is introduced to preserve the constraints which were initialized at the very beginning of processing, $\bar{\mu}$ is the convergent rate and is an input parameter and, finally $\lambda(t)$ is a time-varying and adaptation parameter. The algorithm was formulated (with $\lambda(t) = 1.0$) by Burg et al. (1967) and has been investigated by various authors (Kobayashi, 1970; Frost, 1972; Owsley, 1973; and Gangi and Byun, 1976). The algorithm achieved substantial noise reduction gain relative to the beamsteer (time-align and average) processor. However, experimental work on the recorded seismic data indicated a substantial signal loss as compared with the beamsteer output. That resulted in the optimum signal-to-noise ratio (SNR) gain to be around 1 dB relative to the beamsteer processor.

A better time-domain adaptation is needed to achieve a better SNR gain. It was found that a quasi L_1 norm adaptive filter improved the performance both in reducing the noise and in preventing the desired signal from being degraded. Currently, the L_1 norm ABF has been modified in an attempt to make the ABF processor implementable for optimum operation in various levels of seismic noise. Presently, the time-varying adaptation rate, $\lambda(t)$ is chosen as follows:

$$\lambda(t) = \frac{\bar{y}_{LTS}(t)}{\bar{y}_{STS}(t) \times P(t)} \quad (\text{II-5})$$

where

$$\bar{y}_{LTS}(t) = (1-\alpha) \bar{y}_{LTS}(t-1) + \alpha |y(t)| \quad (\text{II-6})$$

$$\bar{y}_{STS}(t) = (1-\beta) \bar{y}_{STS}(t-1) + \beta |y(t)| \quad (\text{II-7})$$

and

$$P(t) = \sum_{i=1}^N \sum_{j=-J}^J X_i^2(t-j\Delta t). \quad (\text{II-8})$$

α is a long-term smoothing constant of filter output for noise adaptation so that $\bar{\mu}$ would not change significantly when the noise level changes in the operating environment. β is the short-term smoothing constant of filter output intended to prevent the signal loss. It is noted that the performance of the adaptive beamformer is highly dependent on α , β , and $\bar{\mu}$.

Basically an L_1 norm adaptive filter is formulated by minimizing the absolute value of the ABF output. This is in contrast with the more conventional L_2 norm adaptive filter formulated by minimizing the mean square or power of the ABF output. According to Claerbout (1976), the advantage of an L_1 norm filter, which tends to find the median of data samples, is that such a solution is relatively less sensitive to large deviations of the data. By weighting the time-varying adaption rate $\lambda(t)$ inversely as the estimated signal-to-noise ratio of the ABF output, the computation of the update of all of the channel filters is made relatively insensitive to large fluctuations in the ABF output. Thus, when large deviations of the ABF output are encountered due to signals along with the enhanced signal generated noise, the filter update is automatically suppressed to avoid minimizing the power of the signal due to the enhanced signal generated or scattered signal component. In the sense that this feedback to $\lambda(t)$ makes the adaptive filter design much less sensitive to large deviations of the filter output, the filter design is considered closer to a minimum L_1 than a minimum L_2 norm optimum solution. Basically, the L_2 formulation is a matched filter of the ABF output and each channel's deviation from the conventional beamform. The approximate L_1 formulation is a matched filter between the sign of the ABF output and each channel's deviation from a conventional beamform. Our experience indicates that this largely eliminates the previous problem of ABF filters; which is the annihilation of

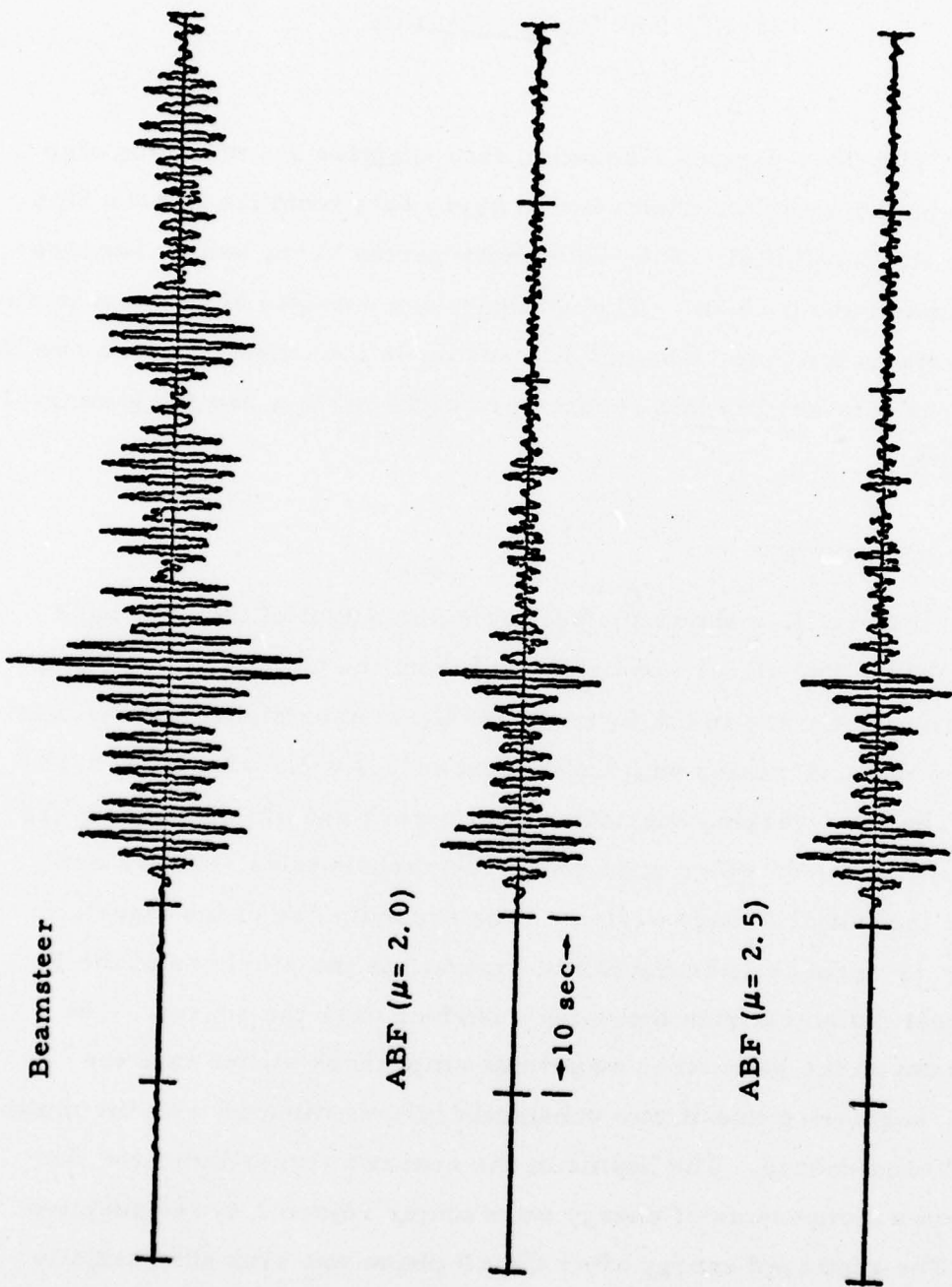
weak signals due to a lack of strict conformity to Levin's constraint (Levin, 1964).

SECTION III DETECTION PERFORMANCE

The time-varying adaptation rate adaptive beamforming algorithm was evaluated using the short-period array data from the Korean Seismic Research Station (KSRS). The KSRS short-period array has 19 sensors with an aperture of about 10 km. The configuration consists of two concentric rings: 6 sensors in the inner ring and 12 sensors in the outer ring with one in the center. The data used in this report were digitized at a sampling interval $\Delta t = 0.1$ seconds.

A. CODA REJECTION

Figure III-1 shows the beamforming output of the wide band (0.5-3.5 Hz) data. The signal was originated from the Ceram Sea on 1 January 1977. The first trace in the figure is the beamsteer signal and the next two traces are the ABF beams with convergent rate $\bar{\mu} = 2.0$ and $\bar{\mu} = 2.5$, respectively. The time-varying adaptation parameters used in processing are $\alpha = 0.0045$, and $\beta = 0.65$ which were found, by various tests, to have optimum SNR for the initial P wave arrival. The second pulse of the signal, which arrived 11 seconds after the initial arrival, is the pP phase of the P wave signal that reflected from the earth's surface near the source. The secondary phase on the beamsteer output has amplitudes higher than the initial phase, suggesting that it was substantially contaminated with the multi-path and scattered energy. The beams of the next two traces indicated that the contaminated components of energy were amply rejected by the adaptive processor. The scattered energy after the pP phase was also substantially suppressed in the ABF beams as compared with the beamsteer output in the



III-2

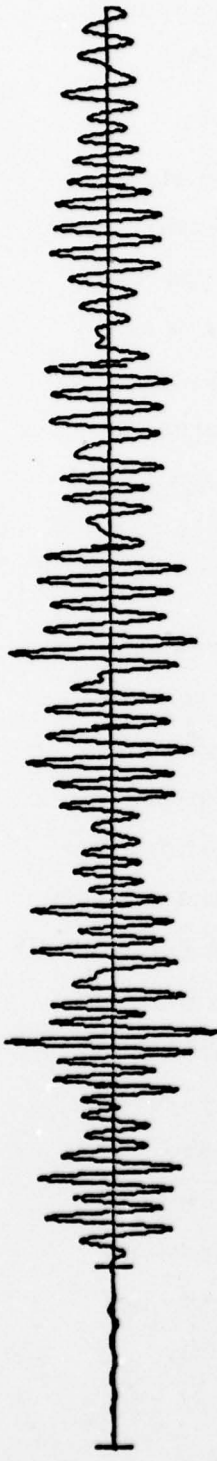
FIGURE III-1
BEAMFORMING OUTPUTS FOR A STRONG EVENT FROM THE CERAM SEA
(0.5-3.5 Hz)

figure. This is due to the fact that the initial arrival of the seismic wavetrains may have better coherency among the channels, while the multi-scattered energy in general shows poorer coherency and therefore was rejected by the adaptive beamformer.

Figure III-2 shows the beamforming outputs for the same signal shown on Figure III-1 with input data in the 0.5-1.5 Hz passband. Rejection of the coda by the adaptive filter is more pronounced in the narrower band data. The pulse which arrived 1 minute 35 seconds later after the initial P wave arrival is PP, the reflected phase of the signal on the earth's surface approximately at the mid-point between the source location and the receiving array. The third identifiable pulse on the ABF beam which arrived 2 minutes and 15 seconds later after the primary signal is possibly the Pcp phase which is due to the reflection from the core of the earth.

To investigate how the beamsteer and ABF processors respond to the wavetrains of different coherency among the channels, the data from the Ceram earthquake were used to form the array beam in various look azimuths with a fixed apparent P wave velocity. Figure III-3 illustrates the beam pattern of the measured peak-to-peak amplitude for the first signal pulse shown in Figure III-1 (in the 0.5-3.5 Hz passband). The decibels are computed relative to the beamsteer output at the 182° azimuth. Because the ABF is designed with the time-varying adaptation rate, the adaptive filter ($\bar{\mu} = 2.0$) response in general follows that of the beamsteer processor in this figure. However, the measured beam patterns on the basis of the second pulse signal in Figure III-1 does show significant difference between the beamsteer and ABF processors as shown in Figure III-4. That is why the adaptive filter is able to achieve more coda rejection than the beamsteer filter. The response pattern actually measured on the basis of recorded data could slightly differ from one signal to the other. The earthquake event used in the study was randomly selected to demonstrate coda rejection.

Beamsteer

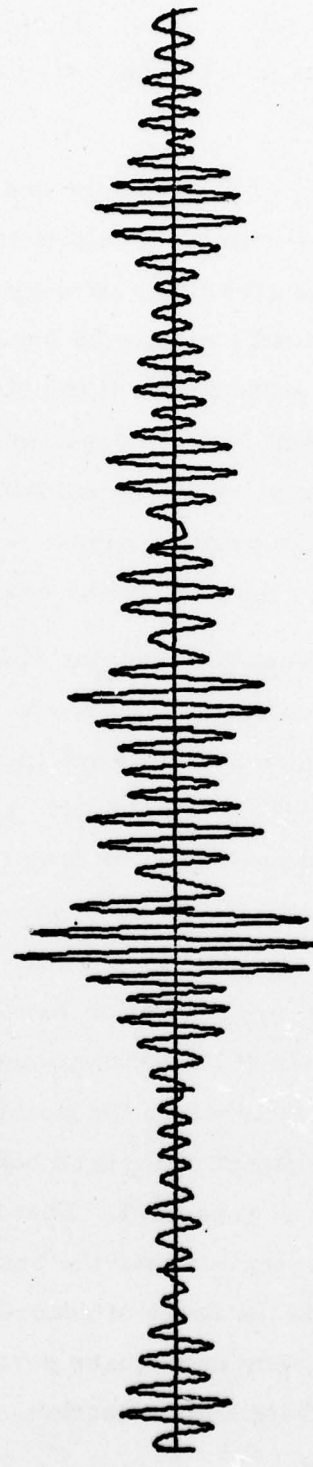


ABF ($\mu = 2.5$)



III-4

Beamsteer (continued)



ABF (continued)

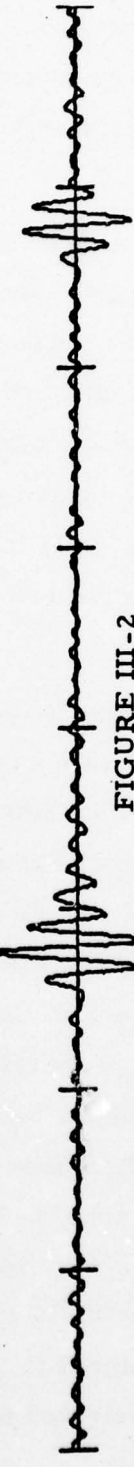


FIGURE III-2

BEAMFORMING OUTPUTS FOR A STRONG EVENT FROM THE CERAM SEA
(0.5-1.5 Hz)

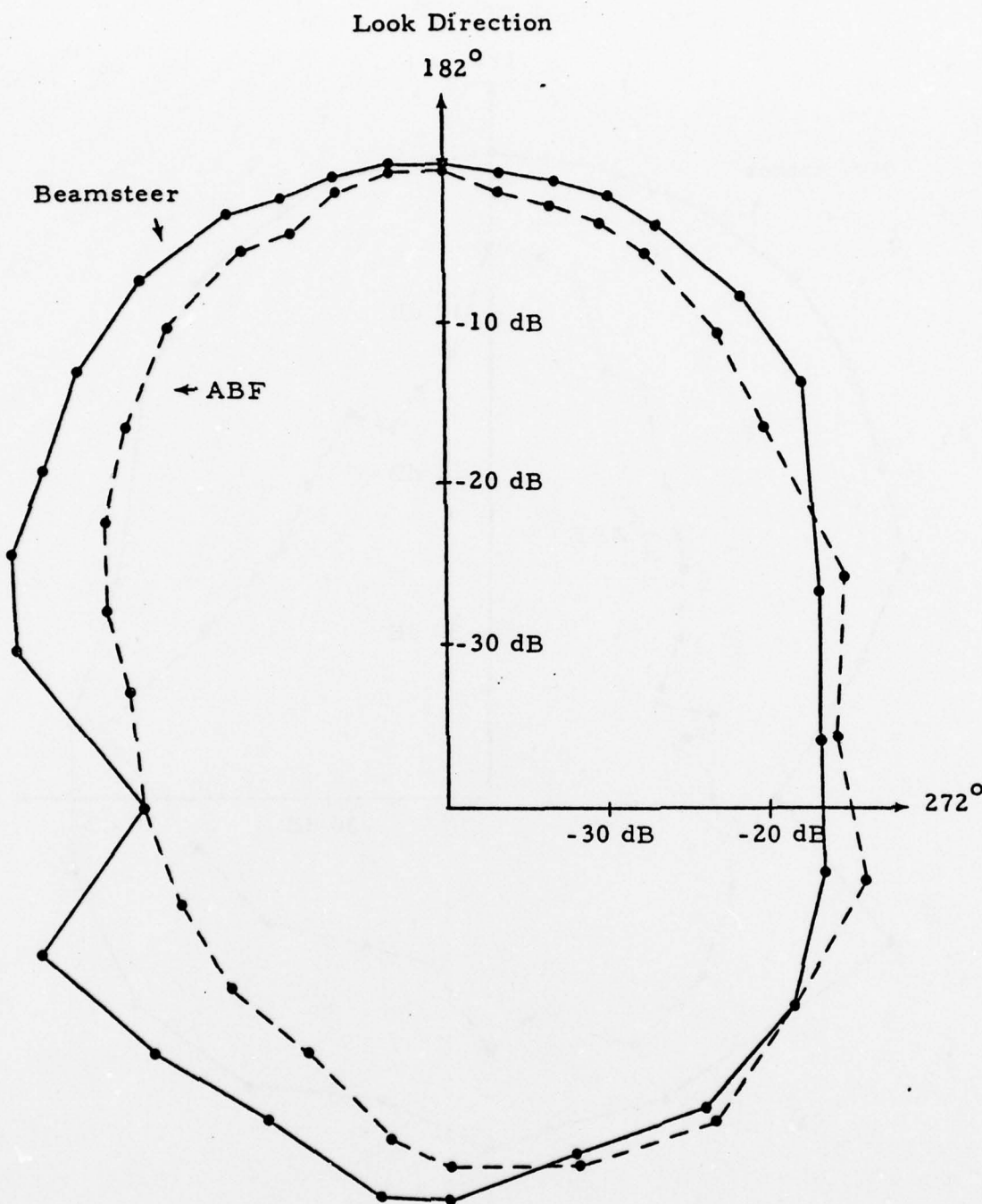


FIGURE III-3

MEASURED BEAMSTEER AND ABF BEAM PATTERN (0.5-3.5 Hz) FOR THE INITIAL SIGNAL PULSE IN FIGURE III-1

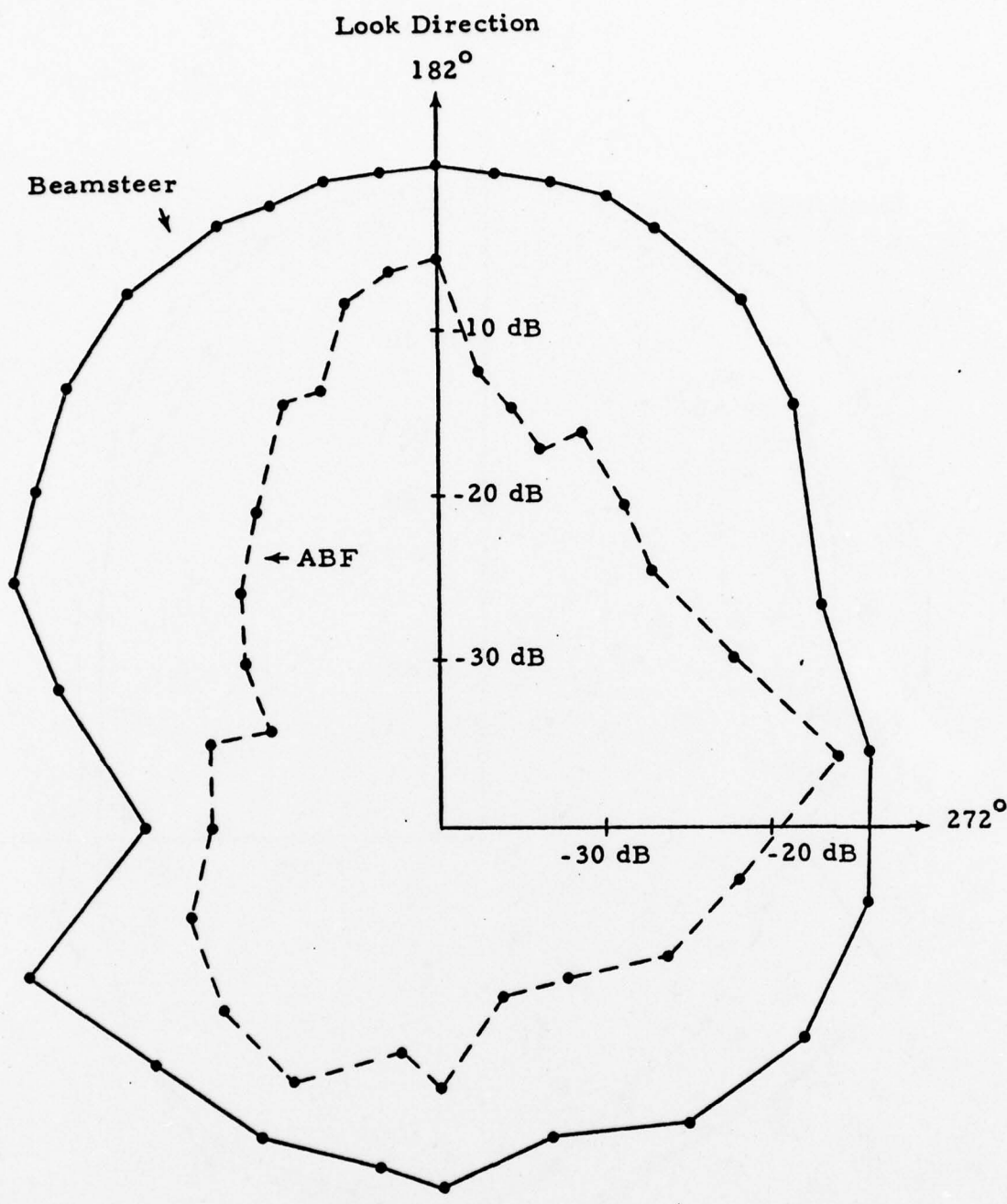


FIGURE III-4

**MEASURED BEAMSTEER AND ABF BEAM PATTERN (0.5-3.5 Hz) FOR THE
SECONDARY SIGNAL PULSE IN FIGURE III-1**

B. DETECTION PROBABILITY MEASUREMENT

The main task in this report is to measure the detection probability as a function of bodywave magnitude (m_b) for the ABF. This involves a statistical estimate and usually requires a substantial data base to form reliable and meaningful results.

1. Data Base

A total of 129 events were processed and used in this evaluation. First, events listed in the January 1977 monthly listing of Preliminary Determination of Epicenters by the U.S. G.S. National Earthquake Information Service (NEIS) were selected, with the following criteria applied:

$$20^\circ \leq \Delta < 100^\circ$$

where Δ is the epicentral distance of a source location to KSRS. This constraint was imposed on event selection because of the intention to design the detector for teleseismic P waves. The processing was performed on 95 events from January 1 to 15, 1977. Table III-1 lists the event information from the NEIS bulletin and our own measurements of m_b . There are four columns on Table III-1 concerning the m_b . From the left, the first m_b is from the NEIS bulletin, the second is the single-site (SS) measurement, and the third and fourth columns are the measurements of m_b by the conventional beamsteer (BS) and the ABF, respectively. A blank in a row means no detection. However, if a SS magnitude is listed (i. e., detected), array beamforming was not performed. Therefore, neither BS nor ABF units were available for that event. But, in the case of detection probability estimates, detections were claimed for both the BS and the ABF. ID, the first column in Table III-1, is the identification number which was used for convenience in referring to the processed traces in Appendix A and Appendix B.

TABLE III-1
PROCESSED EVENT LIST FROM NEIS BULLETIN
(01/01/77 to 01/15/77)
(PAGE 1 OF 4)

ID	DATE	TIME	LAT.	LONG.	DEPTH	A	m _b			
							NEIS	SS	BS	ABF
1	770101	7.20.51.0	40.40N	127.30W	2	76.2	3.7	5.2	5.2	
2	770101	10.52.34.1	8.41N	126.41E	53	29.0	5.0	4.8	4.7	
3	770101	12.19.22.2	10.28N	126.23E	89	27.2	5.0	5.0	4.8	
4	770101	14.24.23.9	28.09S	176.23W	33	83.8	4.9			
5	770101	14.26.35.3	19.34N	155.12W	9	68.3	3.7			
6	770101	17.35.54.9	7.88S	109.01E	113	48.6	5.7	5.9		
7	770101	19.1.39.6	2.53S	126.58E	33	39.9	6.0	6.2		
8	770101	20.45.32.6	1.14S	134.74E	64	39.0	4.9		4.2	
9	770101	21.3.41.6	0.86S	134.33E	33	38.7	4.9		4.1	
10	770101	22.26.40.6	39.20N	43.46E	24	63.7	5.0	5.1	5.0	
11	770102	0.53.6.0	38.05N	91.19E	33	28.9	4.8		4.7	
12	770102	0.55.8.8	6.95S	129.51E	171	44.3	5.0			
13	770102	6.48.15.0	12.02N	143.62E	33	29.0	4.9	4.9	4.8	
14	770102	8.36.35.9	17.51S	167.71E	33	66.4	4.7		4.5	
15	770102	8.47.49.3	17.51S	167.71E	33	66.4	4.7			
16	770102	9.55.28.4	10.17S	118.99E	19	48.3	5.8	6.5		
17	770102	12.59.21.4	63.12N	150.14W	113	53.7	3.8			
18	770102	17.12.19.2	10.22N	126.33E	23	27.2	5.1		5.0	
19	770102	19.37.25.2	39.24N	43.57E	34	63.6	4.9		4.6	
20	770103	0.21.36.9	0.01S	123.90E	131	37.6	5.1		4.9	
21	770103	0.44.7.8	38.21N	23.11E	23	77.6	4.5			
22	770103	1.34.34.2	51.43N	179.08W	33	39.4	4.8		4.8	
23	770103	6.41.7.8	7.23N	60.17E	33	68.0	4.8		4.4	
24	770103	10.5.15.3	29.25S	77.80E	33	81.4	5.1			

TABLE III-1
 PROCESSED EVENT LIST FROM NEIS BULLETIN
 (01/01/77 to 01/15/77)
 (PAGE 2 OF 4)

ID	DATE	TIME	LAT.	LONG.	DEPTH	Δ	NEIS	SS	m _b	BS	ABF
25	770103	13.53.14.2	23.58S	179.96W	540	78.2	5.1		4.9	4.5	
26	770103	15.23.10.2	5.26S	151.92E	65	48.1	5.0		4.9	4.5	
27	770104	1.41.42.8	53.60N	160.50E	157	27.6	4.4		4.6	4.1	
28	770104	11.47. 8.6	1.48S	126.80E	33	38.9	4.9		4.6	4.5	
29	770104	14.56.40.5	59.52N	152.99W	119	53.2	4.2		4.2	4.1	
30	770104	16. 9.58.5	33.09N	47.92E	45	63.5	5.1		5.4	5.3	
31	770104	20.44.39.4	7.43S	38.52E	33	94.0	5.2		5.2	4.8	
32	770105	5.44.39.9	27.46N	56.20E	29	59.9	5.5		5.5		
33	770105	10.20.29.1	23.38S	179.99E	538	78.0	5.0		4.1	4.0	
34	770105	10.36.29.4	16.09S	173.87W	33	76.5	5.0		4.6	4.6	
35	770105	13.29.48.1	20.81S	178.31W	575	77.1	5.2		5.4		
36	770105	14.10.56.5	25.43N	95.18E	104	30.2	4.8		4.7	4.6	
37	770105	14.12.35.0	18.70N	145.52E	136	24.3	4.6		5.3		
38	770105	17.52.19.4	5.41S	146.53E	168	46.2	4.7		4.6	4.4	
39	770106	4.10.17.8	17.94S	178.54W	621	74.8	4.6		4.3	4.3	
40	770106	6.11.40.7	3.63S	144.45E	33	43.8	6.0		6.3		
41	770106	7.55.57.5	49.27N	155.55E	33	23.1	5.4		5.6		
42	770106	9.29. 6.2	7.04S	129.52E	56	44.4	4.3		4.5	4.4	
43	770106	11.16.41.2	3.15S	129.10E	48	40.5	5.0		4.6	4.5	
44	770106	16. 2. 7.6	51.48N	175.48W	38	41.6	5.2		6.0		
45	770106	18.33.43.5	2.51S	28.70E	21	98.8	5.3			5.5	
46	770106	21.50. 8.1	31.05N	88.05E	33	33.3	5.2		4.9	4.8	
47	770107	6.31.13.2	34.55N	70.97E	46	45.5	5.1		5.2	5.1	
48	770107	7. 9.35.3	52.26S	114.59E	33	90.3	5.5		5.0	4.8	
49	770107	7.15.57.5	30.70N	50.69E	67	62.6	4.6		5.4		
50	770107	10.37.18.7	7.48S	129.07E	143	44.9	4.4			4.2	

TABLE III-1
 PROCESSED EVENT LIST FROM NEIS BULLETIN
 (01/01/77 to 01/15/77)
 (PAGE 3 OF 4)

ID	DATE	TIME	LAT.	LONG.	DEPTH	A	m _b			
							NEIS	SS	BS	ABF
51	770107	17.14.47.3	25.18S	176.96W	76	81.2	5.0		4.8	4.7
52	770107	19.9.33.2	5.32N	126.16E	53	32.1	4.7		4.8	4.6
53	770107	21.2.55.2	24.16N	98.45E	42	28.4	4.6			
54	770108	1.6.31.1	20.08N	147.52E	47	24.3	5.2	5.6		
55	770108	6.8.52.7	11.47N	140.38E	24	28.3	4.6		4.8	4.7
56	770108	6.41.4.1	15.32N	121.91E	36	22.7	5.3			
57	770108	7.40.41.9	11.27S	166.11E	42	60.4	5.5			
58	770108	9.38.7.4	37.91N	122.20W	10	80.9	4.8			
59	770108	10.55.19.0	3.58S	140.10E	26	42.5	5.1			
60	770108	11.15.49.3	17.86S	178.62W	571	74.7	4.9			
61	770108	12.24.45.4	5.60S	150.96E	61	48.0	5.3			
62	770108	21.37.16.0	22.24S	170.34E	58	71.7	5.1			
63	770109	3.53.24.6	59.93N	153.36W	132	52.9	4.2			
64	770109	8.31.16.0	6.10N	146.82E	33	35.7	4.9			
65	770109	16.52.11.2	17.88S	178.52W	589	74.7	4.4			
66	770110	3.28.54.9	15.33N	121.86E	47	22.7	5.0			
67	770110	8.18.59.9	8.35N	125.19E	38	29.2	5.4			
68	770110	9.14.43.6	39.58N	27.40E	4	74.1	4.1			
69	770110	9.31.49.9	20.72S	179.25W	653	76.4	5.5			
70	770110	20.40.3.0	7.04S	154.70E	52	51.0	5.0			
71	770110	22.43.43.0	28.41S	176.74W	33	83.7	4.6			
72	770110	23.18.7.0	21.49S	168.66E	16	70.2	5.2			
73	770111	14.51.5.0	12.93N	57.45E	33	66.8	5.1			
74	770111	21.41.26.3	5.36S	133.87E	33	43.1	5.1			
75	770112	10.56.32.6	6.91S	155.34E	102	51.2	4.6			

TABLE III-1
 PROCESSED EVENT LIST FROM NEIS BULLETIN
 (01/01/77 to 01/15/77)
 (PAGE 4 OF 4)

ID	DATE	TIME	LAT.	LONG.	DEPTH	A	m _b			
							NEIS	SS	BS	ABE
76	770112	13. 5. 59. 3	19. 40N	155. 29W	16	68. 2	3. 9			
77	770112	17. 43. 33. 4	28. 22N	102. 59E	33	23. 1	5. 1	5. 5		
78	770112	23. 35. 19. 1	1. 58N	99. 86E	178	44. 1	5. 6	5. 8		
79	770113	5. 54. 59. 0	38. 34N	75. 97E	33	40. 5	5. 0		4. 4	
80	770113	9. 19. 6. 1	43. 55N	17. 10E	20	77. 7	5. 3	5. 7		
81	770113	11. 39. 46. 8	17. 82S	175. 19W	198	76. 8	4. 4		4. 6	4. 3
82	770113	14. 27. 38. 4	2. 05N	125. 08E	156	35. 4	5. 1		4. 8	4. 8
83	770113	16. 26. 29. 7	2. 66N	65. 25E	33	66. 9	4. 7		4. 4	
84	770113	21. 10. 16. 7	51. 96N	175. 03E	51	35. 8	5. 0		5. 4	
85	770113	21. 17. 3. 5	11. 58S	161. 00E	33	58. 0	4. 3		4. 5	
86	770113	22. 5. 59. 3	59. 43N	142. 23W	33	58. 4	4. 5			
87	770114	2. 52. 34. 7	1. 71S	28. 95E	33	98. 1	4. 8			
88	770114	12. 9. 33. 1	34. 70N	82. 71E	33	36. 3	4. 7		4. 8	4. 7
89	770114	15. 46. 11. 1	36. 61N	71. 41E	149	44. 5	4. 8		4. 4	4. 3
90	770114	17. 58. 35. 2	19. 08S	177. 54W	350	76. 8	5. 2		5. 4	
91	770114	23. 26. 42. 5	19. 30N	155. 10W	10	68. 4	4. 2		5. 2	5. 0
92	770115	10. 49. 5. 0	12. 96N	125. 96E	33	24. 5	5. 6		5. 5	
93	770115	10. 55. 47. 2	12. 99N	125. 93E	33	24. 5	5. 5		5. 6	
94	770115	21. 0. 43. 2	62. 80N	150. 37W	100	53. 7	4. 3		4. 9	4. 9
95	770115	23. 58. 46. 8	33. 57N	3. 55W	33	95. 9	4. 4			

Next, a number of events were selected from the January 1978 NORSAR bulletin. The purpose was to select some low-magnitude events for the ABF evaluation. Three constraints were imposed on the event selection as follows:

- <1> NORSAR $m_b \leq 4.5$
- <2> NORSAR Bulletin $V_p \leq 14.0 \text{ km/sec}$
- <3> Event-KSRS Distance $20^\circ \leq \Delta \leq 99^\circ$

where V_p is the apparent P wave velocity at NORSAR and was listed in the NORSAR event bulletin. The first constraint was intended to improve the ABF evaluation by selecting additional low-magnitude events not available on the NEIS list. The second constraint was applied to ensure a satisfactory degree of reliability for a given event listed in the bulletin. Finally, the third constraint was imposed to limit the evaluation to teleseismic P waves. Processing was performed on 34 events from January 1 to 31, 1978. Table III-2 lists the information from the NORSAR bulletin and the measured m_b . Appendix B presents the processed traces for those events. (Note: Event ID was introduced in Table III-2 and Appendix B for the convenience of the reader.)

2. Comparison of Station m_b and Bulletin m_b

Measurement of bodywave m_b magnitude was done when a signal was detected. An analyst-type of detection criteria was used in which signal amplitude rise was about twice that of the maximum noise amplitude, in a one minute time gate. The measured m_b was computed by the expression

$$m_b = \log \left(\frac{A}{T} \right) + p(\Delta, h)$$

where A is the peak-to-peak amplitude in $\text{m}\mu$, T is the period and $P(\Delta, h)$ is a correction factor, which is a function of epicentral distance, Δ (in degree) and the depth, h (in km).

The P factors in Table 2 of Veith and Clawson (1972) were used for the computations.

TABLE III-2
 PROCESSED WEAK EVENT LIST FROM NORSAR BULLETIN
 (01/01/78 to 01/31/78)
 (PAGE 1 OF 2)

ID	DATE	TIME	LAT.	LONG.	Δ	m_b			
						NORSAR	SS	BS	ABF
1	780101	4. 22. 49. 0	40. 00N	33. 00E	70. 3	3. 8			
2	780102	1. 45. 33. 0	32. 00N	74. 00E	44. 1	4. 1			
3	780105	3. 26. 29. 0	27. 00N	67. 00E	51. 7	4. 3	5. 0	4. 8	
4	780105	14. 45. 16. 0	37. 00N	71. 00E	44. 6	4. 2			
5	780105	19. 29. 54. 0	27. 00N	60. 00E	57. 2	4. 1	4. 3		
6	780105	19. 35. 3. 0	28. 00N	65. 00E	60. 6	4. 0	4. 9	4. 8	
7	780106	2. 36. 8. 0	34. 00N	46. 00E	64. 4	3. 7			
8	780106	5. 27. 9. 0	28. 00N	55. 00E	60. 6	4. 1	4. 4		
9	780107	2. 58. 32. 0	38. 00N	77. 00E	39. 8	4. 2	4. 0		
10	780107	23. 44. 5. 0	37. 00N	71. 00E	44. 6	4. 0	4. 2		
11	780110	12. 36. 40. 0	34. 00N	46. 00E	64. 4	4. 0	4. 4		
12	780111	1. 44. 31. 0	35. 00N	77. 00E	40. 7	4. 5	4. 4		
13	780111	3. 58. 8. 0	39. 00N	28. 00E	74. 0	4. 0	4. 6		
14	780111	5. 7. 31. 0	36. 00N	22. 00E	79. 6	3. 7			
15	780112	11. 7. 23. 0	27. 00N	60. 00E	57. 2	3. 9			
16	780112	20. 8. 27. 0	35. 00N	24. 00E	79. 0	4. 5	5. 4		
17	780113	11. 30. 5. 0	46. 00N	27. 00E	70. 6	3. 6			
18	780113	16. 1. 55. 0	35. 00N	27. 00E	77. 0	4. 3			
19	780115	7. 3. 29. 0	31. 00N	50. 00E	62. 9	4. 0	5. 0	4. 9	
20	780115	10. 26. 39. 0	46. 00N	27. 00E	70. 6	4. 1	5. 1	4. 9	
21	780115	11. 30. 31. 0	37. 00N	71. 00E	44. 6	3. 9			
22	780121	1. 21. 4. 0	37. 00N	71. 00E	44. 6	4. 1	4. 2		
23	780121	8. 11. 24. 0	35. 00N	24. 00E	79. 0	4. 0			
24	780121	14. 33. 44. 0	37. 00N	71. 00E	44. 6	3. 7	4. 1		
25	780124	10. 7. 8. 0	35. 00N	77. 00E	40. 7	4. 5	4. 2		

TABLE III-2
 PROCESSED WEAK EVENT LIST FROM NORSAR BULLETIN
 (01/01/78 to 01/31/78)
 (PAGE 2 OF 2)

ID	DATE	TIME	LAT.	LONG.	Δ	m_b			
						NORSAR	SS	BS	ABF
26	780126	8.29.45.0	39.00N	24.00E	76.5	3.7			
27	780126	14.54.37.0	27.00N	60.00E	57.2	4.0			
28	780128	10.13. 6.0	39.00N	24.00E	76.5	3.6			
29	780128	14.18.17.0	34.00N	46.00E	64.4	4.1			
30	780129	9.40.43.0	37.00N	71.00E	44.6	3.9			
31	780129	10.25.10.0	44.00N	26.00E	72.4	4.0			
32	780129	17.32. 8.0	15.00N	56.00E	66.7	4.4			
33	780130	7.53.14.0	35.00N	24.00E	79.0	3.9			
34	780131	1.55.54.0	37.00N	71.00E	44.6	4.1			

The KSRS short-period array has an instrument response peak centered at 1.0Hz (0.488 m μ /computer count) and thereby, T = 1.0 second was used for all m_b computations. The NEIS bulletin lists depths while the NORSAR bulletin does not. In the absence of depth from the NORSAR bulletin, the 40 km 'normal depth' was used for P (Δ , h) corrections.

Figure III-5 compares the site 1 measured m_b at the KSRS with the NEIS or NORSAR m_b (numerical m_b units are listed in Tables III-1 and III-2, and are separately and repeatedly listed in the seismic trace figures in Appendices A and B for convenience to the reader). The dashed slant line in Figure III-5 indicates the difference between the average bulletin m_b and the average measured m_b at site 1. In other words, the measured m_b units at site 1, on the average, yielded 0.35 units higher than those in the bulletins. A number of factors could possibly attribute to the bias or difference in the averaged m_b units. First, single seismometer measurement tends to increase the m_b unit by noise contribution to the signal amplitude (Note: measurement was done by peak-to-peak amplitudes). Second, NORSAR body-wave magnitude in general was about 0.2-0.3 unit smaller than the NEIS m_b (Ringdal and Whitelaw, 1973).

Figure III-6 shows the comparison of NEIS or NORSAR m_b versus the measured m_b by the conventional beamsteer at the KSRS. The slant line is

$$\text{Beamsteer } m_b = -0.1 + \text{NEIS or NORSAR } m_b$$

which indicated that the average KSRS beamsteer m_b was 0.1 unit smaller than those of the bulletin. This difference is due to the beamforming loss at the KSRS short-period array. The same method of comparing the bulletin m_b with ABF m_b is shown in Figure III-7 where the dashed slant line is

$$\text{ABF } m_b = -0.1 + \text{NEIS or NORSAR } m_b$$

Considering the average of all signals detected by the ABF, the ABF m_b was

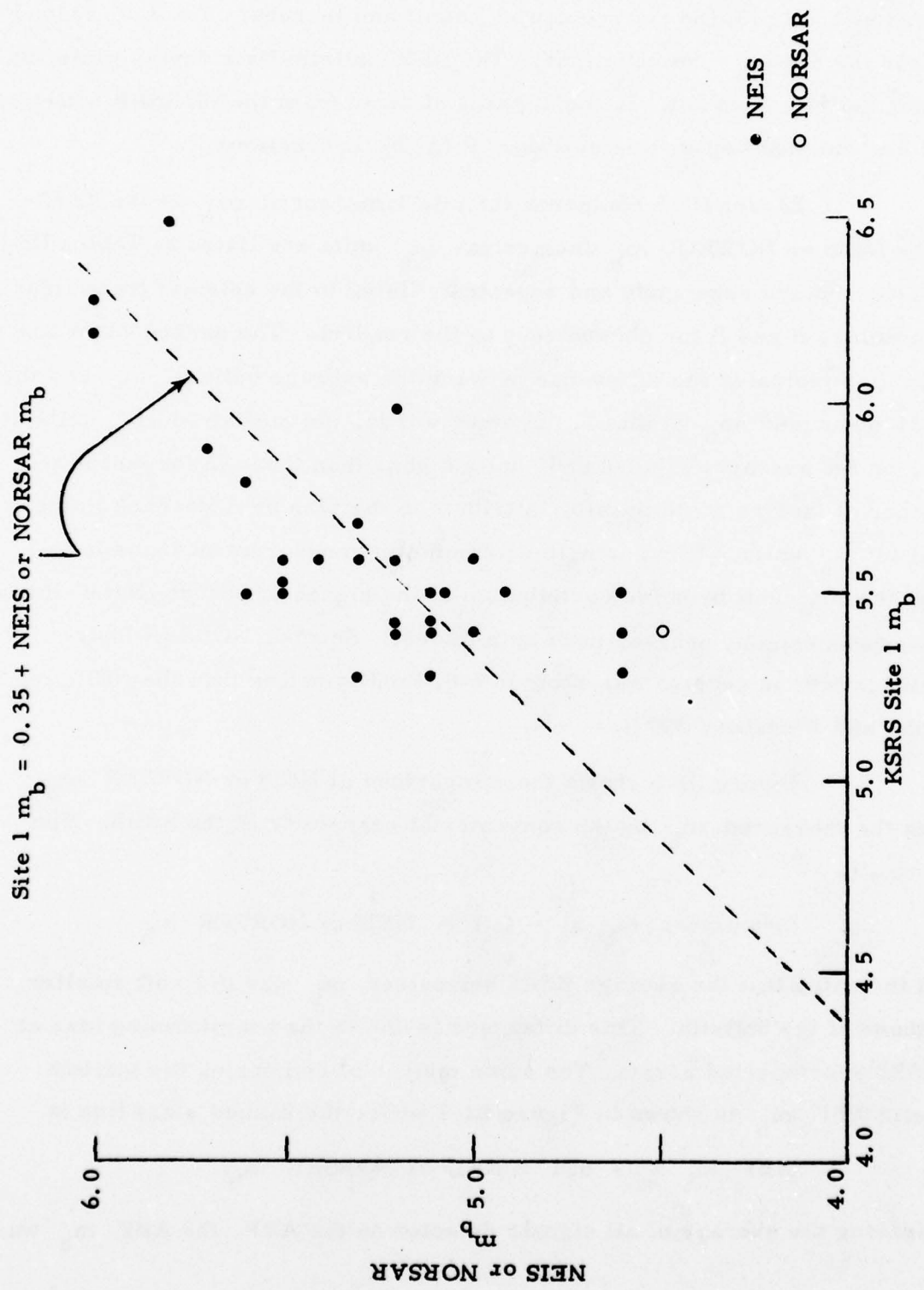
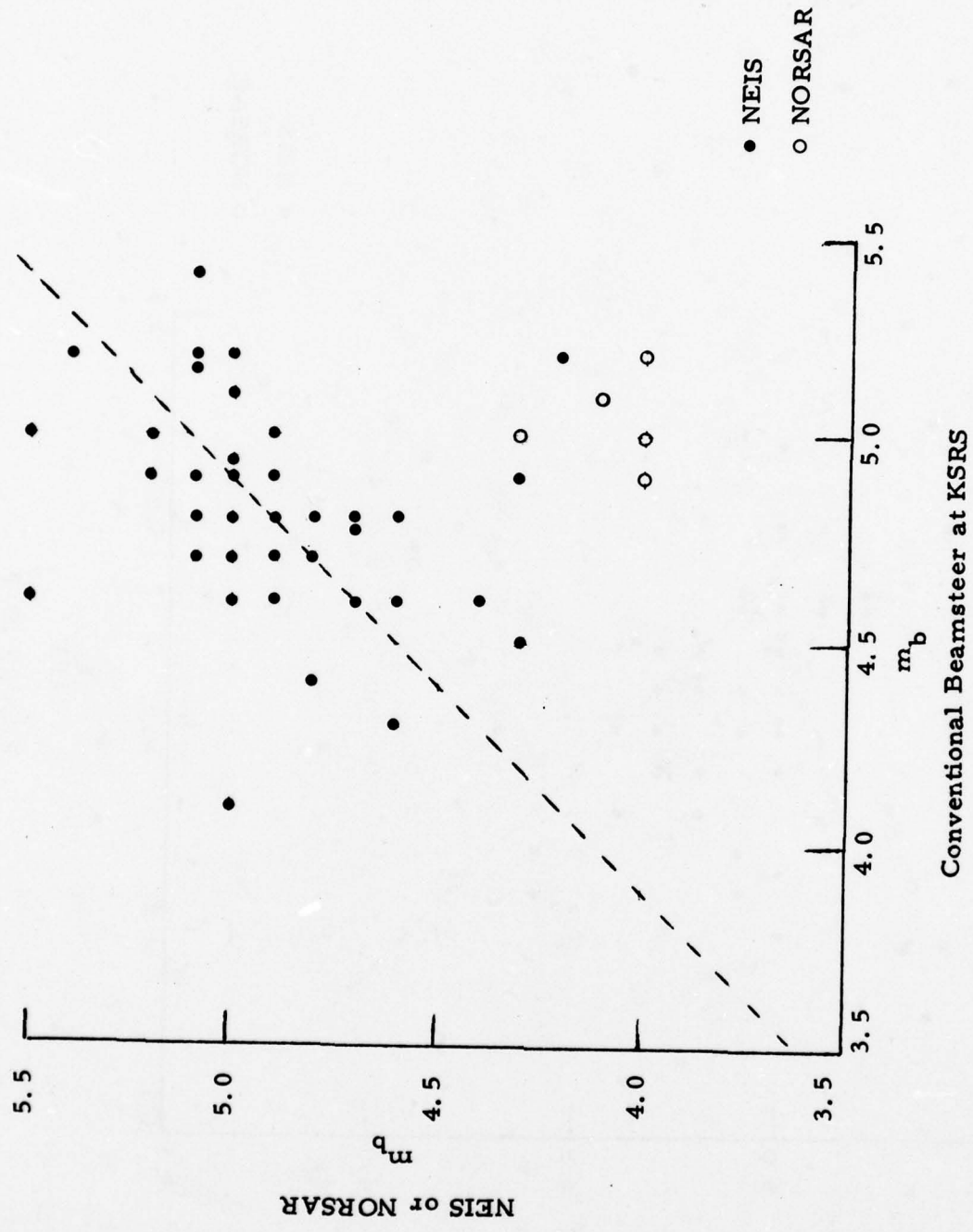


FIGURE III-5
NEIS OR NORSAR m_b VERSUS MEASURED m_b BY SITE 1 OF THE KSRS



Conventional Beamsteer at KSRS

FIGURE III-6

NEIS OR NORSAR m_b VERSUS KSRS BEAMSTEER m_b

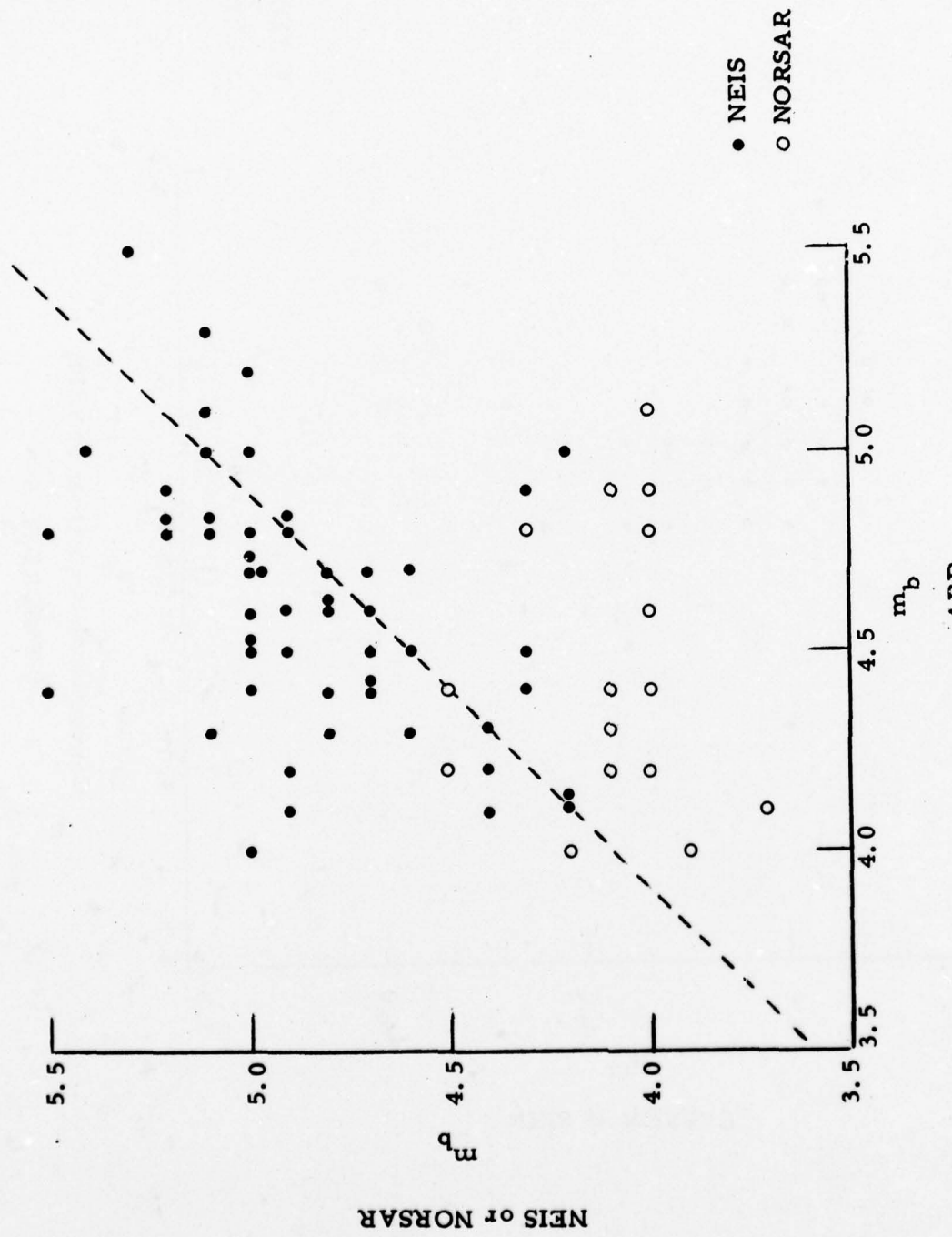


FIGURE III-7
NEIS OR NORSAR m_b VERSUS ABF m_b

0.1 unit smaller than those in the bulletin. This difference is the same magnitude of loss as the conventional beamsteer.

3. ABF, Beamsteer, and Single Site Detection Probabilities at KSRS

Histograms of detection and non-detection as a function of body-wave magnitudes m_b were generated from the results listed in Tables III-1 and III-2. For a given event in the tables, if a signal was detected by site 1(i.e., m_b value is printed in m_b SS column), detections are automatically claimed for the beamsteer and ABF processors. The detection percentages (in terms of m_b) were fitted to Gaussian probabilities by use of a least-square procedure with uniform unity correct decision probability (Shen, 1976). Curves of 90% confidence were also computed.

Figure III-8 shows the KSRS site 1 detection and non-detection histogram and detection probability. In the figure, MB50 means, in terms of m_b , the 50% detection probability, and MB90 the 90% detection probability. In this case, the bodywave magnitude for a 50% detection probability is a mean value $\mu m_b = 5.23$, with a standard deviation $\sigma m_b = 0.34$.

For the array beamforming results, Figure III-9 shows the KSRS beamsteer detection and non-detection histogram and detection probability. The 50% detection probability is $\mu m_b = 4.62$ and the standard deviation is $\sigma m_b = 0.58$. The conventional beamforming improvement at the KSRS short-period array is 0.61 m_b units or 12.2 dB for the MB50 and 0.30 m_b units or 6 dB for the MB90. The 12.2 dB beamforming detection improvement agrees with \sqrt{N} array gain, where N is the number of channels of an array. (i.e., 12.78 dB for N = 19).

The array detection capability was enhanced further by the ABF. Figure III-10 shows KSRS ABF detection and non-detection histogram and detection probability where MB50 is 4.14 and MB90 4.84, with $\sigma m_b = 0.54$. Detection improvement of the ABF over the conventional beamsteer is 0.48.

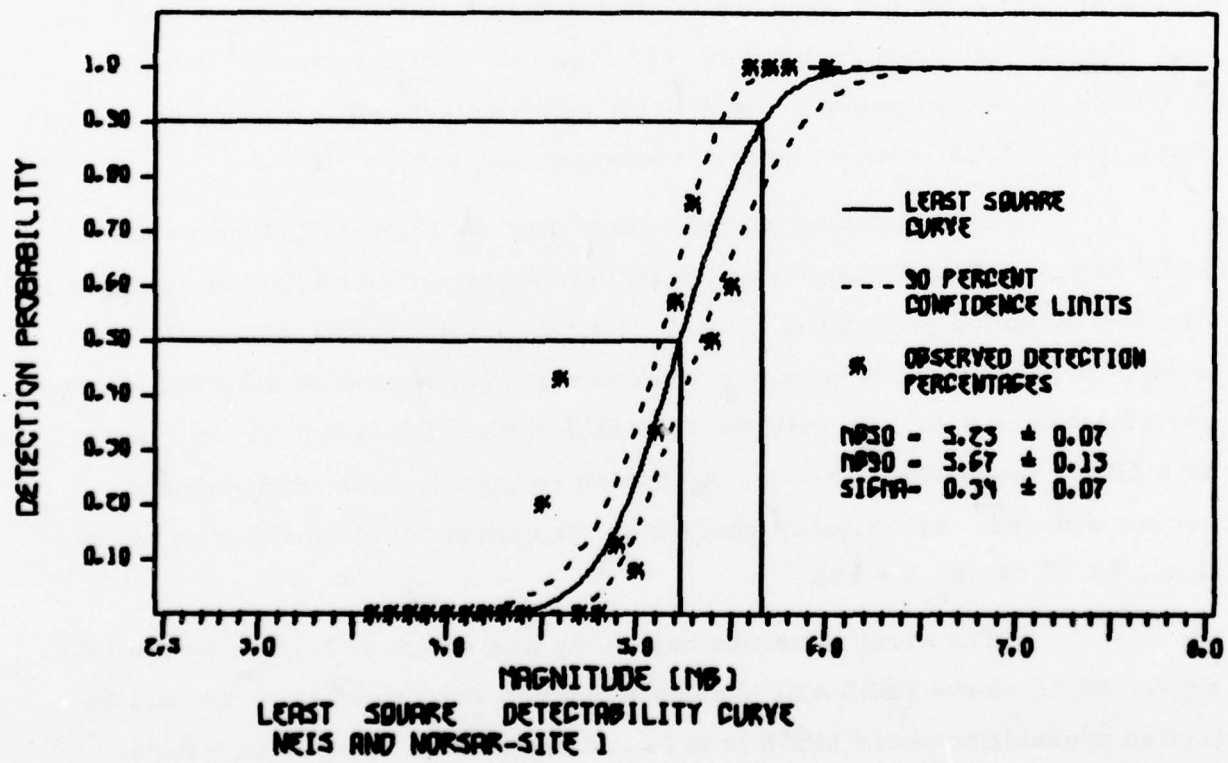
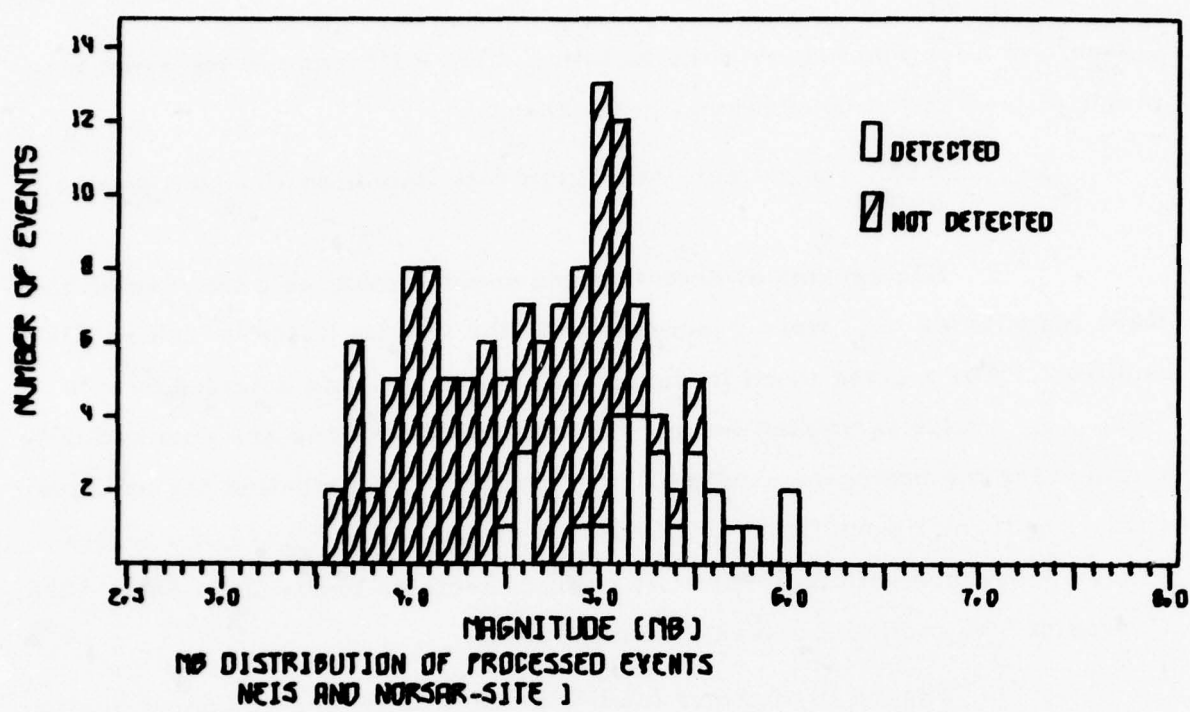


FIGURE III-8

KSRS SITE 1 DETECTION AND NON-DETECTION HISTOGRAM
AND DETECTION PROBABILITY

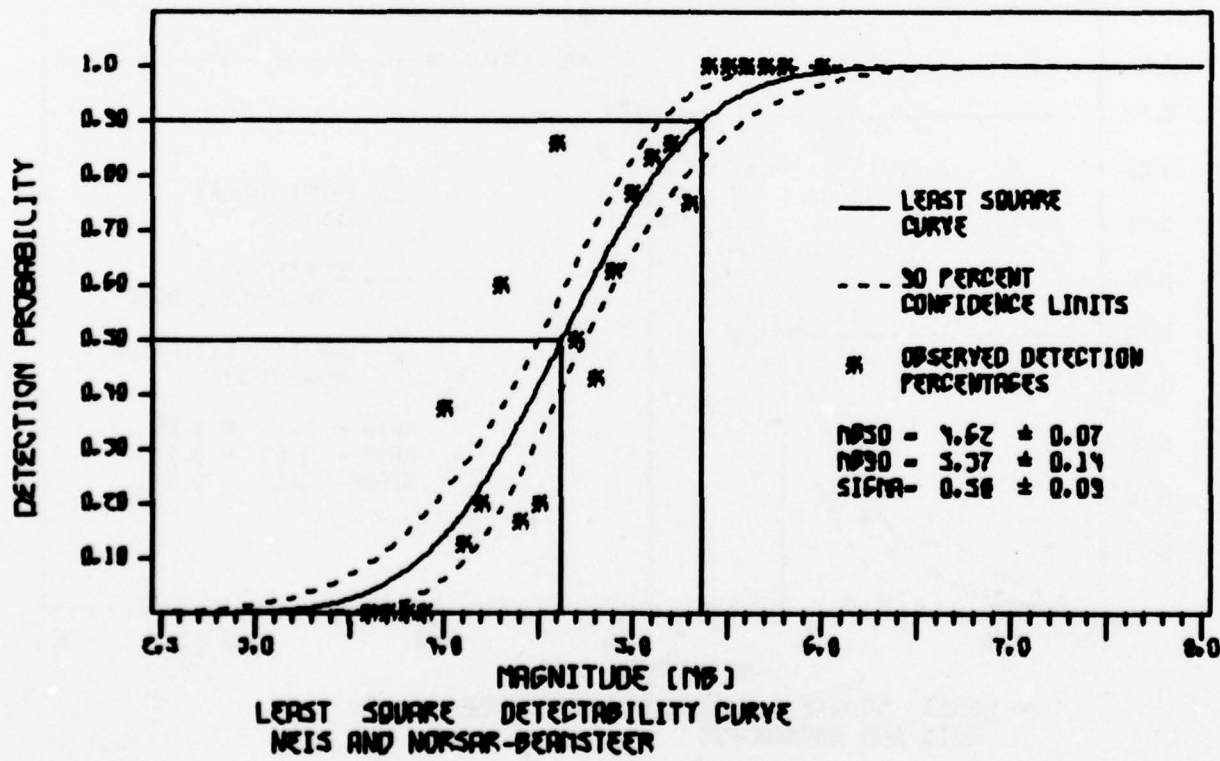
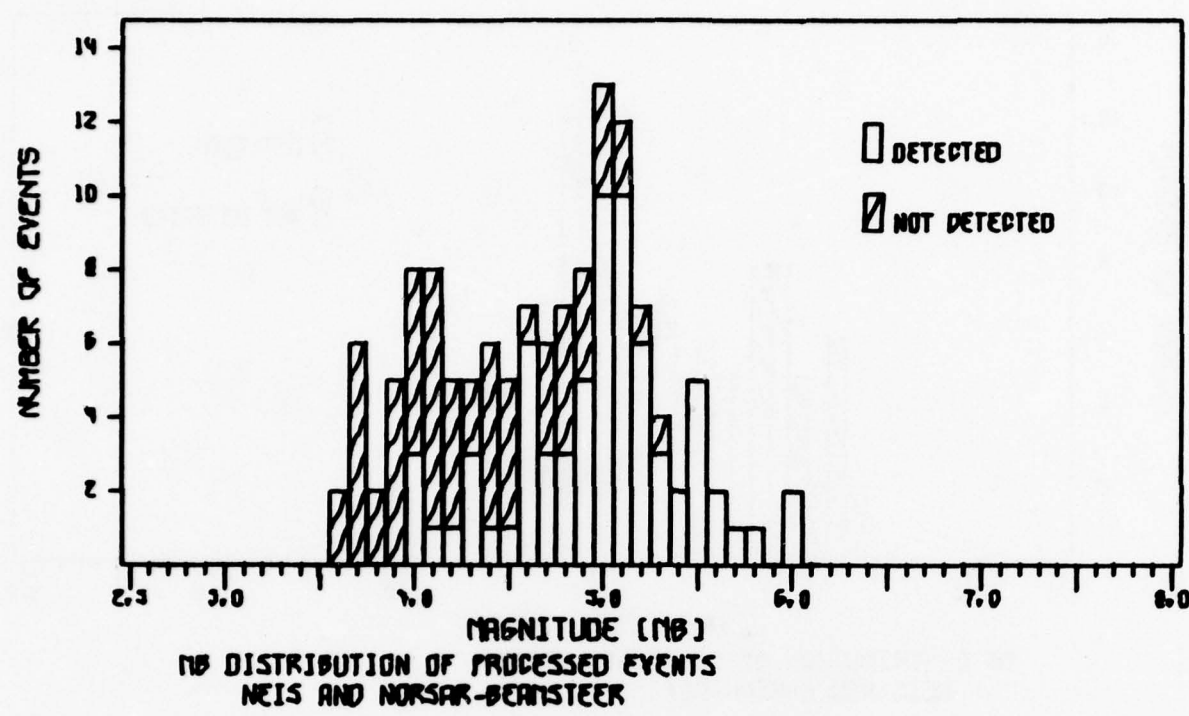


FIGURE III-9

KSRS BEAMSTEER DETECTION AND NON-DETECTION HISTOGRAM
AND DETECTION PROBABILITY
III-21

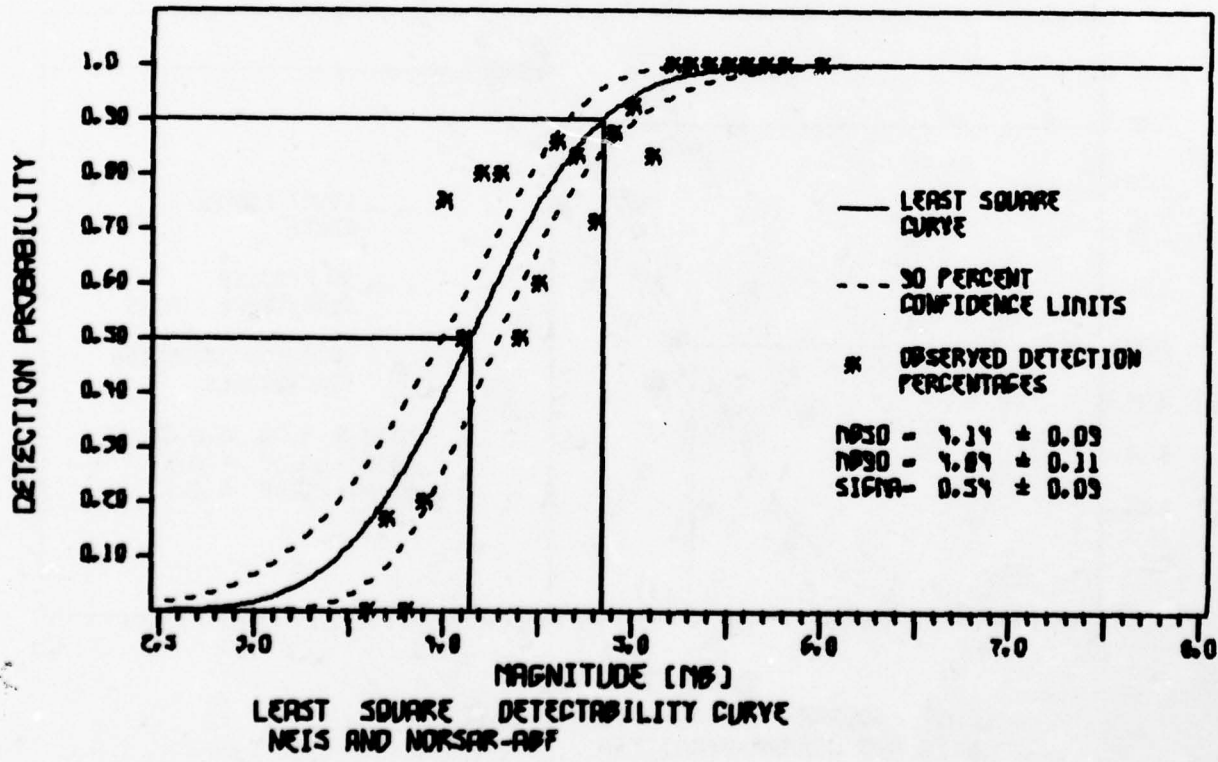
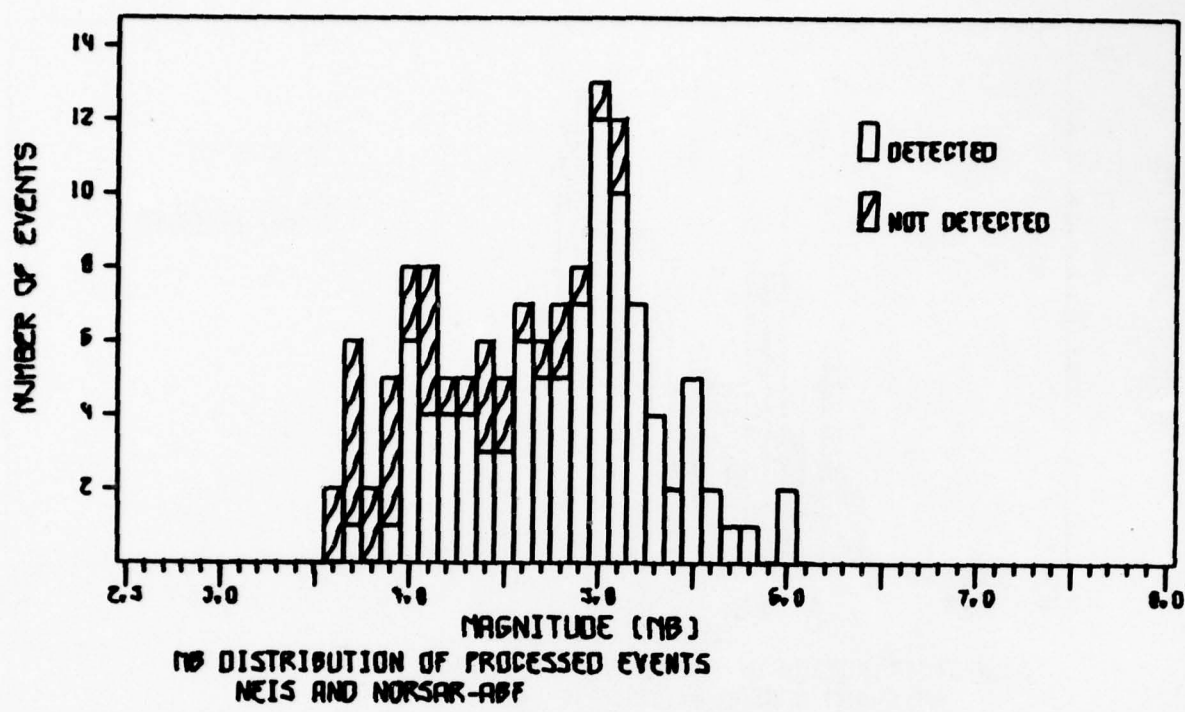


FIGURE III-10

KSRS ABF DETECTION AND NON-DETECTION HISTOGRAM
AND DETECTION PROBABILITY
III-22

m_b units or 9.6 dB at MB50 and 0.53 m_b units, or 10.6 dB at MB90. This demonstrated ABF improvements enhanced the KSRS (19 sites) detection capability to the equivalence of a conventional beamsteer operating on an array consisting of 190 sensors. That increase in capability is significant.

It should be noted that the detection improvement (in dB or m_b units) mentioned here was the threshold reduction rather than SNR processing gain. One would expect that the SNR processing gain should be equal to the threshold reduction if processing is linear, in terms of input-output SNR relationship, such as the conventional beamsteer. Previous study by adding scaled noise to signal (Shen, 1977) indicated that the ABF processing gain was not equal to its threshold reduction.

Bodywave magnitudes used in Figures III-8, III-9, and III-10 were directly taken from NEIS or NORSAR bulletins. The events vary over a wide range of epicentral distances and thus potentially represent a wide range of signal amplitudes corresponding to each m_b value. Because the epicentral distances range from 20° to 99° , it was felt that the detection probability might not be well-behaved in terms of Gaussian distribution and result in a large event population standard deviation. Therefore, for the purpose of statistical study, bodywave magnitude was adjusted to an equivalent 50° epicentral distance from the KSRS by the transformation

$$m_b(50, h) = m_b(\Delta, h) - p(\Delta, h) + p(50, h)$$

where Δ is epicentral delta (in degrees) and h is depth (in km). $m_b(\Delta, h)$ is the bulletin magnitude, and $p(\Delta, h)$ is a correction factor for Δ and h .

Figure III-11 shows the site 1 detection and non-detection histogram and detection probability where the magnitudes, m_b have been adjusted for the location being at 50° from the KSRS. The adjusted Gaussian parameters are $\mu m_b = 5.18$ and $\sigma m_b = 0.29$. The same procedure was accomplished for the beamsteer and the ABF. Figure III-12 shows the histogram and

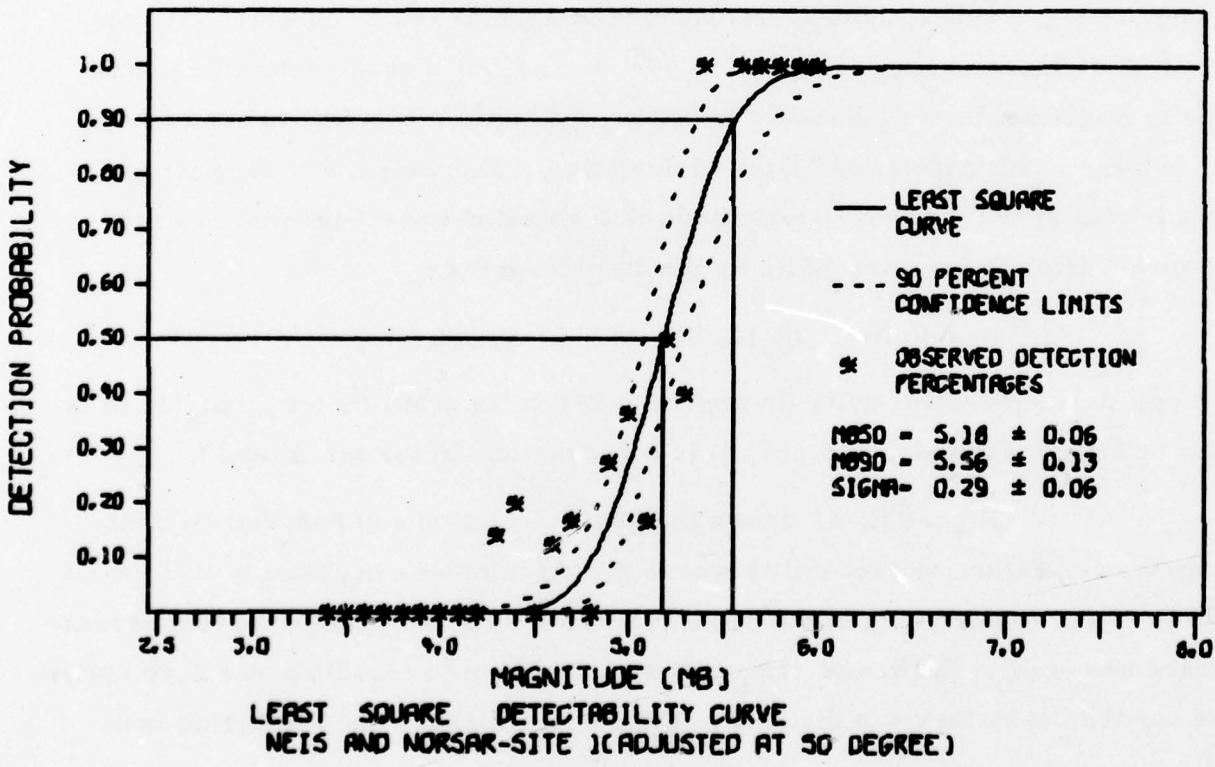
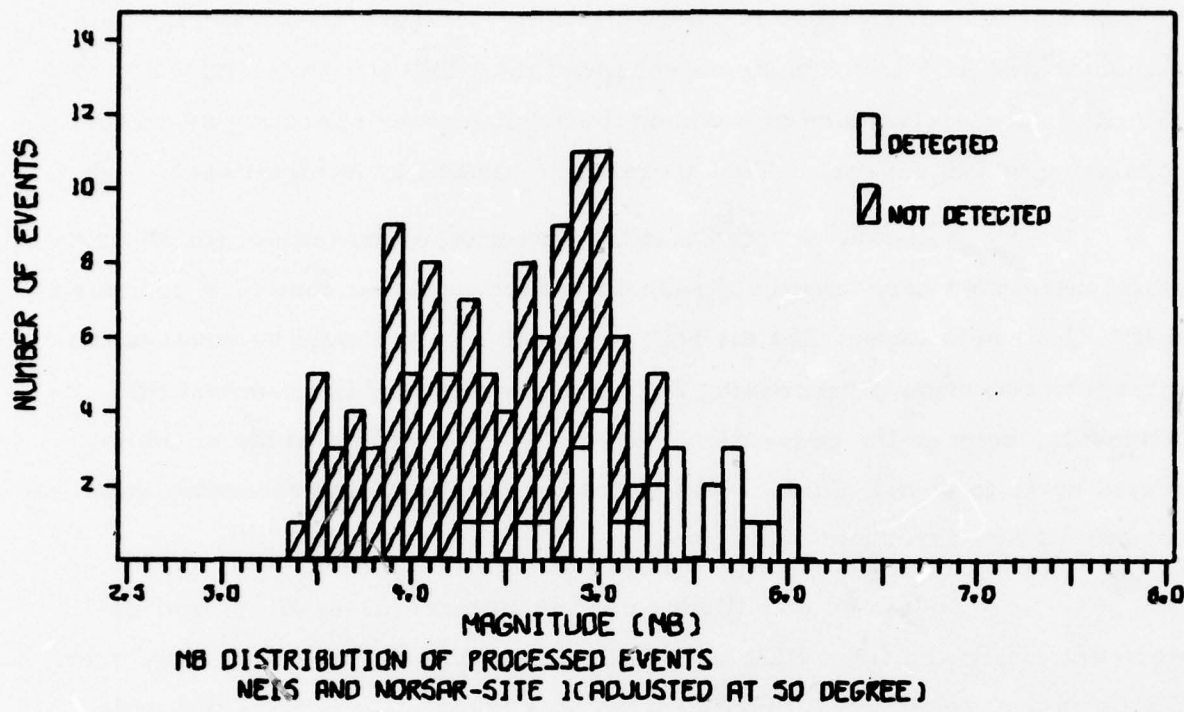


FIGURE III-11

KSRS SITE 1 DETECTION HISTOGRAM AND PROBABILITY
BY ADJUSTING m_b AT 50° DELTA

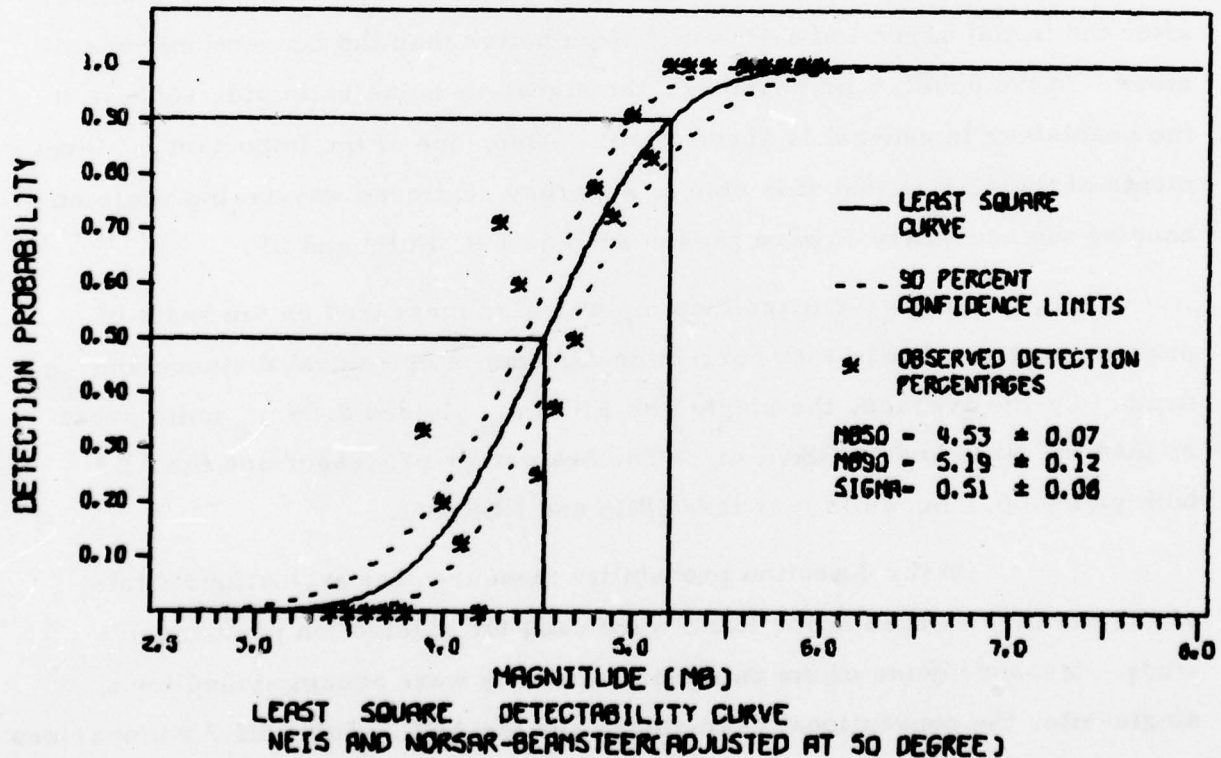
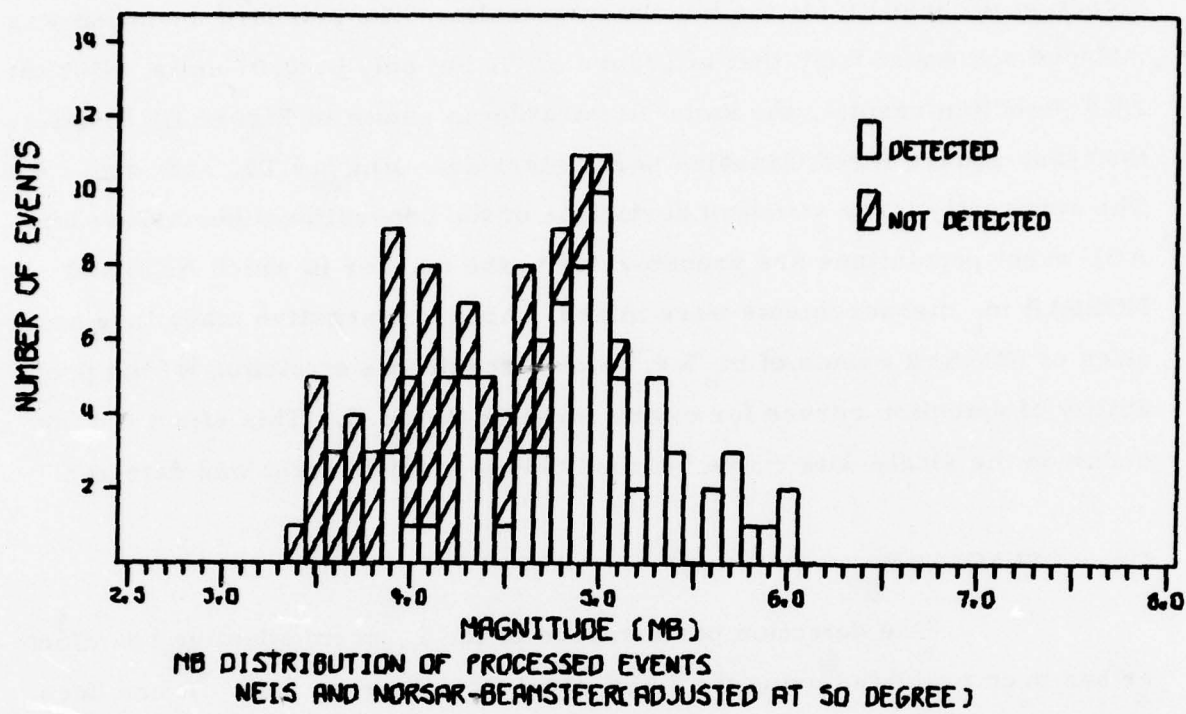


FIGURE III-12

KSRS BEAMSTEER DETECTION HISTOGRAM AND PROBABILITY
BY ADJUSTING m_b AT 50° DELTA

detection probability for the beamsteer results. The standard deviation was reduced somewhat from that of Figure III-9, but only by 0.07 units. For the ABF detection results, the same illustration is shown in Figure III-13 where the least-square fitted Gaussian parameters are $\mu m_b = 4.05$, and $\sigma m_b = 0.47$. The apparently large standard deviations of the conventional beamsteer and ABF event populations are probably due to the manner in which NEIS and NORSAR m_b measurements were mixed. Apparent negative magnitude anomalies of NORSAR events of $m_b \leq 4.5$ would result in a stretching of the probability of detection curves for events smaller than 4.5. This effect did not occur on the single-site curve because only one small event was detected.

C. SUMMARY

The detection performance of the L_1 norm adaptive beamformer has been evaluated using the KSRS short-period array data. It has been demonstrated that the ABF is able to suppress the coda, the scattered energy after the initial arrival of a P wave, much better than the conventional beamsteer. In the 0.5-1.5 Hz passband, the signal-to-noise ratio gain relative to the beamsteer in general is above 10 dB. Also, one of the important achievements of the ABF is that it is able to suppress scattered wavetrains while enhancing the secondary P wave phases such as PP, PcP, and pP.

Bodywave magnitude m_b was also measured on the basis of peak-to-peak amplitude with correction for source epicentral distance and depth. On the average, the single site KSRS m_b yielded 0.35 m_b units greater than the NEIS and NORSAR m_b . The beamsteer processor and the ABF both yielded 0.1 m_b units less than NEIS and NORSAR.

On the detection probability measurement evaluation, a total of 129 events recorded at the KSRS were used for a detection performance study. Measurements of the detection capability were accomplished for a single-site, the conventional beamsteer, and the ABF. Table III-3 summarizes

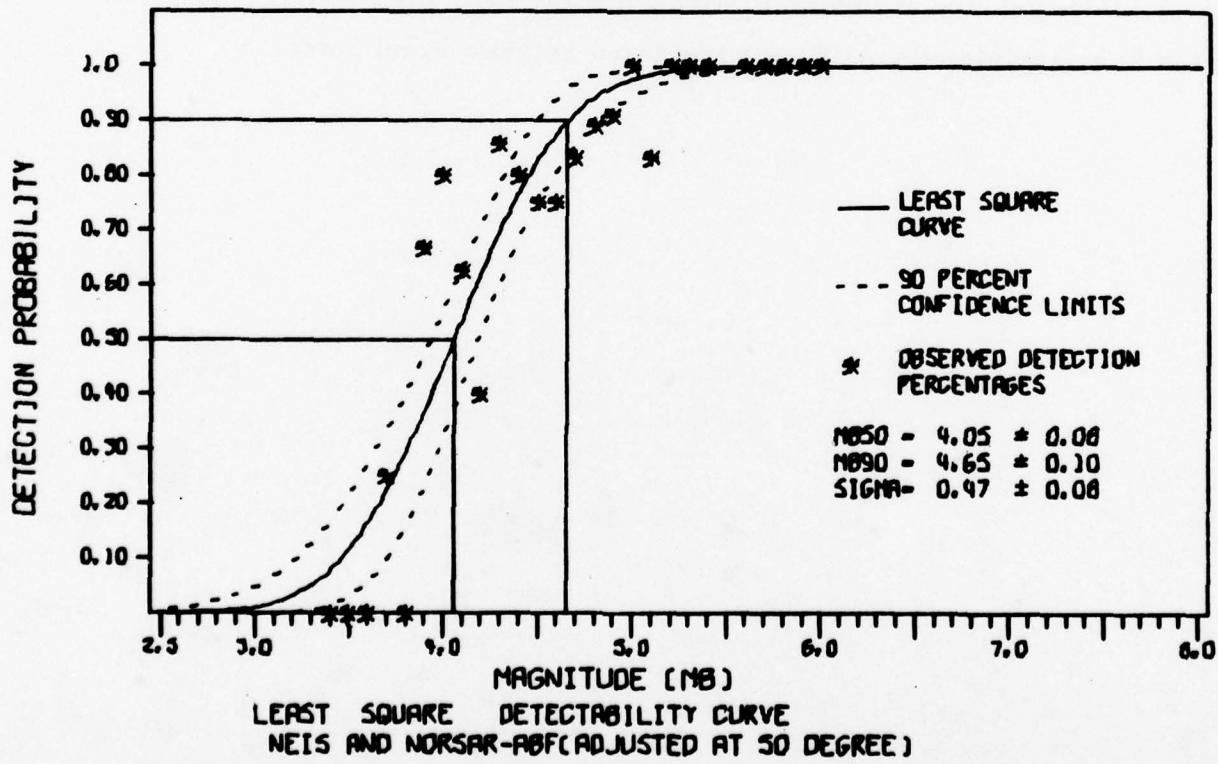
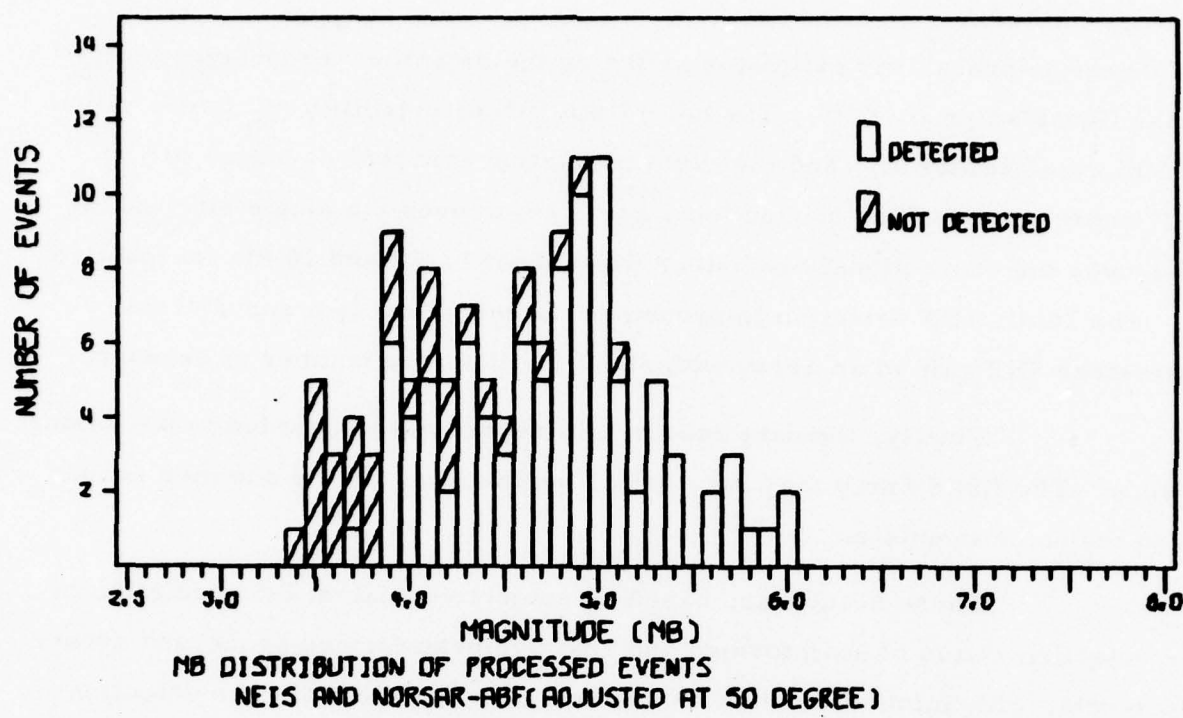


FIGURE III-13

KSRS ABF DETECTION HISTOGRAM AND PROBABILITY
BY ADJUSTING m_b at 50° DELTA

the detection probability estimates by fitting the detection percentages of m_b to the Gaussian probability. The table lists 50% detectability m_b (mean value, μ) 90% detectability m_b , and the event population standard deviation (σm_b). SNR improvement of the conventional array beam over the single site and the ABF over the conventional beamsteer were about 12 dB and 10 dB, respectively. The 10 dB ABF detection improvement is equivalent to a conventional beamsteer SNR gain of an array with about 10 times the number of sensors.

Finally, the data used in this report were recorded in the winter season. The KSRS array may have better performance in the summer season when the noise is quieter.

These results are based on subjective analyst interpretation of the detection status of beamformed and adaptive beamformed processed events. More data, with automatic detection criteria used to determine the detection status of events, are needed to more accurately estimate the detection gains possible by applying the ABF as a front-end seismic event detector.

TABLE III-3
SUMMARY OF DETECTION PROBABILITIES AND IMPROVEMENTS
FOR ABF, BEAMSTEER, AND SINGLE SITE

	50% Detectability (μm_b)	90% Detectability (m_b)	Standard Deviation (σm_b)	Comments
Site 1	5.23	5.67	0.34	Bulletin
Beamsteer	4.62	5.37	0.58	m_b
ABF	4.14	4.84	0.54	
Beamsteer Improvement Over Single Site	0.61 (12.2 dB)	0.30 (0.60 dB)	----	
ABF Improvement Over Beamsteer	0.48 (9.6 dB)	0.53 (6.0 dB)	----	
Site 1	5.18	5.56	0.29	Bulletin
Beamsteer	4.53	5.19	0.51	m_b are adjusted to the locations
ABF	4.05	4.65	0.47	50° from KSRS
Beamsteer Improvement Over Single Site	0.65 (13.0 dB)	0.37 (7.4 dB)	----	
ABF Improvement Over Beamsteer	0.48 (9.6 dB)	0.53 (10.6 dB)	----	

SECTION IV

CONCLUSION AND SUGGESTIONS

A. CONCLUSION

The ABF was developed as an array processor for signal detection and extraction. There is no need to inject a pilot signal or noise statistics to train the system. The ABF can be implemented as a front-end detector.

Using the KSRS short-period array data, evaluation for its detection performance has been accomplished in terms of its capability to suppress coda wavetrains or the scattered energy following the initial arrival, to enhance the secondary P wave phases, accuracy of its m_b measurement, and estimates of its detection probability as compared with the conventional beamsteer. A total of 129 events were used. On the average, the ABF yielded the same magnitude difference of 0.1 m_b units as the beamsteer when compared with the bulletin m_b . However, the ABF improved the KSRS detection capability by 0.5 m_b units from the conventional beamsteer as suggested from the statistical estimate of the processed results.

B. SUGGESTIONS FOR FURTHER STUDY

The present ABF algorithm, programmed for and catalogued in the IBM/360 TS44 system, was used in the real-time mode except for off-line processing using recorded field tapes and was limited to one beam (i. e., one azimuth and one velocity). The processed data were stored in a data buffer for a Calcomp plot and for other purposes. The ABF can be improved to speed-up computation. To implement the ABF in a real-time front-end

detection system, additional software work is needed. Examples of this software work are an automatic control of data quality among the channels in an array, power detector decision rules, and multiple beams to cover a certain area.

The L_1 norm ABF has proved very successful for a seismic short-period array. On the basis of short-period and long-period array studies, it is expected that the present ABF would have better performance for the long-period array than for the short-period array. Application of the L_1 norm ABF to long-period seismic arrays for surface wave detection and extraction would enhance the detection and discrimination capability of seismic arrays.

The recent growth of interest in regional seismic signal detection and identification strongly suggests that applications of the ABF in small arrays (5 to 7 channels) for both long-period and short-period data may provide an effective and economical solution to the problem. A feasibility study and investigation of this application would be beneficial.

SECTION V
REFERENCES

- Burg, J. P., A. H. Booker, and M. Holyer, 1967; Adaptive Filtering of Seismic Array Data, Advanced Array Research, Report No. 1, Texas Instruments Incorporated, Science Services Division, Dallas, TX and a number of technical reports by Booker and his co-workers.
- Claerbout, J. F., 1976; Fundamentals of Geophysical Data Processing, McGraw-Hill, New York, NY.
- Frost, O. L. III, 1972; An algorithm for linearly constrained adaptive array processing, Proceedings of the IEEE, vol. 60, No. 8, p. 926-935.
- Gangi, A. F., and B. S. Byun, 1976; The corrective gradient projection method and related algorithms applied to seismic array processing, Geophysics, vol. 41, No. 5, p. 970-984.
- Kobayashi, H., 1970; Iterative synthesis methods for a seismic array processor, IEEE Transactions on Geoscience Electronics, vol. GE-8, No. 3, p. 169-178.
- Levin, M. J., 1964; Maximum-likelihood array processing, in M. I. T. Lincoln Laboratory Semi-Annual Technical Summary Report, DDC45 5743, 31 December.
- Owsley, N., 1973; A recent trend in adaptive spatial processing for sensor arrays: Constrained adaptation, in signal processing, edited by J. W. R. Griffiths, P. L. Stocklin, and C. Van Schooneveld, Academic Press, New York, NY.

Ringdal, F., and R. L. Whitelaw, 1973; Continued Evaluation of the Norwegian Short-Period Array, Special Report No. 9, Texas Instruments Incorporated, Dallas, TX.

Shen, W. W., 1976; Evaluation of Two Automatic Signal Detectors Using the Korean Seismic Research Station Short-Period Array, Technical Report No. 3, Texas Instruments Incorporated, Dallas, TX.

Shen, W. W., 1977; Study of Adaptive Beamforming Algorithms for Low Magnitude Seismic P-Wave Detection, Technical Report No. 5, Texas Instruments Incorporated, Dallas, TX.

Shen, W. W., 1978a; Mixed-Signal Separation and Coda Rejection by Adaptive Beamforming Filter, J. Acoustical Society of America, vol. 63, Supplement No. 1, S48.

Shen, W. W., 1978b; Feasibility Study of Mixed-Signal Separation Techniques, Technical Report No. 19, Texas Instruments Incorporated, Dallas, TX.

Veith, K. F., and G. E. Clawson, 1972; Magnitude From Short-Period P-Wave Coda, Bulletin of Seismological Society of America, p. 435.

APPENDIX A

PROCESSED DATA PLOTS FROM NEIS BULLETIN

This appendix presents the processed data plots for those events taken from the NEIS bulletin dated January 1 to 15, 1977. Time in the figure is depicted as Julian date, hour, minutes, and seconds. In general, the computed P-wave arrival is 70 seconds after the start time. In the present size of figure, it is about 10 seconds for 0.5 inch scale. The line of computer print on the top of each figure also appears in Table III-1 herein. The parameters $\alpha = 0.003$ and $\beta = 0.5$ were used for processing.

770101 7.20.5" 0 4C.NCN 127.3CW 2 76.2 3.7

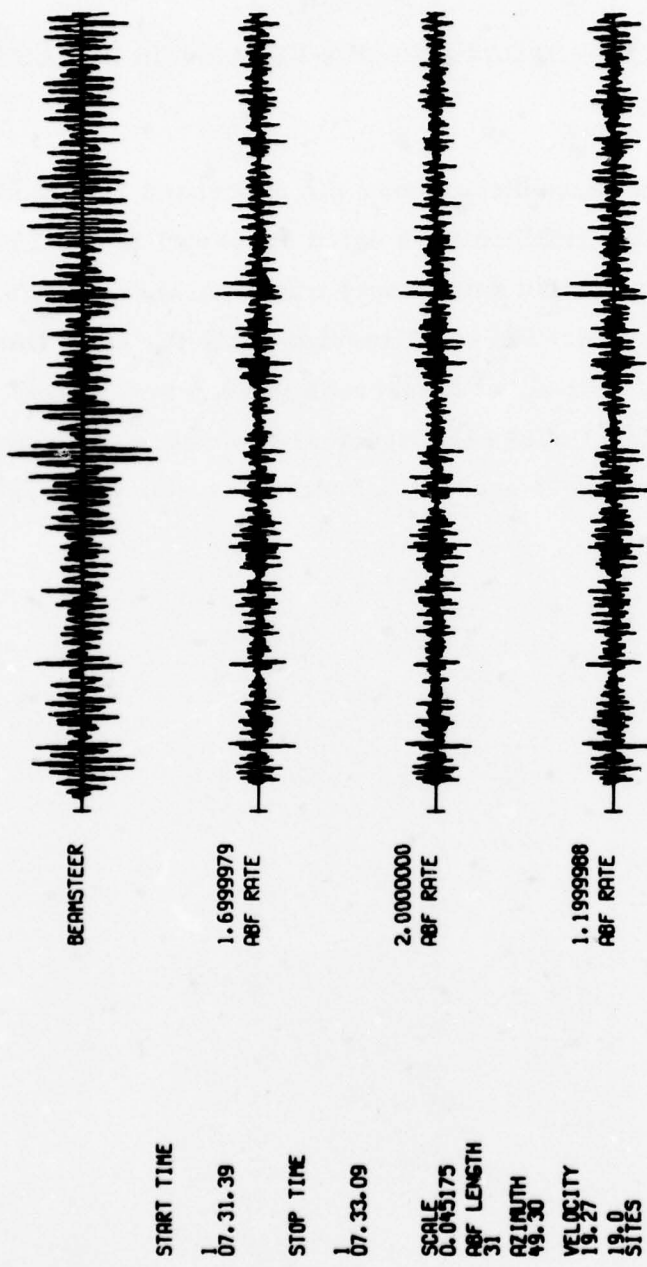
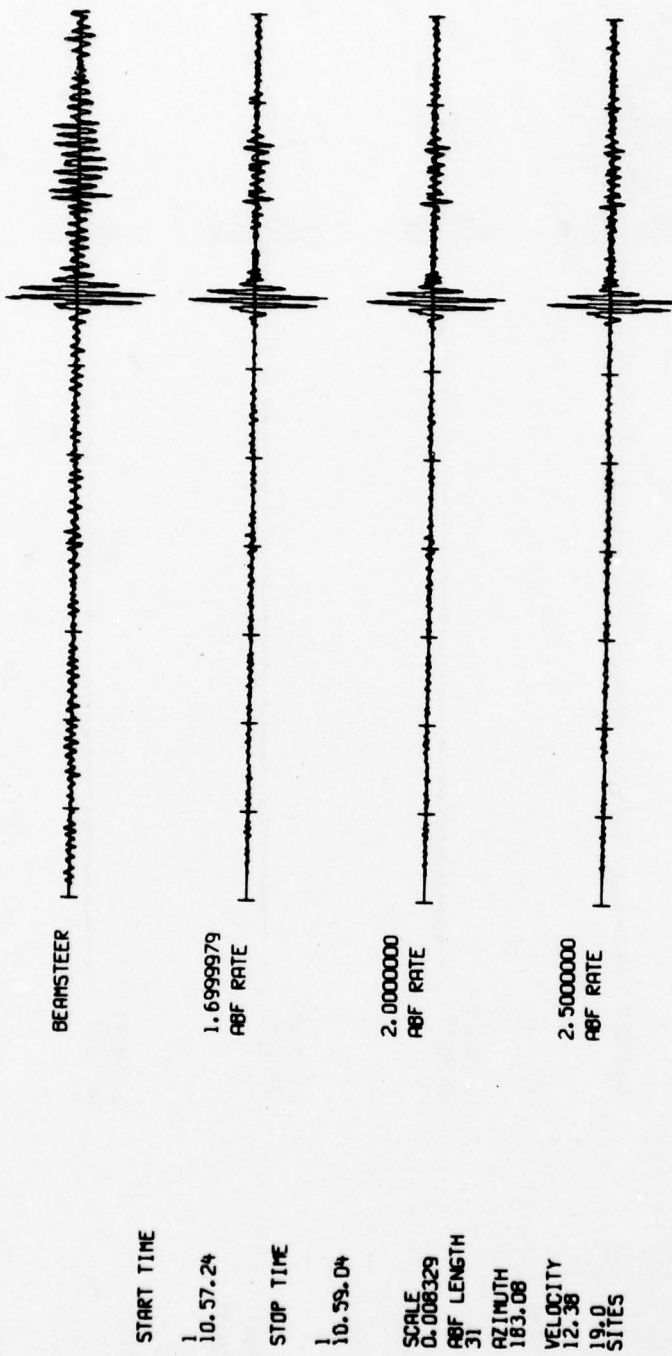


FIGURE A-1
PROCESSED TRACES FOR EVENT A-1

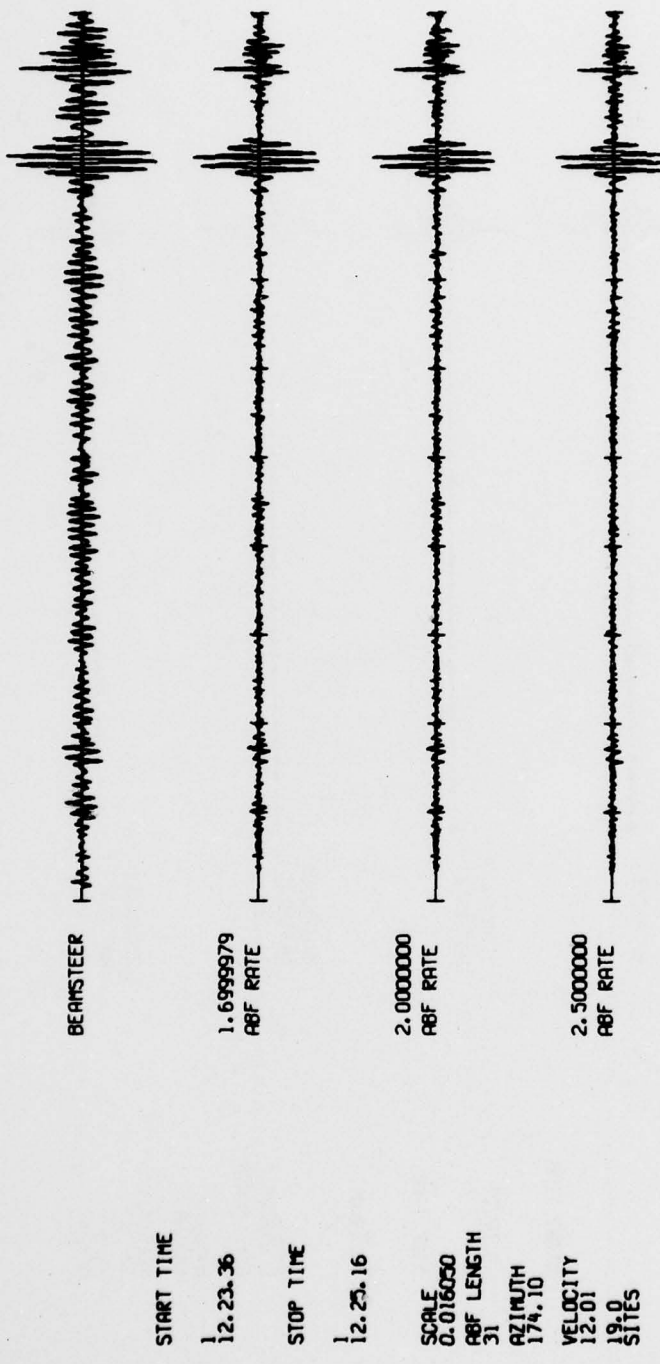
2 770101 10.52.34.1 8.41N 126.49E 53 29.0 5.0 5.2 5.2



A-3

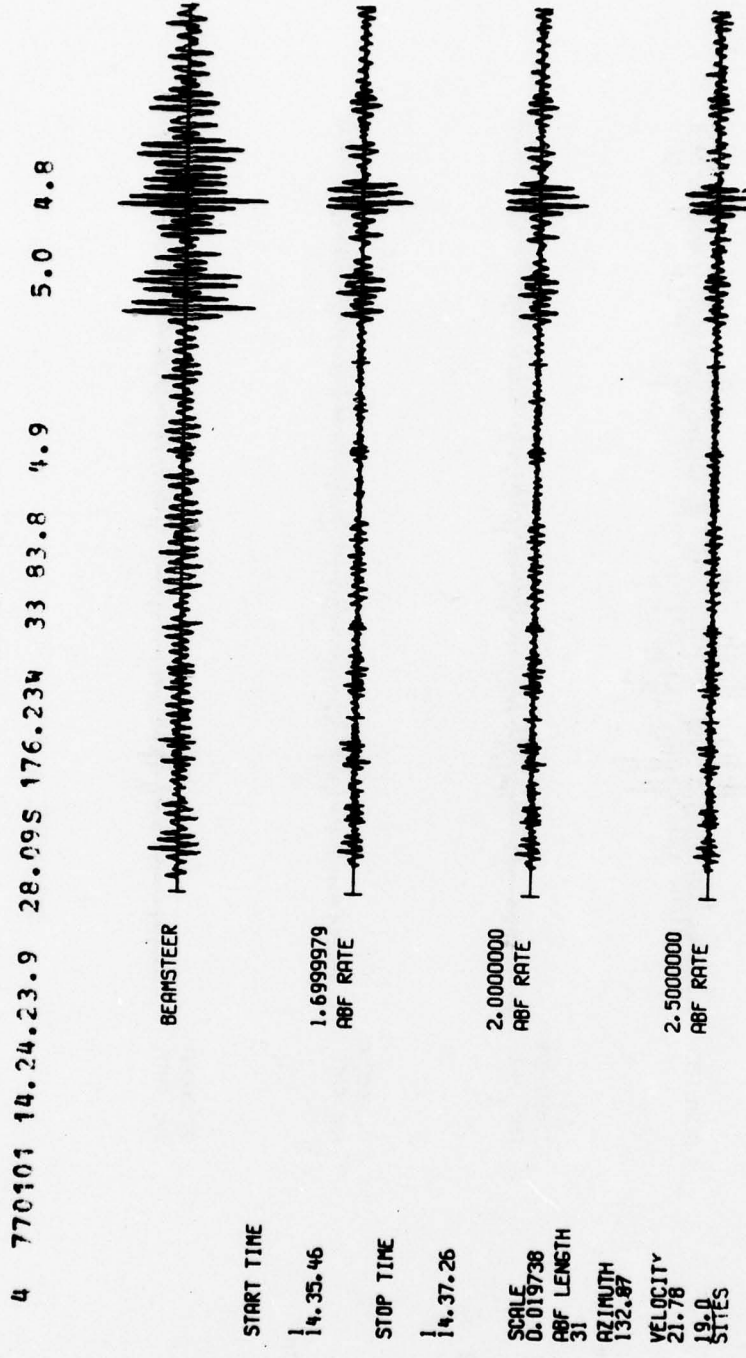
FIGURE A-2
PROCESSED TRACES FOR EVENT A-2

3 770101 12.19.22.2 10.28N 126.23E 89 27.2 5.0 4.8 4.7



A-4

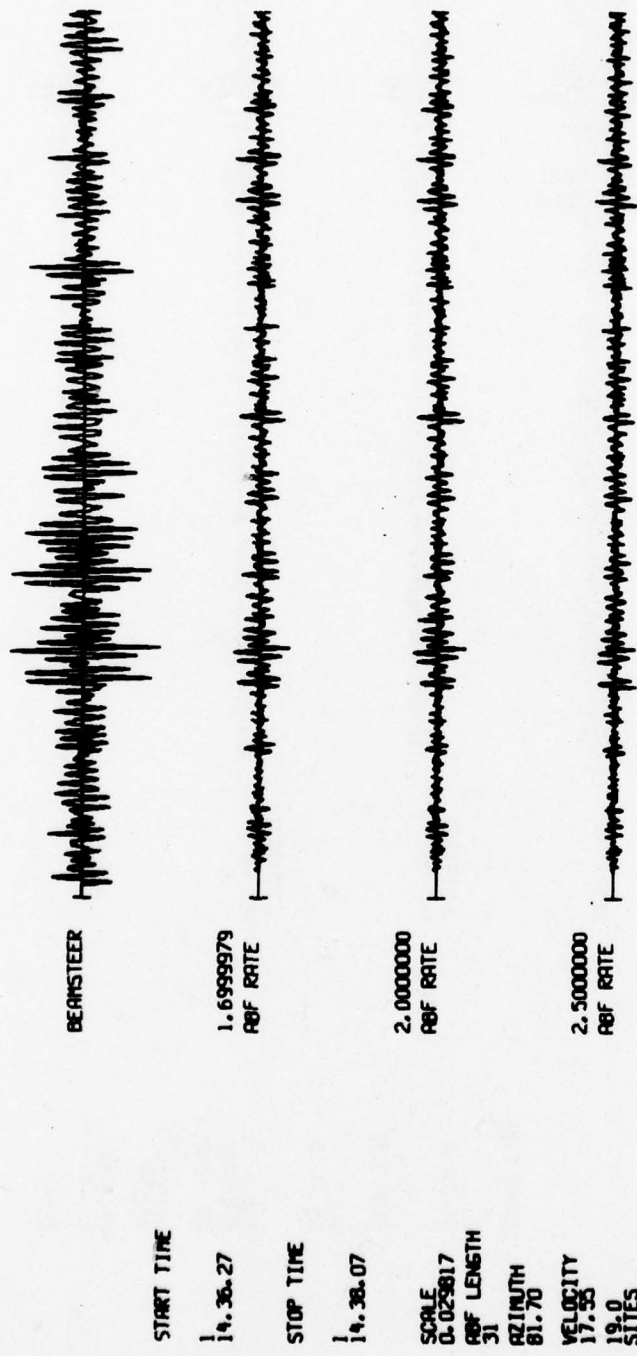
FIGURE A-3
PROCESSED TRACES FOR EVENT A-3



A-5

FIGURE A-4
PROCESSED TRACES FOR EVENT A-4

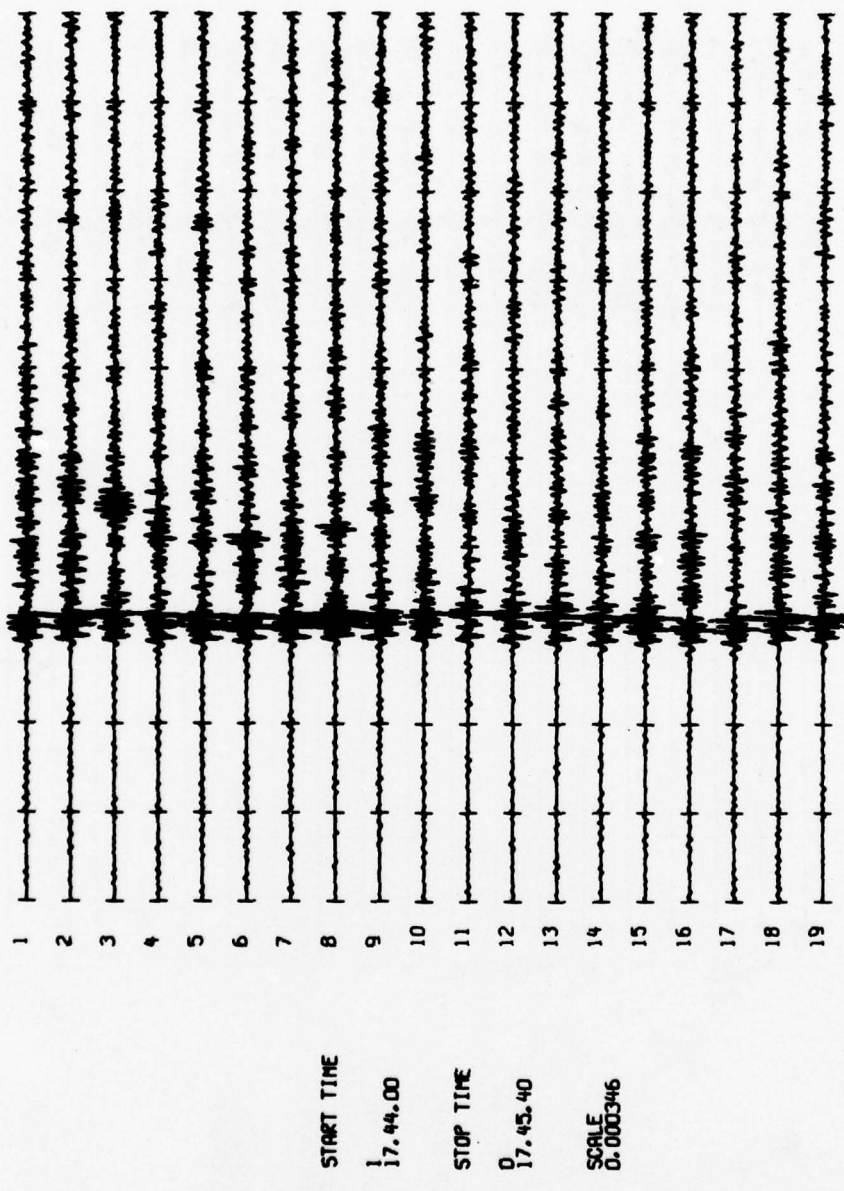
5 770101 14.26.35.3 19.34N 155.12W 9 68.3 3.7



A-6

FIGURE A-5
PROCESSED TRACES FOR EVENT A-5

6 770101 17.35.53.9 7.885 109.01E 113 48.6 5.7 5.0



A-7

FIGURE A-6
PROCESSED TRACES FOR EVENT A-6

7 770101 19. 1.39.6 2.53S 126.58E 33 39.9 6.0 6.2

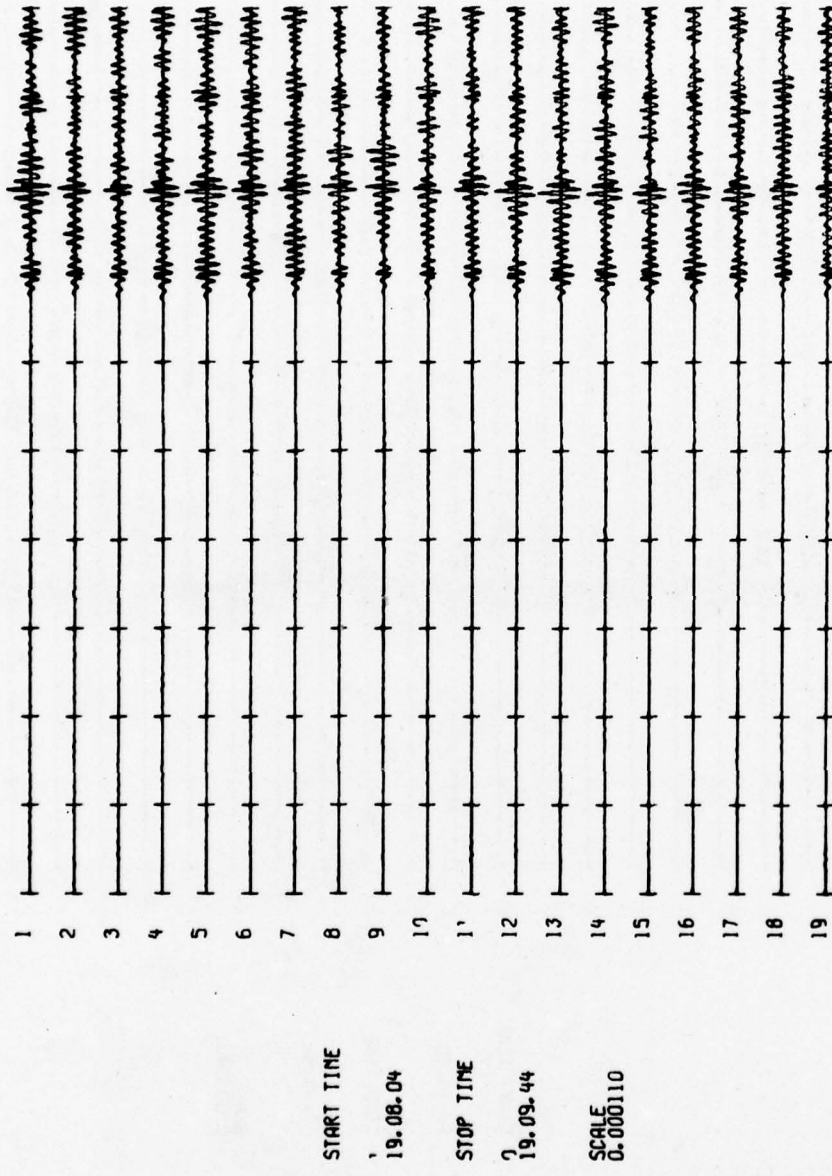
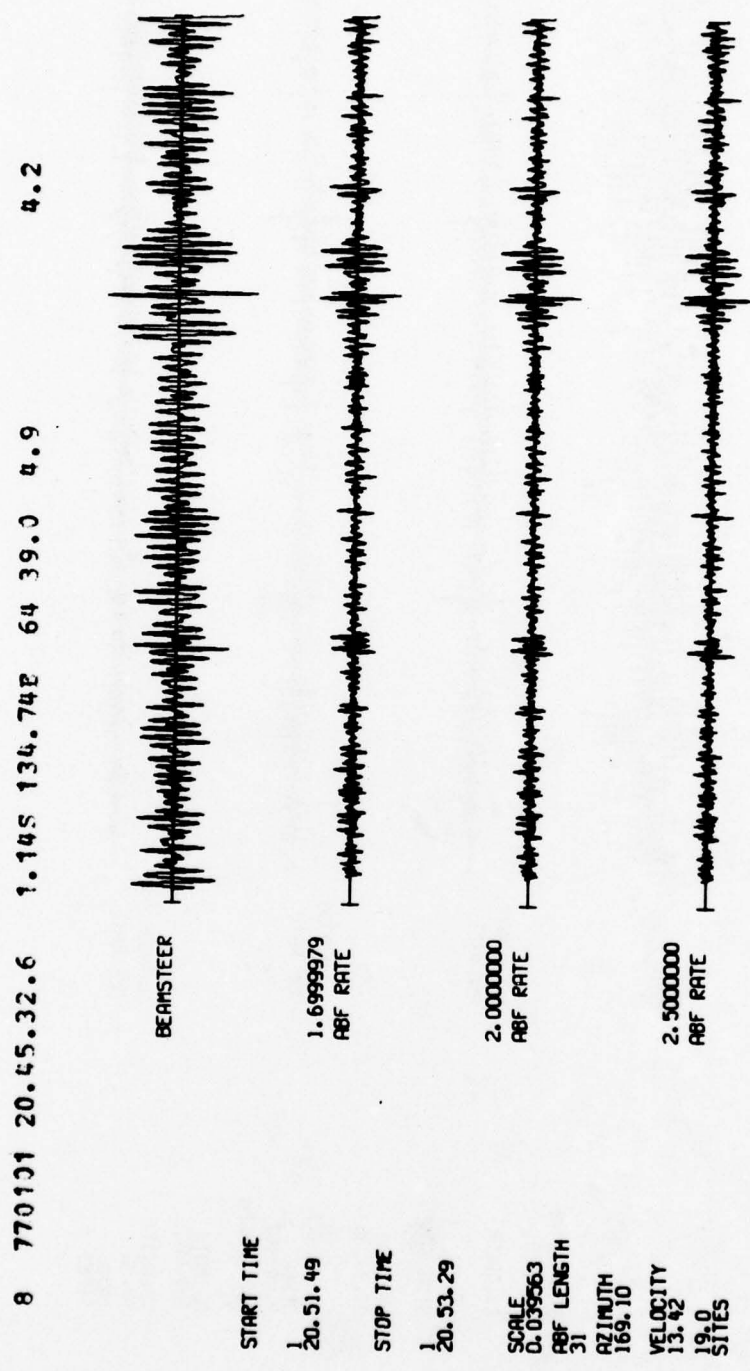
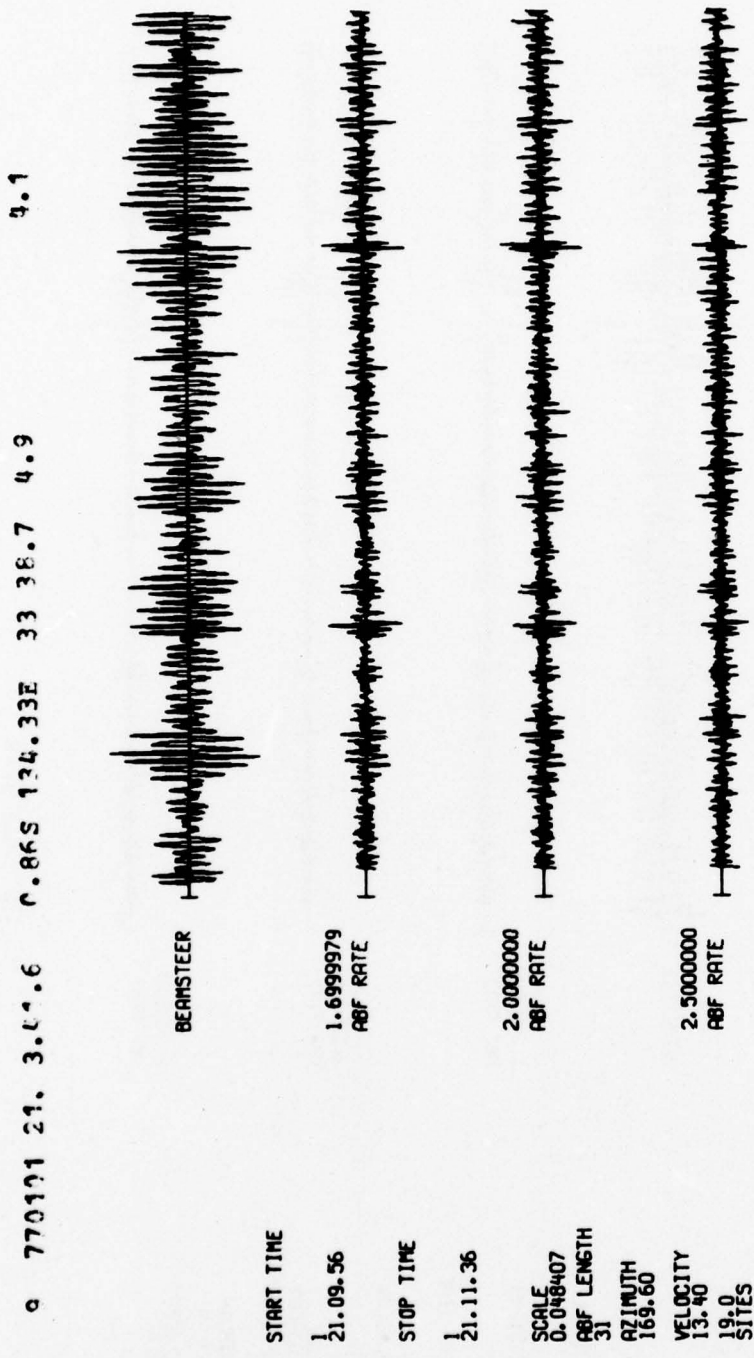


FIGURE A-7
PROCESSED TRACES FOR EVENT A-7



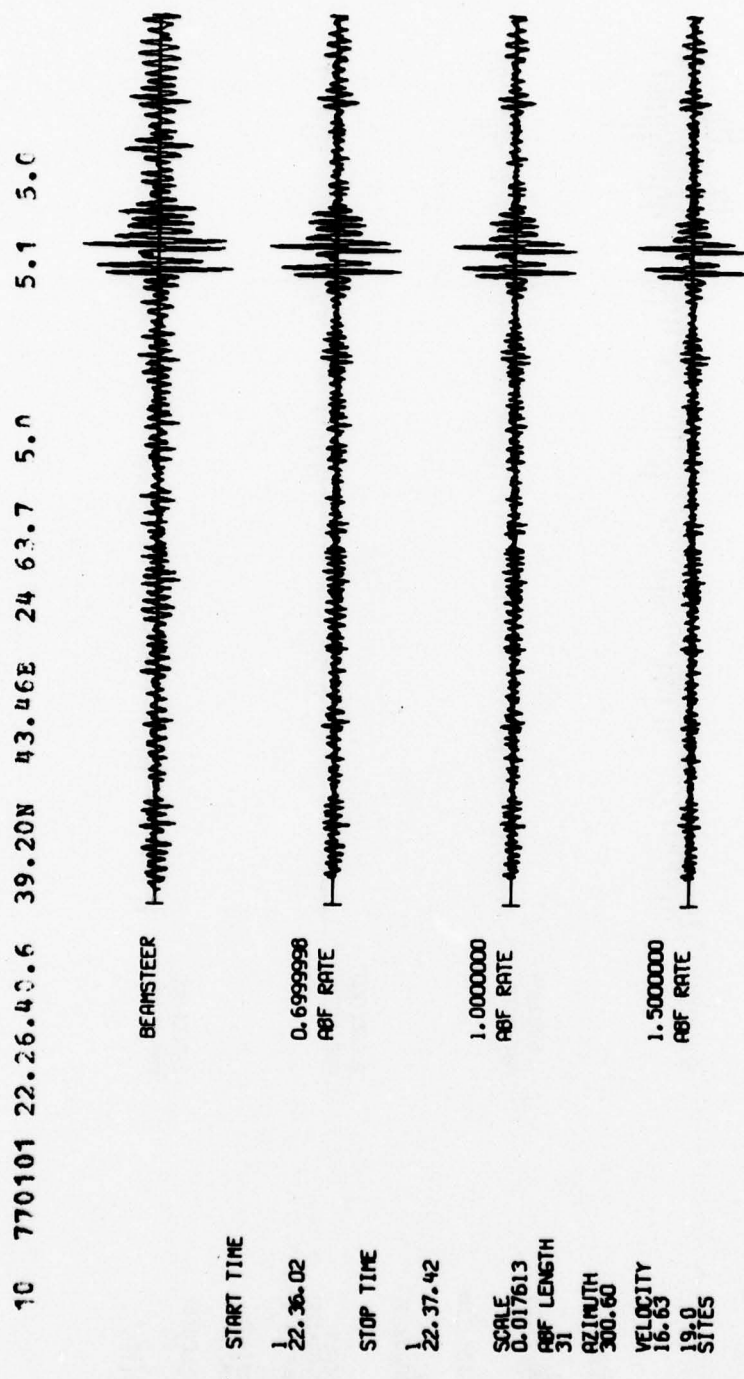
A-9

FIGURE A-8
PROCESSED TRACES FOR EVENT A-8



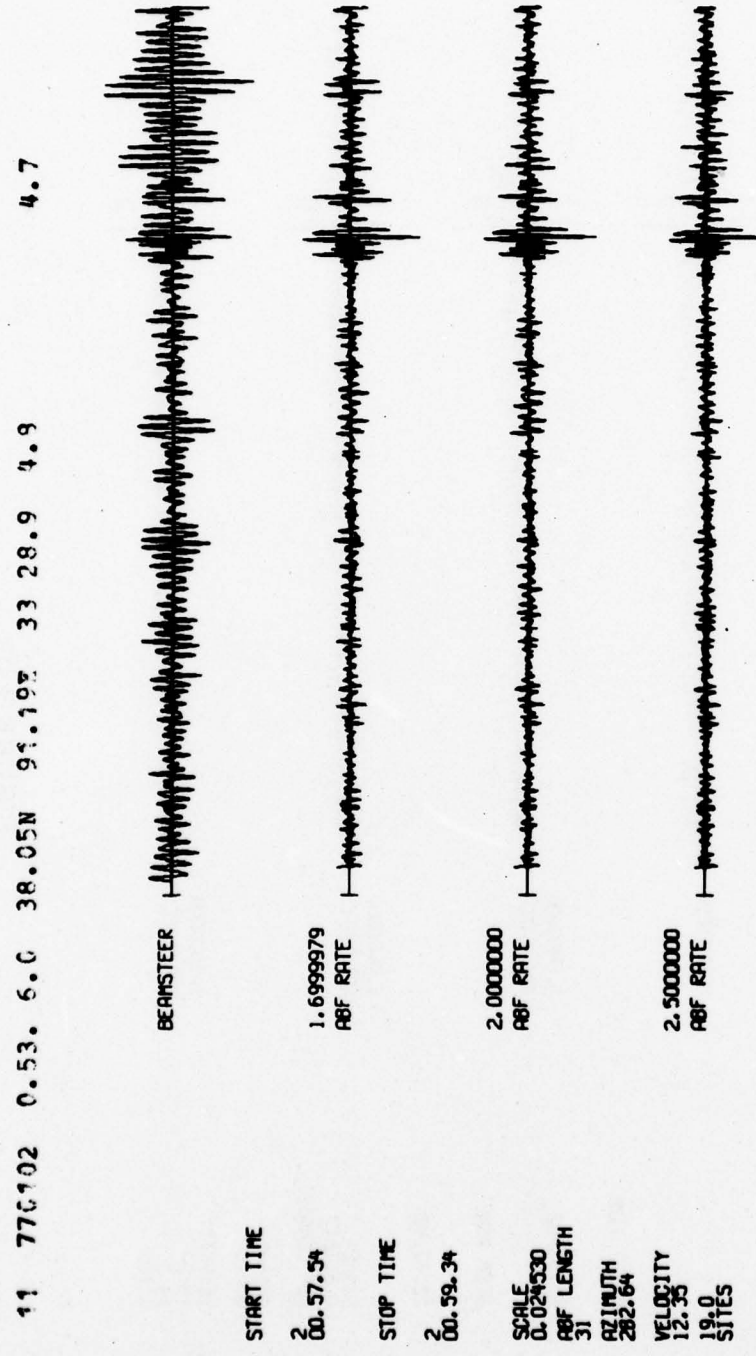
A-10

FIGURE A-9
PROCESSED TRACES FOR EVENT A-9



A-11

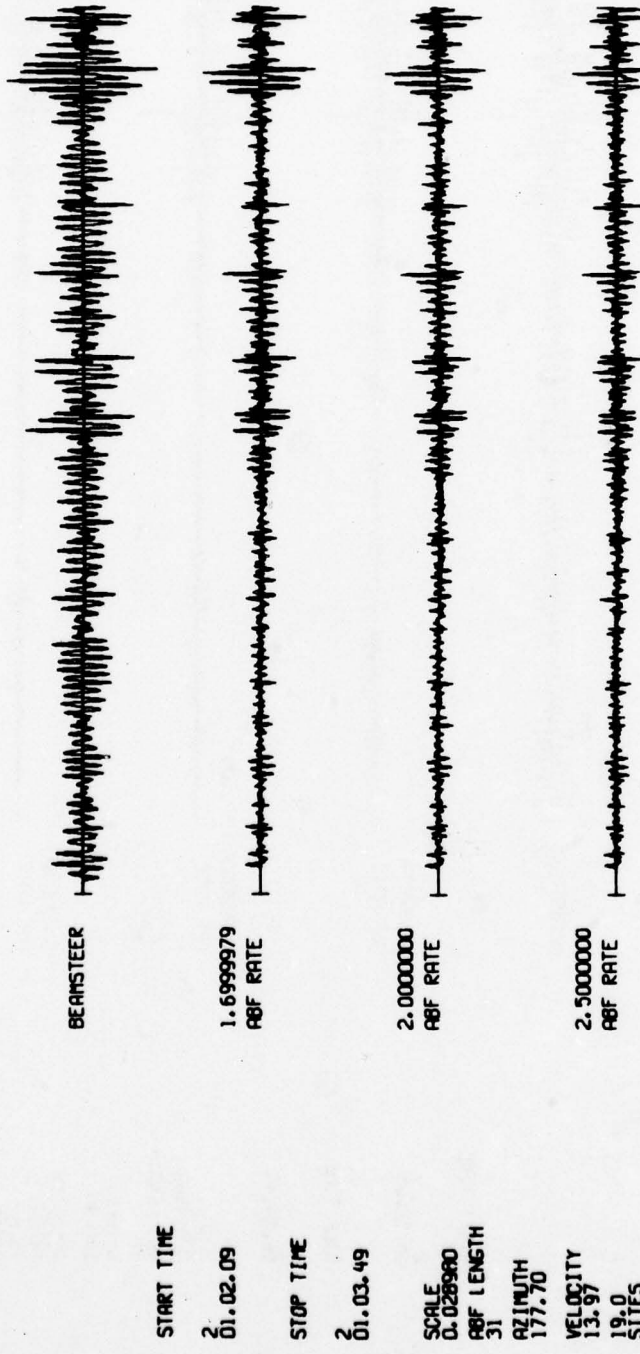
FIGURE A-10
PROCESSED TRACES FOR EVENT A-10



A-12

FIGURE A-11
PROCESSED TRACES FOR EVENT A-11

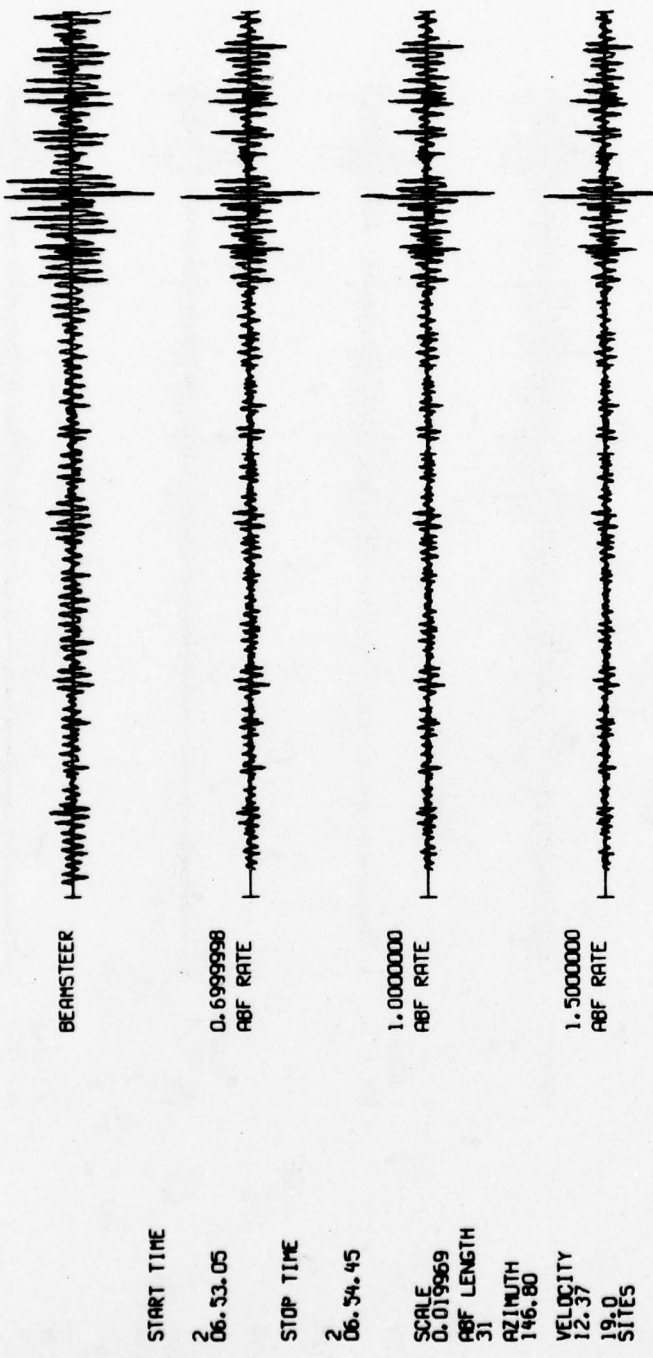
12 770102 0.55. 8.0 6.95S 129.51E 171 40.3 5.0



A-13

FIGURE A-12
PROCESSED TRACES FOR EVENT A-12

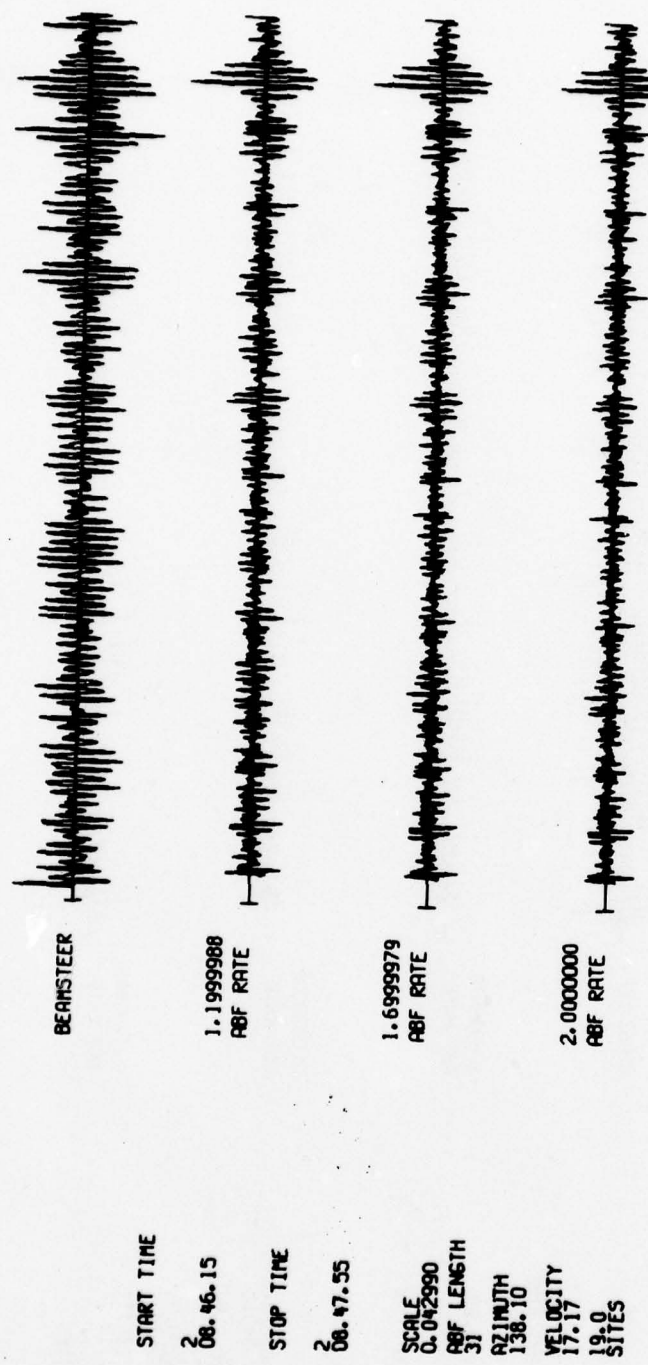
13 770102 6.48.15.0 12.02N 143.62E 33 29.0 4.9 4.9 4.8



A-14

FIGURE A-13
PROCESSED TRACES FOR EVENT A-13

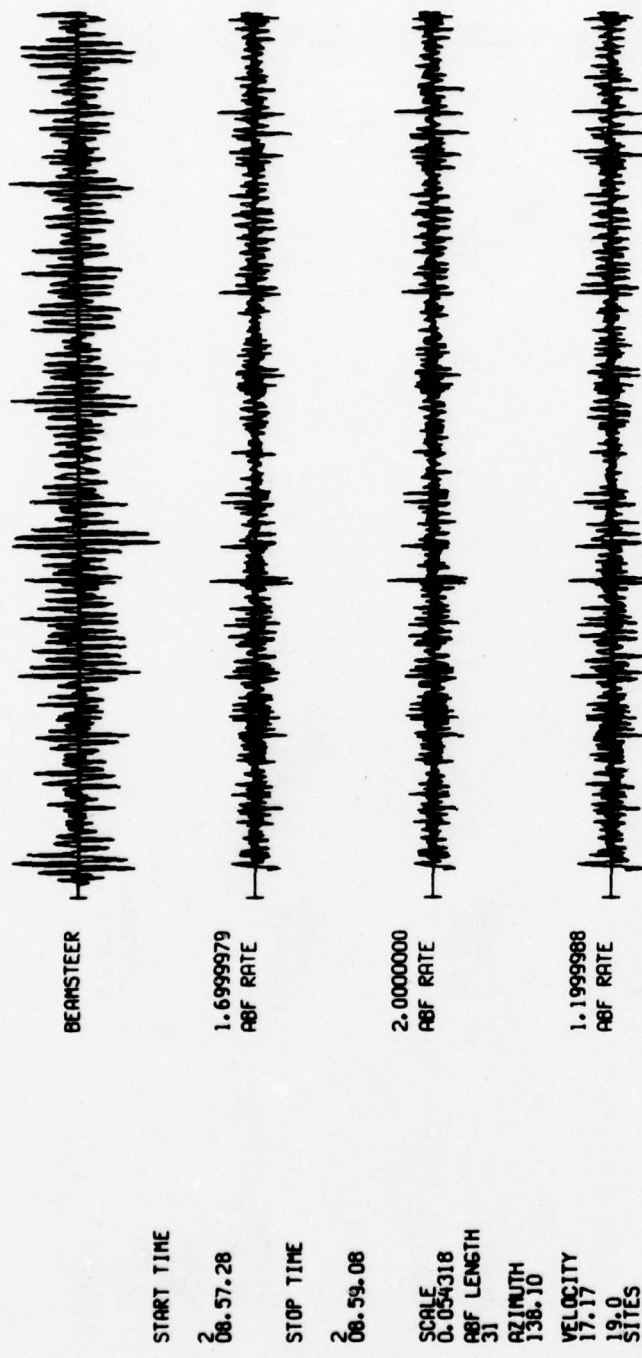
1a 77C102 8.36.35.9 17.51S 167.71E 33 66.4 4.7 4.5



A-15

FIGURE A-14
PROCESSED TRACES FOR EVENT A-14

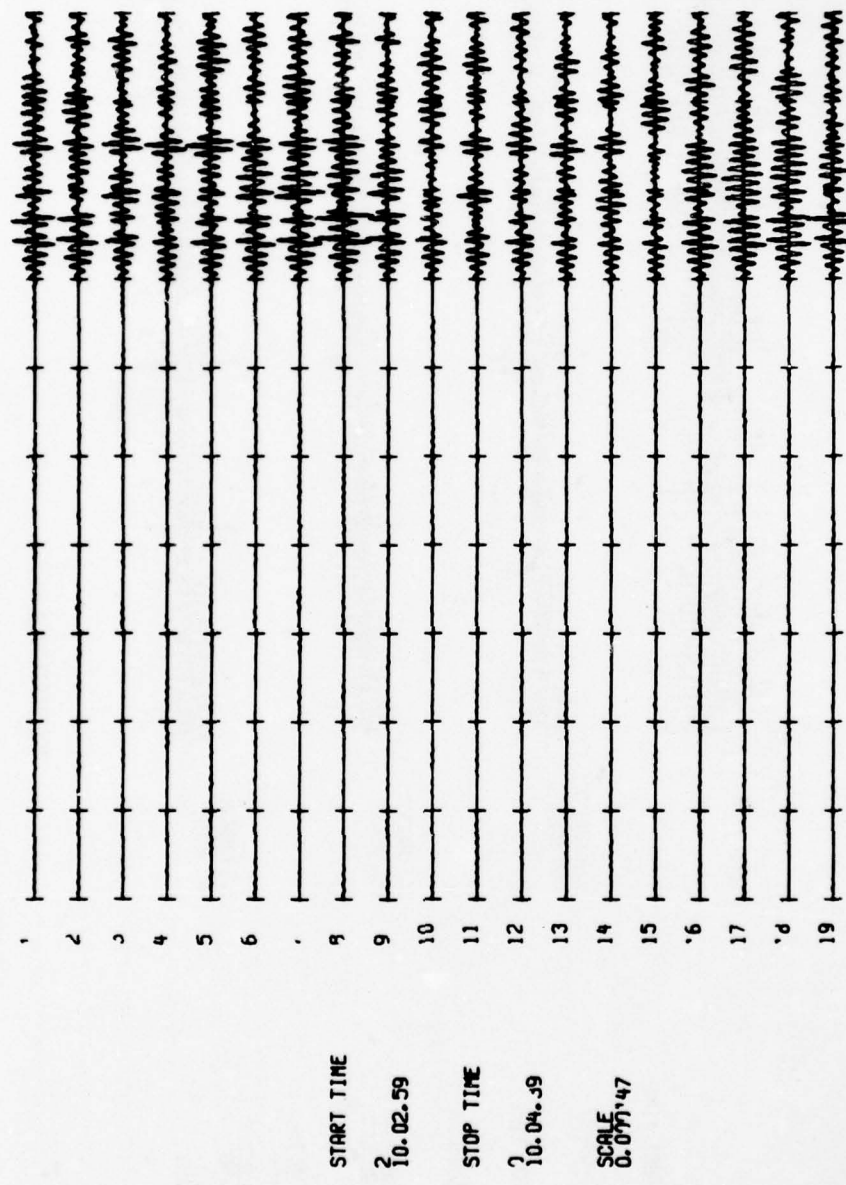
15 770192 8.47.49.3 17.51S 167.71E 33 66.0 4.7



A-16

FIGURE A-15
PROCESSED TRACES FOR EVENT A-15

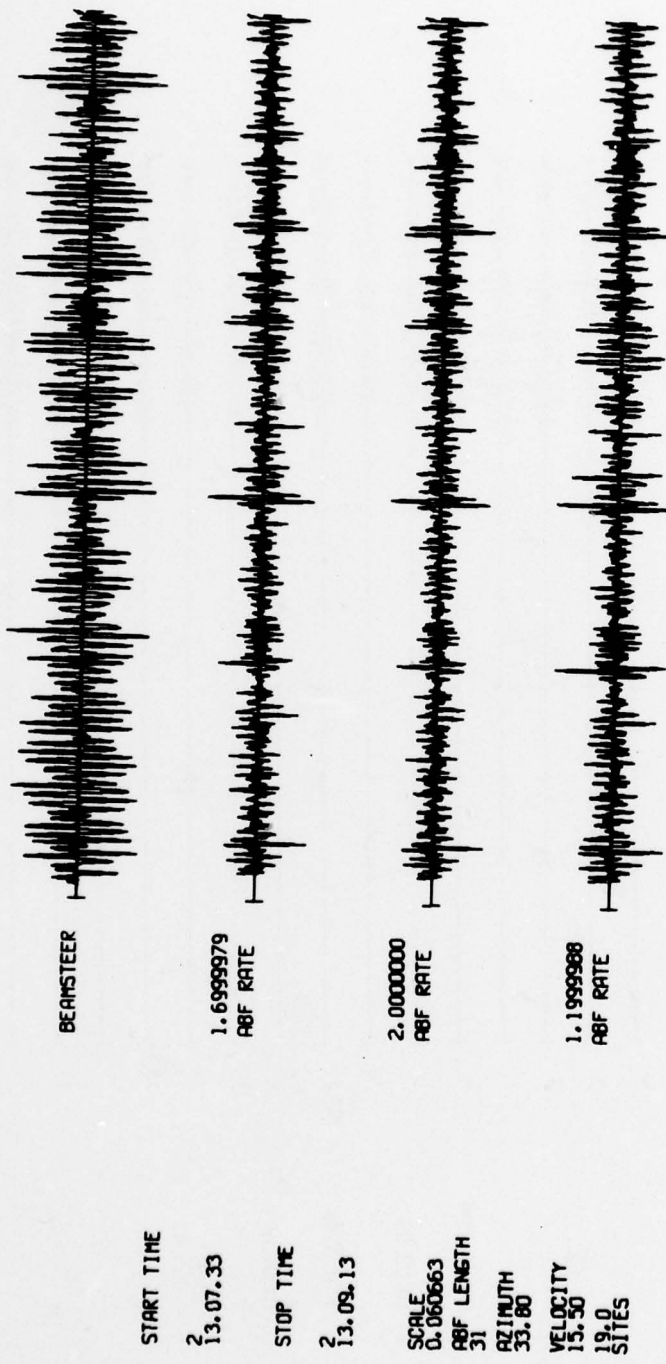
16 770102 9.55.28.n 10.17s 118.99P 19 48.3 5.9 6.5



A-17

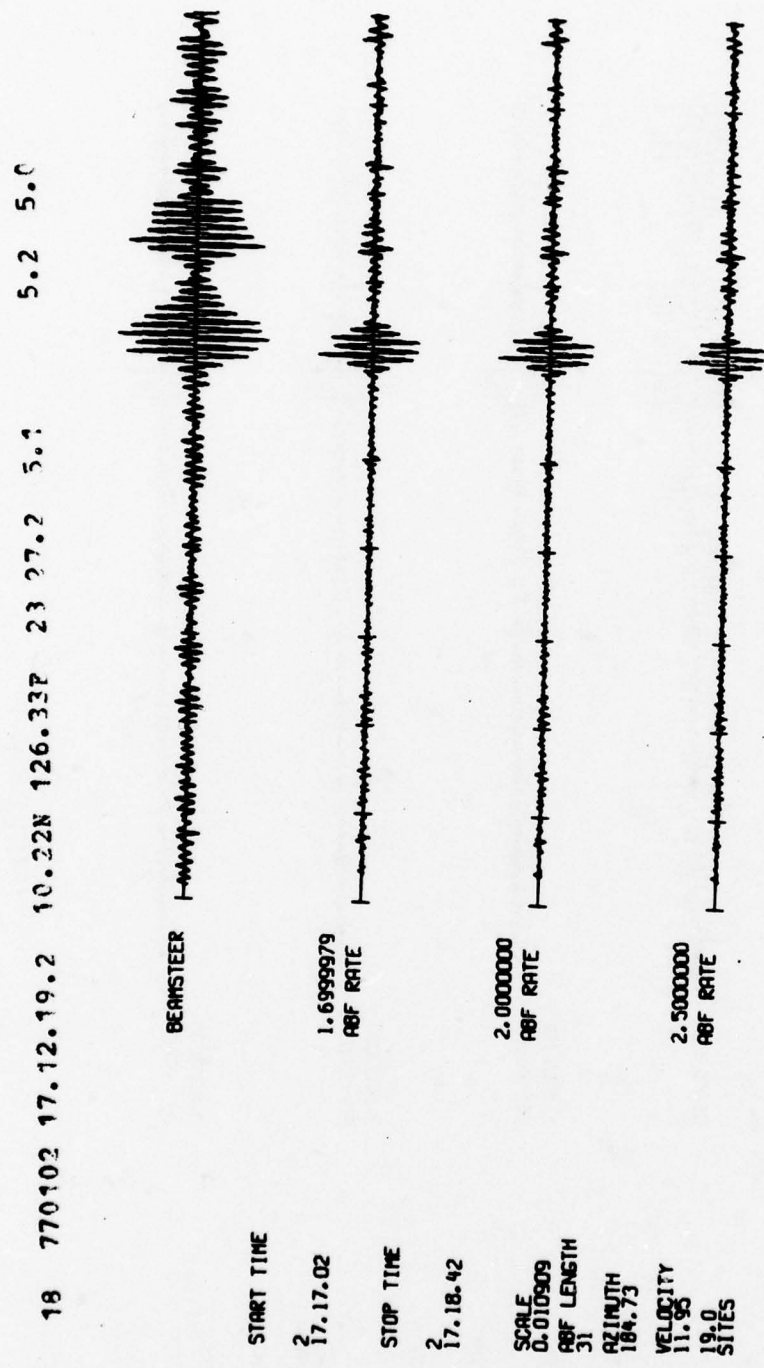
FIGURE A-16
PROCESSED TRACES FOR EVENT A-16

17 770102 12.59.21.4 63.12N 150.12W 113 53.07 3.8



A-18

FIGURE A-17
PROCESSED TRACES FOR EVENT A-17



A-19

FIGURE A-18
PROCESSED TRACES FOR EVENT A-18

19 770102 19.37.25.2 39.24N 43.57E 34 63.6 4.9 4.7 4.6

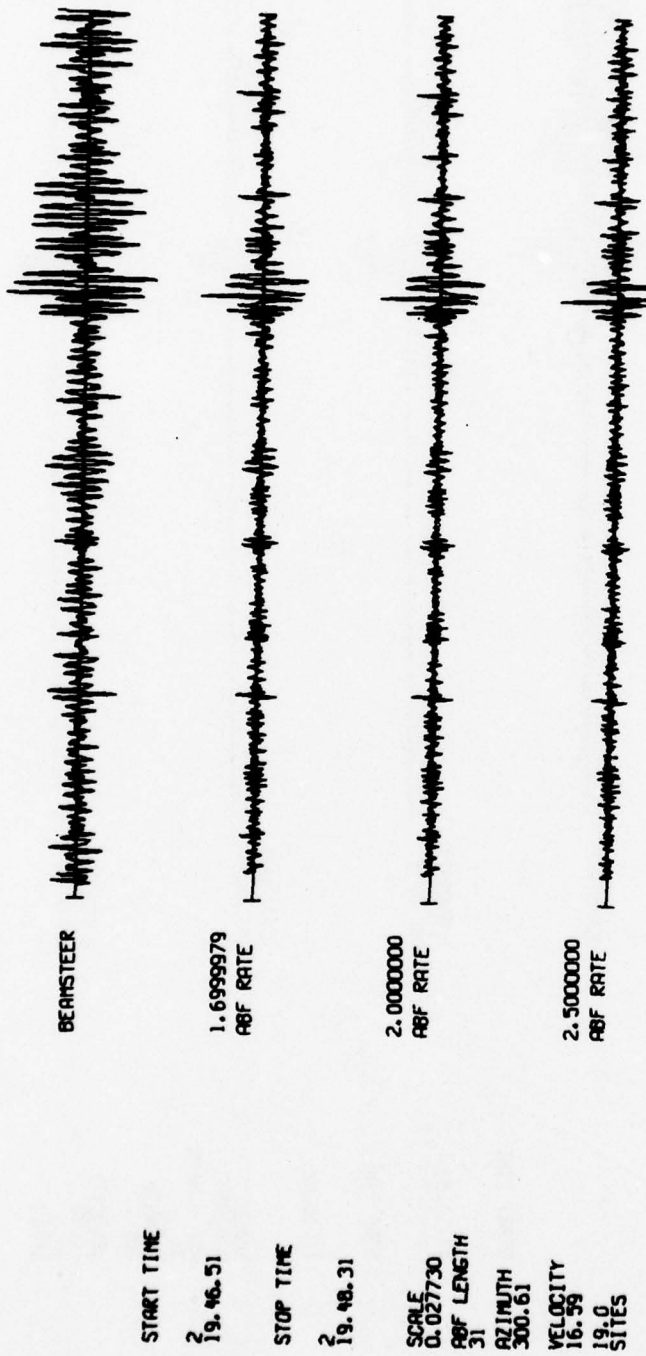
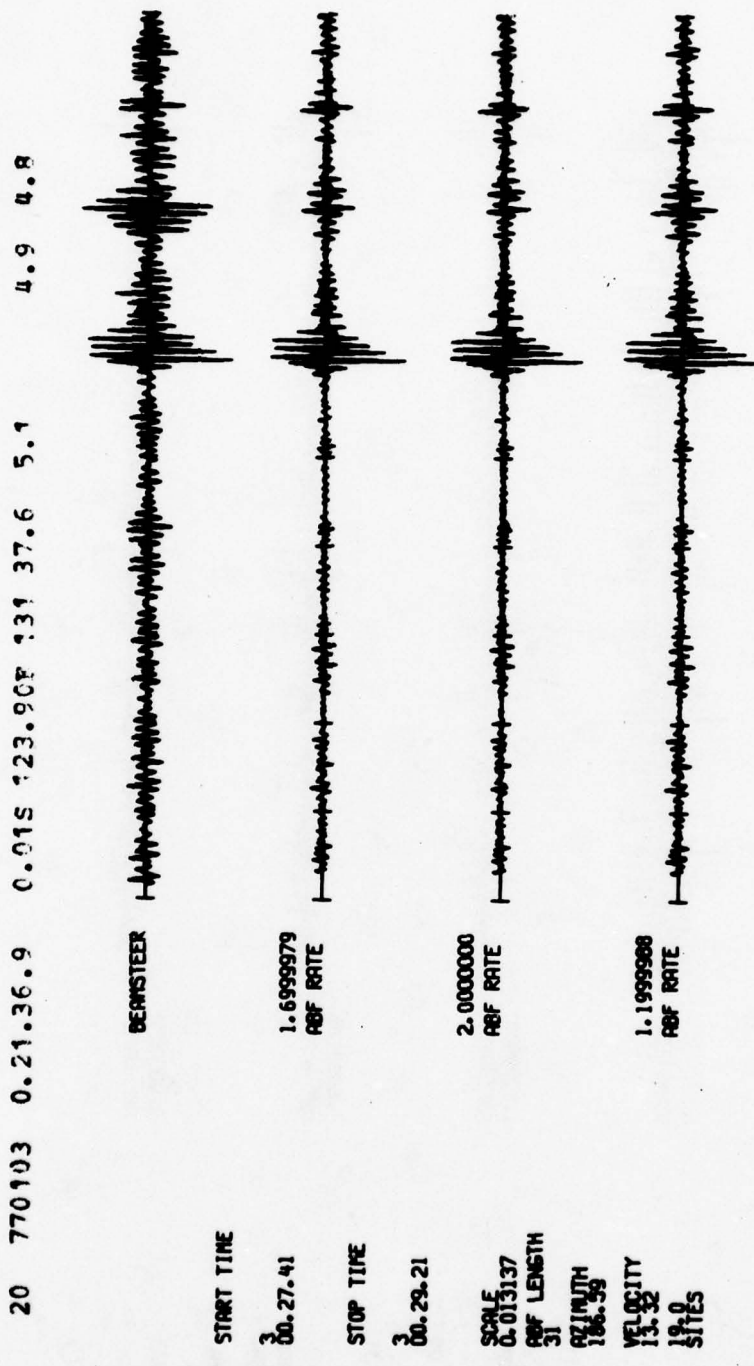


FIGURE A-19
PROCESSED TRACES FOR EVENT A-19



A-21

FIGURE A-20
PROCESSED TRACES FOR EVENT A-20

21 770103 C.44. 7.8 29.21N 23.11E 23 77.6 4.5

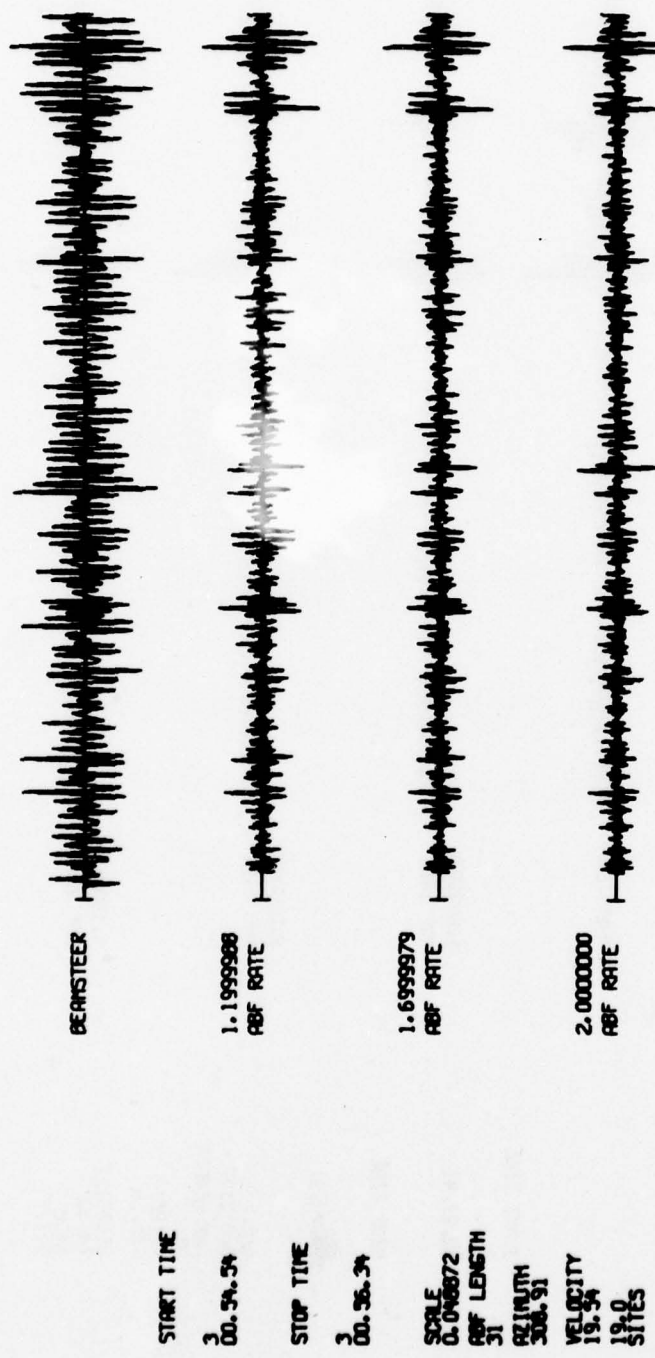


FIGURE A-21
PROCESSED TRACES FOR EVENT A-21

22 770103 1.34.34.2 51.43N 179.08W 33 39.0 4.0 4.8 4.6

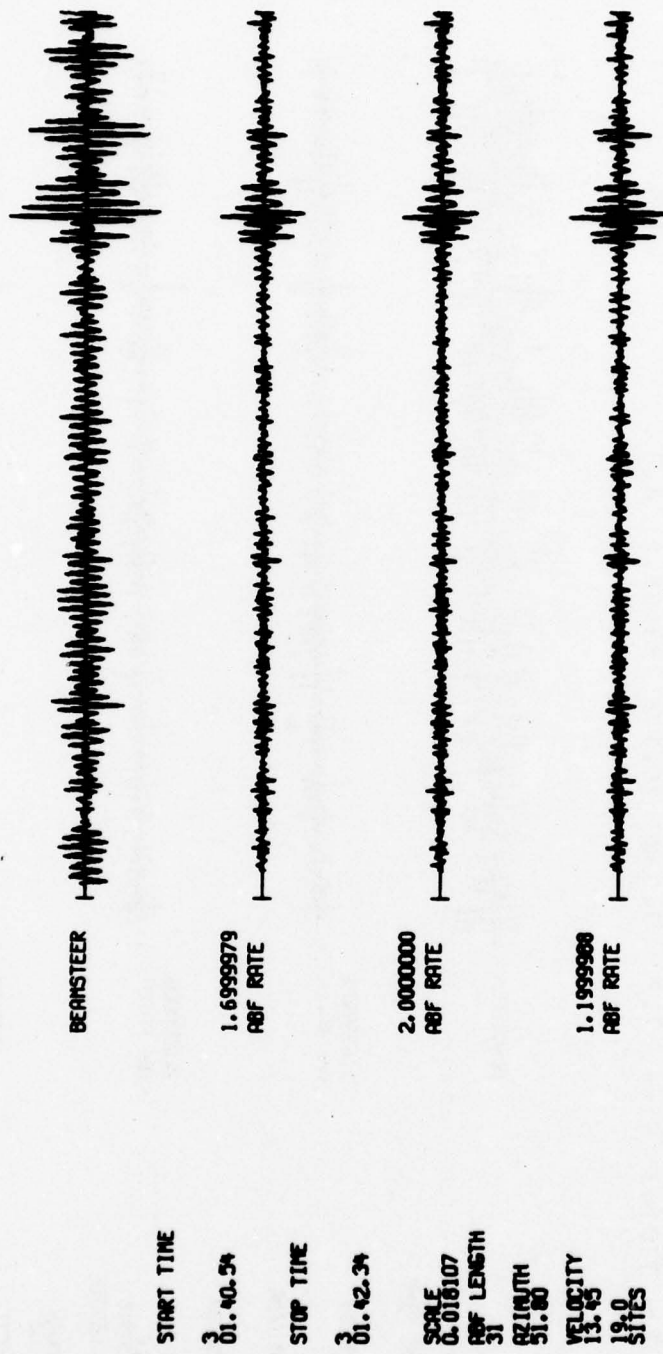


FIGURE A-22
PROCESSED TRACES FOR EVENT A-22

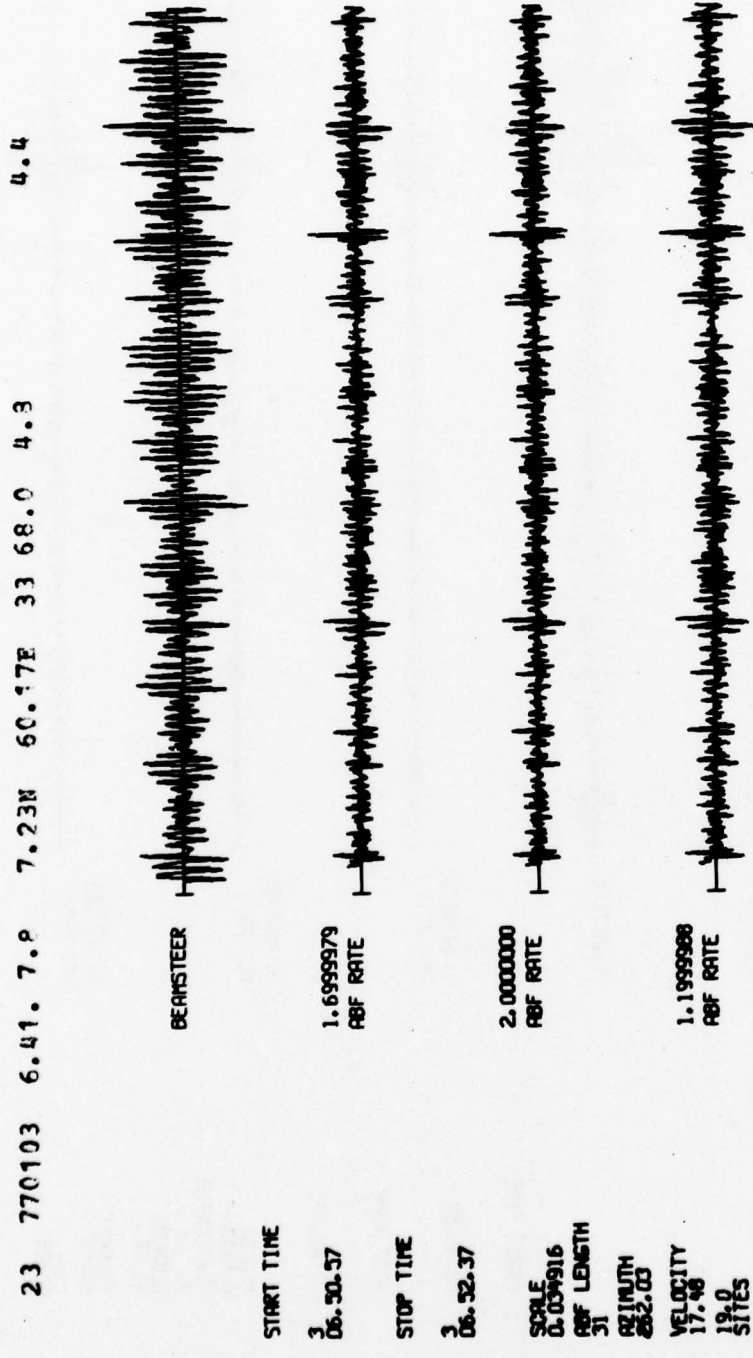
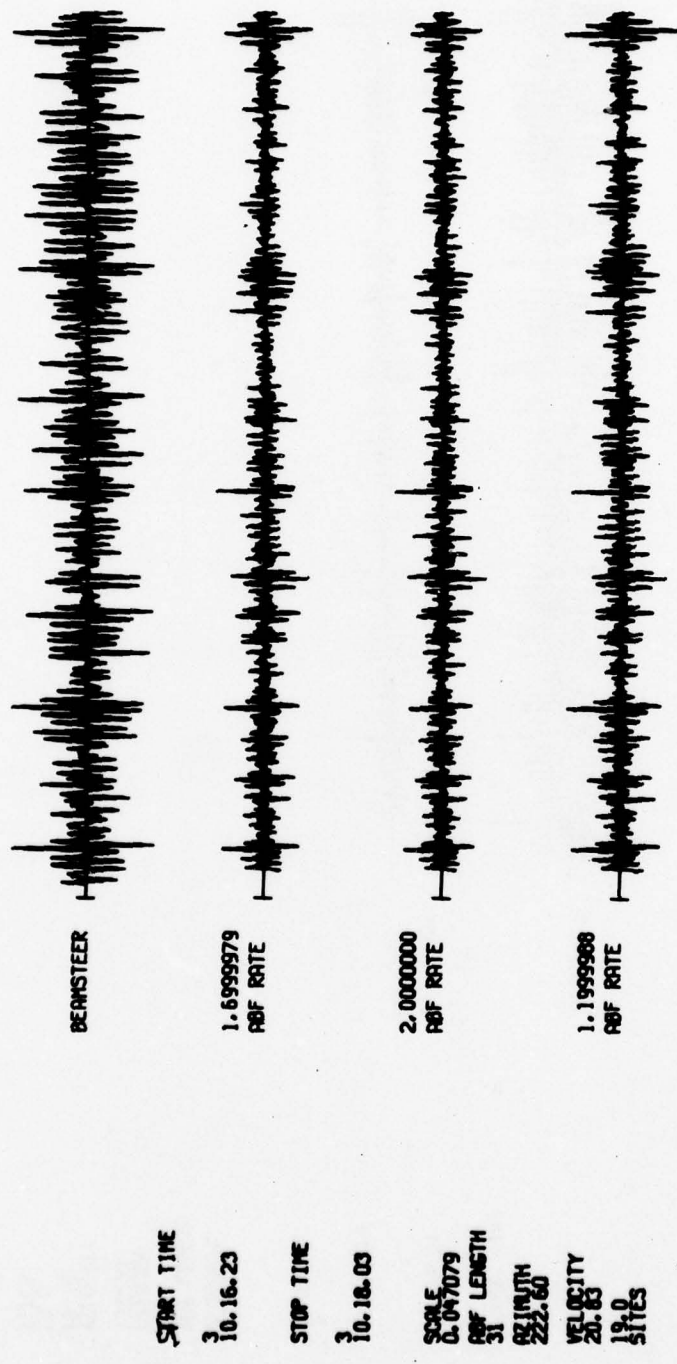


FIGURE A-23

PROCESSED TRACES FOR EVENT A-23

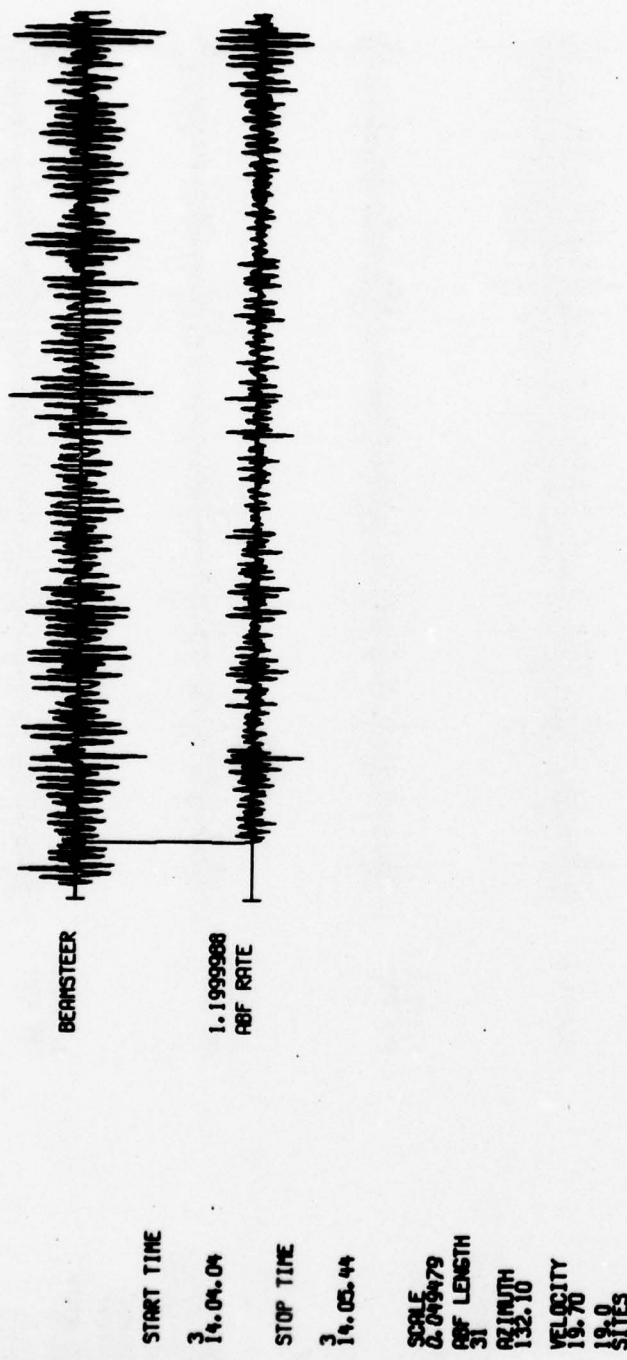
24 770103 10. 5.15.3 29.253 77.80P 33 94.4 5.1



A-25

FIGURE A-24
PROCESSED TRACES FOR EVENT A-24

25 770103 13.53.14.2 23.58S 179.96W 540 78.2 5.1



A-26

FIGURE A-25
PROCESSED TRACES FOR EVENT A-25

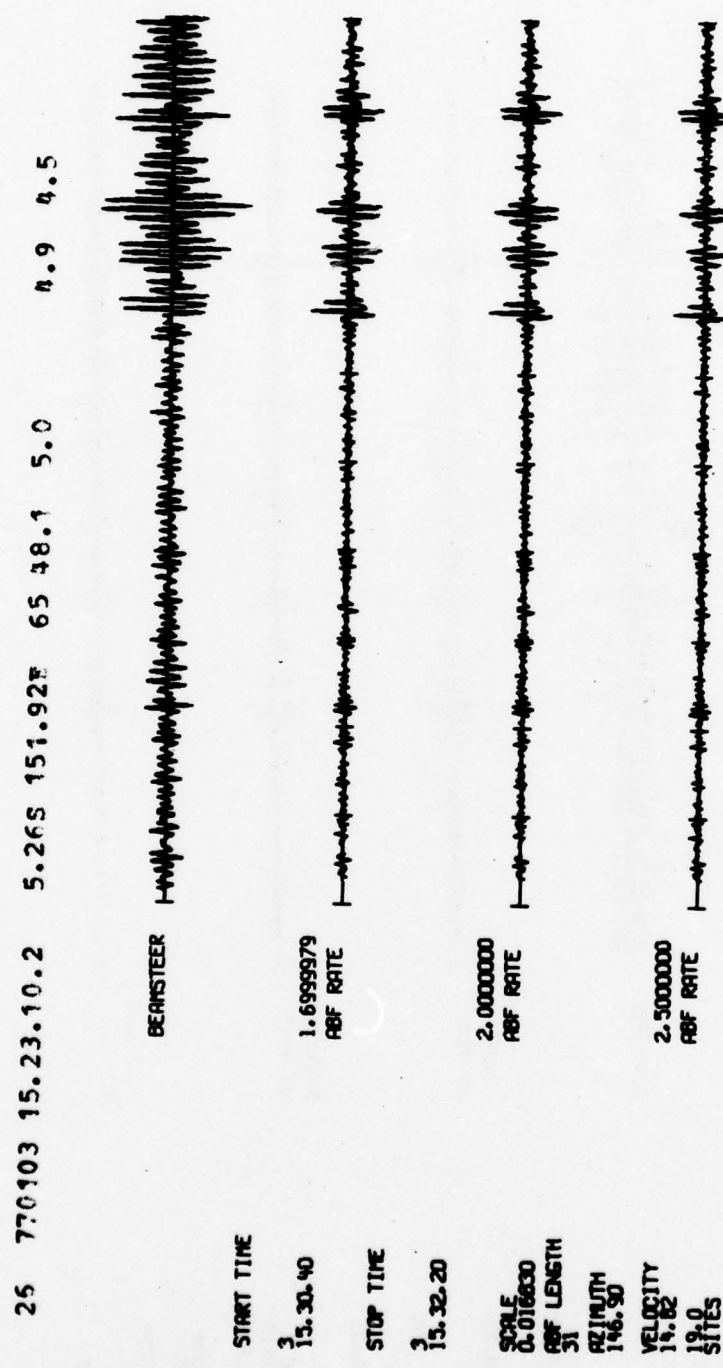


FIGURE A-26

PROCESSED TRACES FOR EVENT A-26

27 770104 1.41.42.8 53.67N 160.50E 157 27.6 4.4 9.1

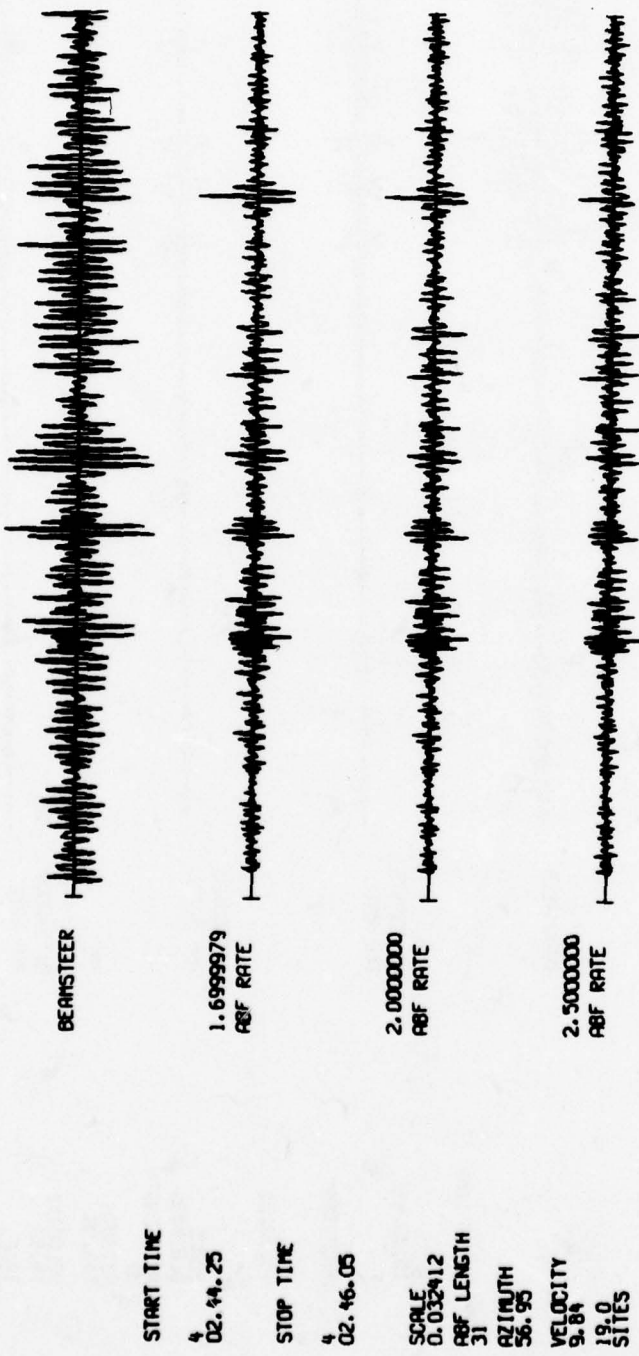
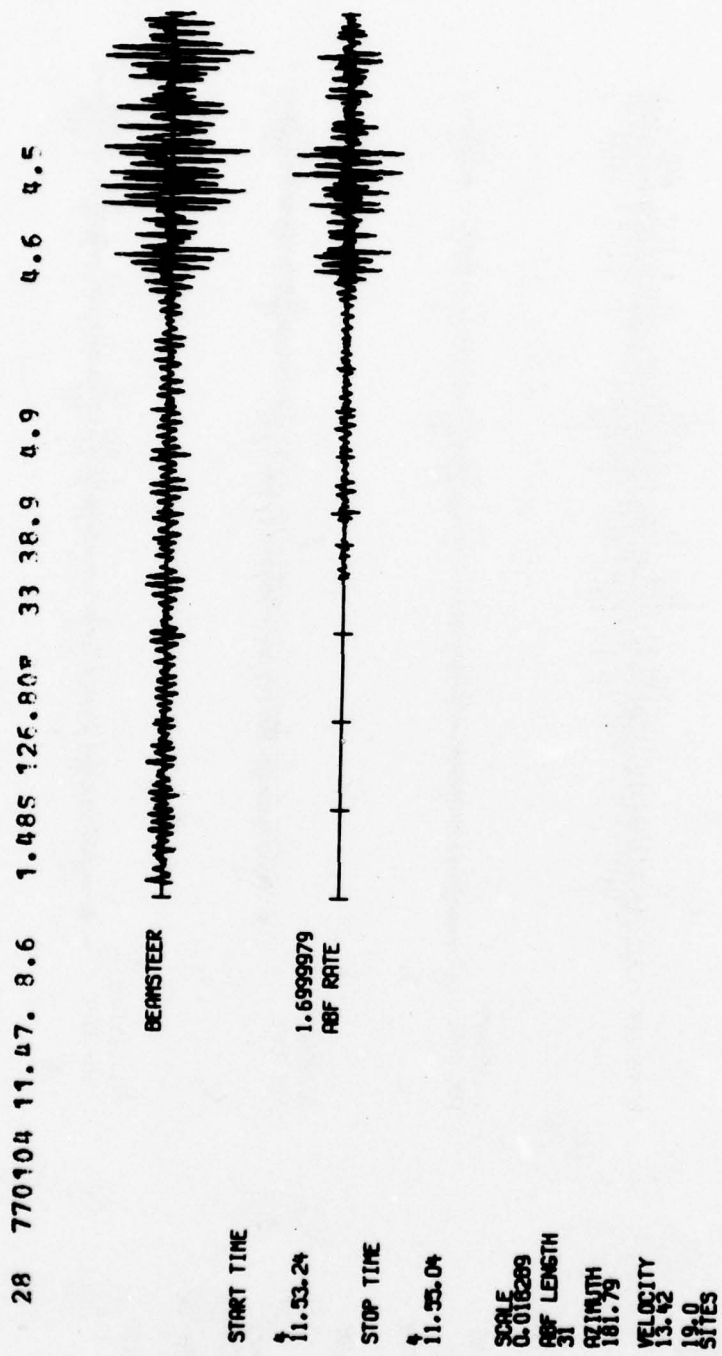
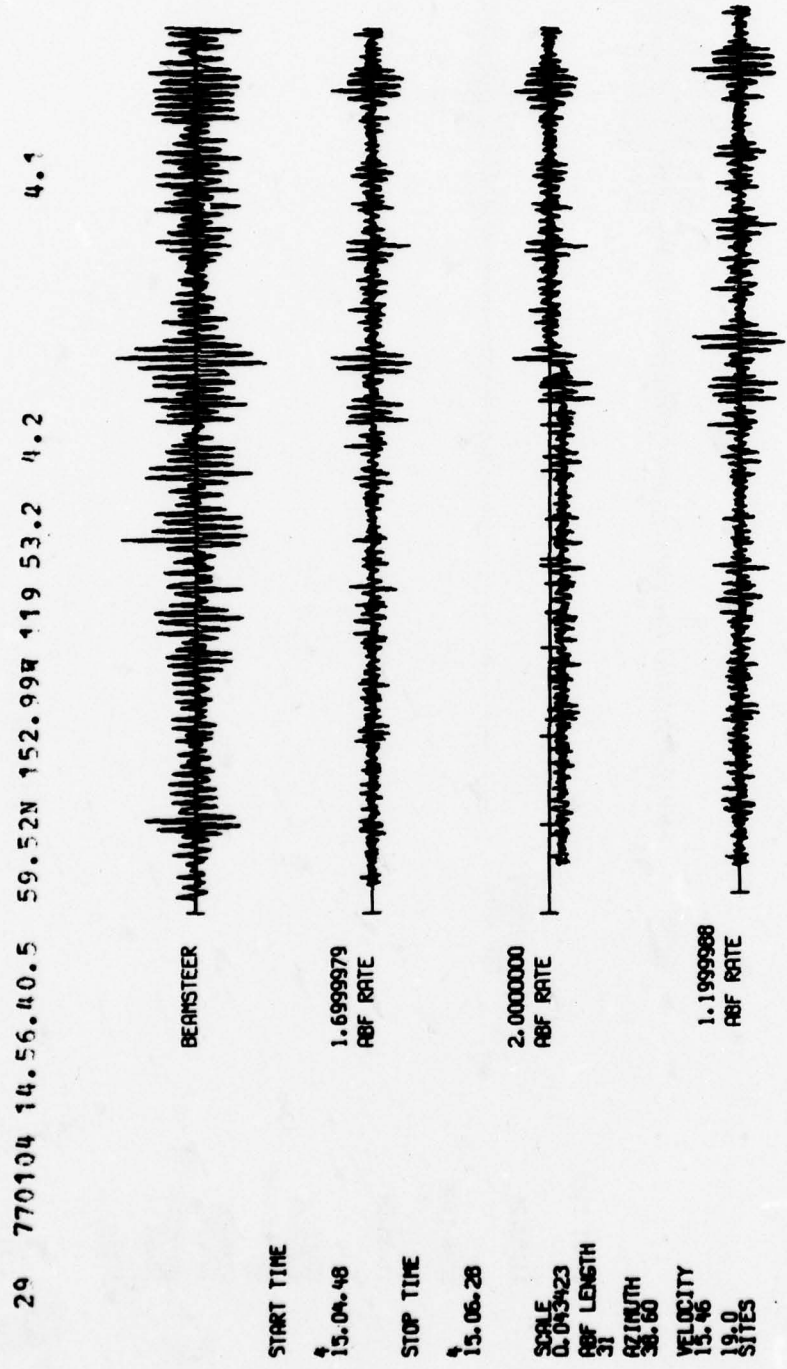


FIGURE A-27
PROCESSED TRACES FOR EVENT A-27



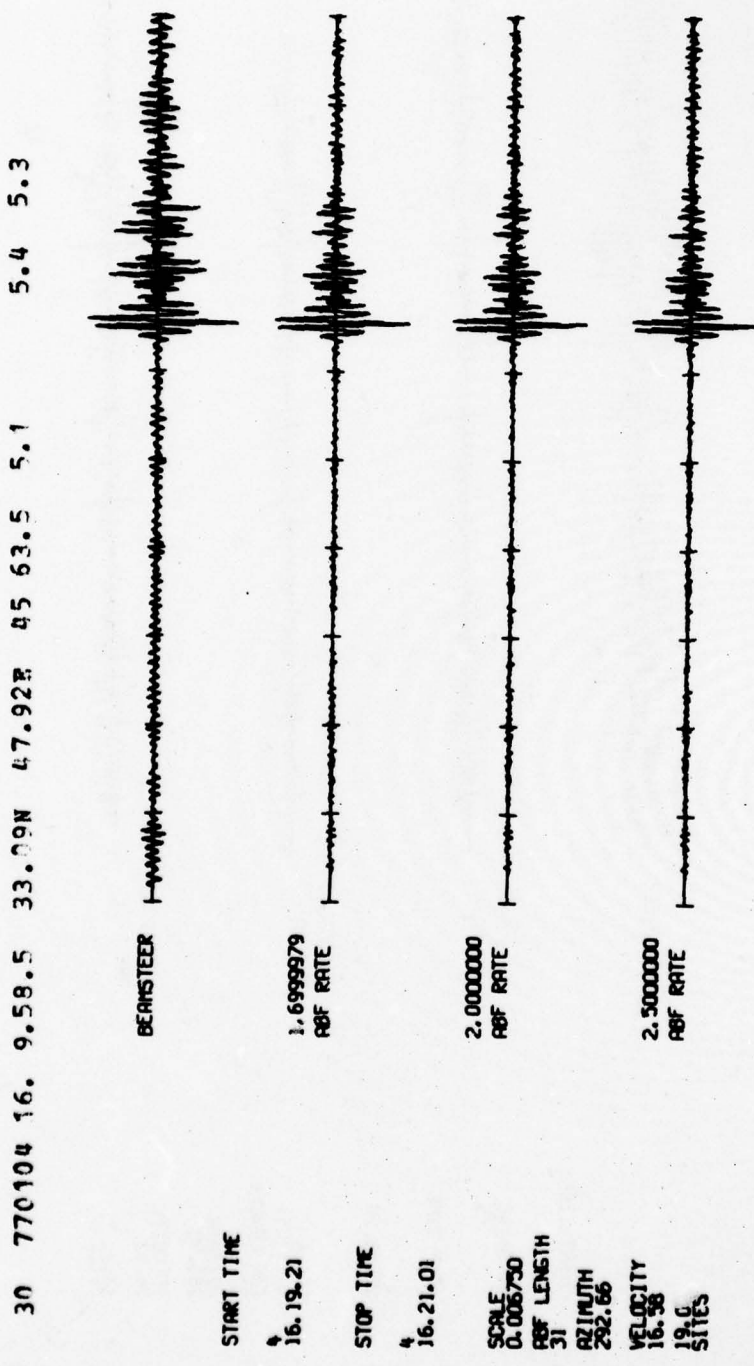
A-29

FIGURE A-28
PROCESSED TRACES FOR EVENT A-28



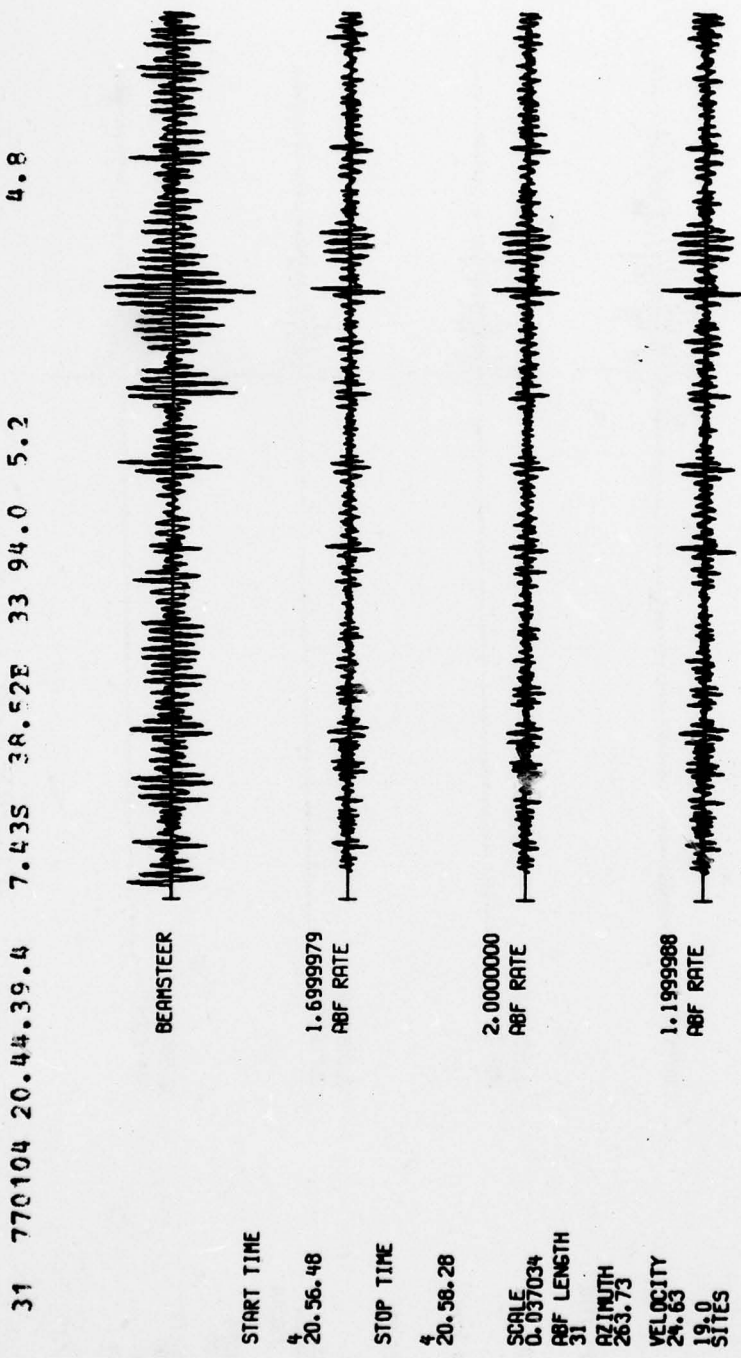
A-30

FIGURE A-29
PROCESSED TRACES FOR EVENT A-29



A-31

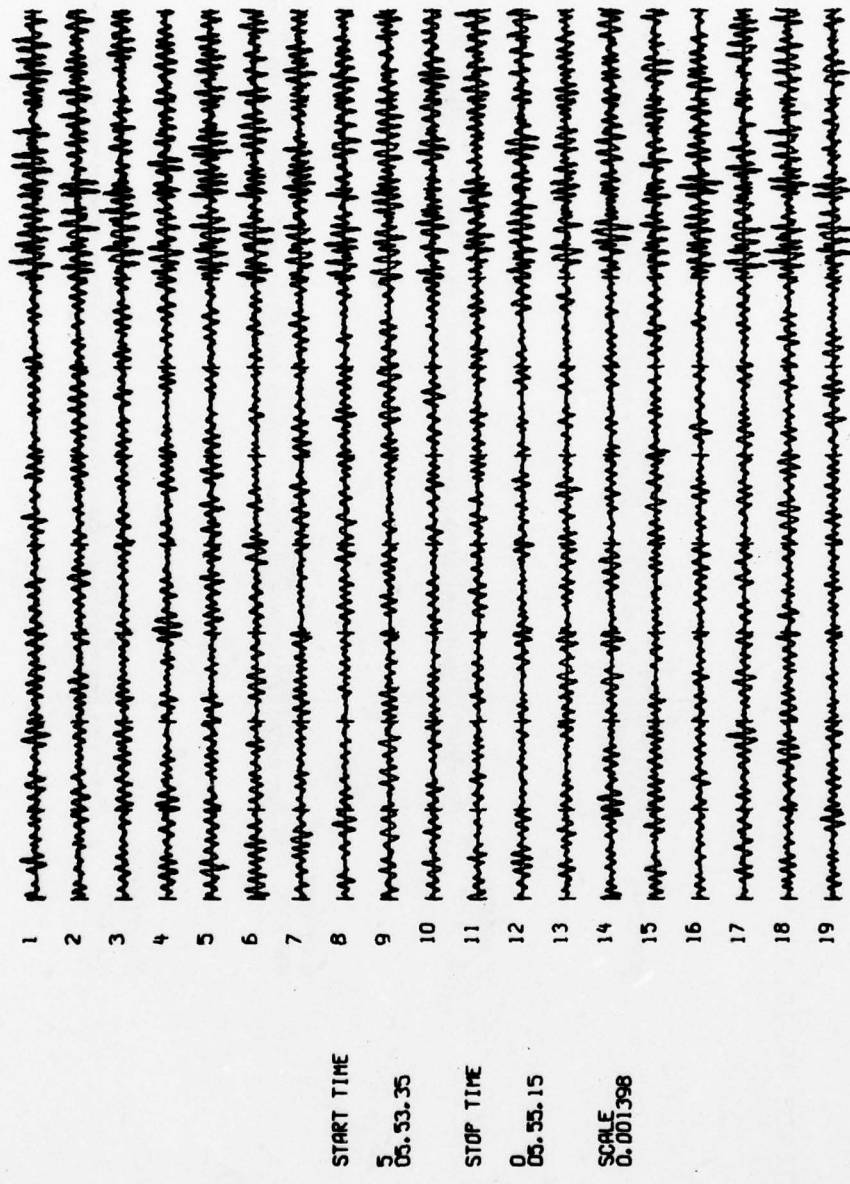
FIGURE A-30
PROCESSED TRACES FOR EVENT A-30



A - 32

FIGURE A-31
PROCESSED TRACES FOR EVENT A-31

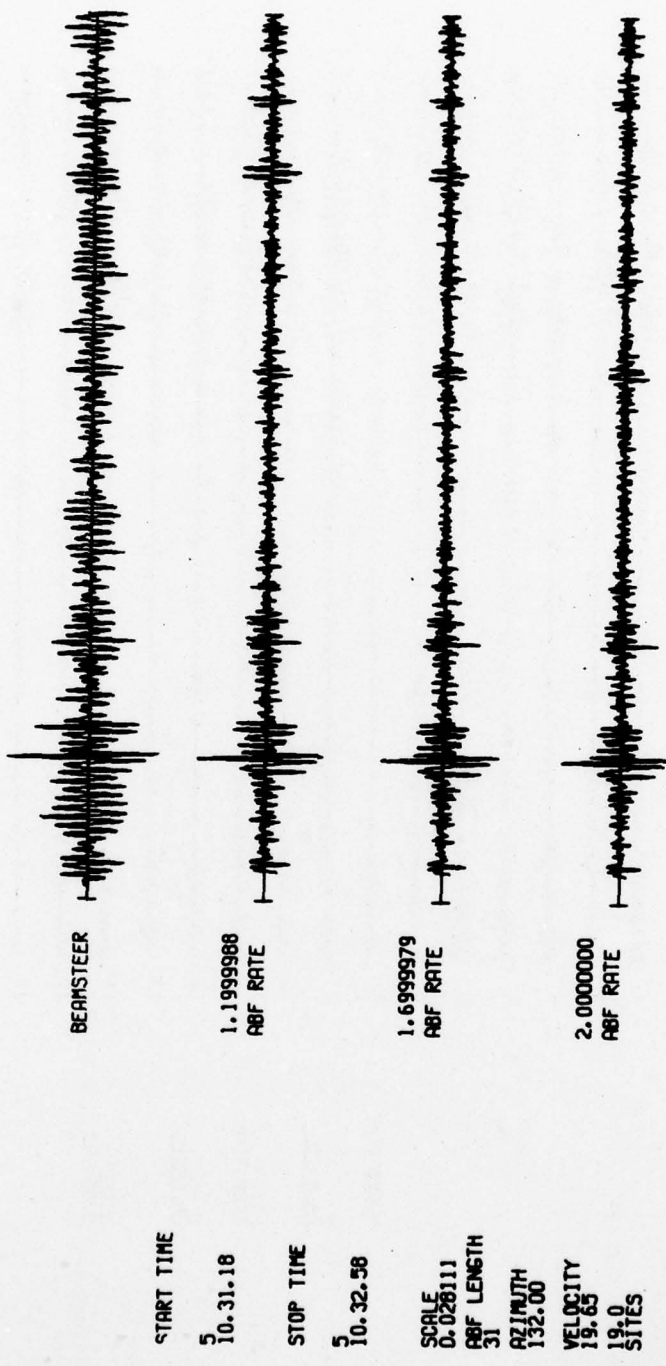
32 770195 5.44.39.9 27.46N 56.70E 29 59.9 5.5 5.5



A-33

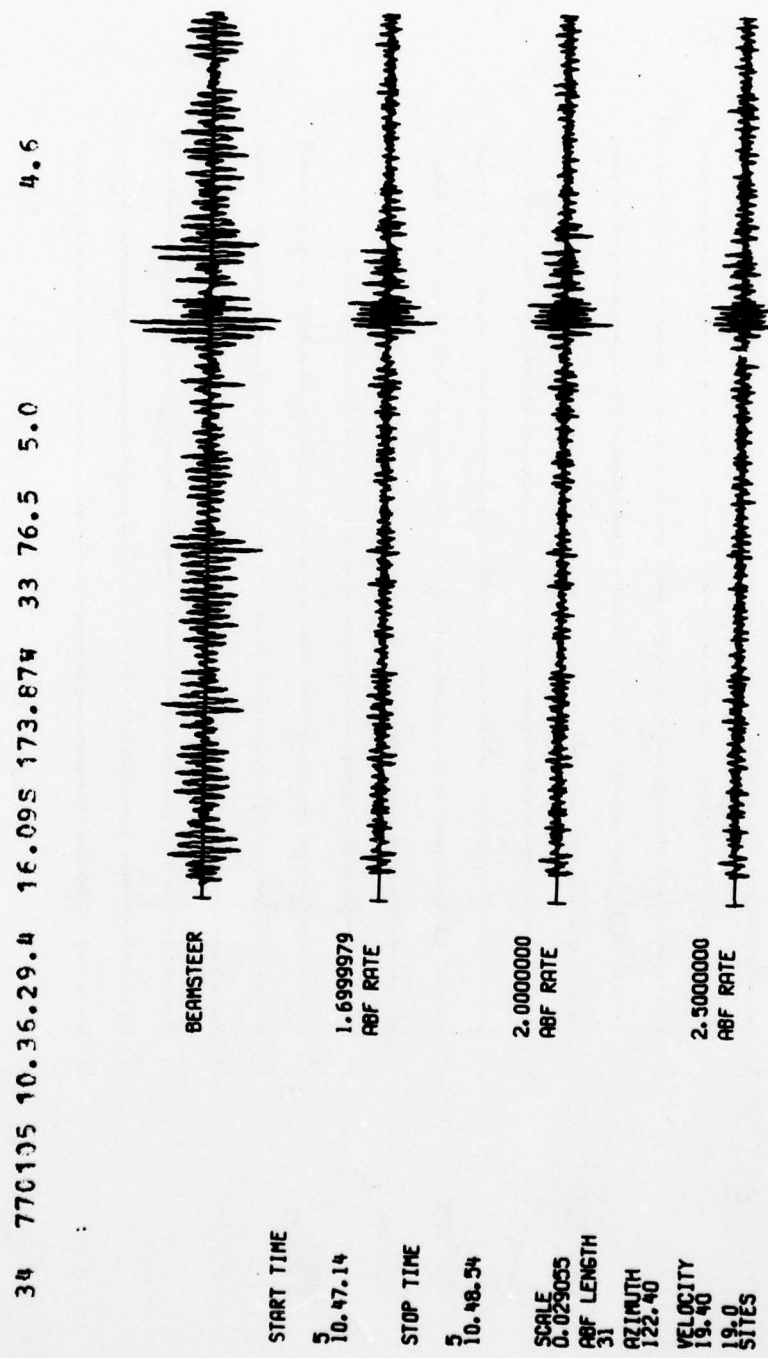
FIGURE A-32
PROCESSED TRACES FOR EVENT A-32

33 770105 10.20.29.1 23.38S 179.99E 538 78.0 5.0 R.1 4.0



A - 34

FIGURE A-33
PROCESSED TRACES FOR EVENT A-33



A-35

FIGURE A-34
PROCESSED TRACES FOR EVENT A-34

35 770105 13.29.48.1 20.915 178.314 575 77.1 5.2 5.4

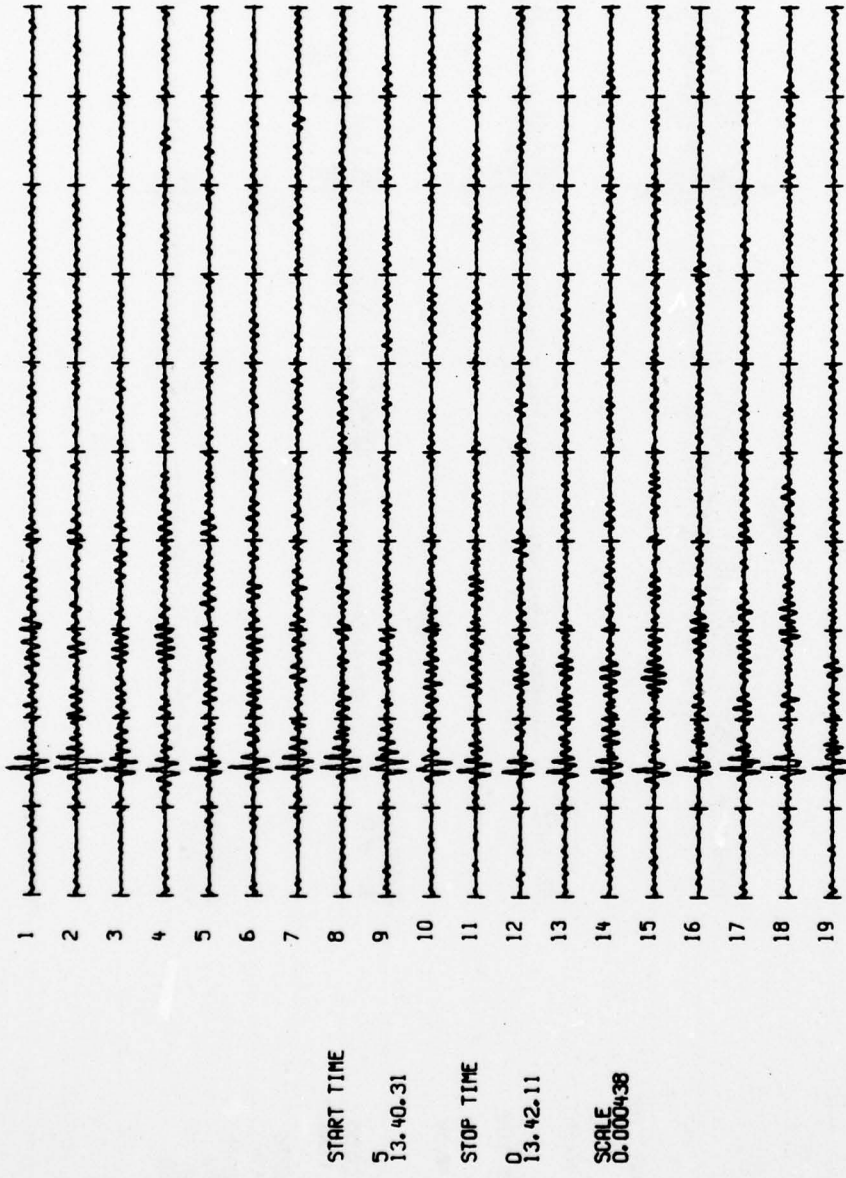


FIGURE A-35
PROCESSED TRACES FOR EVENT A-35

36 770105 14.10.56.5 25.43N 95.19E 104 30.2 4.8 4.7 4.6

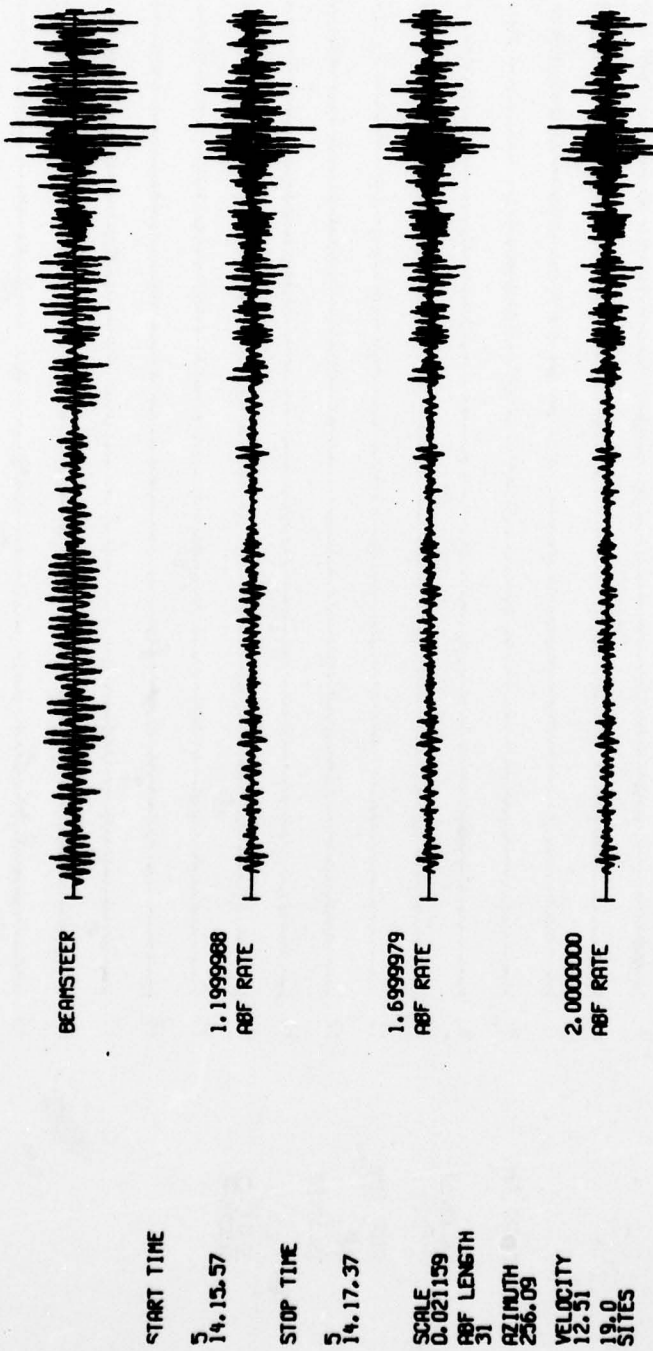


FIGURE A-36

PROCESSED TRACES FOR EVENT A-36

37 770105 14.12.35.0 18.70N 145.52E 136 24.3 4.6 5.3

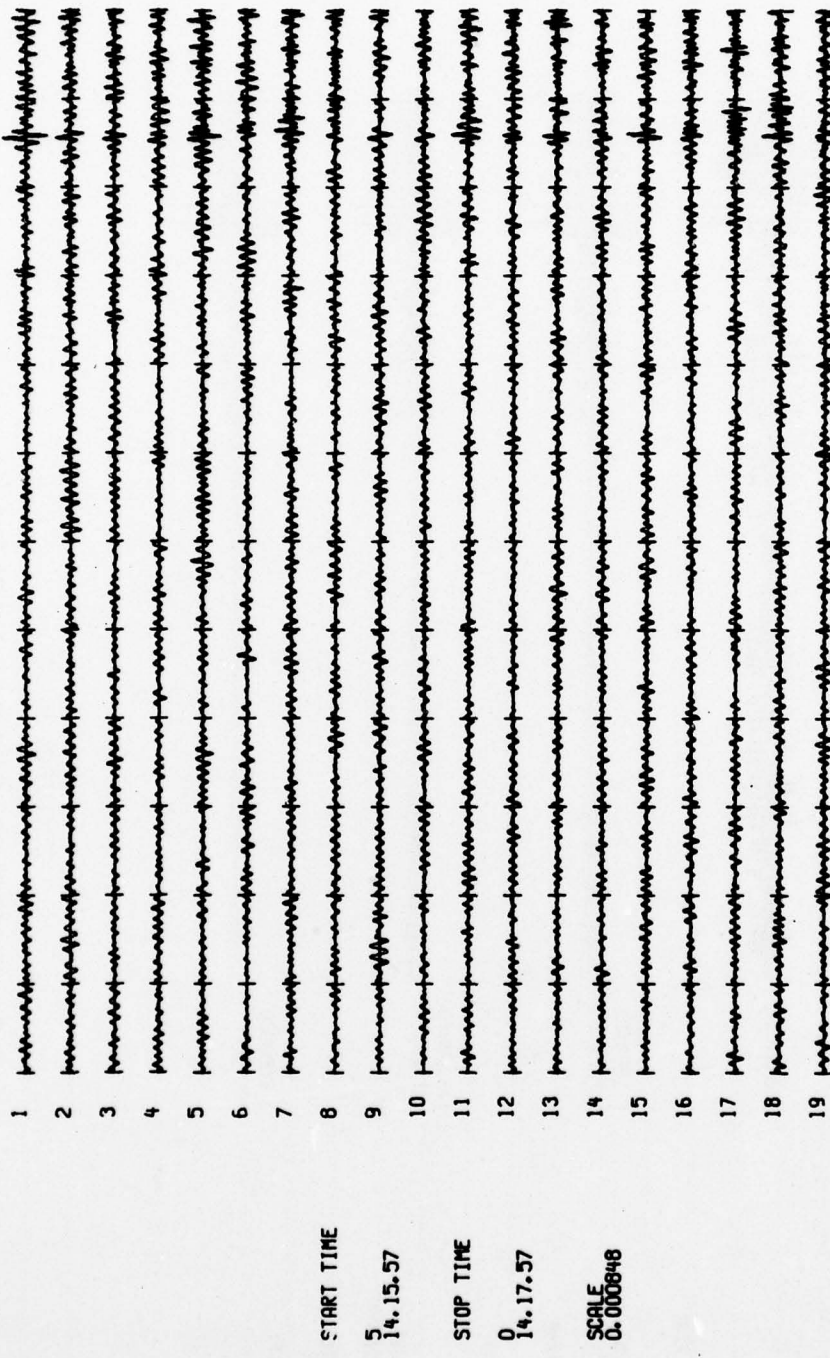
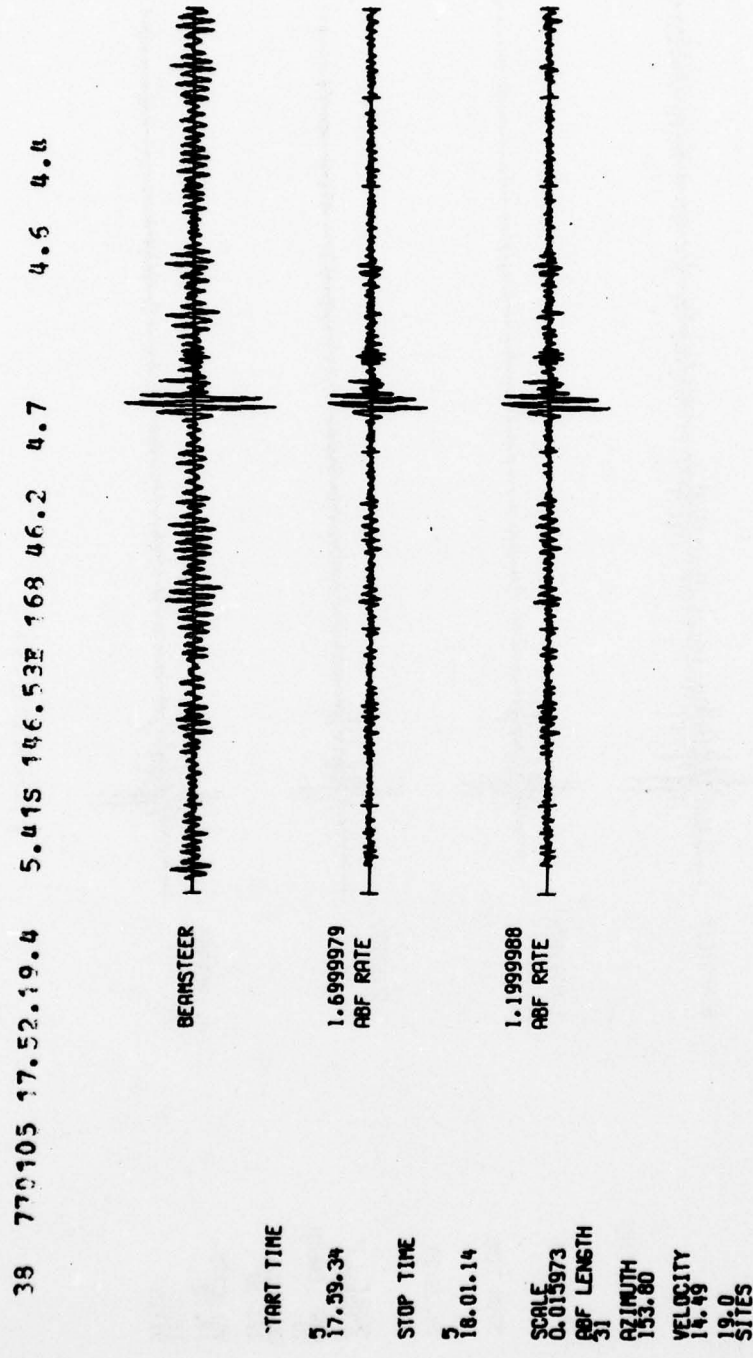


FIGURE A-37
PROCESSED TRACES FOR EVENT A-37



A-39

FIGURE A-38
PROCESSED TRACES FOR EVENT A-38

39 770106 4.10.17.8 17.945 178.544 621 74.8 4.6 4.3 4.6

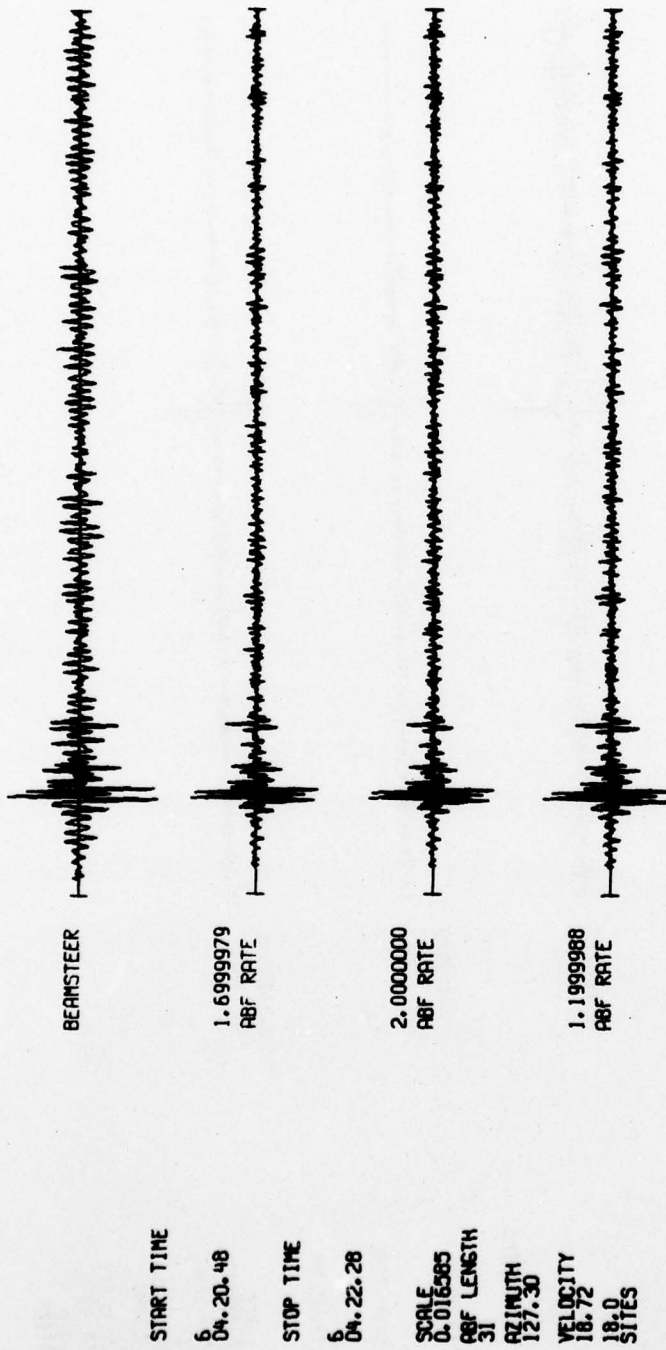


FIGURE A-39
PROCESSED TRACES FOR EVENT A-39

40 770106 6.11.00.7 3.63S 144.45F 33 43.8 6.0 6.3

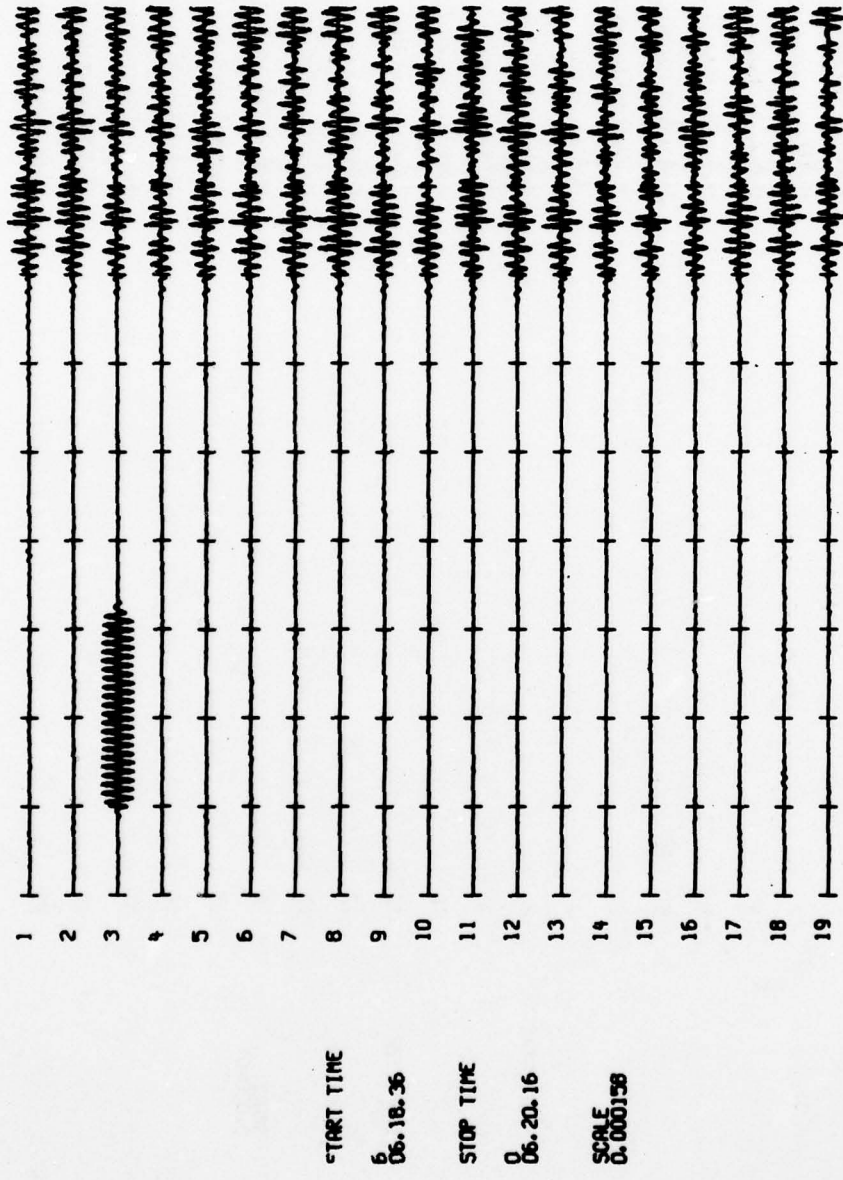


FIGURE A-40
PROCESSED TRACES FOR EVENT A-40

41 770106 7.55.57.5 49.27N 155.55E 33 23.1 5.4 5.6

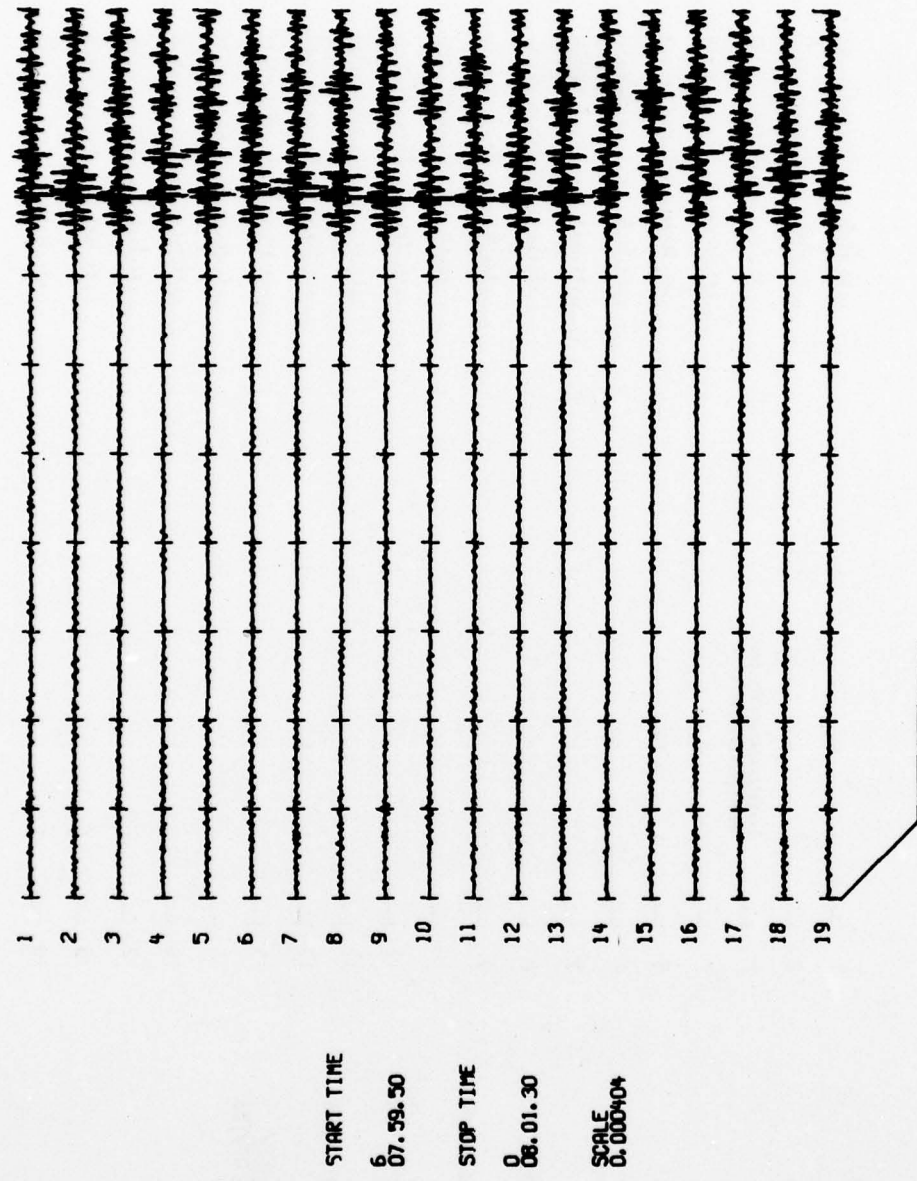
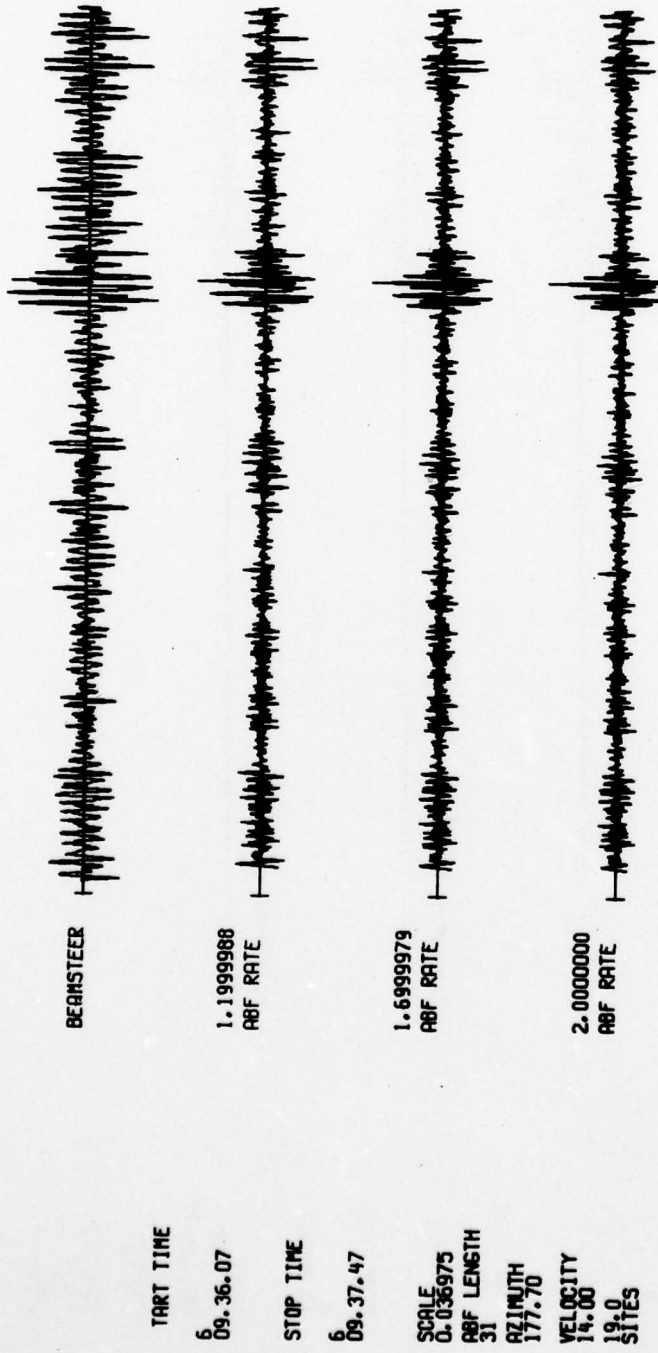


FIGURE A-41
PROCESSED TRACES FOR EVENT A-41

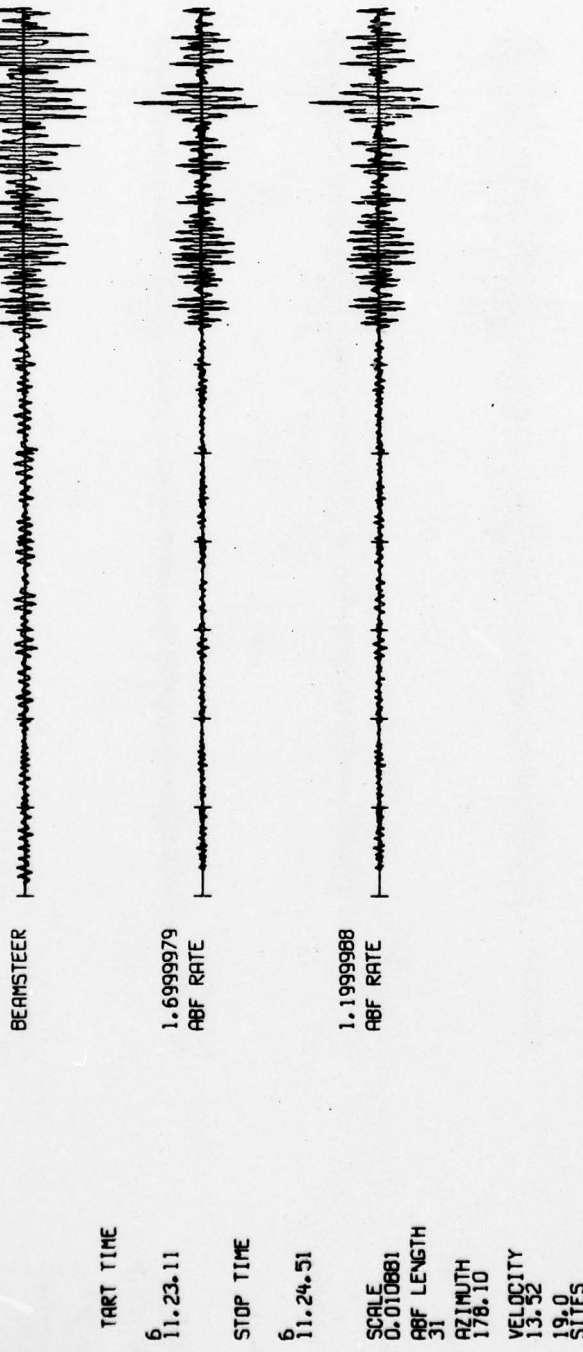
42 77C106 9.29. 6.2 7.04S 129.52E 56 46.4 4.3 4.5 4.4



A-43

FIGURE A-42
PROCESSED TRACES FOR EVENT A-42

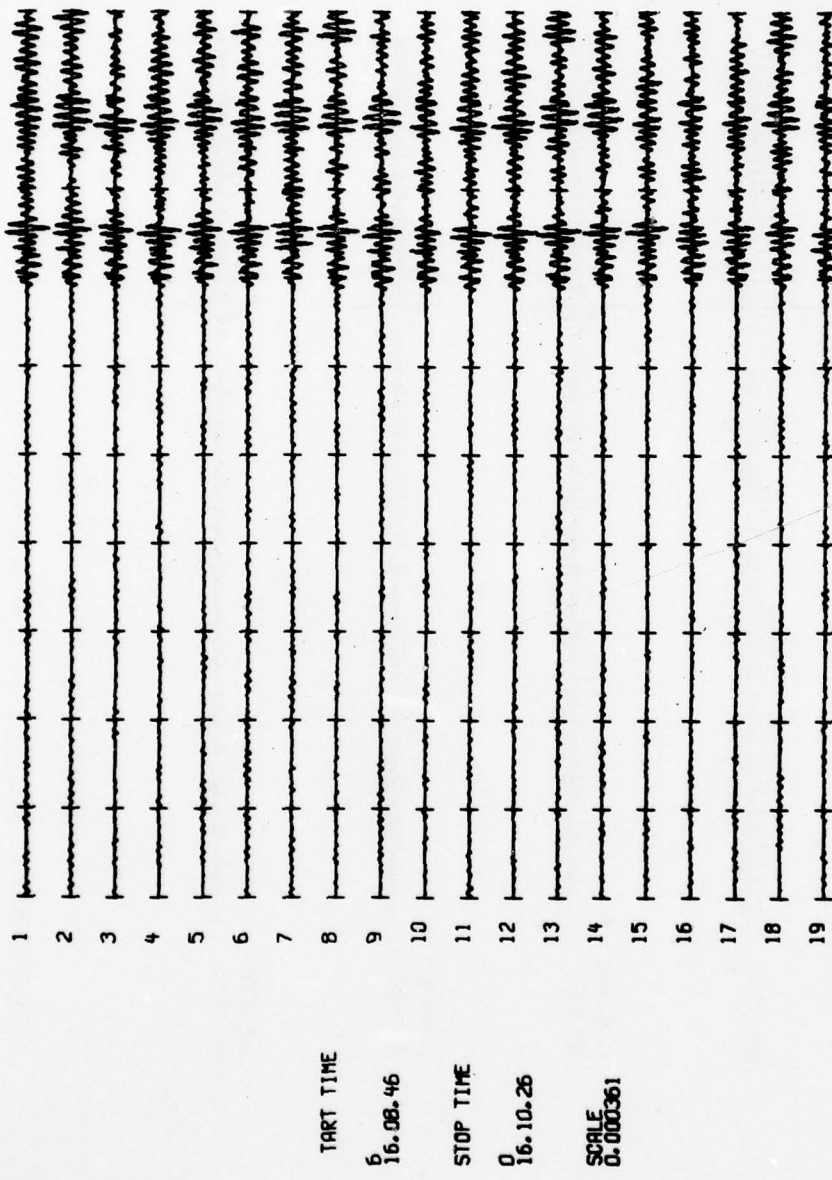
43 770106 11.16.51.2 3.15S 129.10E 48 40.5 5.0 4.6 4.5



A-44

FIGURE A-43
PROCESSED TRACES FOR EVENT A-43

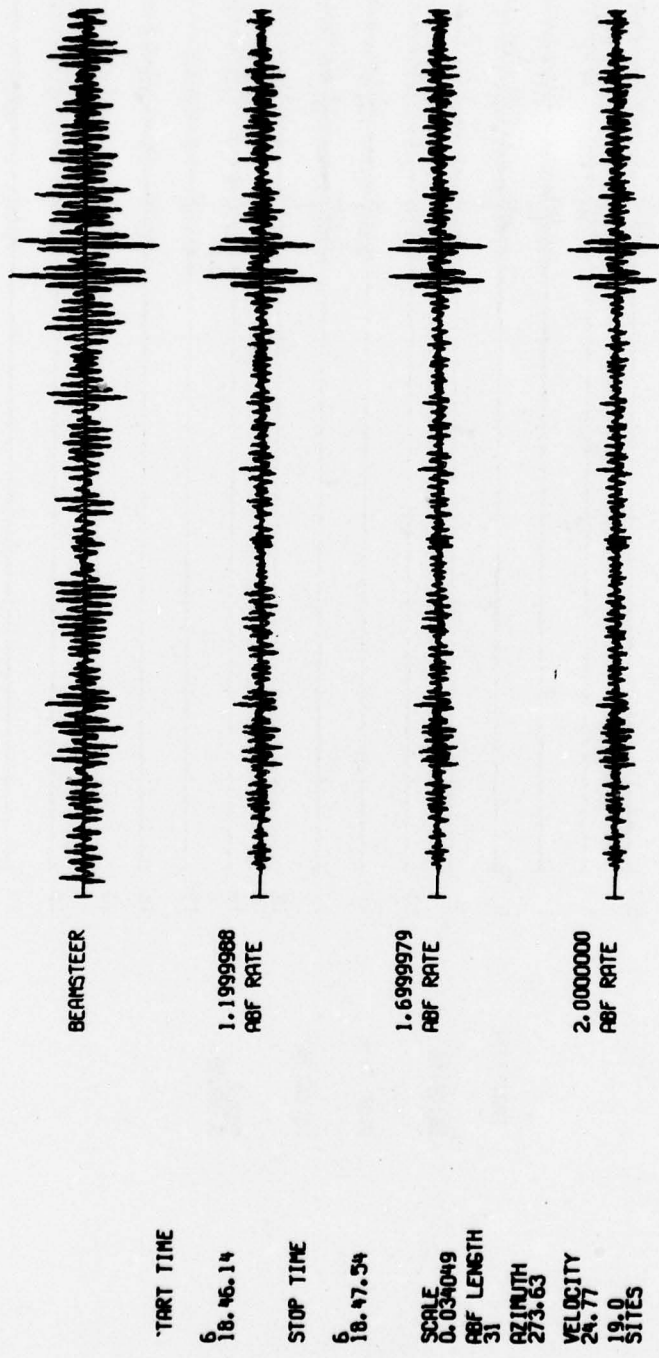
44 770105 16. 2. 7.6 51.48N 175.48W 33 41.6 5.2 6.0



A-45

FIGURE A-44
PROCESSED TRACES FOR EVENT A-44

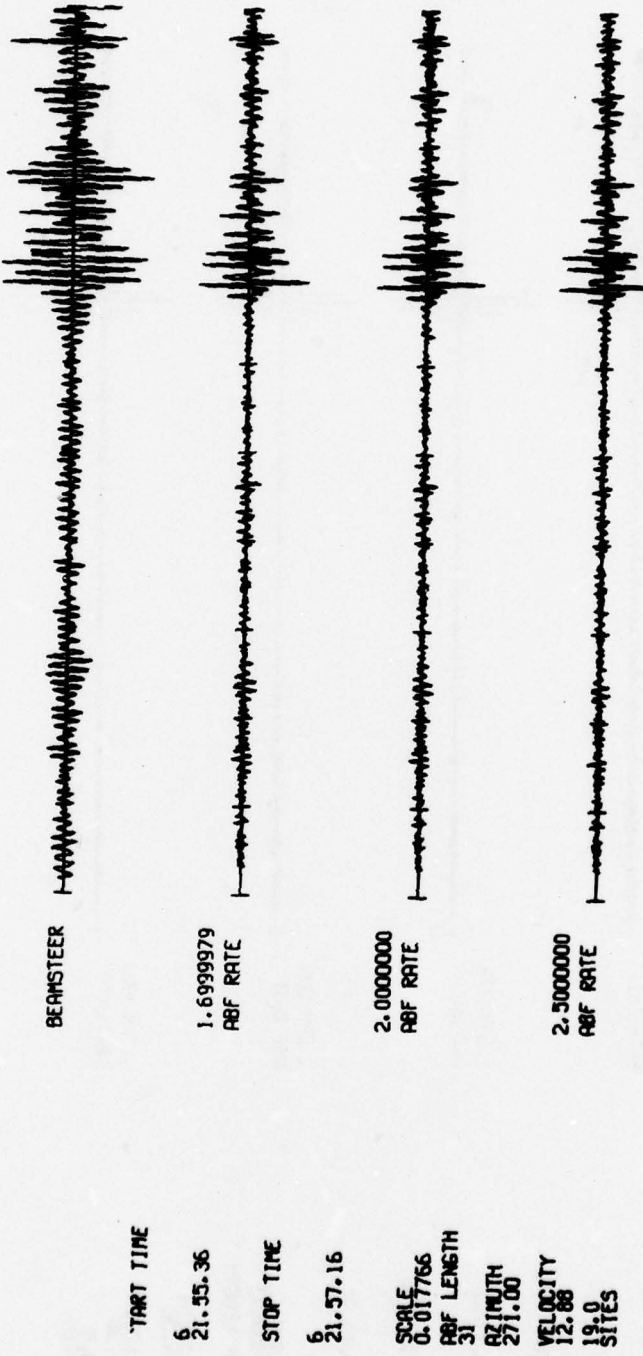
45 770106 18.33.43.5 2.515 28.70F 21 98.8 5.3 5.5



A-46

FIGURE A-45
PROCESSED TRACES FOR EVENT A-45

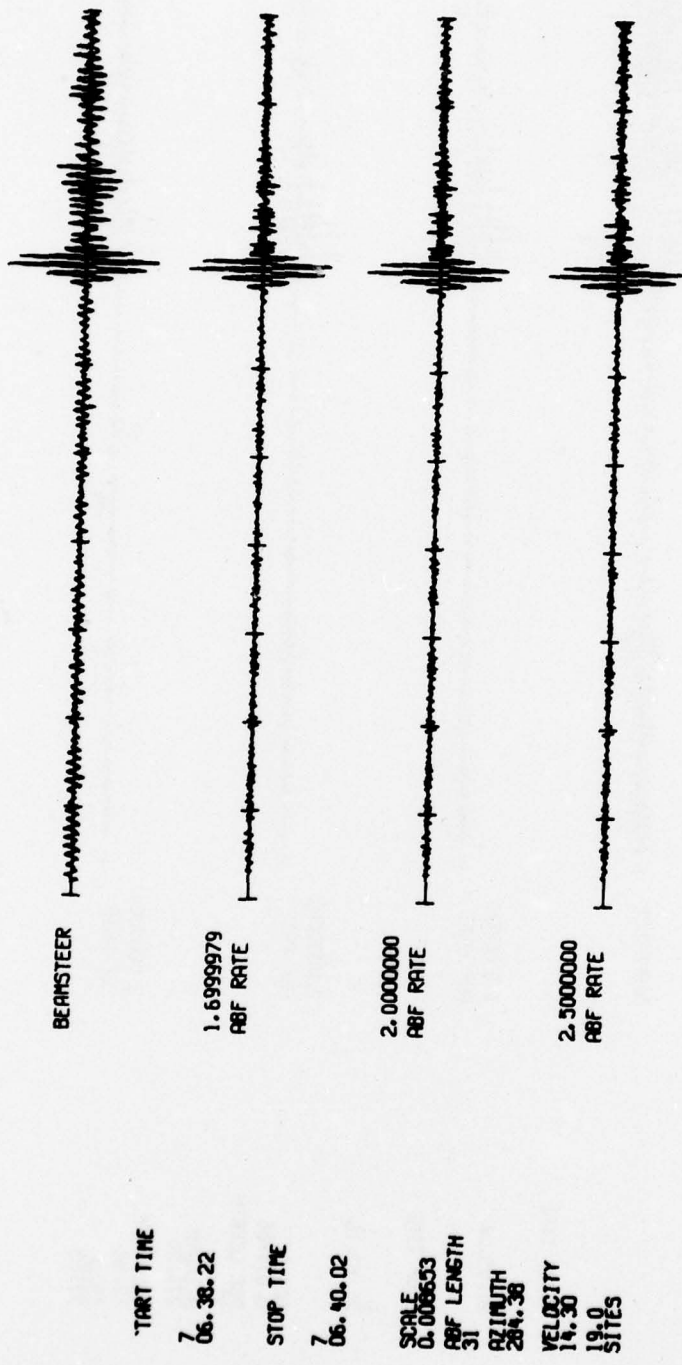
46 770106 21.50. 8.1 31.05N 88.05E 33 33.3 5.2 4.9 4.8



A-47

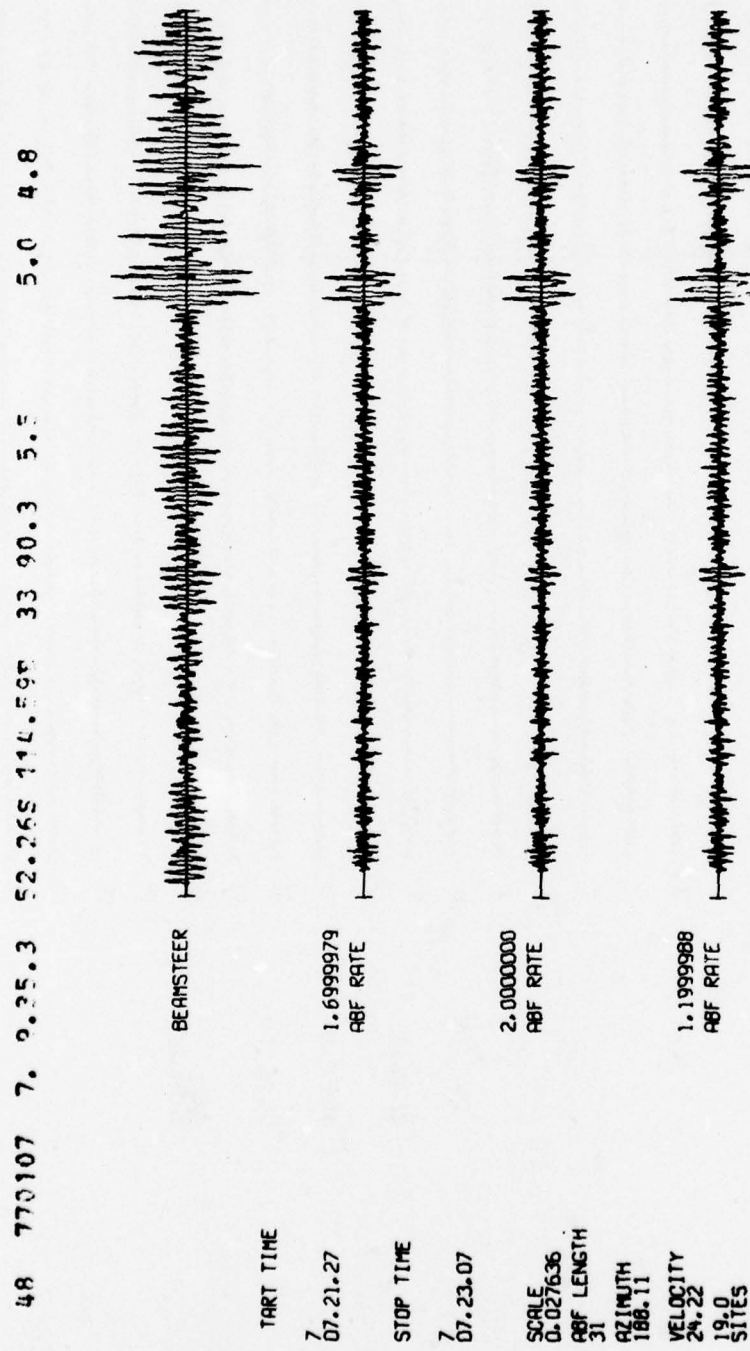
FIGURE A-46
PROCESSED TRACES FOR EVENT A-46

47 770107 6.31.13.2 34.55N 70.97E 45 45.5 5.1
5.2 5.1



A-48

FIGURE A-47
PROCESSED TRACES FOR EVENT A-47



A-49

FIGURE A-48
PROCESSED TRACES FOR EVENT A-48

49 770107 7.15.57.5 30.701 50.698 67 62.6 4.6 5.4

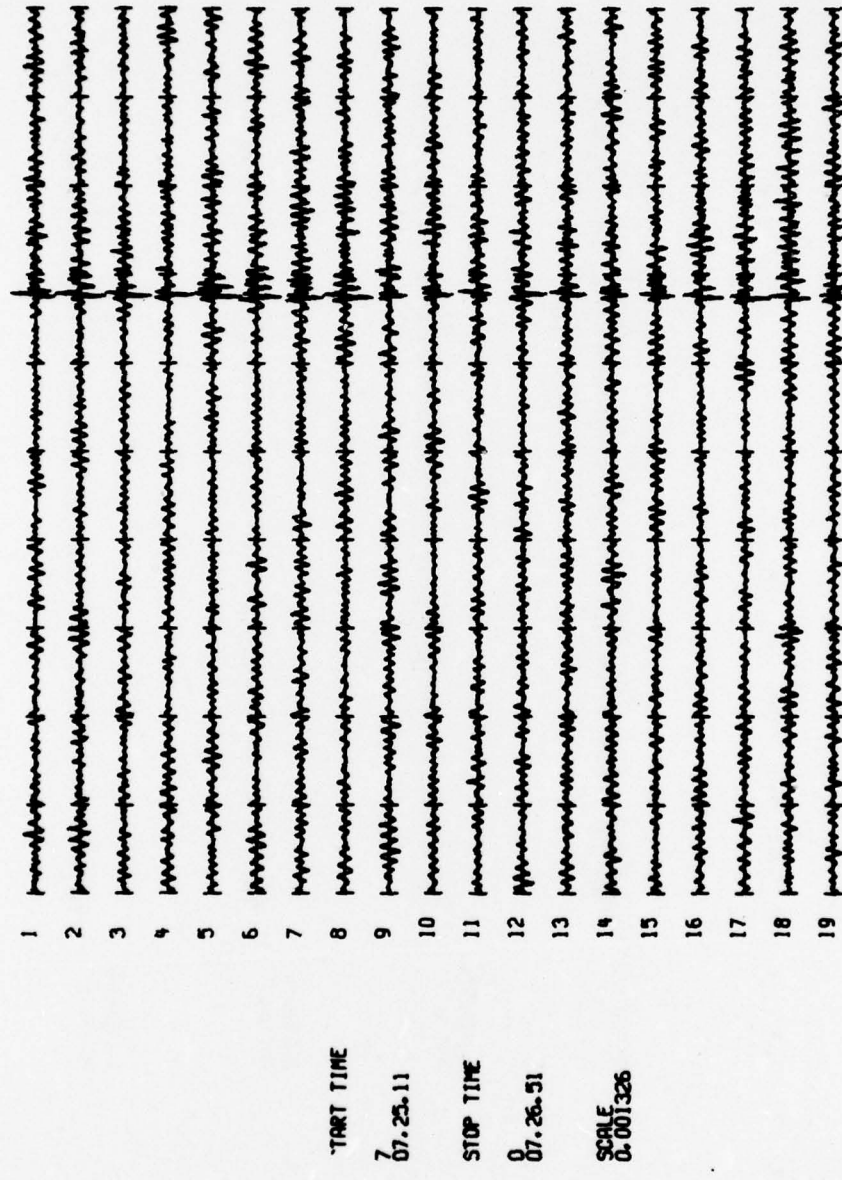
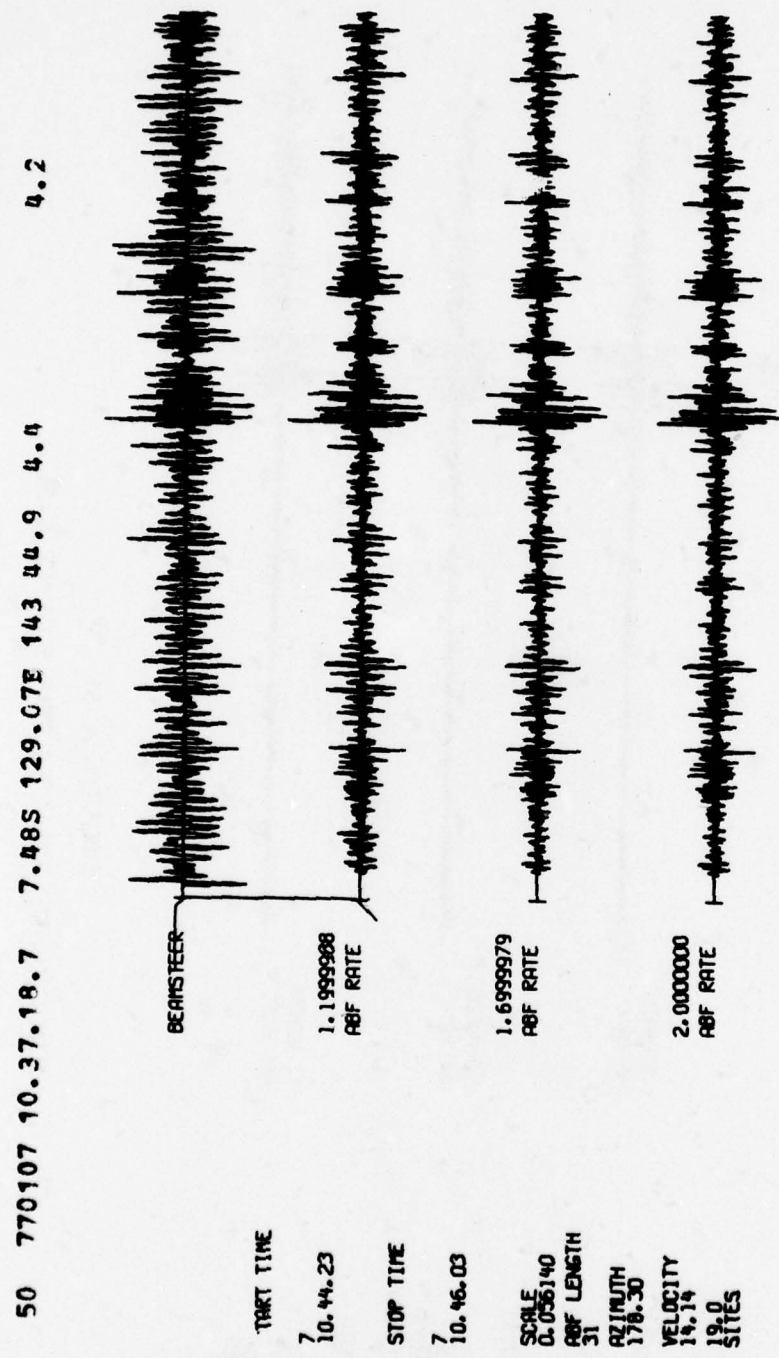


FIGURE A-49

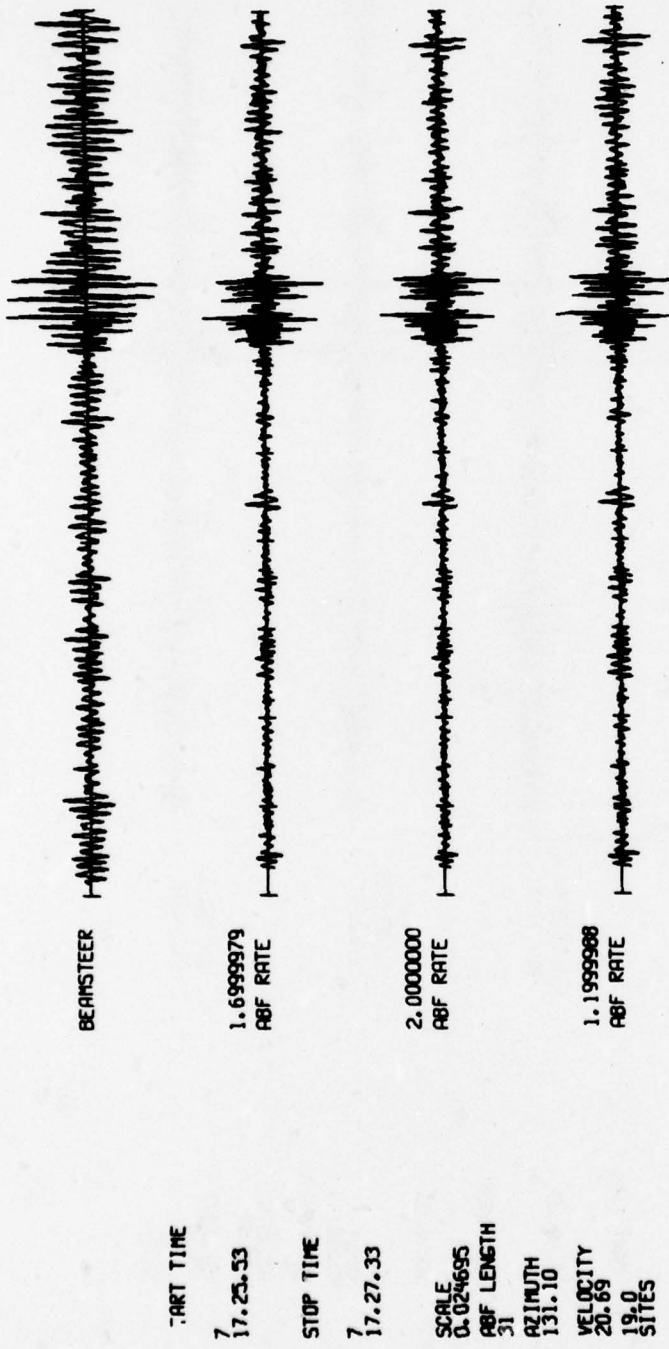
PROCESSED TRACES FOR EVENT A-49



A-51

FIGURE A-50
PROCESSED TRACES FOR EVENT A-50

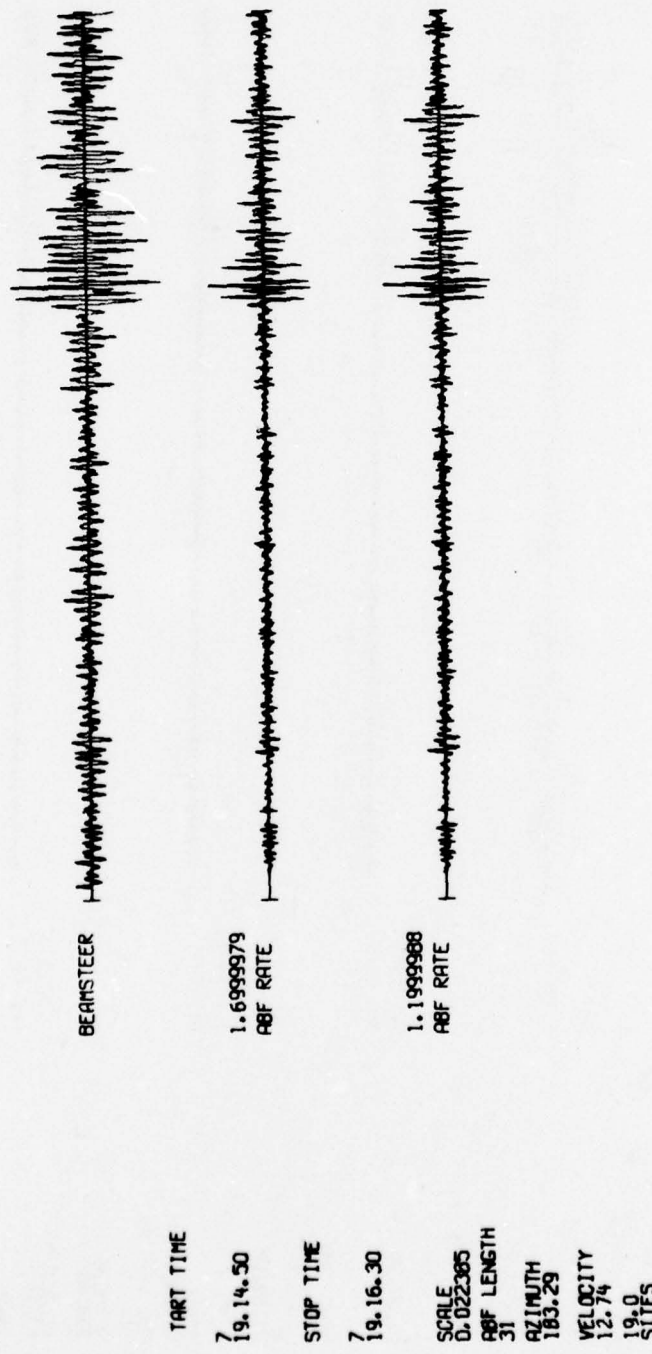
51 770107 17.14.47.3 25.185 176.964 76 91.2 5.0 4.8 4.7



A-52

FIGURE A-51
PROCESSED TRACES FOR EVENT A-51

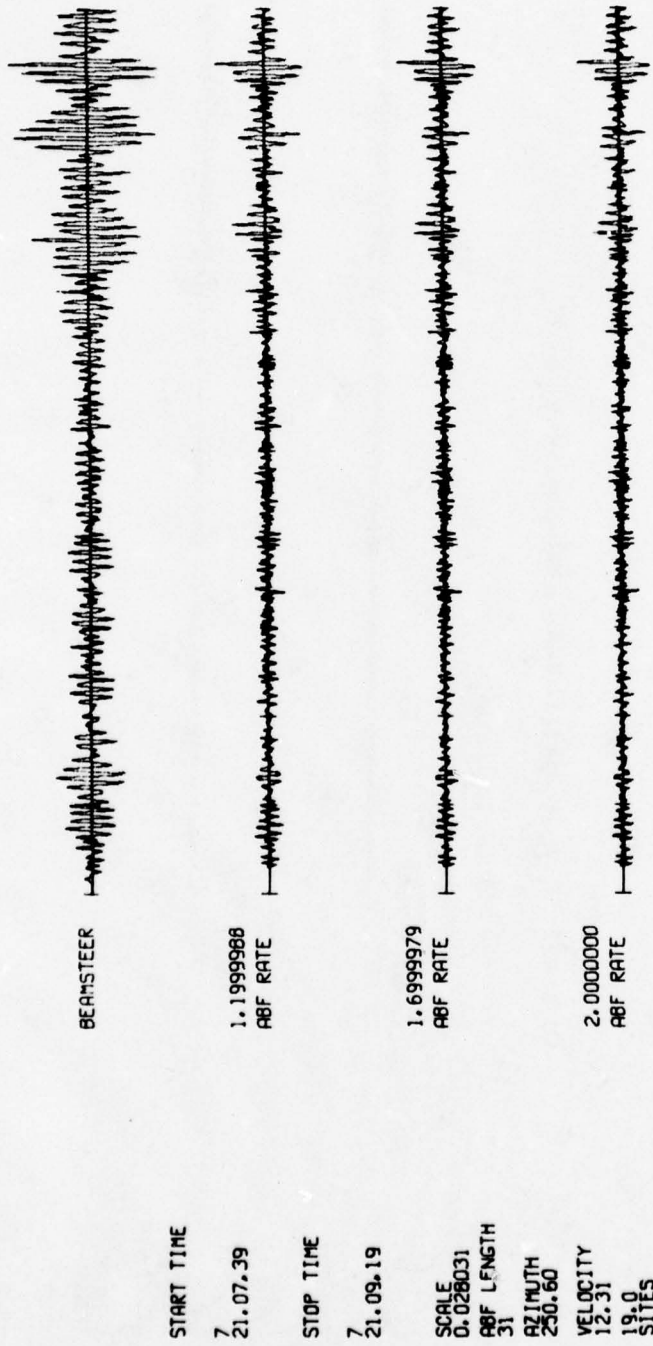
52 770107 19. 0.33.2 5.32N 126.16E 53 32.0 3.7 4.8 4.6



A-53

FIGURE A-52
PROCESSED TRACES FOR EVENT A-52

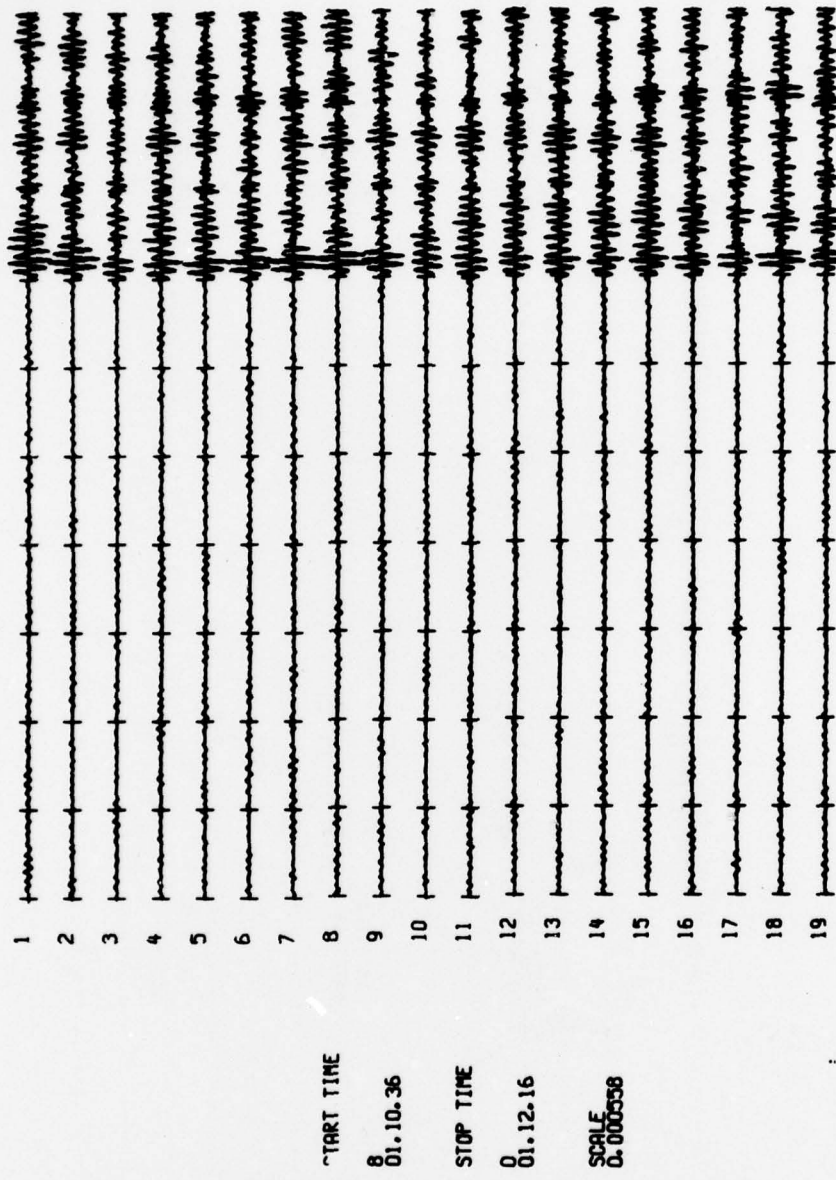
53 770107 21. 2.55.2 24.16N 98.45E 42 28.4 4.5



A-54

FIGURE A-53
PROCESSED TRACES FOR EVENT A-53

54 770108 1. 6.31.1 20.08N 147.52E 47 24.3 5.2 5.6



A-55

FIGURE A-54
PROCESSED TRACES FOR EVENT A-54

55 770108 6. 8.52.7 11.47N 140.39E 24 28.3 4.6 4.8 4.7

ART TIME

SEAMSTEER



STOP TIME

1.6999979
ABF RATE



SCALE

2.0000000
ABF RATE



ABF LENGTH

31

AZIMUTH

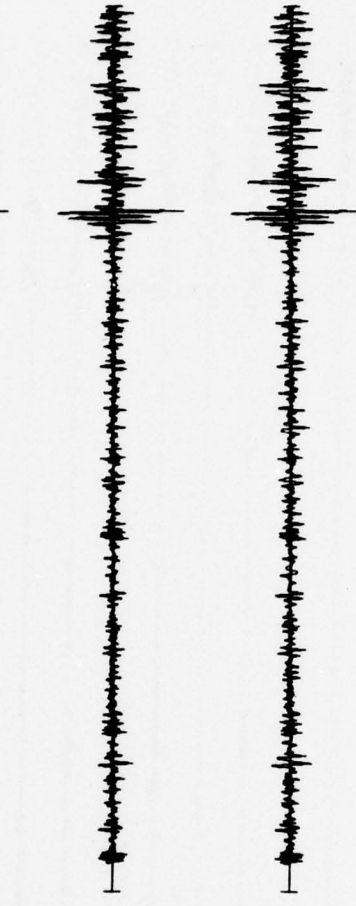
153.40

VELOCITY

12.29

19.0

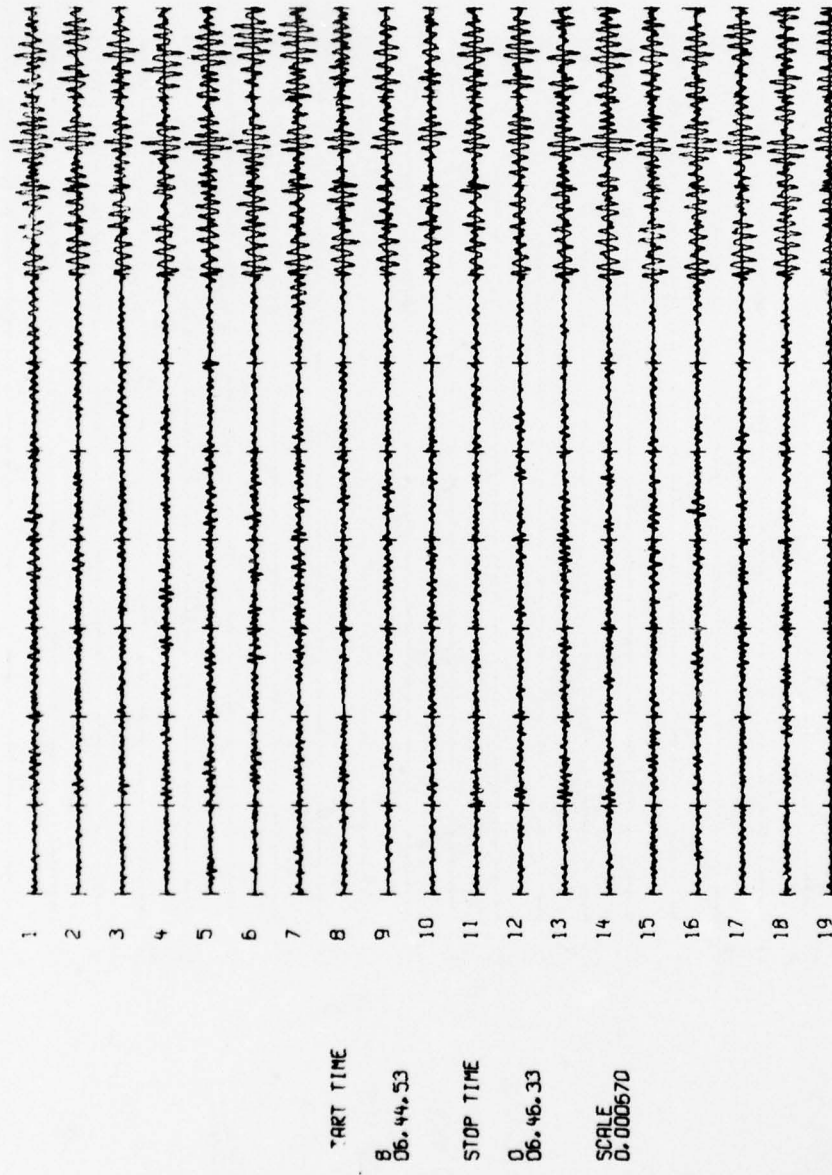
SITES



A-56

FIGURE A-55
PROCESSED TRACES FOR EVENT A-55

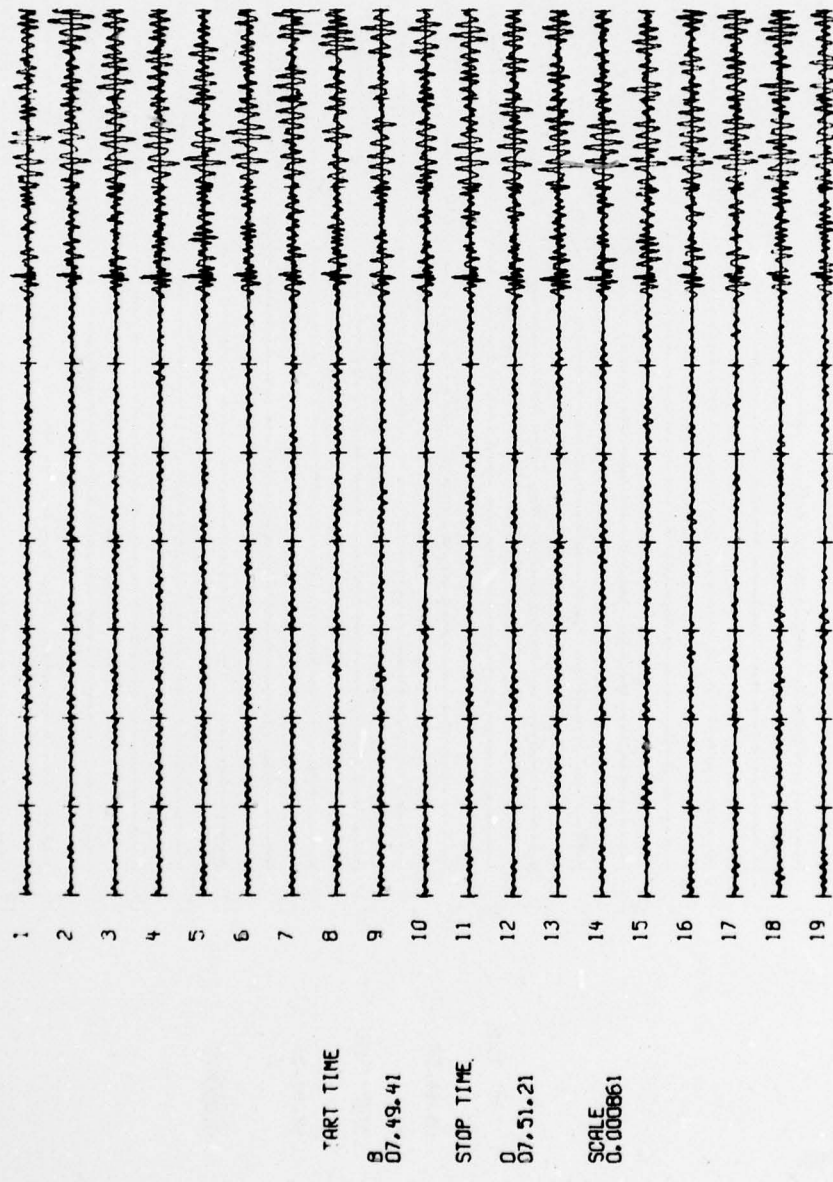
56 770108 6.41.4.1 15.32N 129.91E 36 22.7 5.3 5.3



A-57

FIGURE A-56
PROCESSED TRACES FOR EVENT A-56

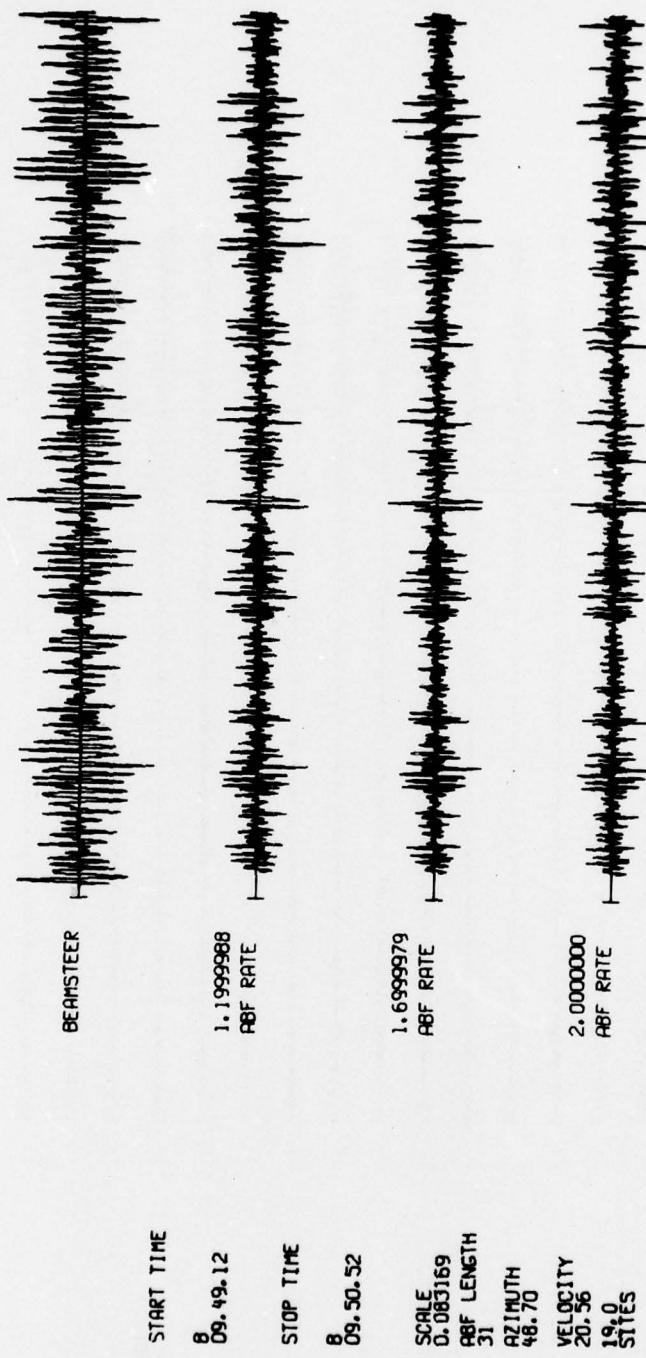
57 770108 7.00.41.9 11.27S 166.11E 42 60.4 5.5 5.5



A-58

FIGURE A-57
PROCESSED TRACES FOR EVENT A-57

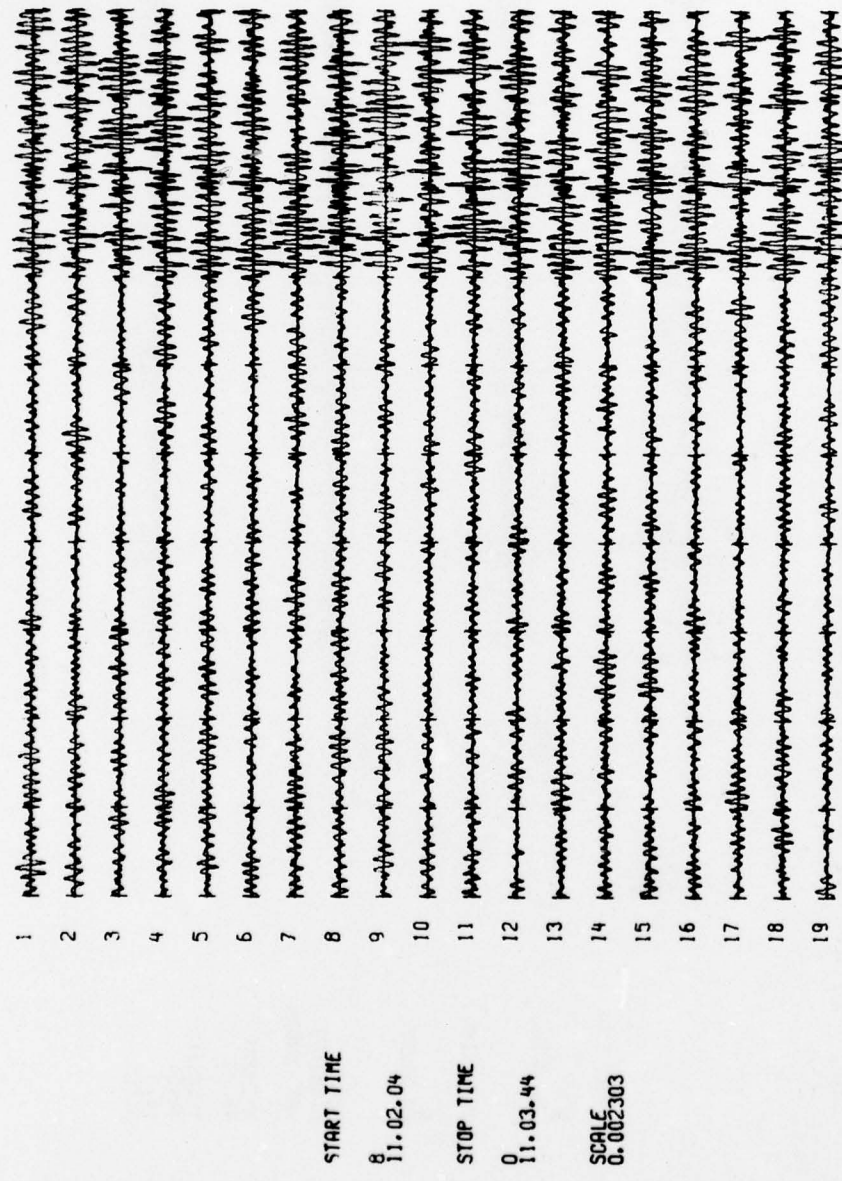
58 770108 9.28.7.4 37.91N 122.20W 10 80.9 4.8



A-59

FIGURE A-58
PROCESSED TRACES FOR EVENT A-58

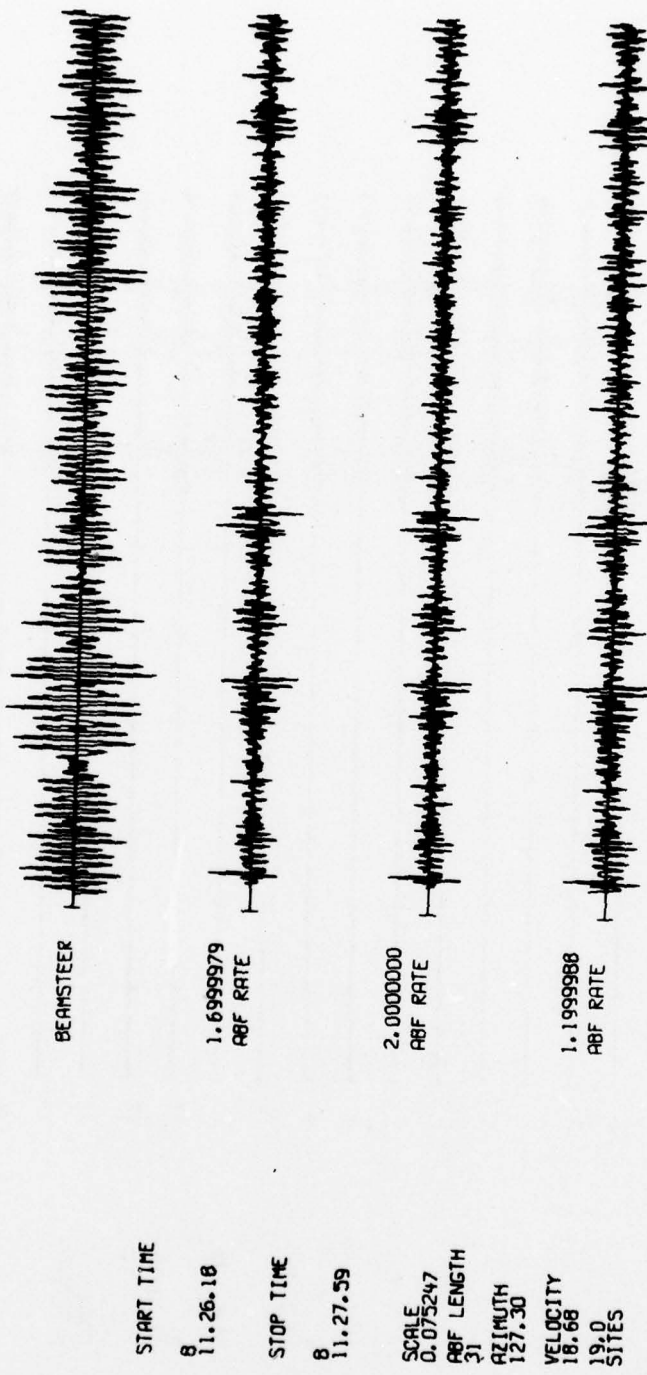
59 770109 10.55.19.0 3.585 140.10P 26 42.5 5.1 5.1



A-60

FIGURE A-59
PROCESSED TRACES FOR EVENT A-59

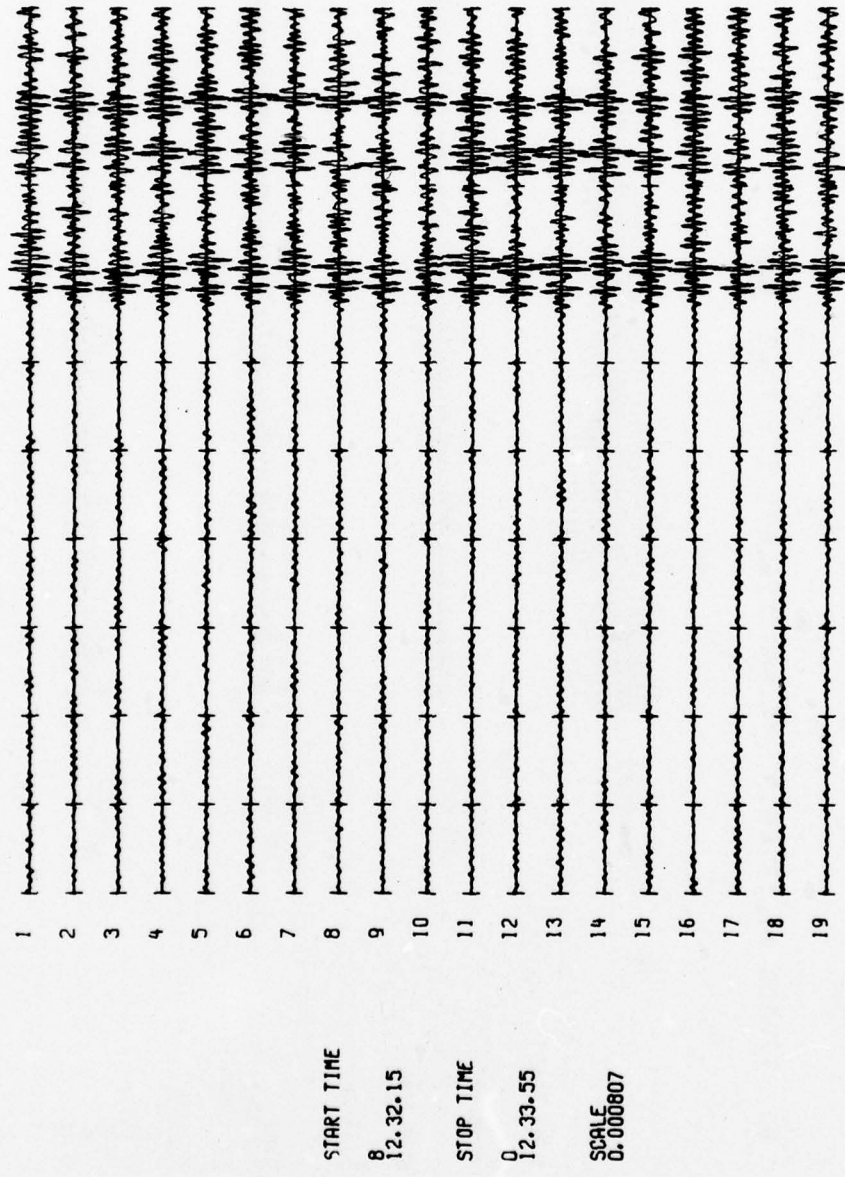
60 770108 11.15.49.3 17.96S 178.62W 571 74.7 4.9



A-61

FIGURE A-60
PROCESSED TRACES FOR EVENT A-60

61 770109 12.24.05.4 5.60S 150.96E 61 48.0 5.3 5.6



A-62

FIGURE A-61
PROCESSED TRACES FOR EVENT A-61

62 770108 21.37.16.0 22.245 170.318 58 71.7 5.1 5.4

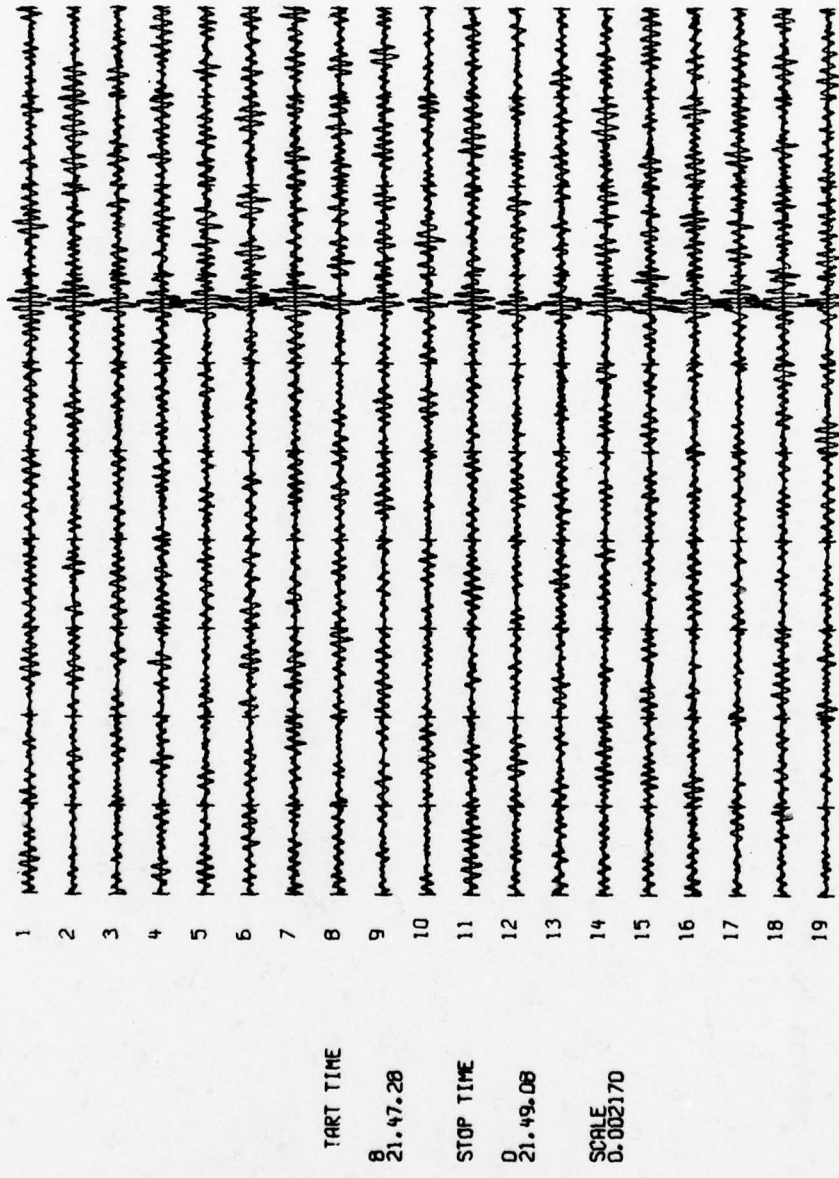
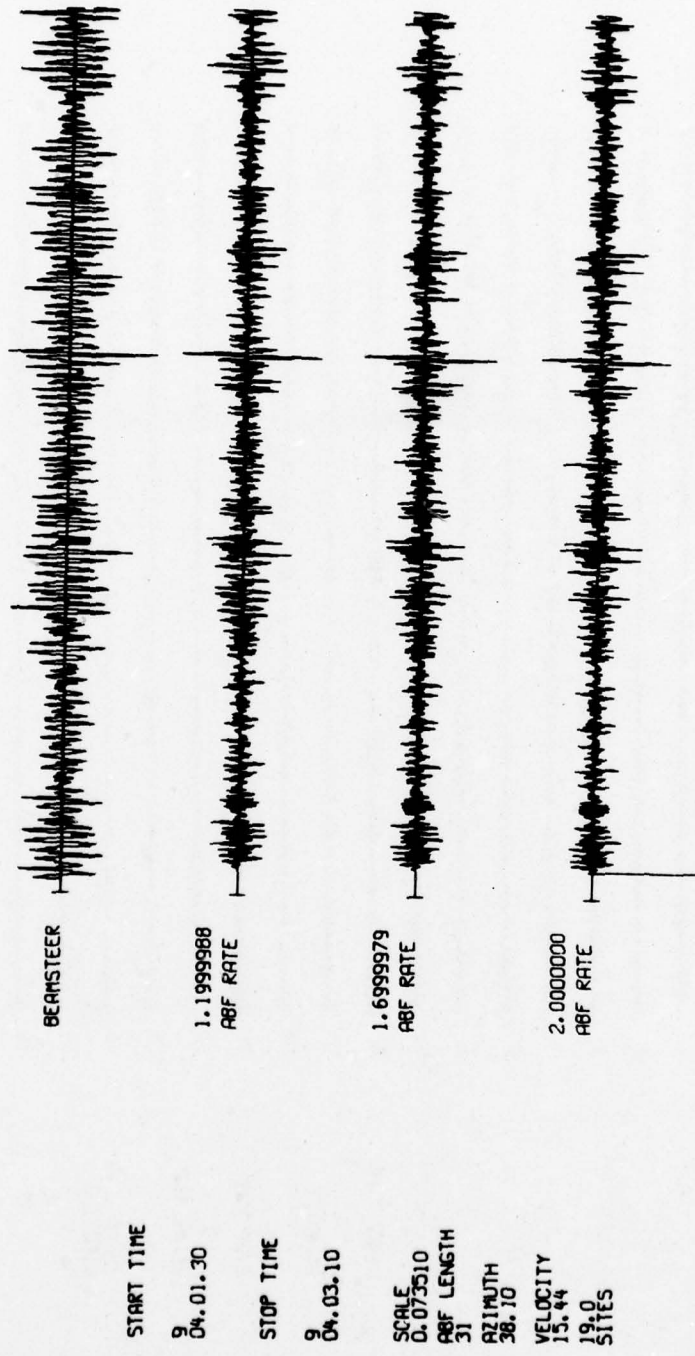


FIGURE A-62
PROCESSED TRACES FOR EVENT A-62

63 770109 3.53.24.6 59.93N 153.36W 132 52.9 4.2

4.1



A-64

FIGURE A-63
PROCESSED TRACES FOR EVENT A-63

64 770109 8.31.13.0 6.19N 146.82E 33 25.7 4.9 5.5

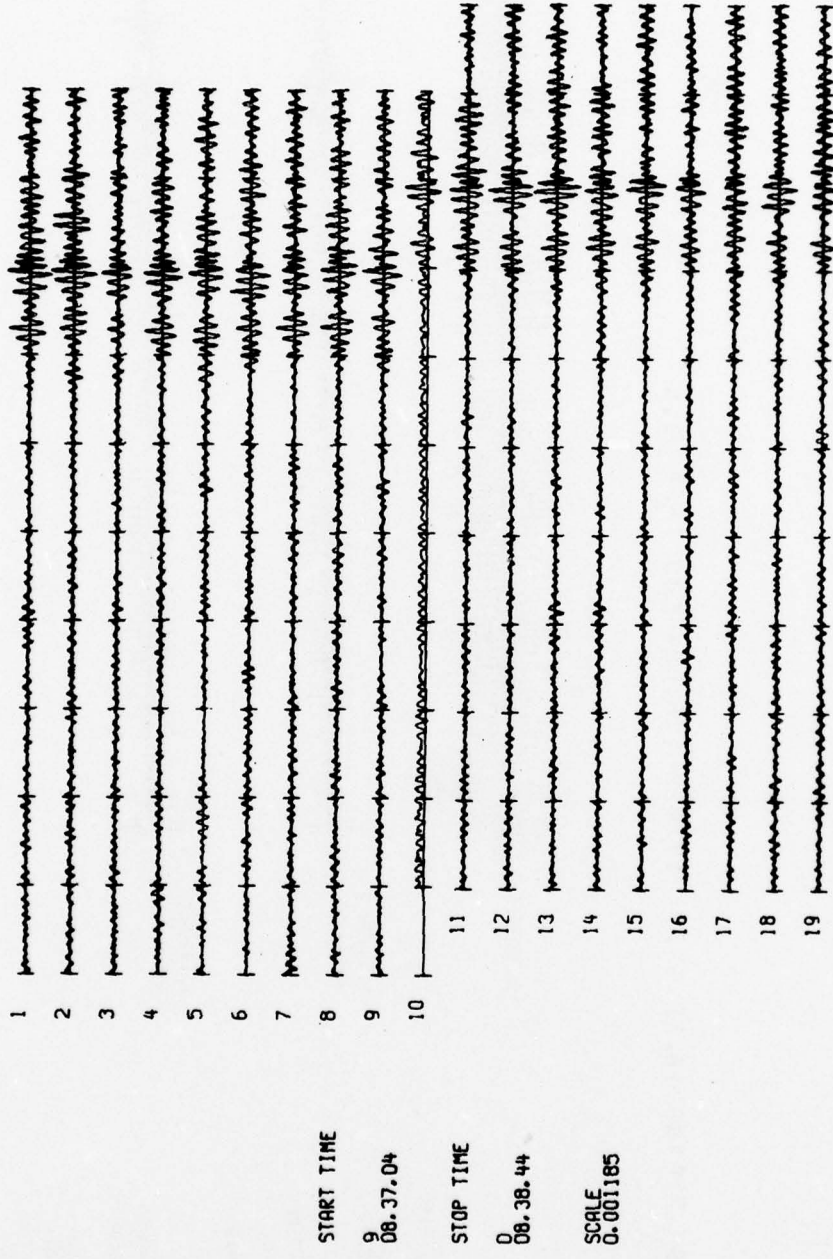
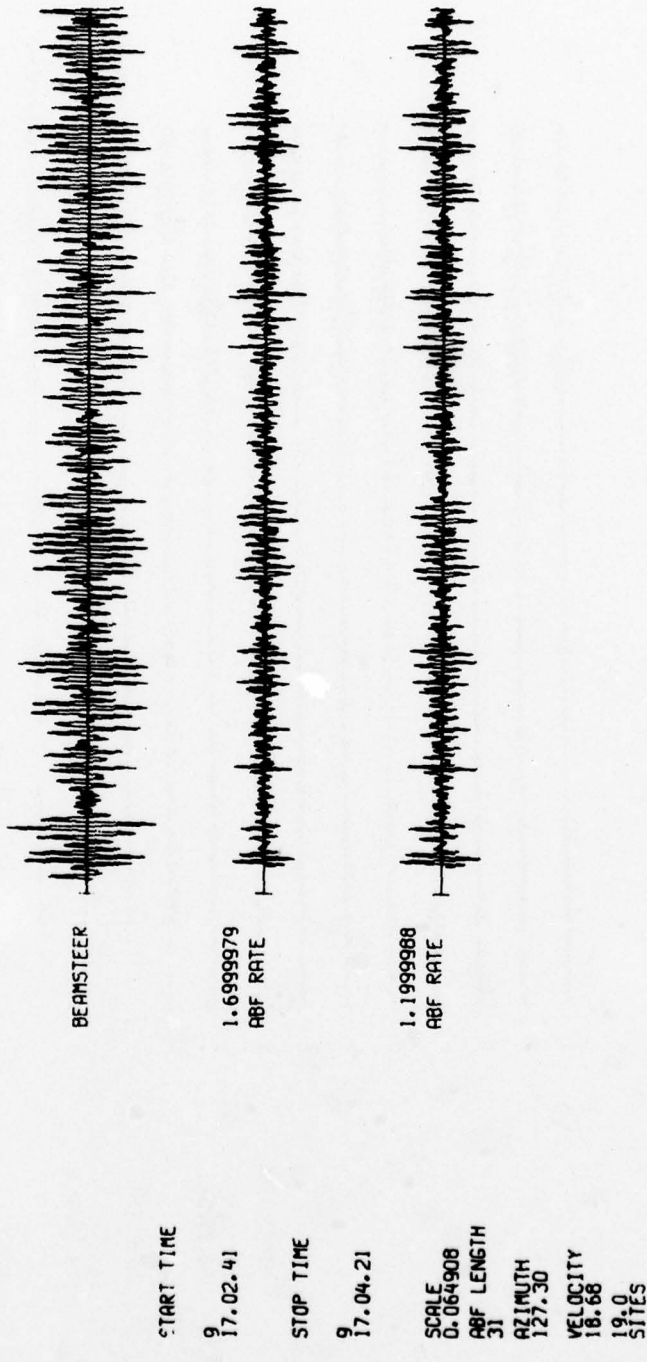


FIGURE A-64
PROCESSED TRACES FOR EVENT A-64

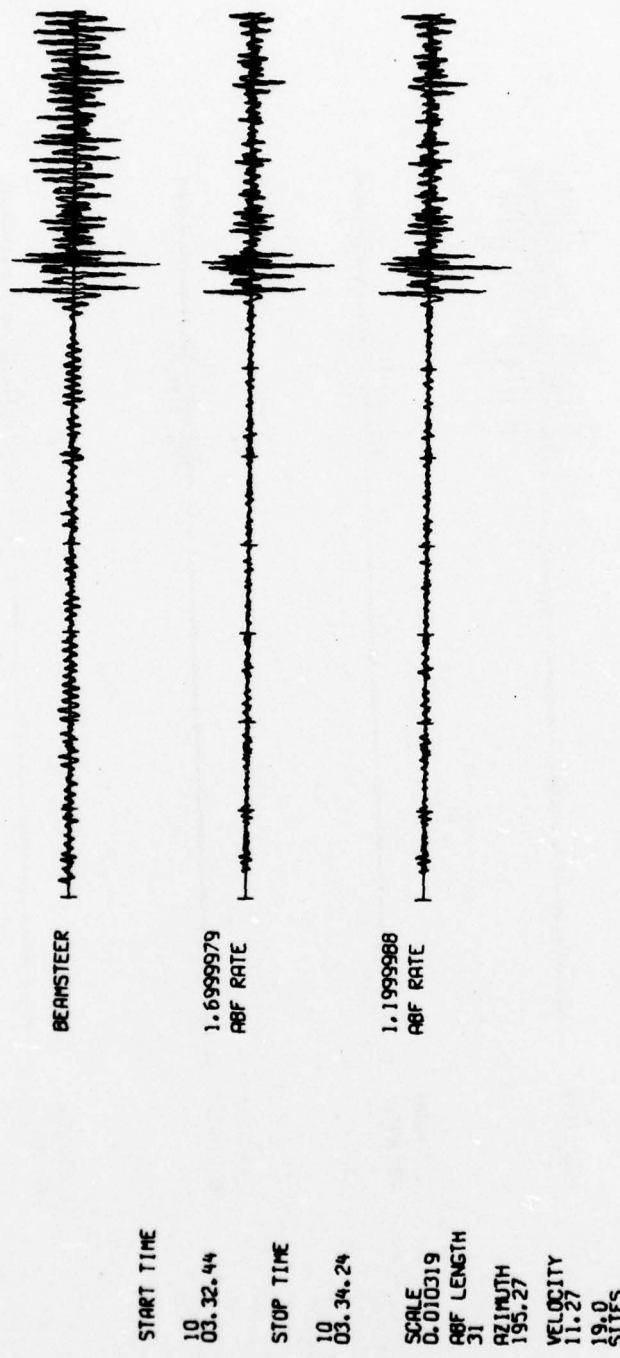
65 770109 16.52.11.2 17.83S 178.52W 589 75.7 4.4



A-66

FIGURE A-65
PROCESSED TRACES FOR EVENT A-65

66 770110 3.28.54.9 15.33N 124.86E 47 22.7 5.0 4.7 4.7



A-67

FIGURE A-66
PROCESSED TRACES FOR EVENT A-66

67 770110 8.19.59.0 8.35N 125.19E 38 29.2 5.4 5.2 5.0

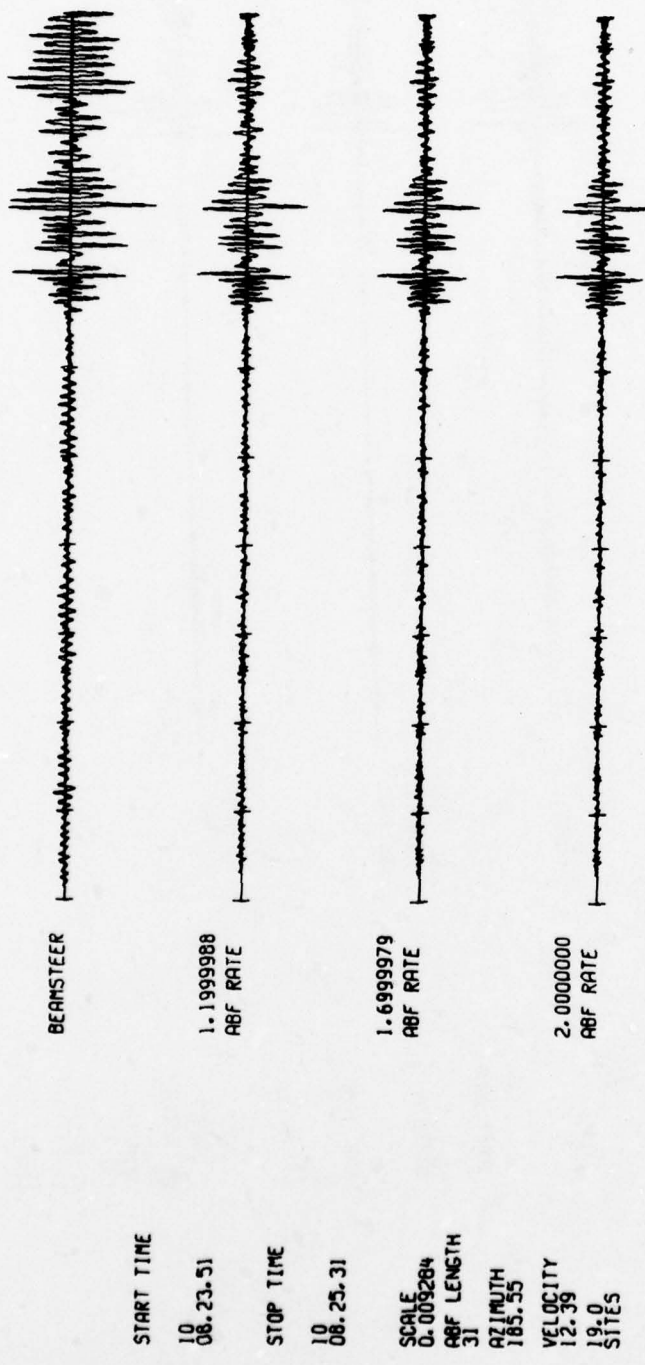
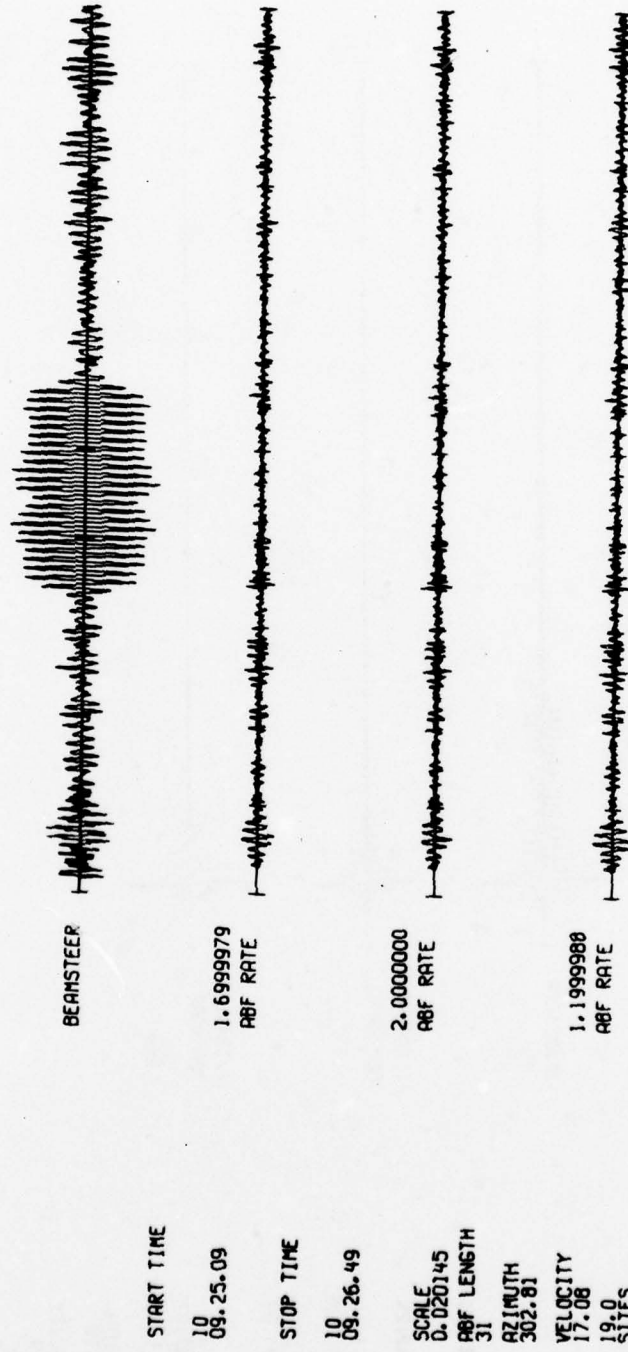


FIGURE A-67
PROCESSED TRACES FOR EVENT A-67

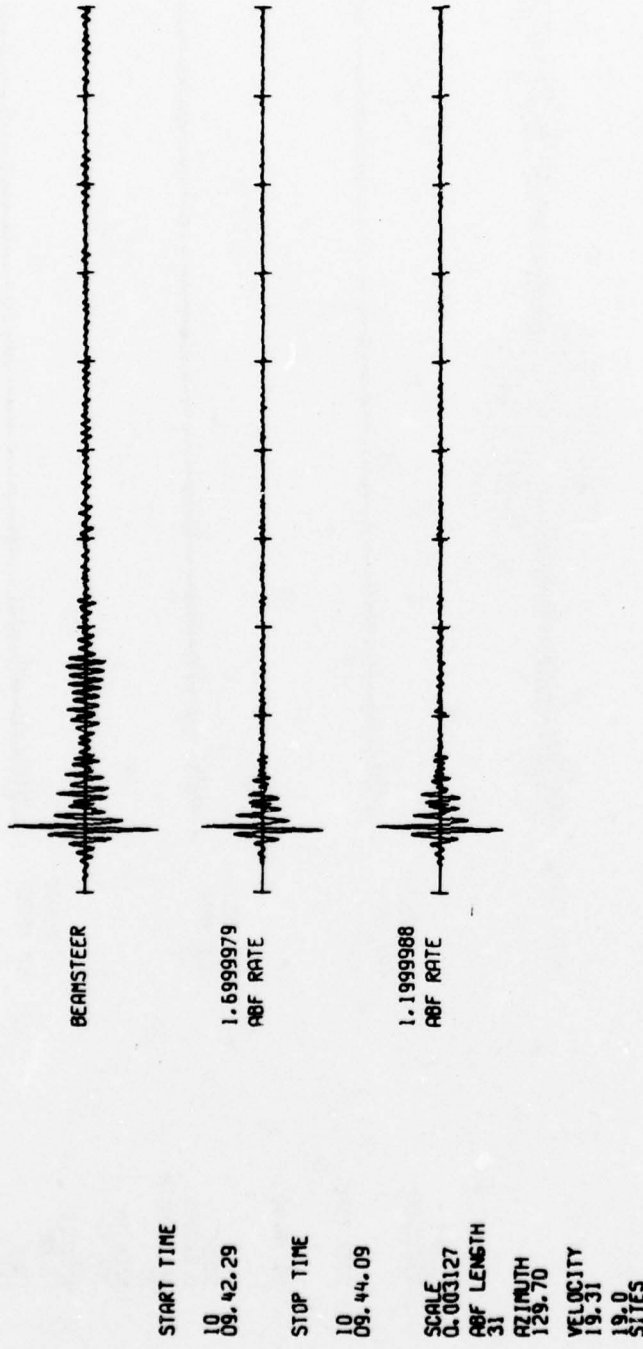
68 770110 9.10.43.6 39.58N 27.40E 4 72.4 4.1



A-69

FIGURE A-68
PROCESSED TRACES FOR EVENT A-68

69 770110 9.31.49.9 20.72S 179.75W 653 76.4 5.5 4.6 4.4



A-70

FIGURE A-69
PROCESSED TRACES FOR EVENT A-69

79 770110 20.40. 3.0 7.04S 154.70E 52 51.0 5.0 4.9 4.8

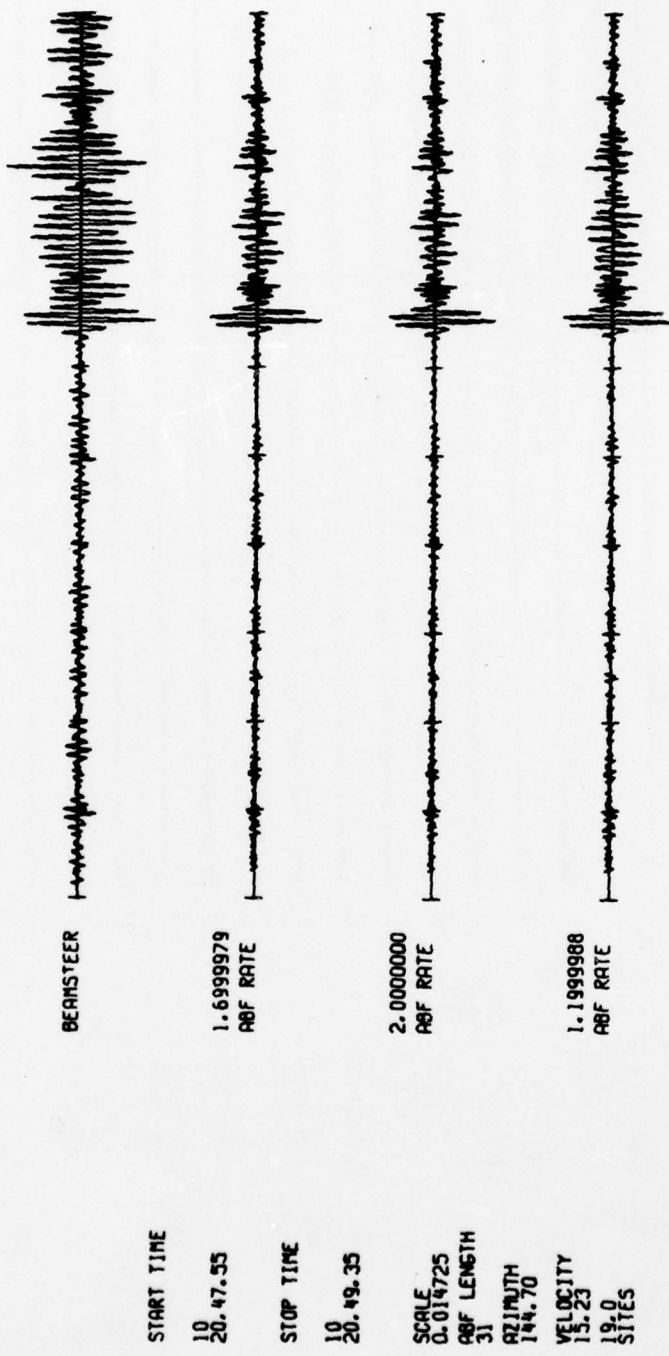
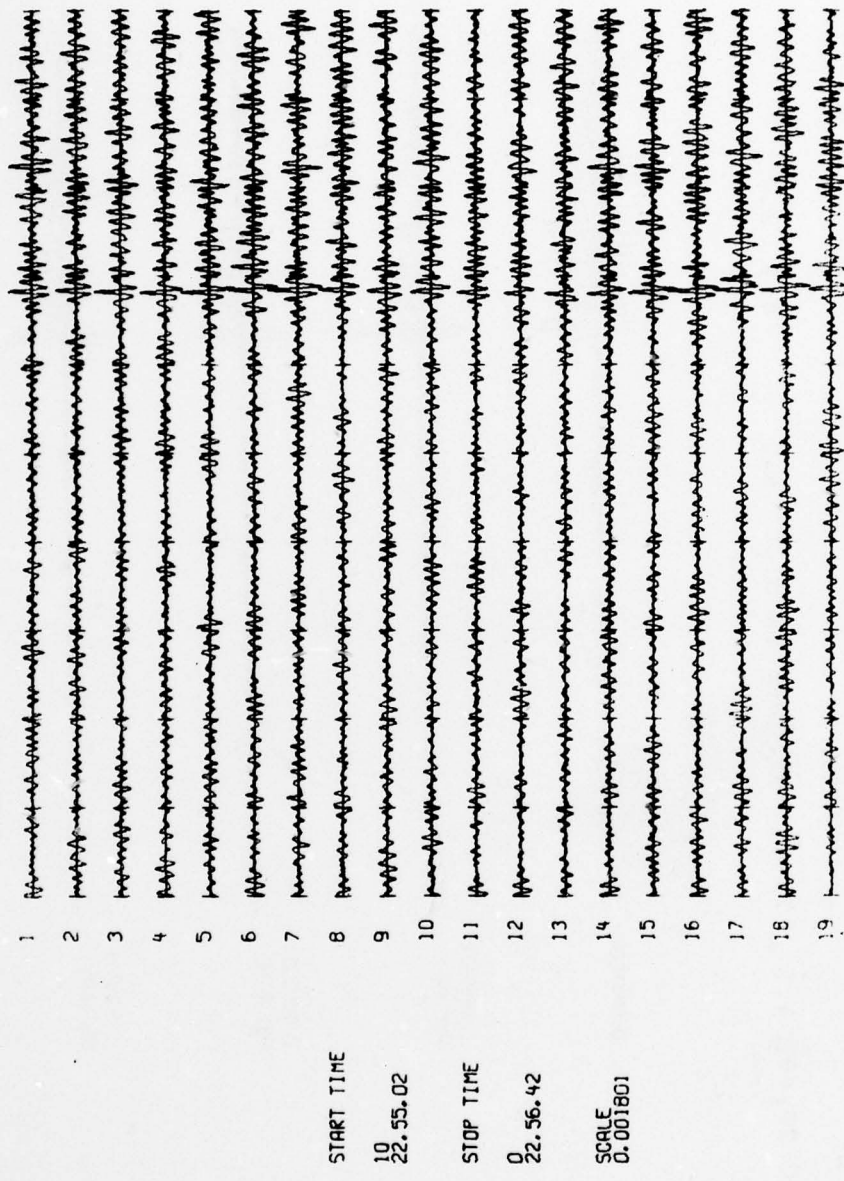


FIGURE A-70

PROCESSED TRACES FOR EVENT A-70

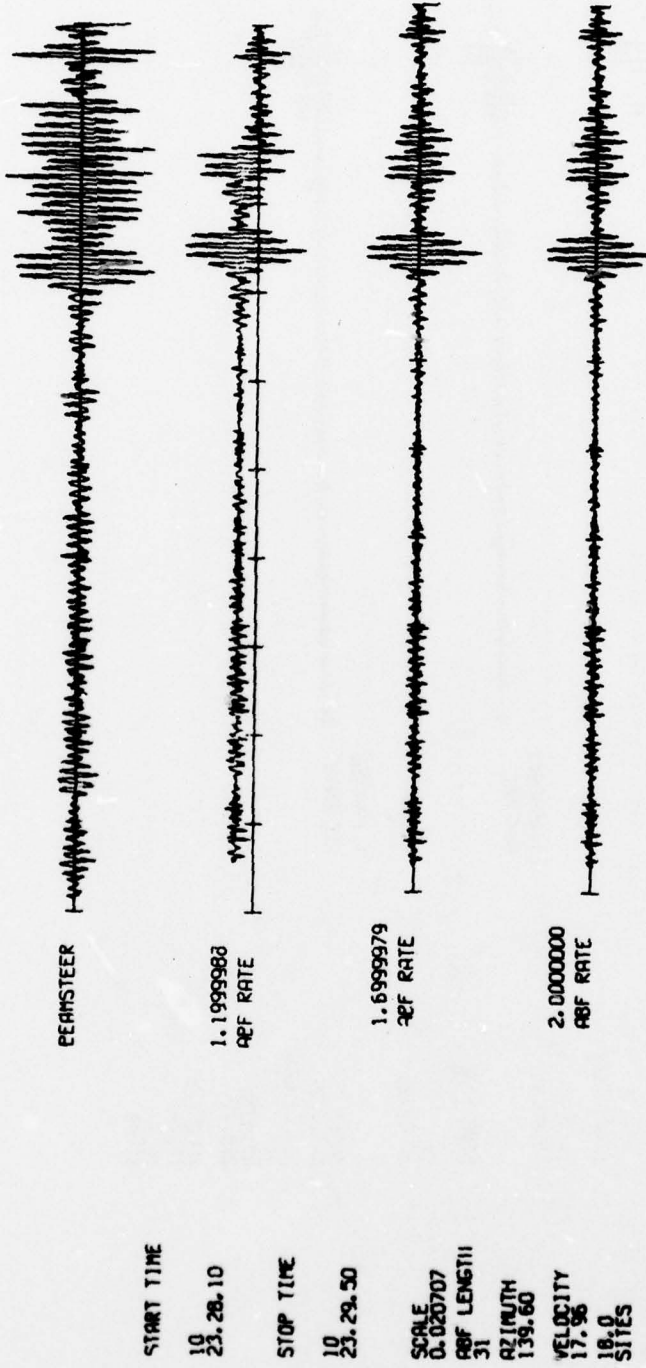
71 770110 22.43.43.0 28.415 176.748 33 93.7 4.6 5.5



A-72

FIGURE A-71
PROCESSED TRACES FOR EVENT A-71

72 770110 23.18. 7.0 21.495 168.667 16 70.2 5.2 5.0 8.9



A-73

FIGURE A-72
PROCESSED TRACES FOR EVENT A-72

73 770111 14.51. 5.0 12.93N 57.45E 33 66.8 5.1 4.7 4.3

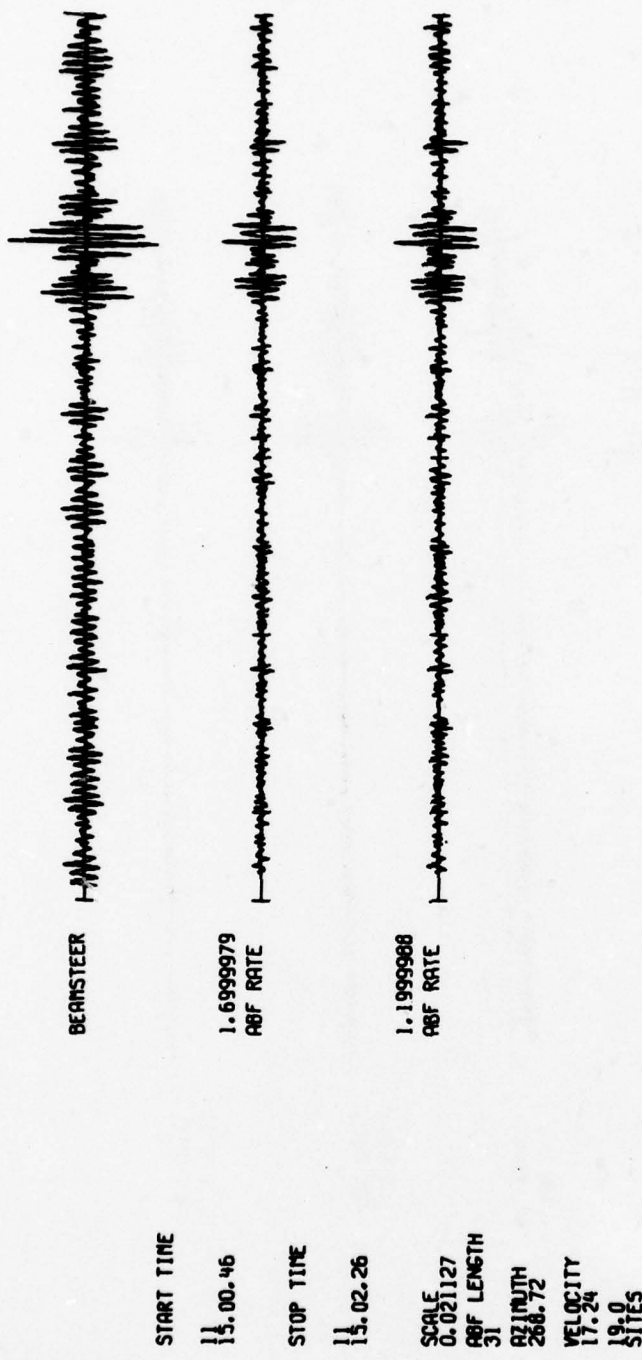
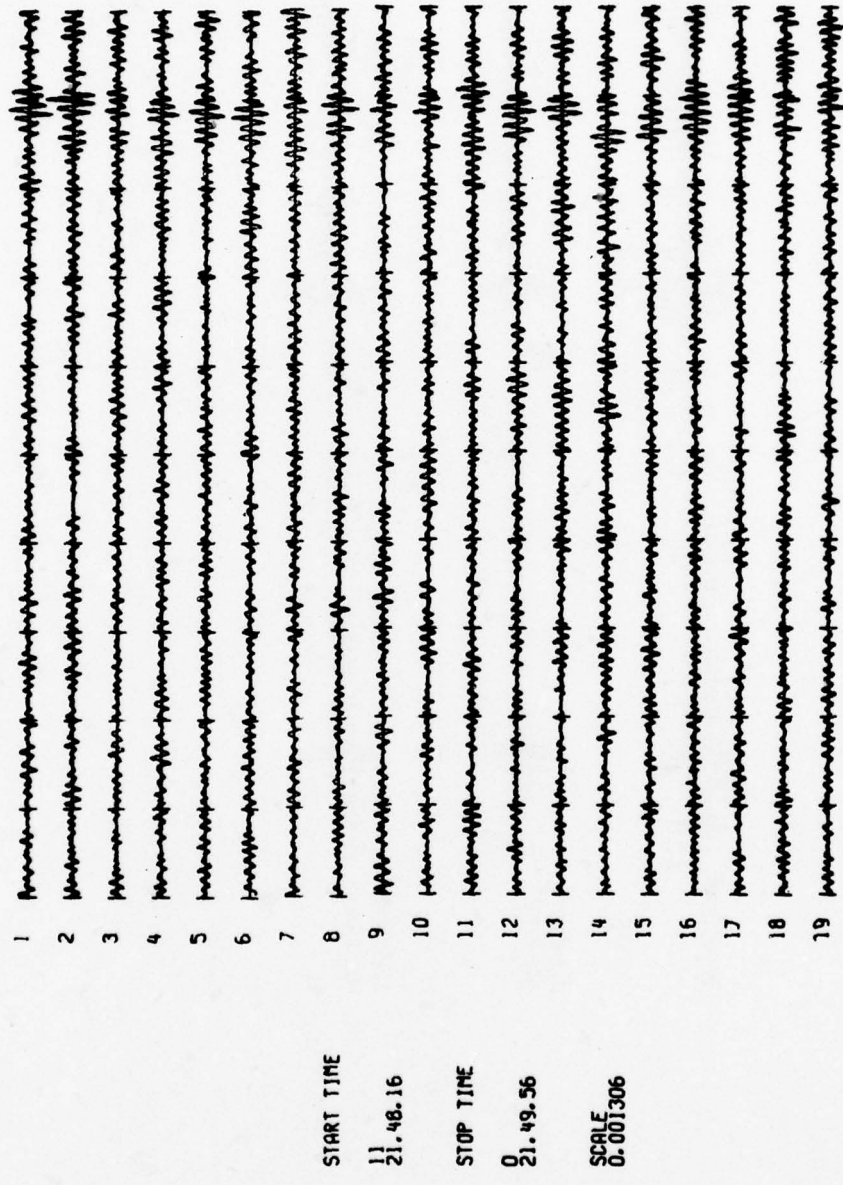


FIGURE A-73
PROCESSED TRACES FOR EVENT A-73

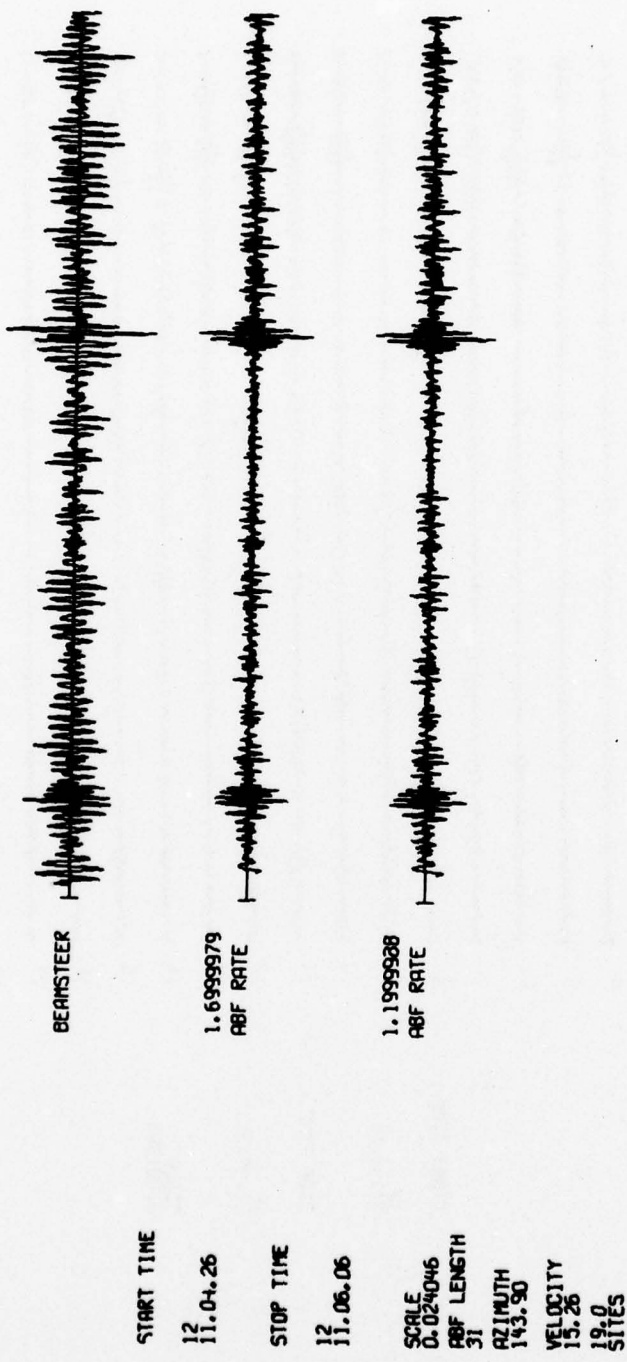
74 770111 21.49.26.3 5.36S 133.87E 33 43.1 5.1 5.4



A-75

FIGURE A-74
PROCESSED TRACES FOR EVENT A-74

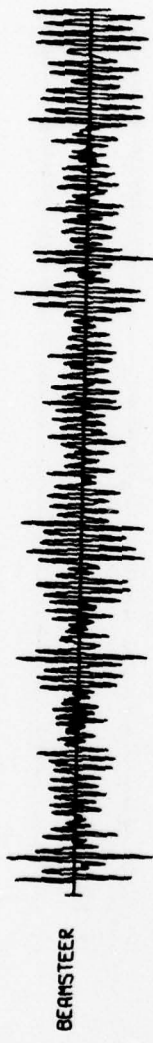
75 770112 10.56.32.6 6.91S 155.34E 192 51.2 4.6 4.6 4.5



A-76

FIGURE A-75
PROCESSED TRACES FOR EVENT A-75

76 770112 13. 5.59.3 19.40N 155.29W 16 6P.2 3.9



START TIME

12
13.15.49

SCALE
1.6999979
ABF RATE

STOP TIME
12
13.17.29

SCALE
0.01,62/
ABF LENGTH
31
AZIMUTH
61.10
VELOCITY
17.32
sites

A-77

FIGURE A-76
PROCESSED TRACES FOR EVENT A-76

77 770112 17.43.33.4 28.22N 102.59E 33 23.1 5.1 5.5

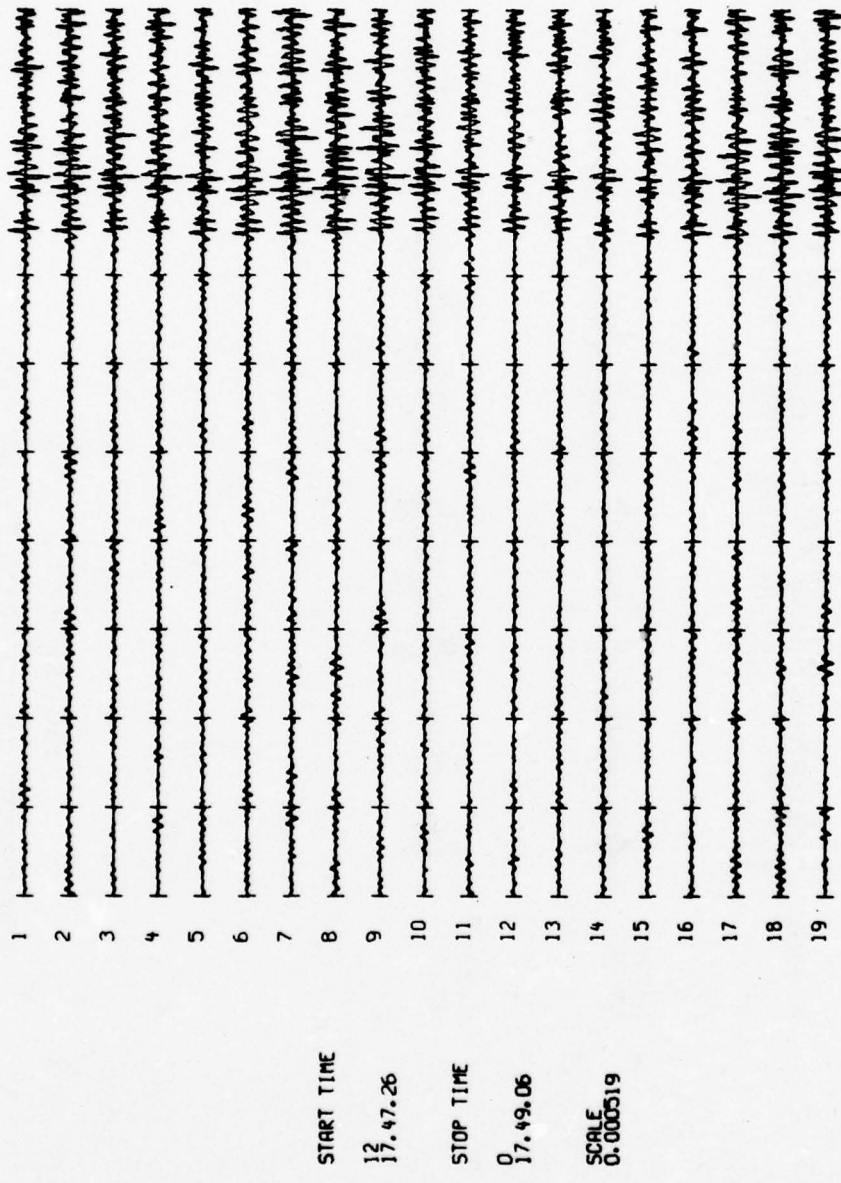


FIGURE A-77
PROCESSED TRACES FOR EVENT A-77

78 770112 23.35.19.1 1.58X 99.868 178 44.1 5.6 5.9

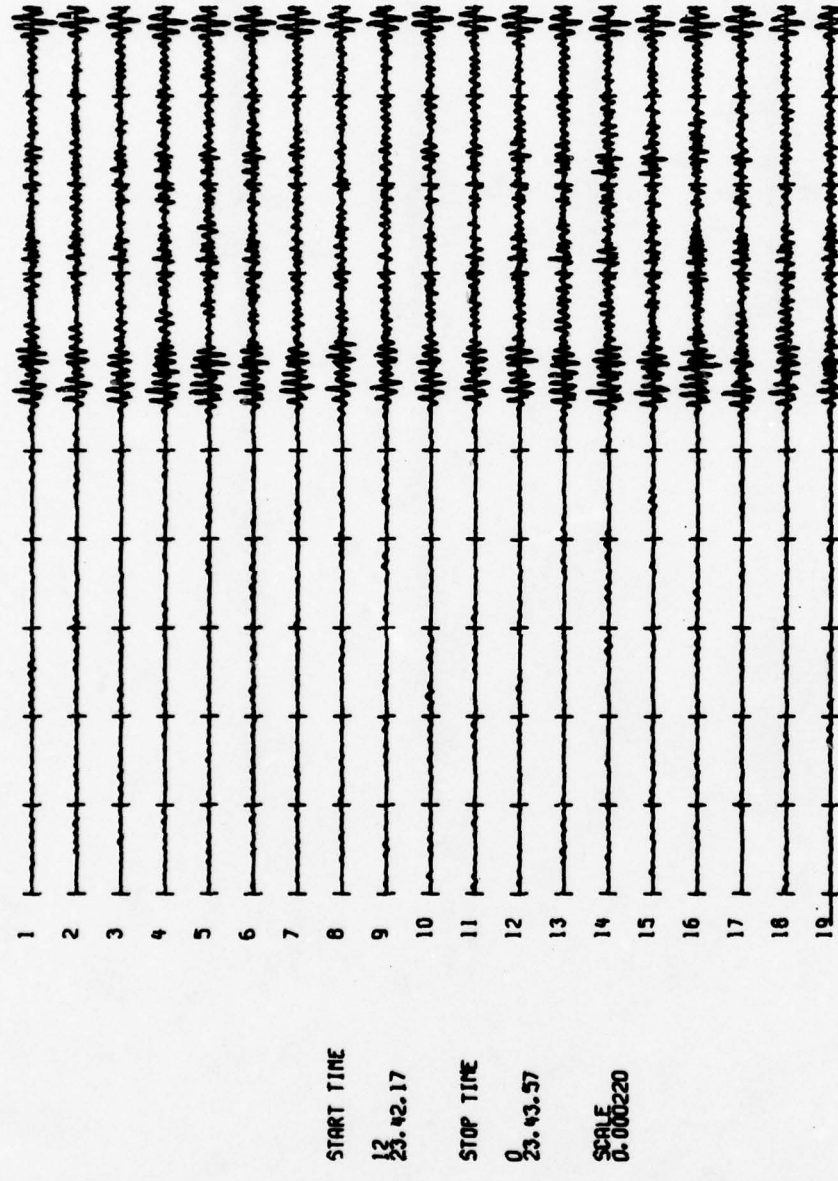
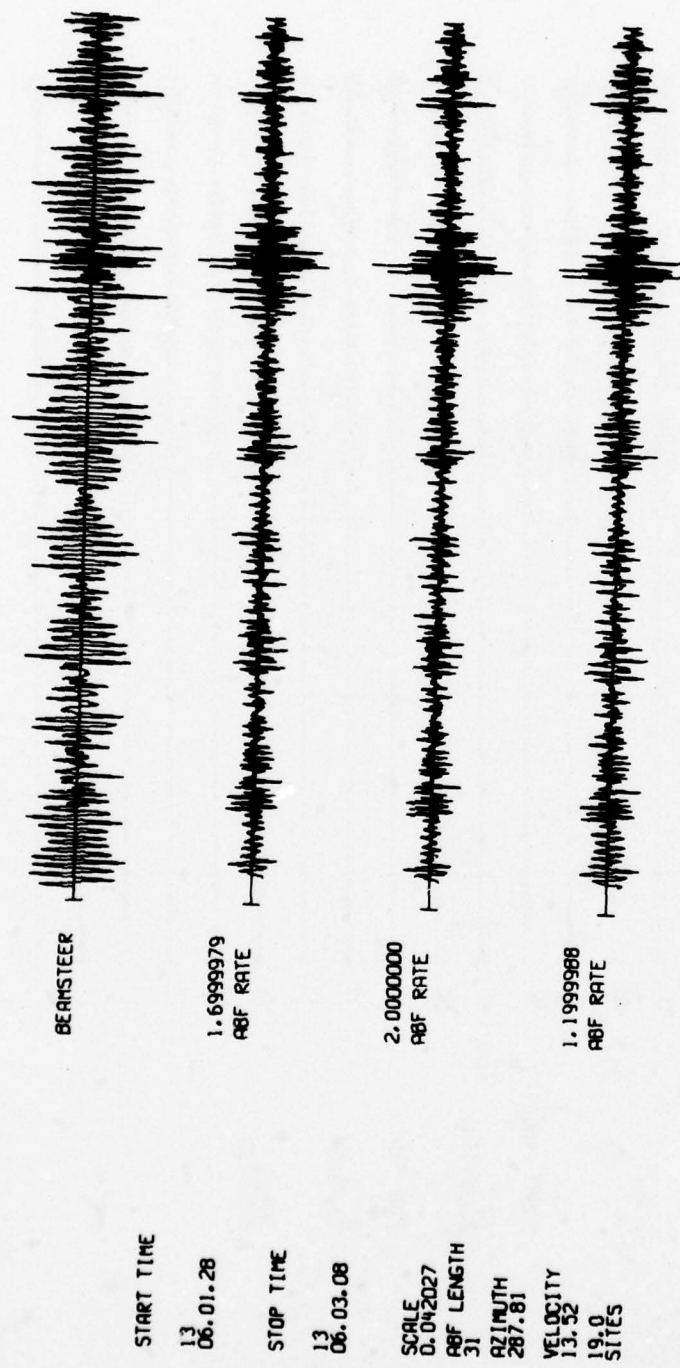


FIGURE A-78
PROCESSED TRACES FOR EVENT A-78

70 770113 5.54.59.0 39.34N 75.97E 33 40.5 5.0 4.4



A-80

FIGURE A-79
PROCESSED TRACES FOR EVENT A-79

90 770113 9.13. 6.1 03.55N 17.10E 20 77.7 5.3 5.7

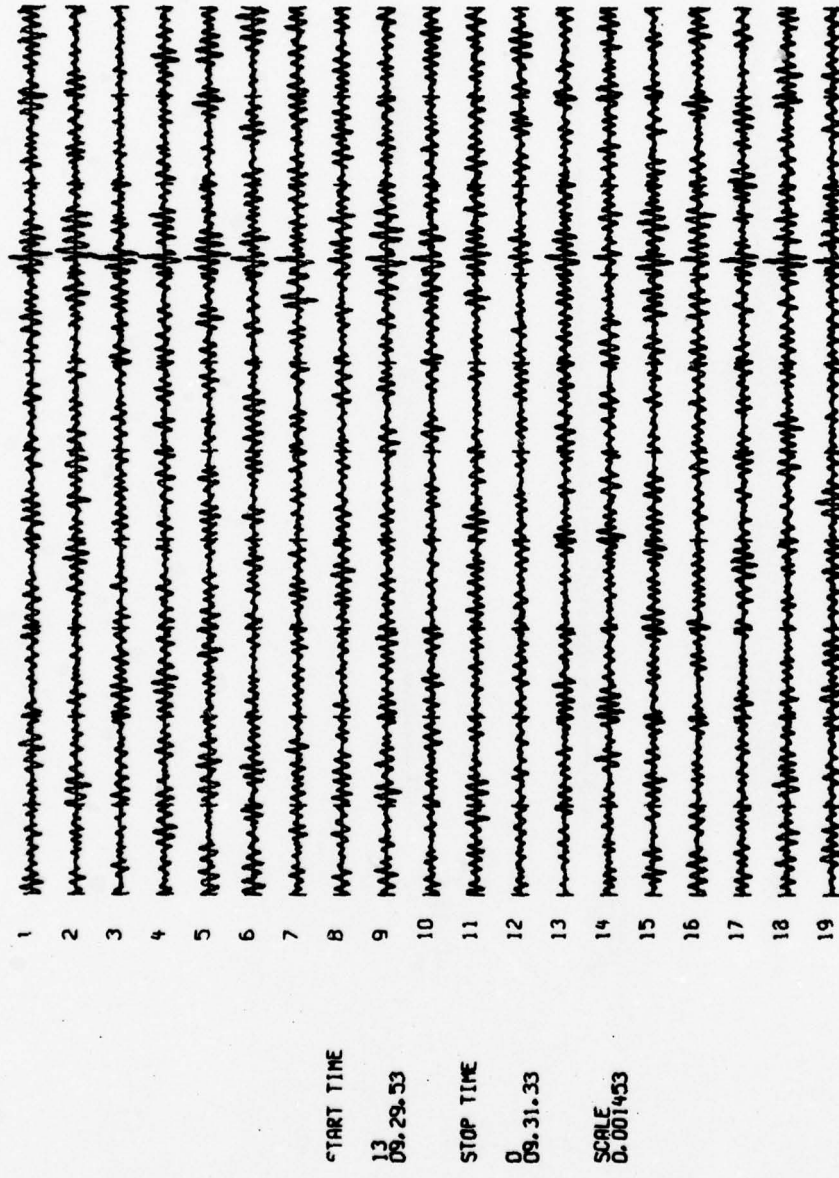
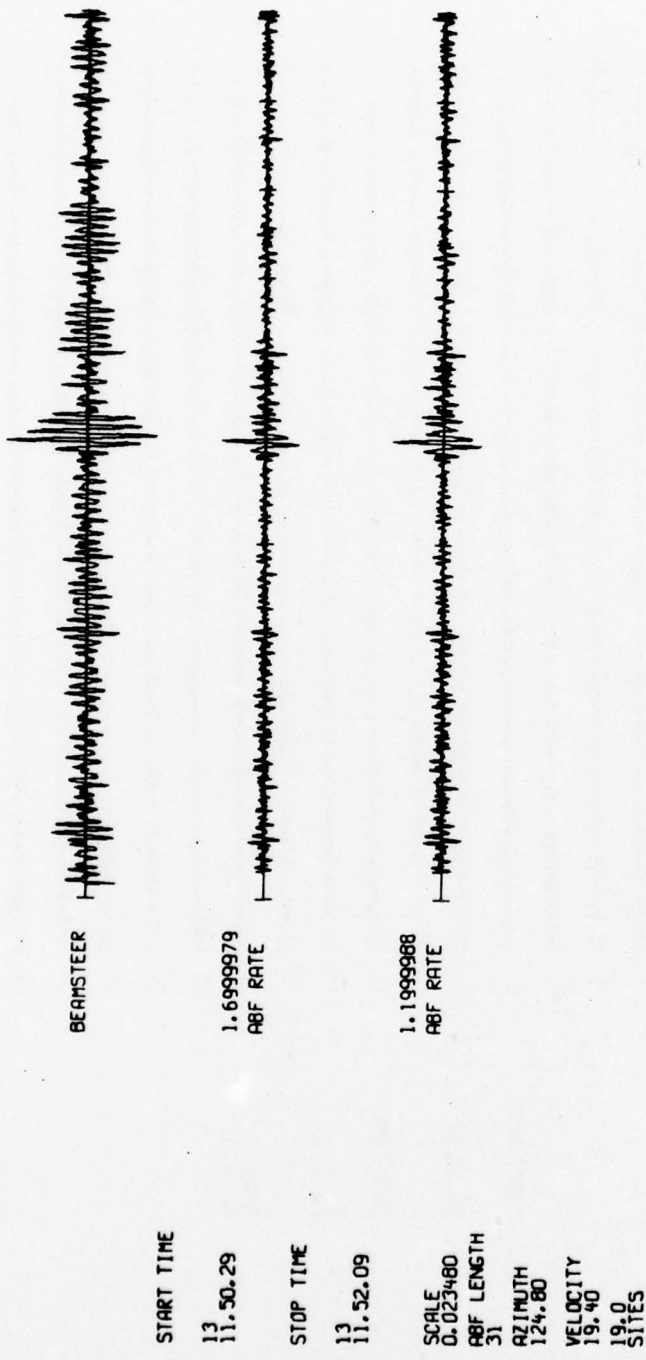


FIGURE A-80

PROCESSED TRACES FOR EVENT A-80

81 770113 11.39.16.8 -7.82S 175.19W 199 76.8 4.4 4.6 4.3



A-82

FIGURE A-81
PROCESSED TRACES FOR EVENT A-81

92 770113 14.27.38.4 2.05N 125.08E 156 35.4 5.1 4.8 4.8

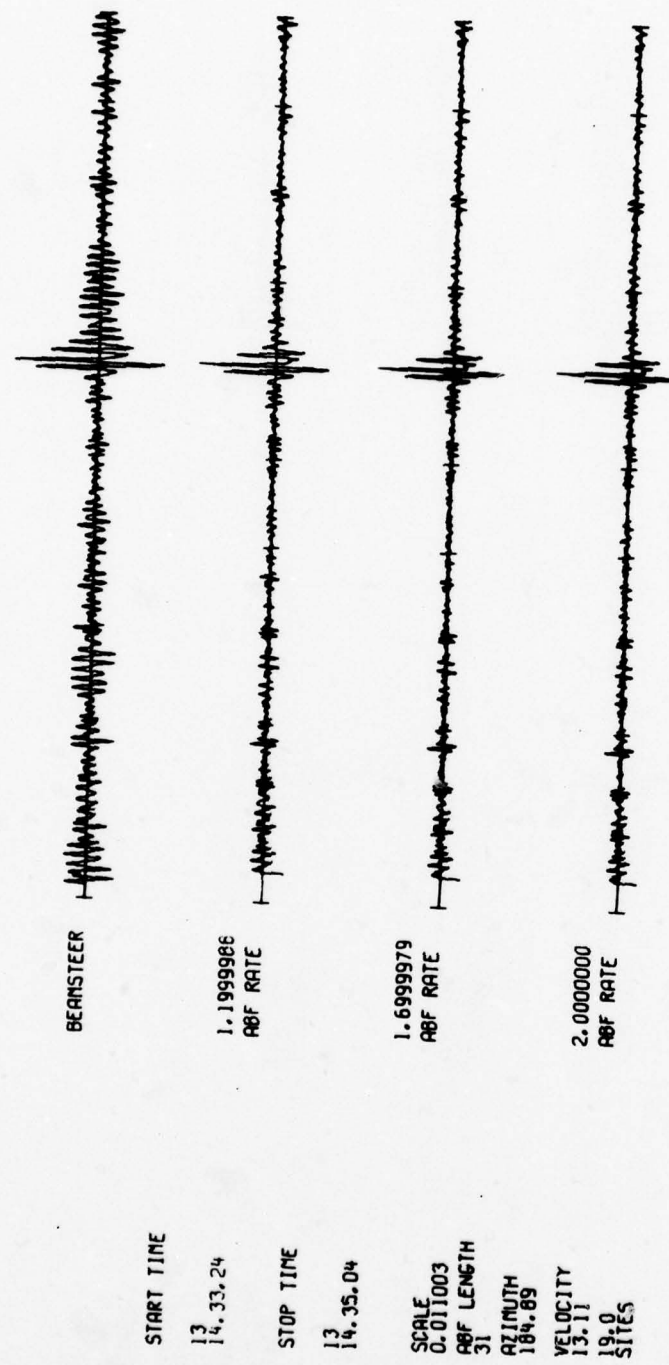
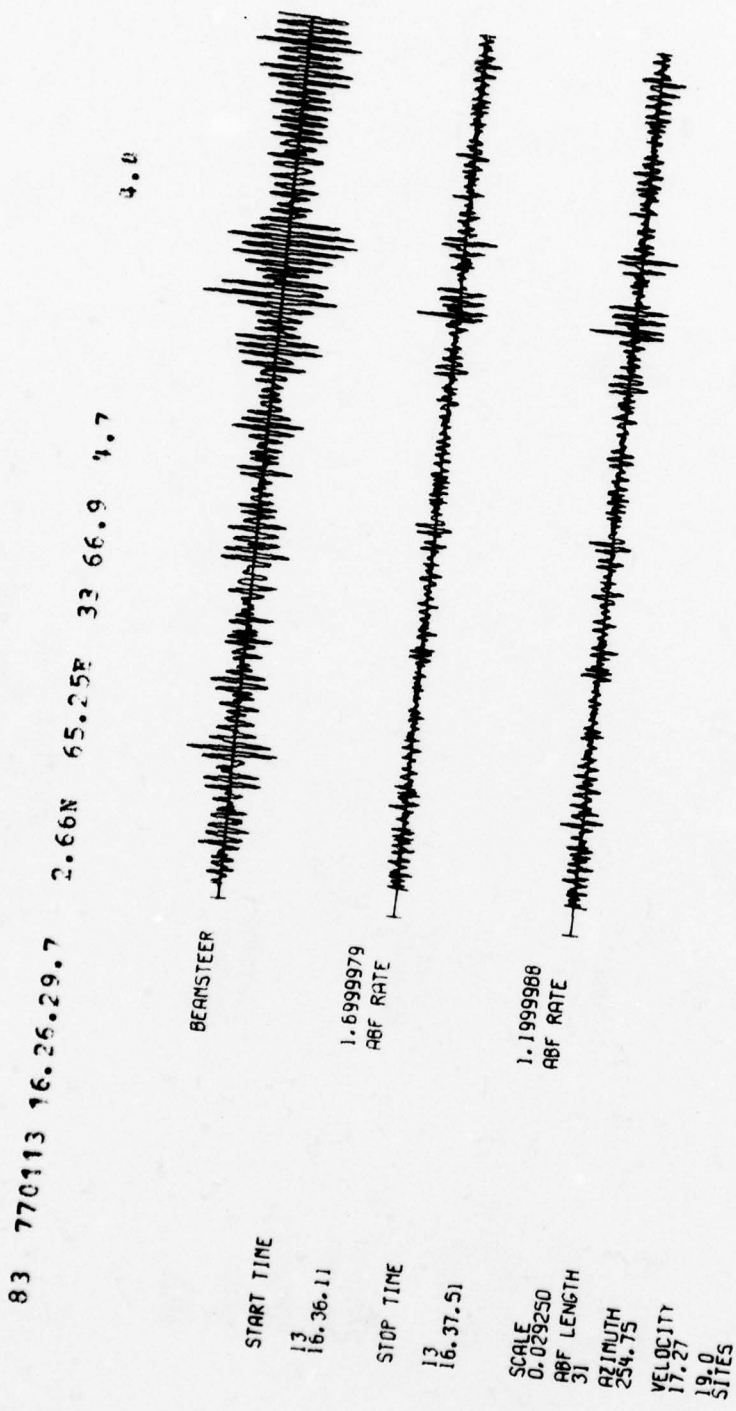


FIGURE A-82

PROCESSED TRACES FOR EVENT A-82



A-84

FIGURE A-83
PROCESSED TRACES FOR EVENT A-83

84 770113 21.06.16.7 54.06N 175.03E 51 35.3 5.0 5.0

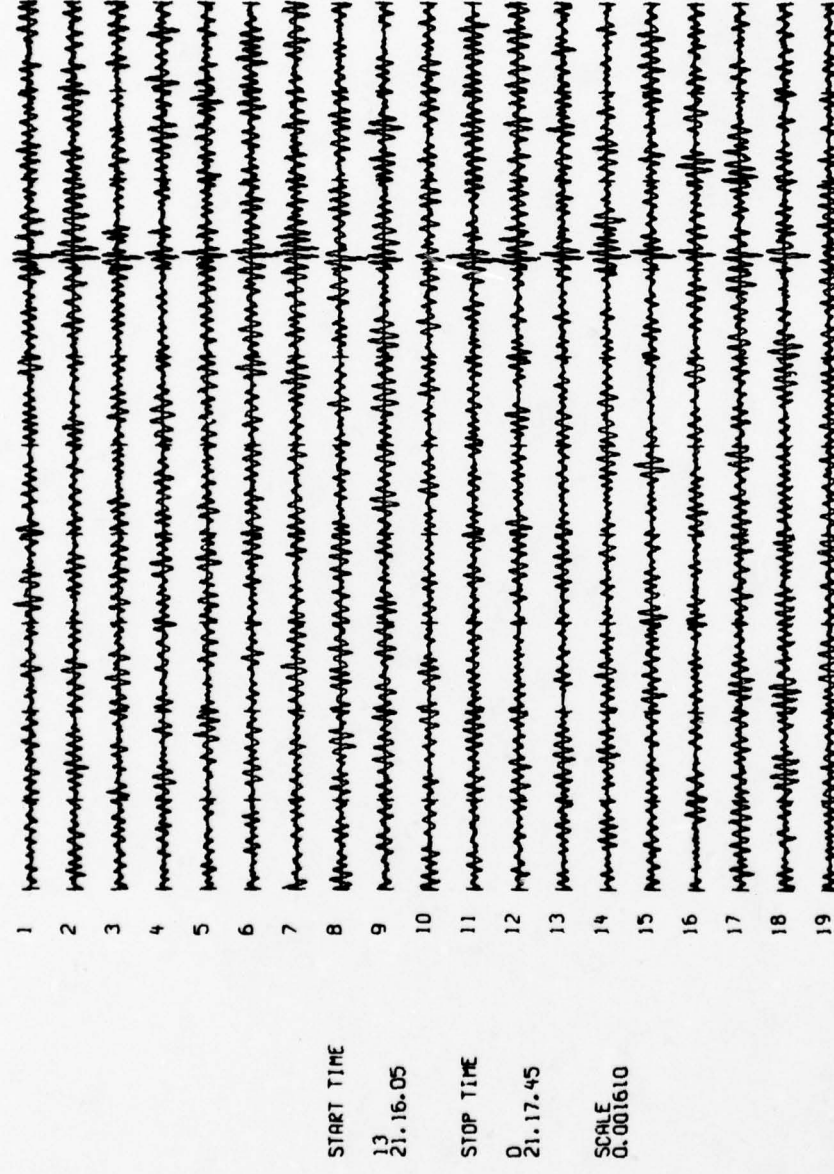
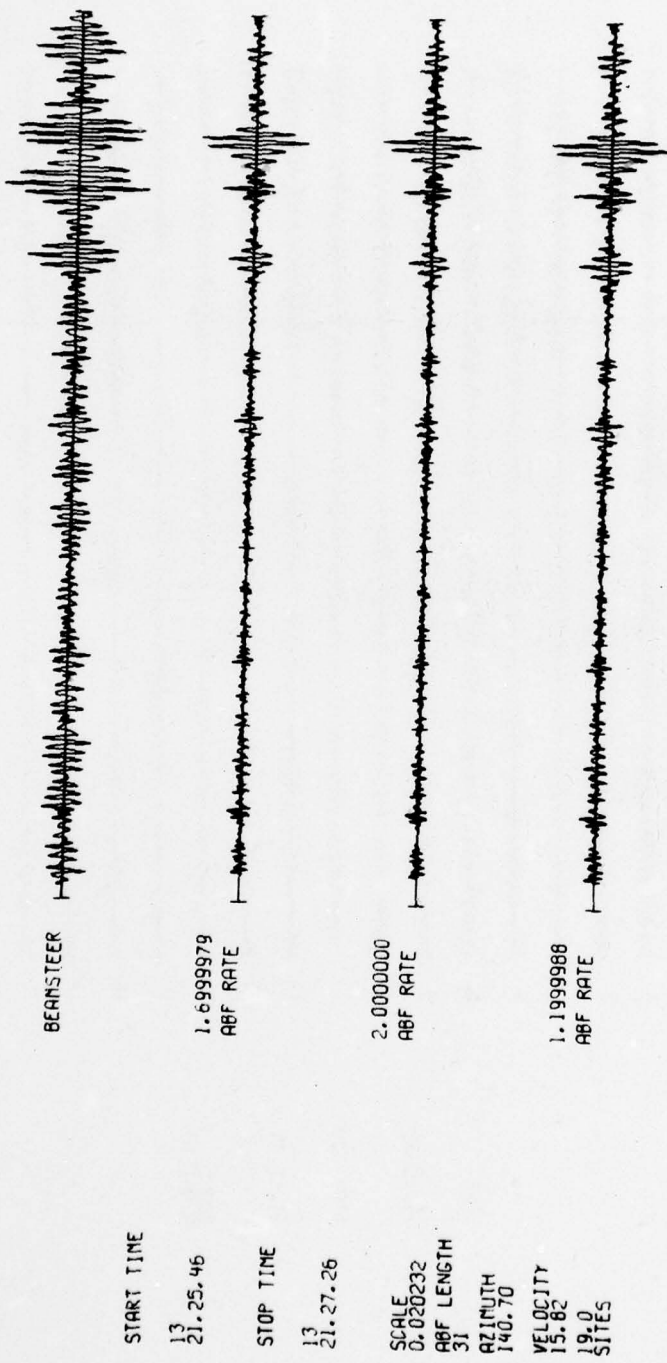


FIGURE A-84

PROCESSED TRACES FOR EVENT A-84

85 770113 21.17. 3.5 11.58S 161.00E 33 58.0 4.2 4.5



A-86

FIGURE A-85
PROCESSED TRACES FOR EVENT A-85

96 770113 22. 5.59.3 59.03N 102.23W 33 58.4 4.5

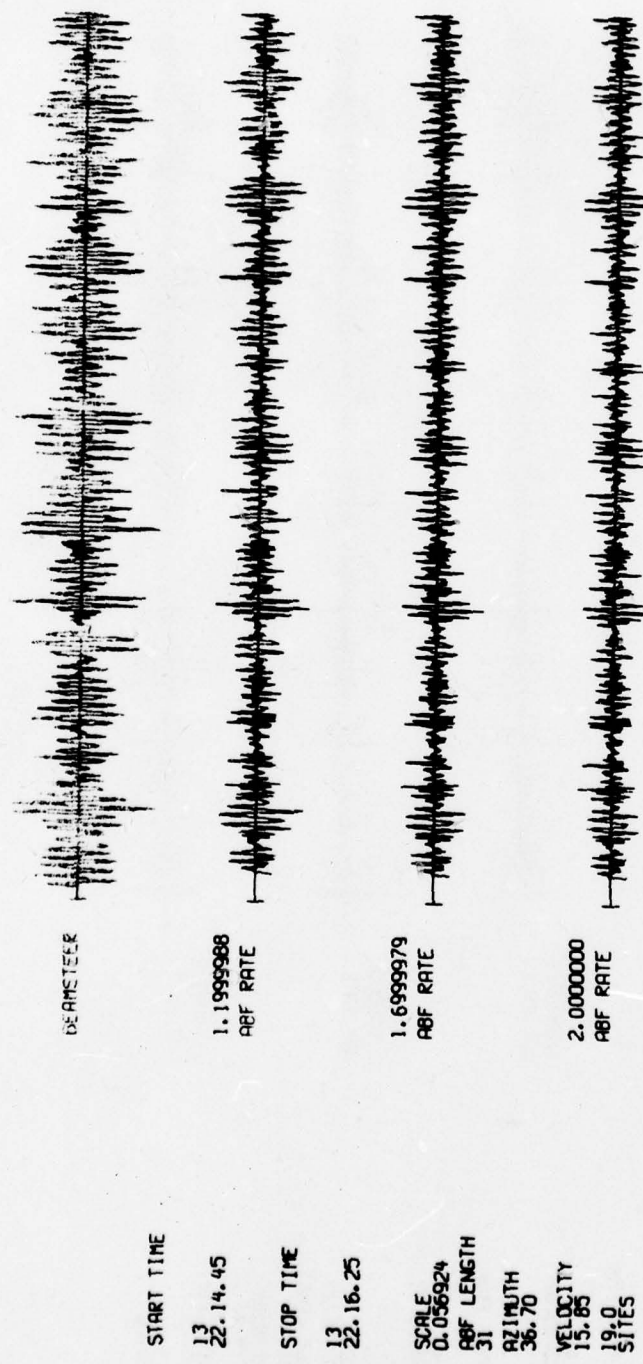
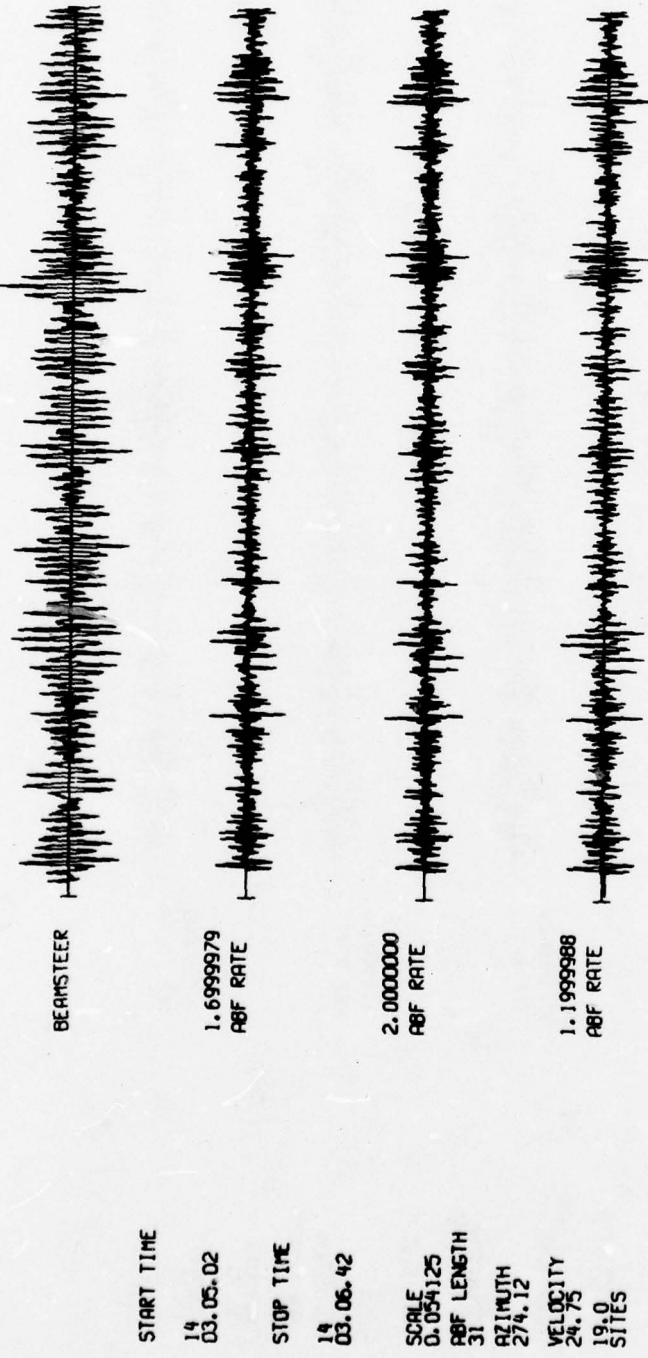


FIGURE A-86
PROCESSED TRACES FOR EVENT A-86

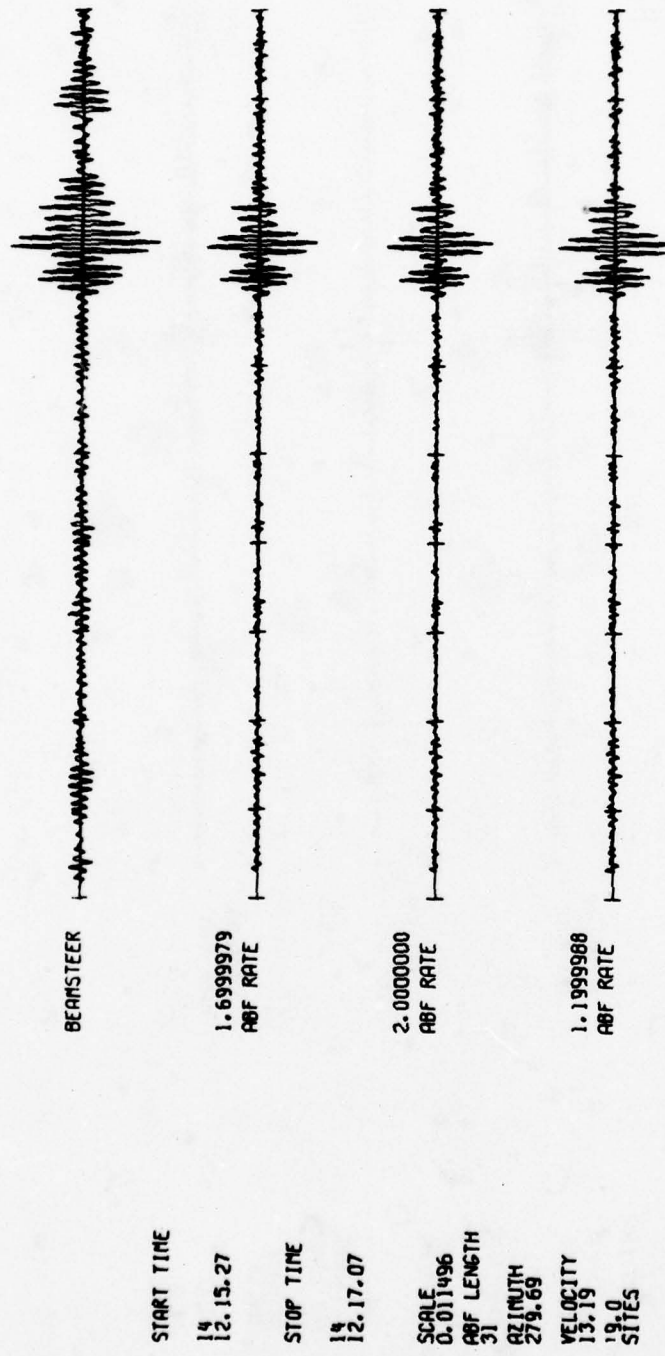
97 770111 2.52.34.7 1.715 28.95E 33 99.1 4.9



A-88

FIGURE A-87
PROCESSED TRACES FOR EVENT A-87

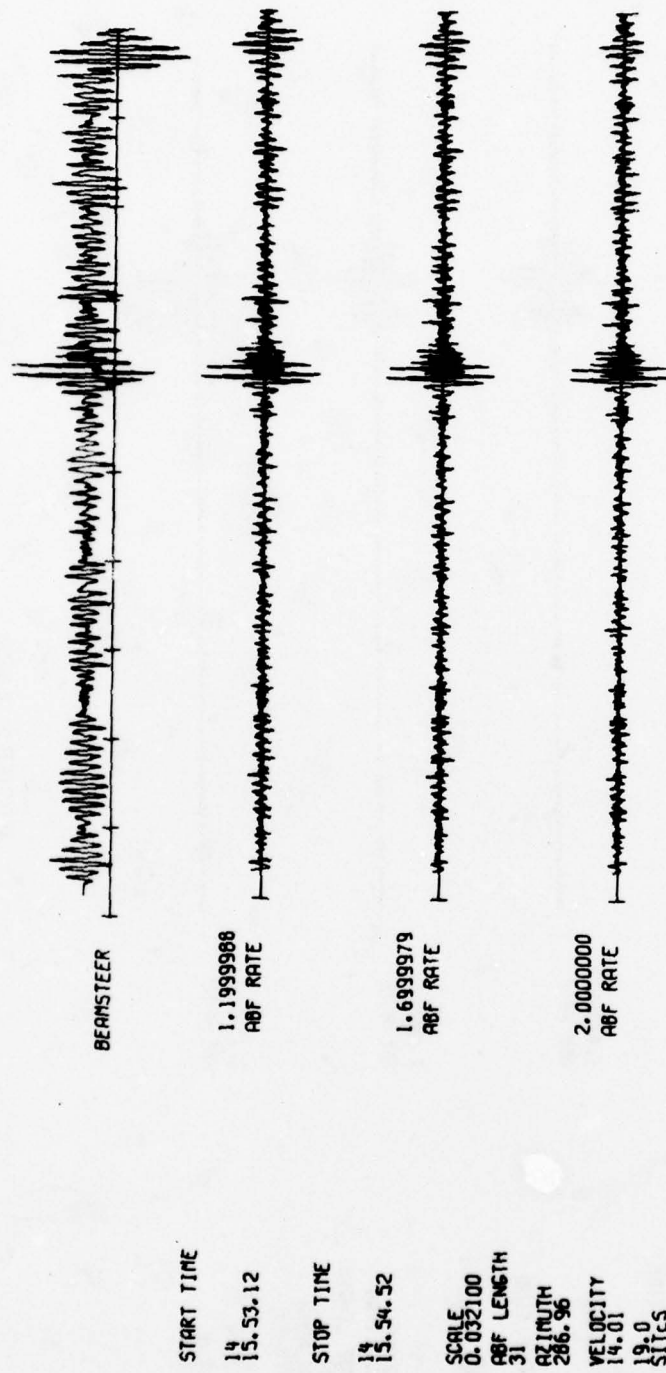
88 770114 12. 9.33.1 34.70N 82.71E 33 36.3 4.7 4.8 4.7



A-89

FIGURE A-88
PROCESSED TRACES FOR EVENT A-88

39 770114 15.46.11.1 36.61N 71.01E 149 04.5 1.9 11.4 4.3



A-90

FIGURE A-89
PROCESSED TRACES FOR EVENT A-89

90 770114 17.58.35.2 19.805 177.544 350 76.8 5.2 5.4

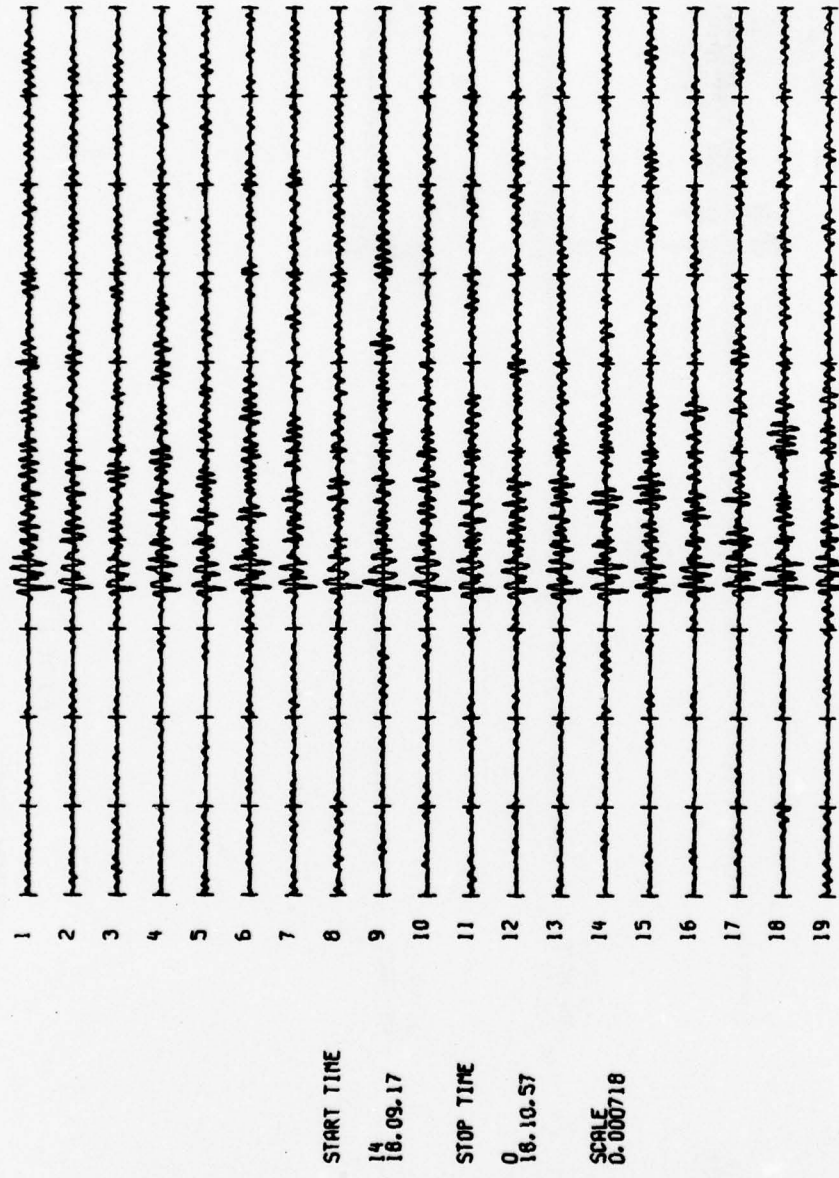
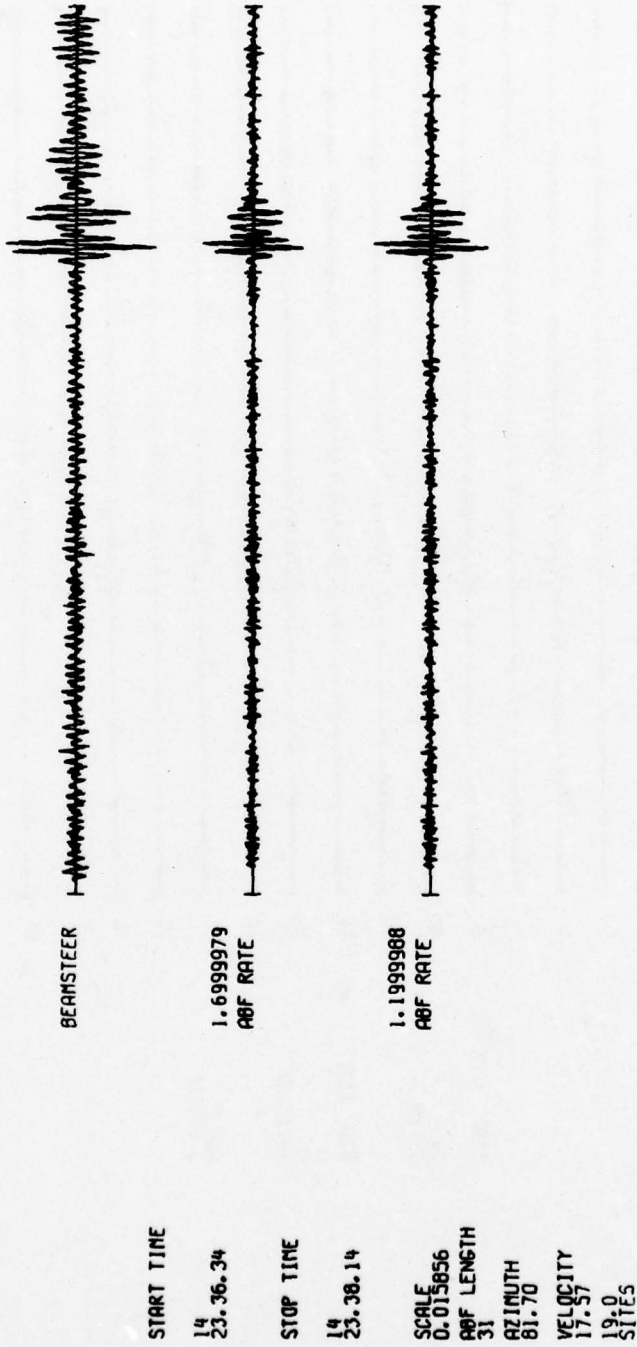


FIGURE A-90

PROCESSED TRACES FOR EVENT A-90

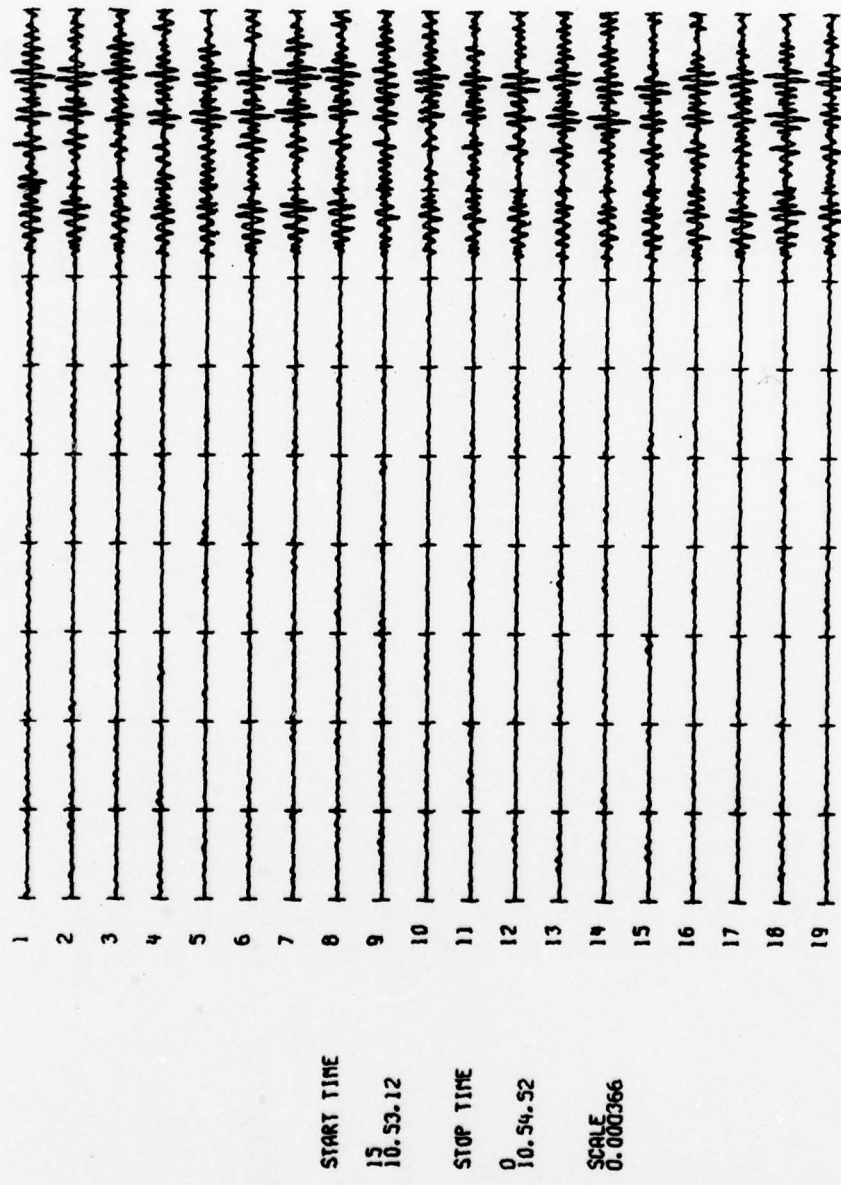
91 770114 23.26.42.5 19.30N 155.10W 10 59.4 4.2 5.2 5.0



A-92

FIGURE A-91
PROCESSED TRACES FOR EVENT A-91

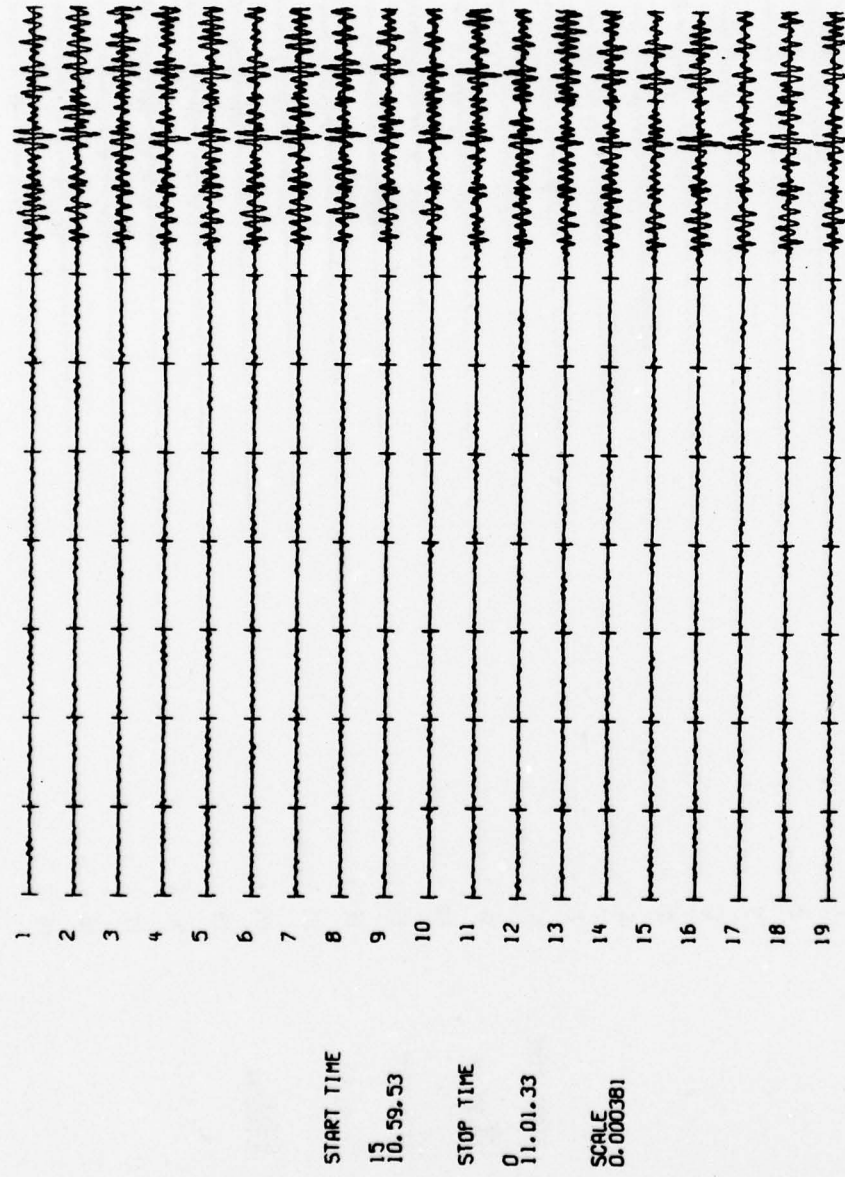
92 770115 10.49.5.0 12.96N 125.96E 33 24.5 5.6 5.5



A-93

FIGURE A-92
PROCESSED TRACES FOR EVENT A-92

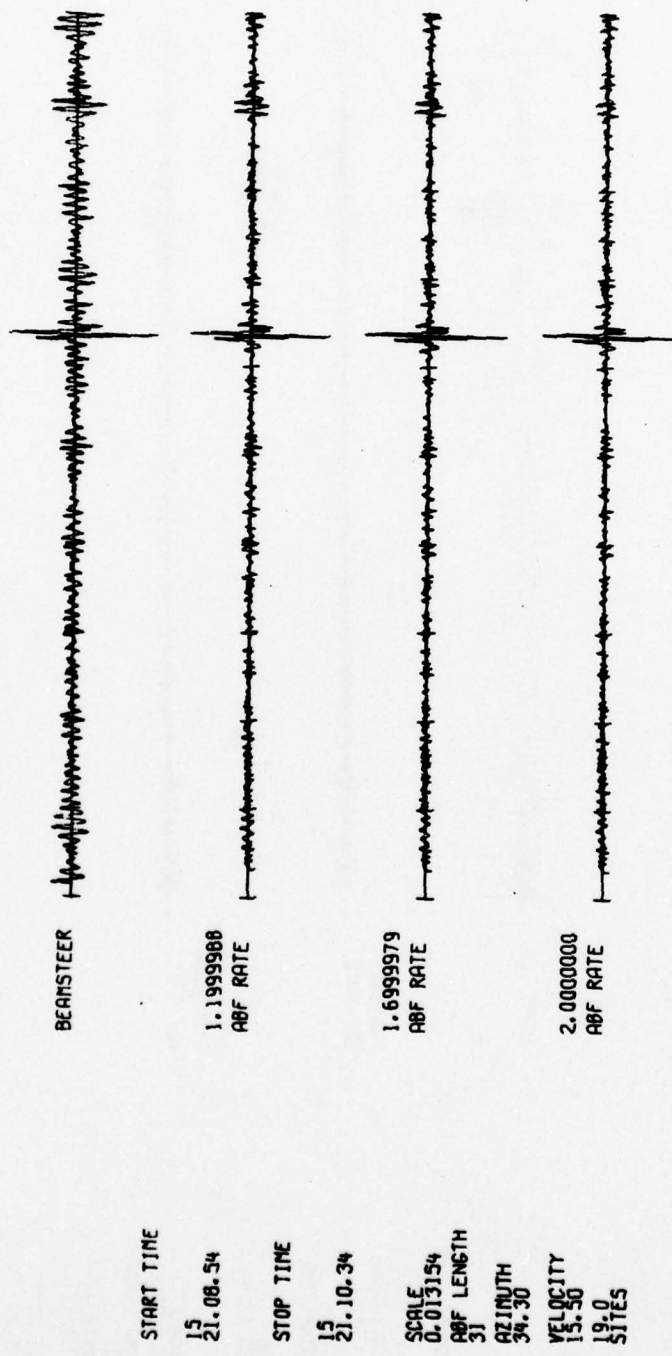
93 770115 10.55.47.2 12.99N 125.93E 33 24.5 5.5 5.6



A - 94

FIGURE A-93
PROCESSED TRACES FOR EVENT A-93

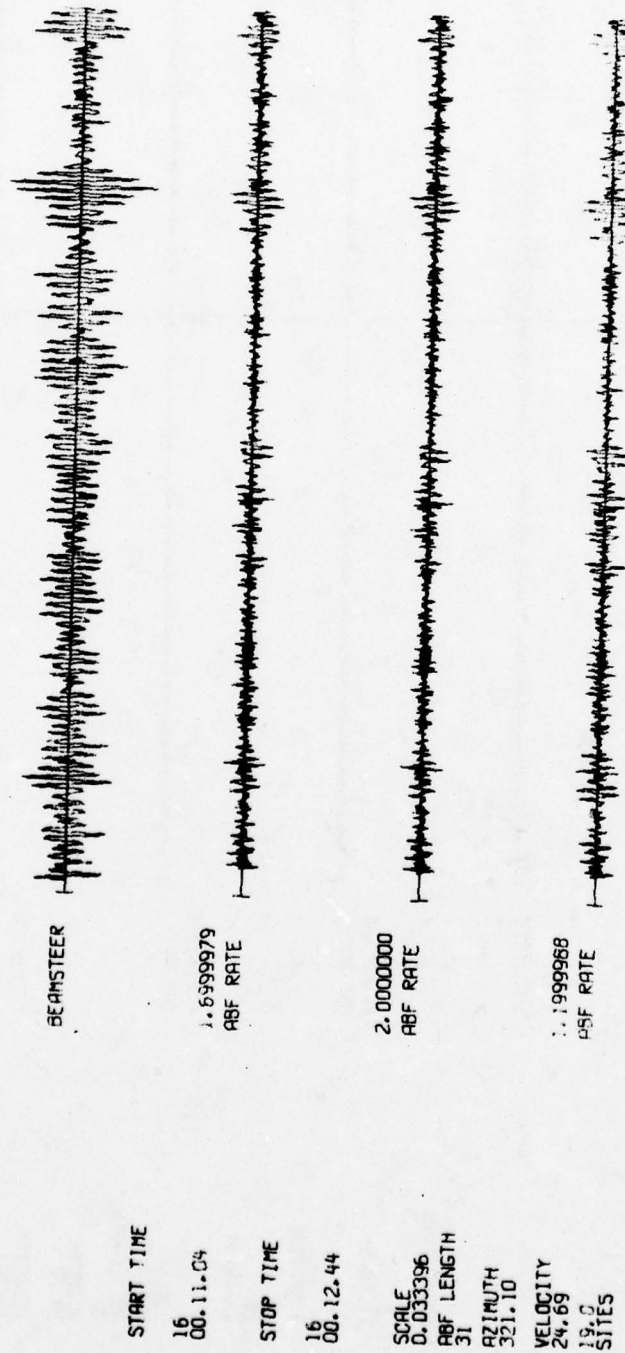
94 770115 21. 0.43.2 62.80N 150.37W 100 53.7 4.3 4.9 4.9



A-95

FIGURE A-94
PROCESSED TRACES FOR EVENT A-94

95 770115 23.58.46.8 33.57N 3.55W 33 95.9 4.4



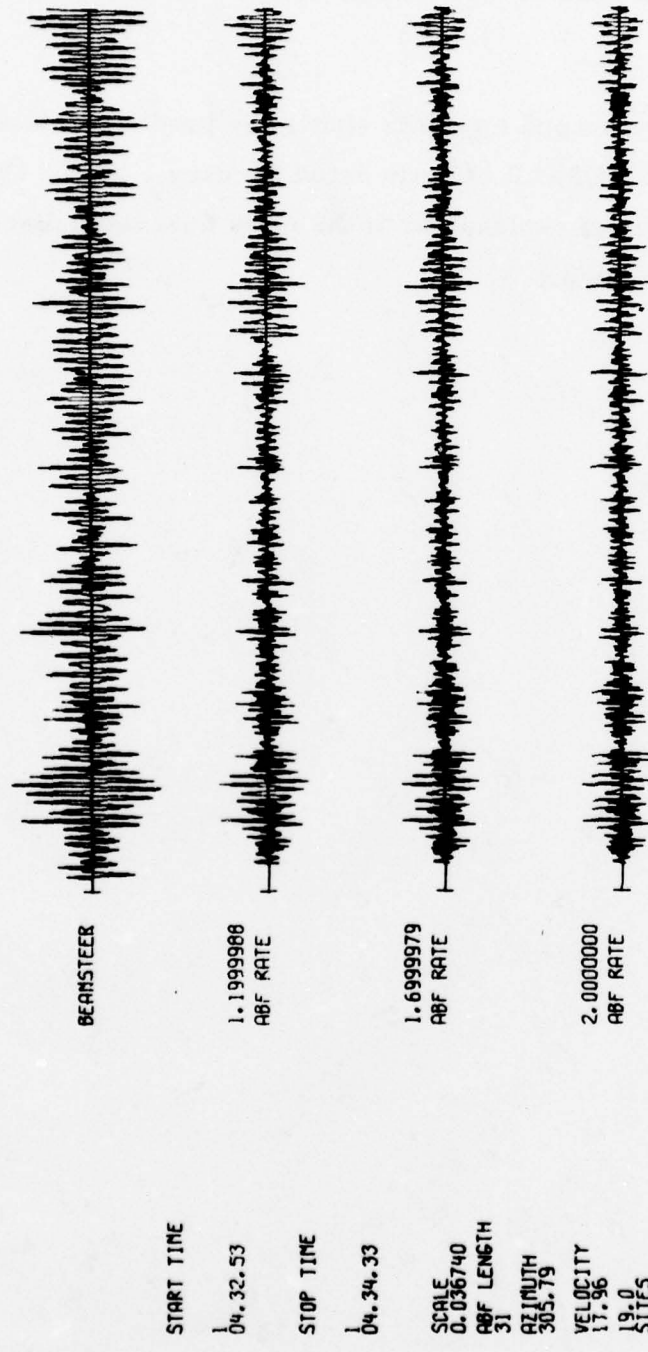
A-96

FIGURE A-95
PROCESSED TRACES FOR EVENT A-95

APPENDIX B
PROCESSED DATA PLOTS FROM NORSAR BULLETIN

The second appendix shows the processed data plots for the events taken from NORSAR bulletin dated January 1 to 31, 1978. The selection criteria and brief explanation of the plots have been discussed in an earlier portion of this report.

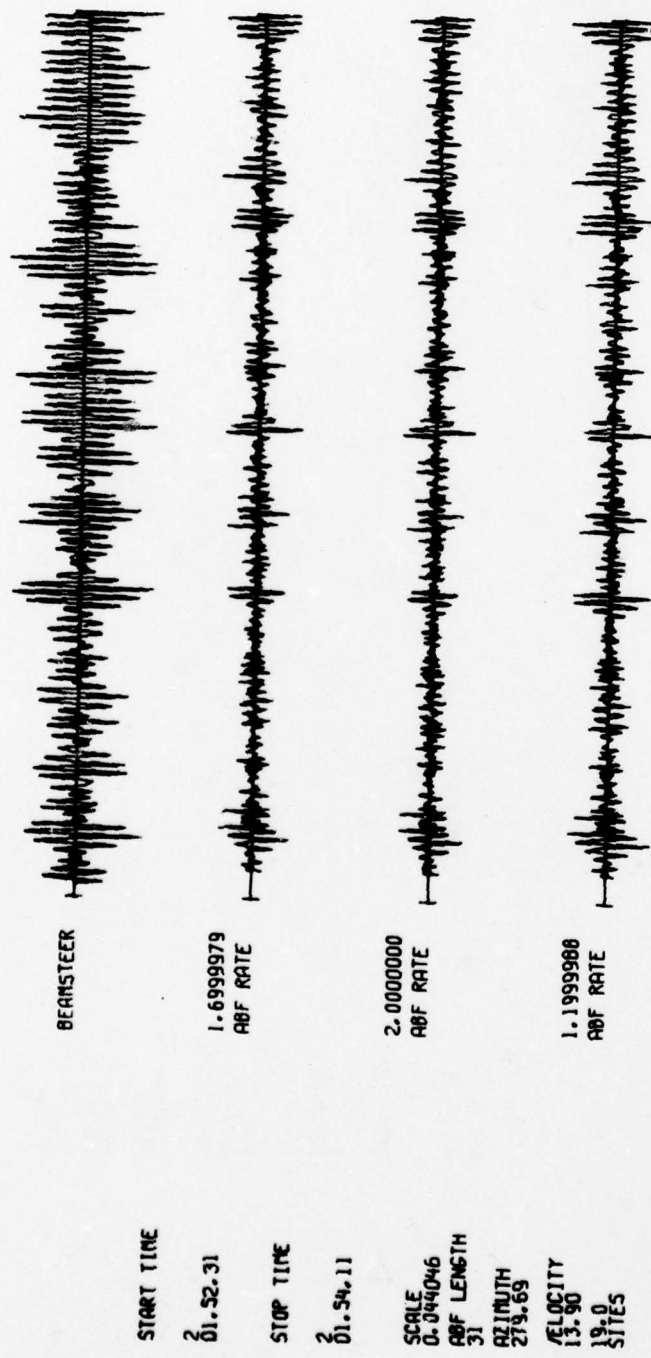
1 780101 4.22.49.0 40.00N 33.00E 0 70.3 3.8



B-2

FIGURE B-1
PROCESSED TRACES FOR EVENT B-1

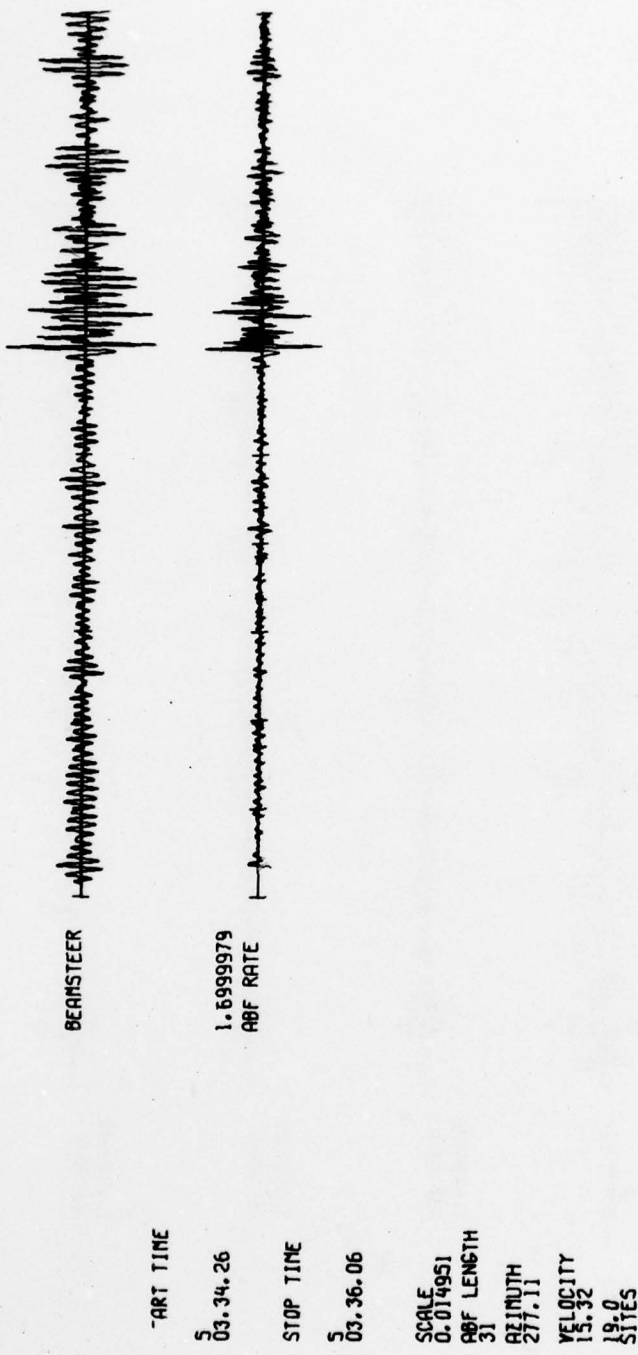
2 780102 1.45.33.0 32.00N 74.00E 0 44.1 4.1



B-3

FIGURE B-2
PROCESSED TRACES FOR EVENT B-2

3 780175 3.26.29.0 77.00N 67.00P 0 51.7 n.3 5.0 4.8



B-4

FIGURE B-3
PROCESSED TRACES FOR EVENT B-3

4 780105 14.45.16.0 37.0CN 71.CDF 0 42.6 4.2

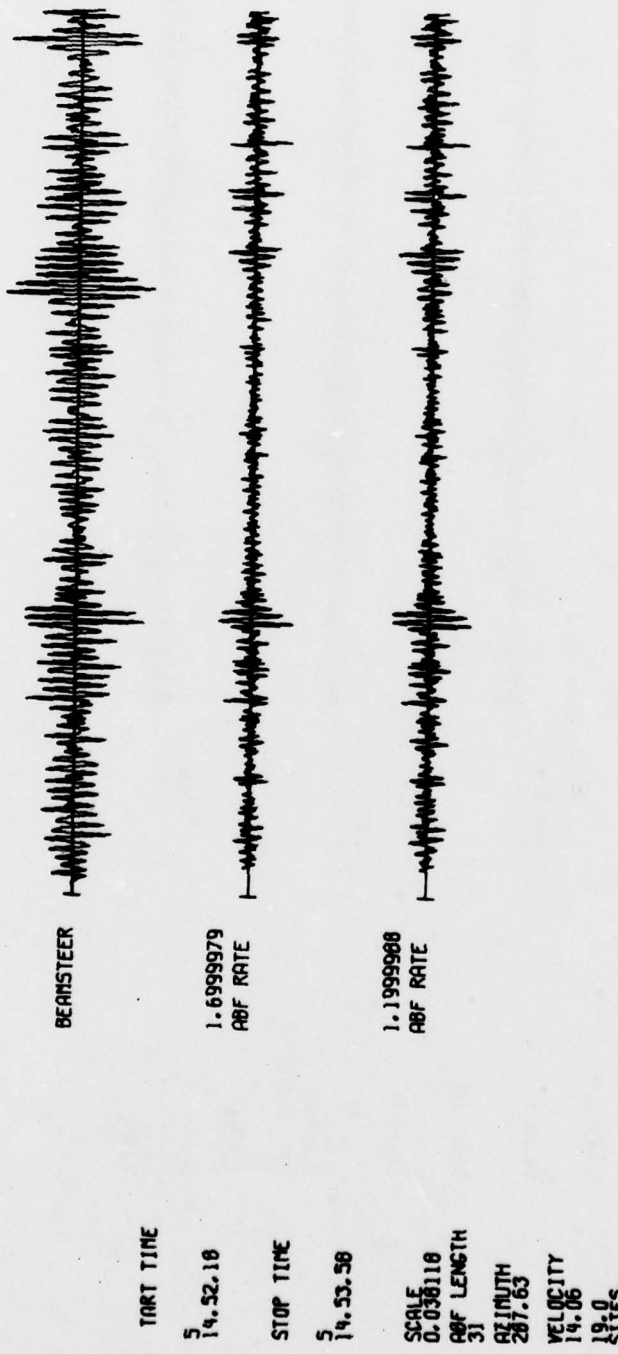
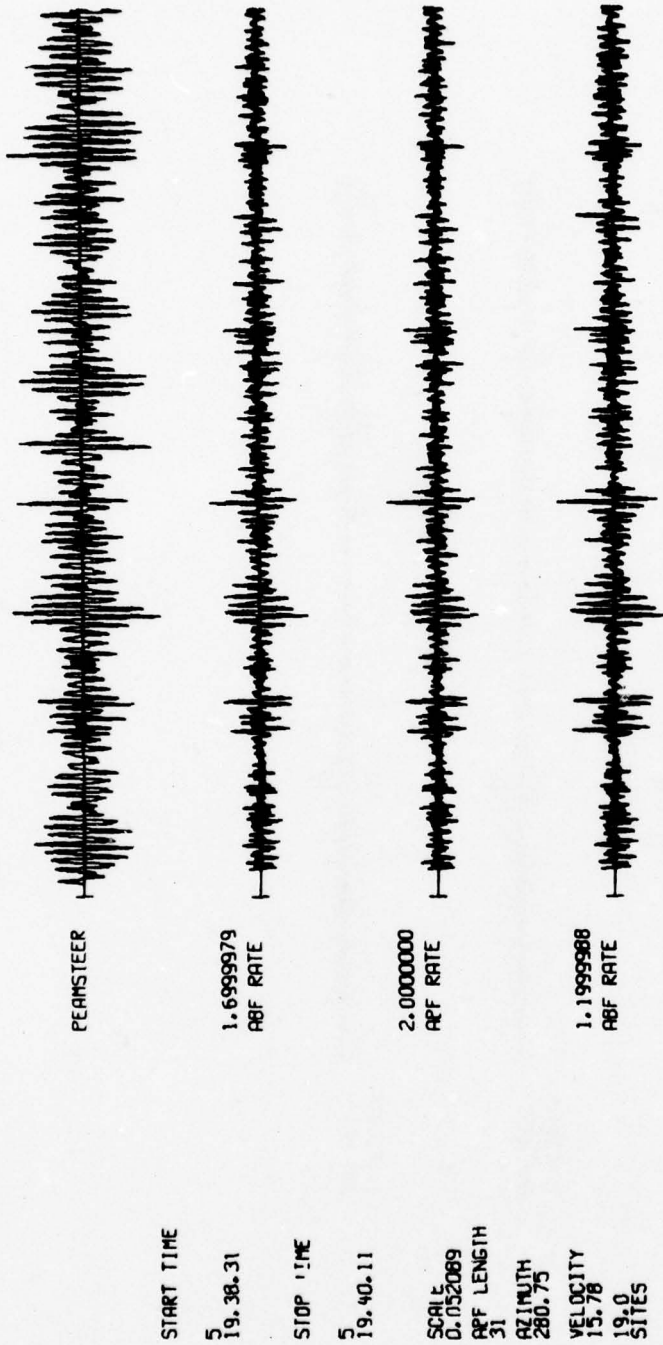


FIGURE B-4
PROCESSED TRACES FOR EVENT B-4

5 780105 19.29.54.0 27.00N 60.00E 0 57.2 4.?

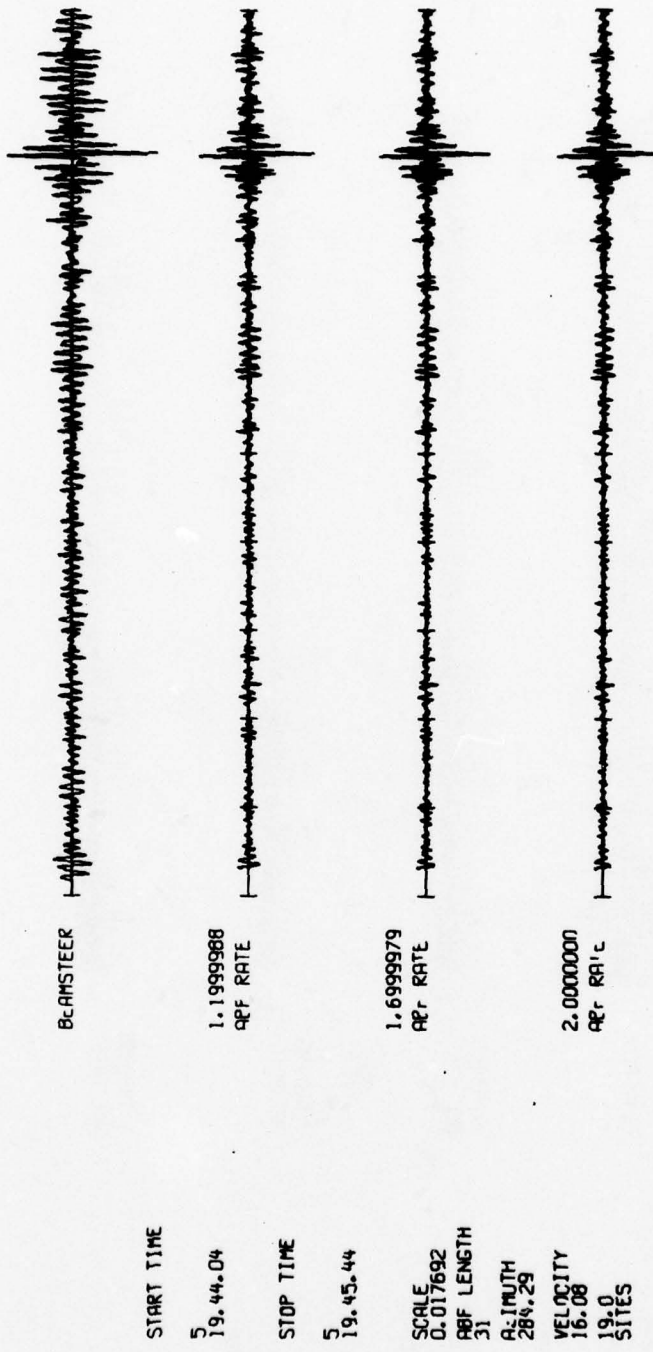
4.3



B-6

FIGURE B-5
PROCESSED TRACES FOR EVENT B-5

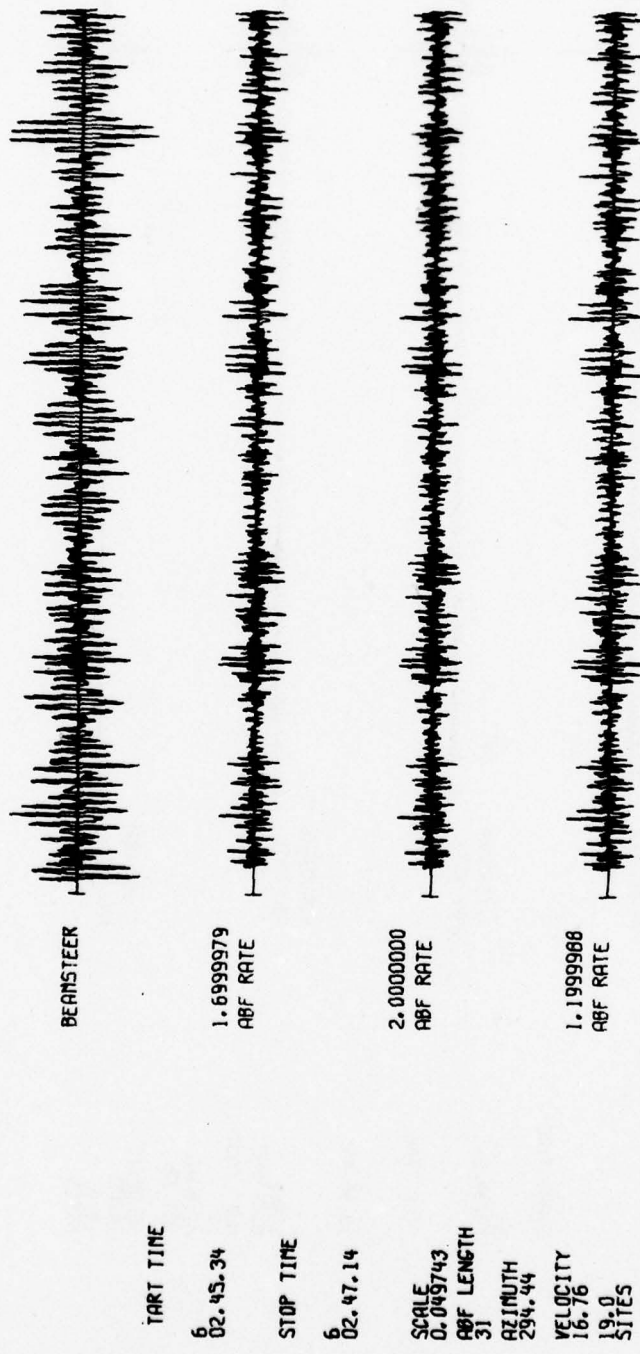
6 790105 19.35. 3.0 28.00N 55.00E 0 60.6 4.0 4.9 4.8



B-7

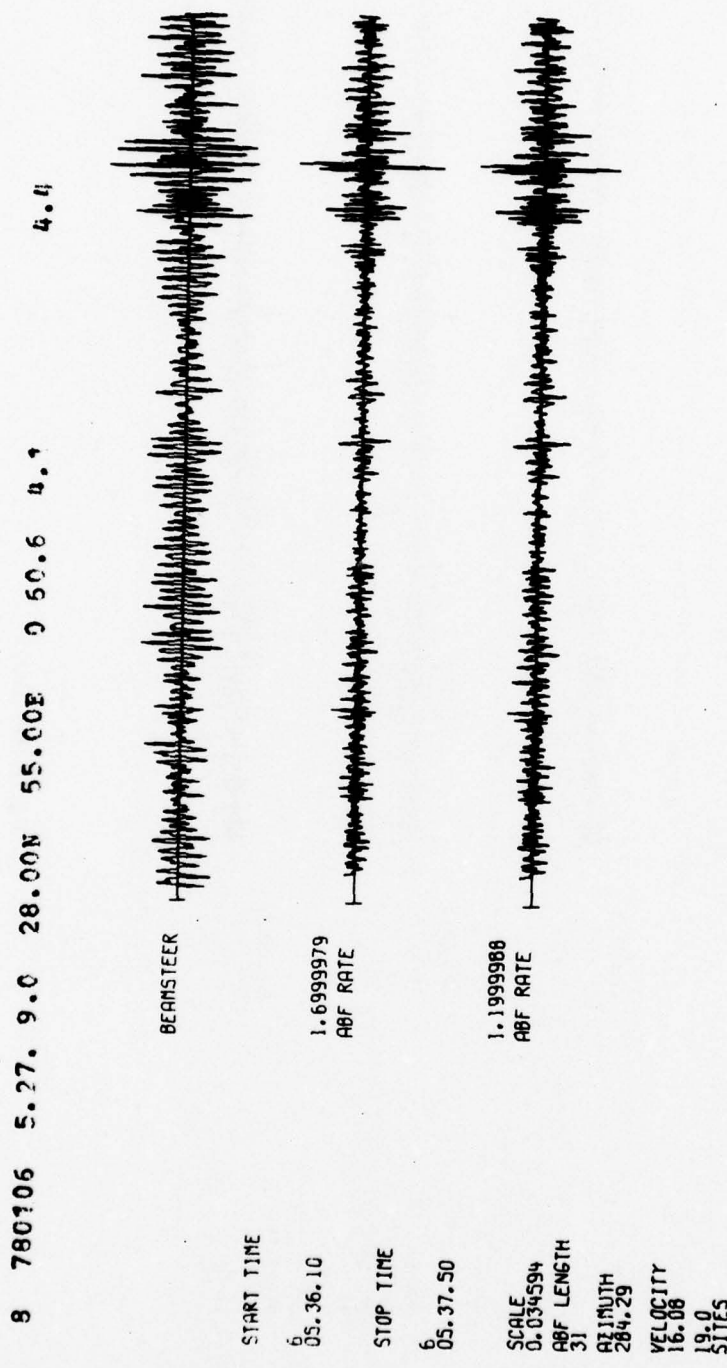
FIGURE B-6
PROCESSED TRACES FOR EVENT B-6

7 780196 2.36. 8.0 34.0CN 46.00E 0 64.4 3.7



B-8

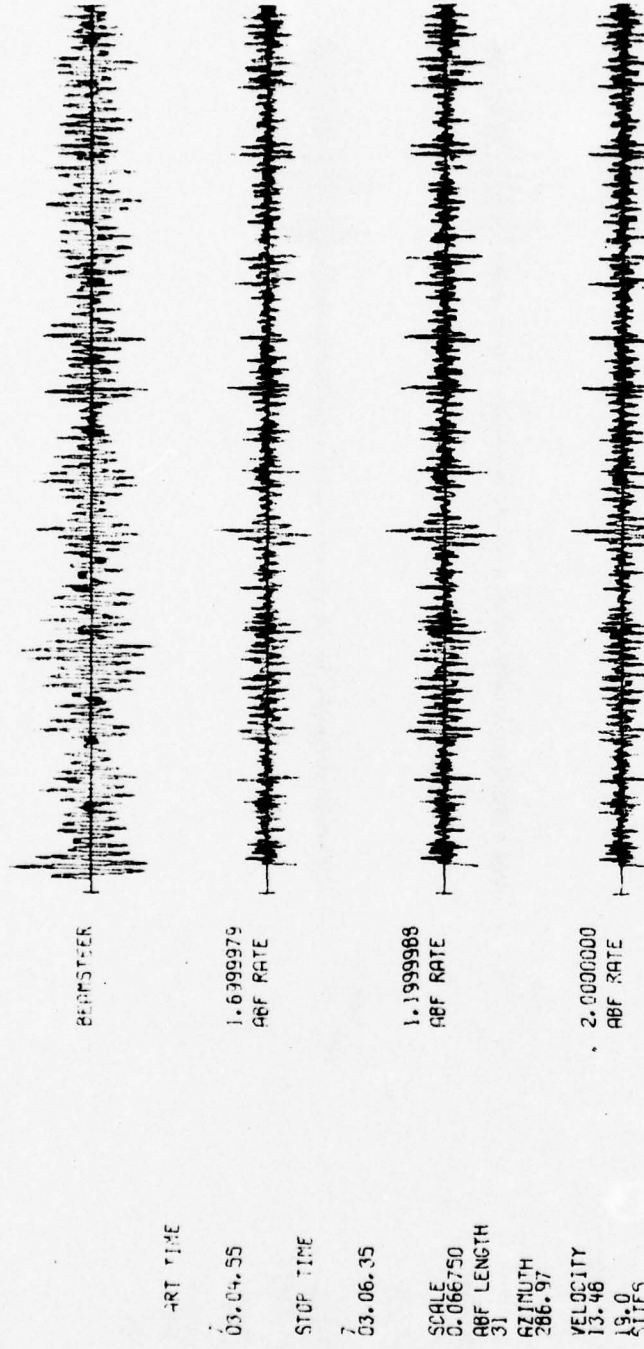
FIGURE B-7
PROCESSED TRACES FOR EVENT B-7



B-9

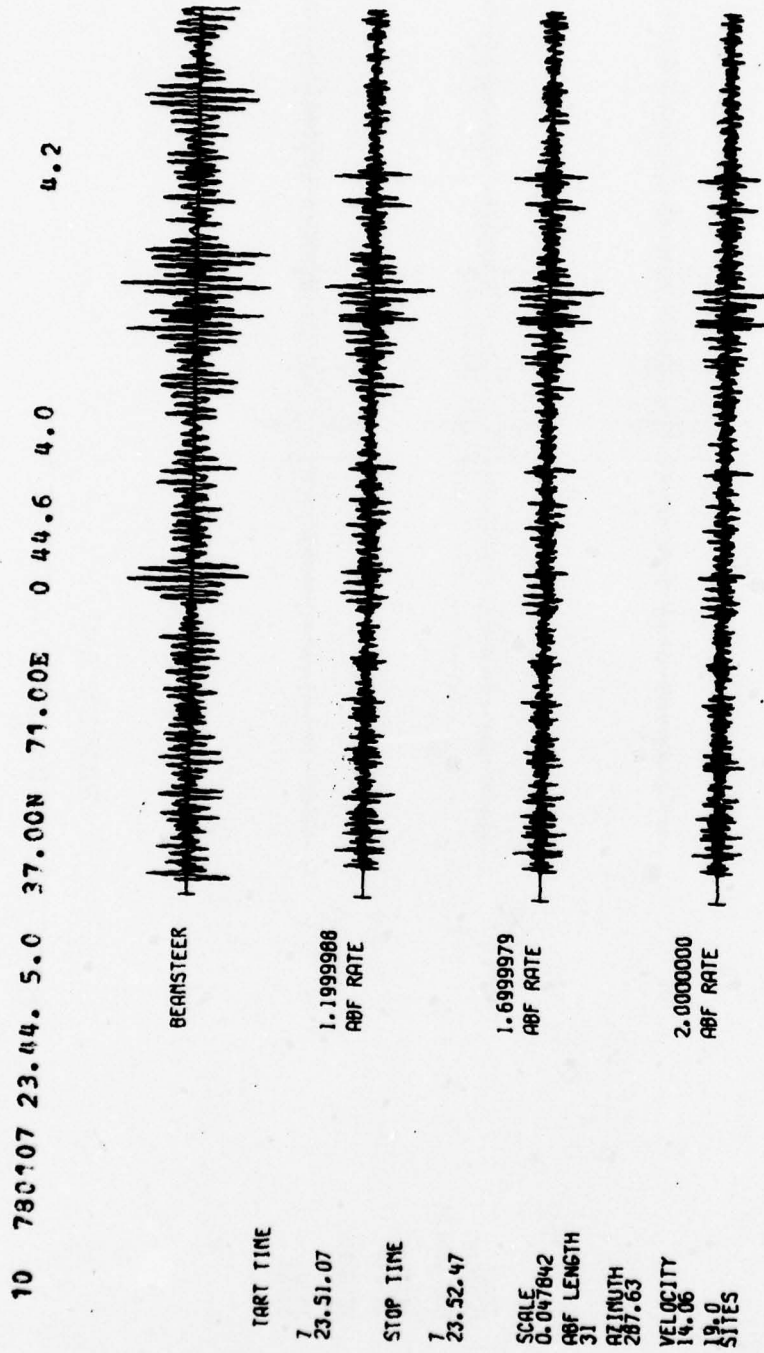
FIGURE B-8
PROCESSED TRACES FOR EVENT B-8

9 780107 2.58.32.0 38.00N 77.00E 0 39.8 4.2 4.0



B-10

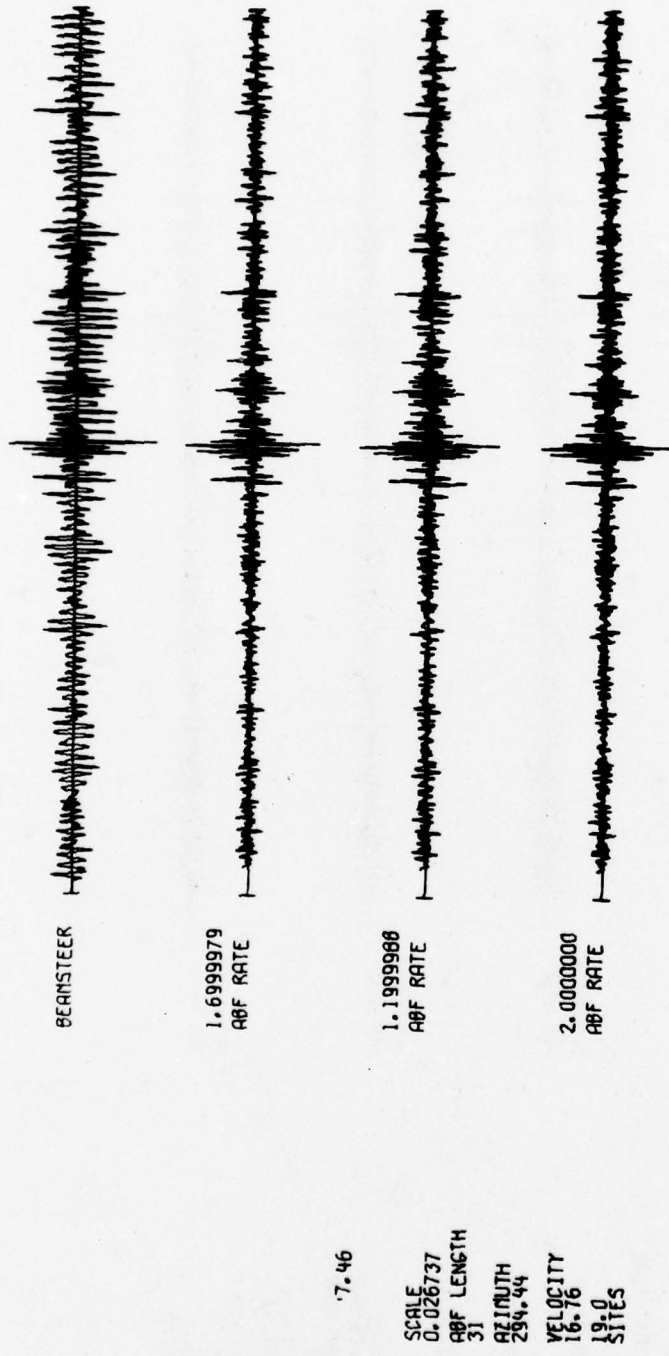
FIGURE B-9.
PROCESSED TRACES FOR EVENT B-9



B-11

FIGURE B-10
PROCESSED TRACES FOR EVENT B-10

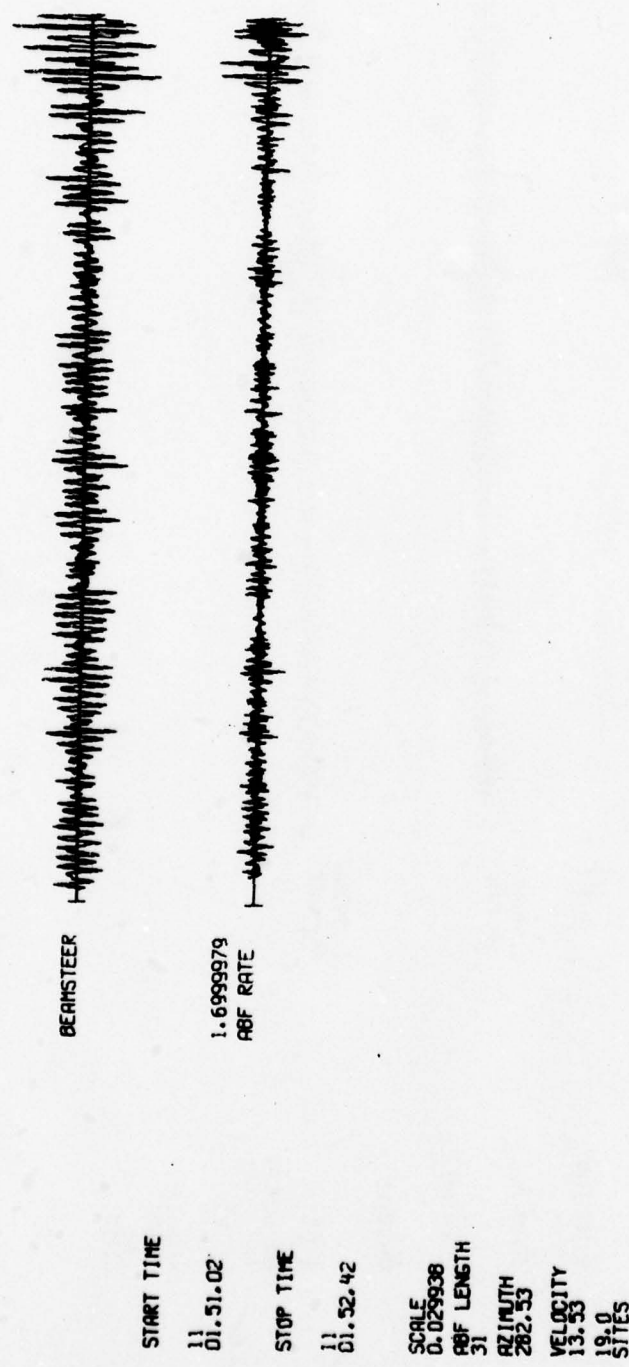
11 780110 12.36.40.0 34.00N 46.00E 0 64.4 u.u



B-12

FIGURE B-11
PROCESSED TRACES FOR EVENT B-11

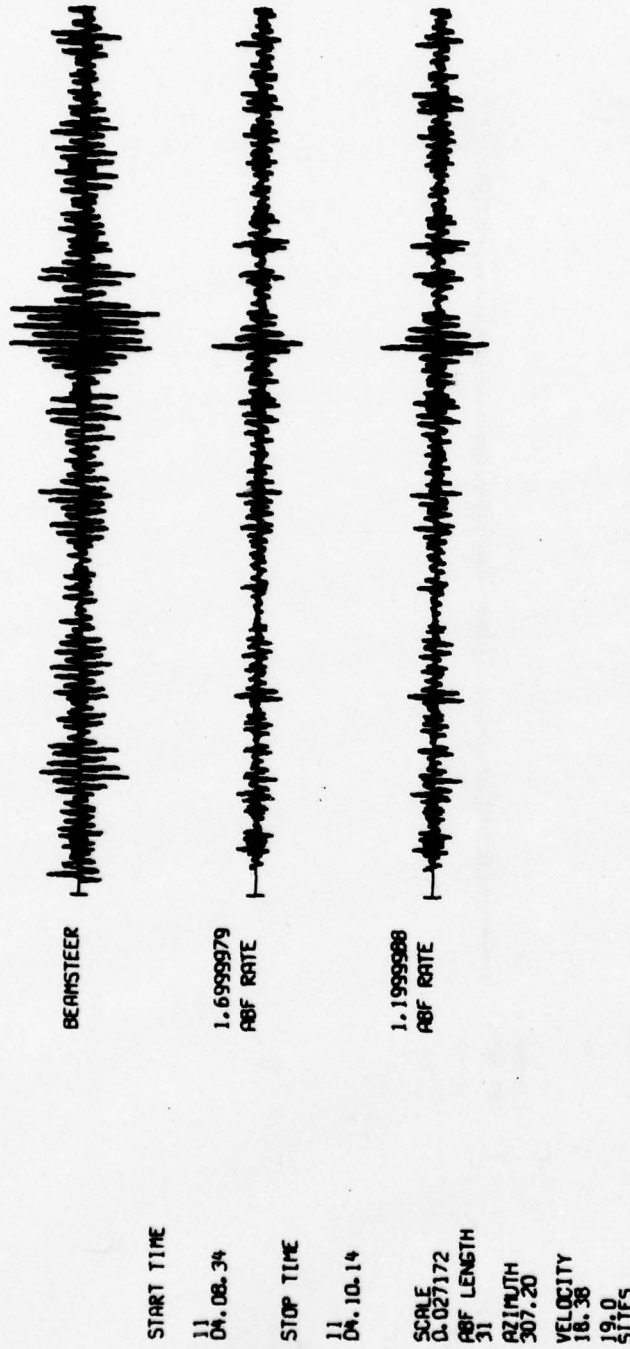
12 780111 1.44.31.0 35.00N 77.00E 0 40.7 4.5 4.4



B-13

FIGURE B-12
PROCESSED TRACES FOR EVENT B-12

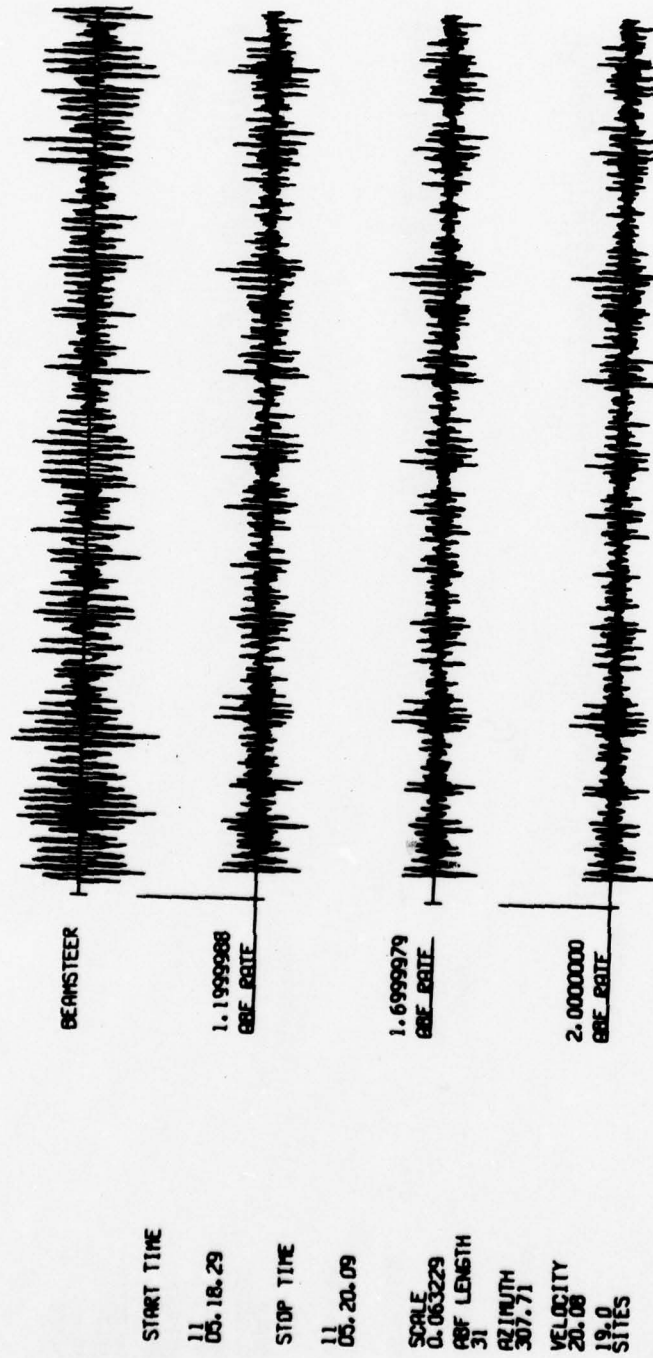
13 790111 3.58. 8.0 39.00N 28.00E 070.0 4.0 4.6



B-14

FIGURE B-13
PROCESSED TRACES FOR EVENT B-13

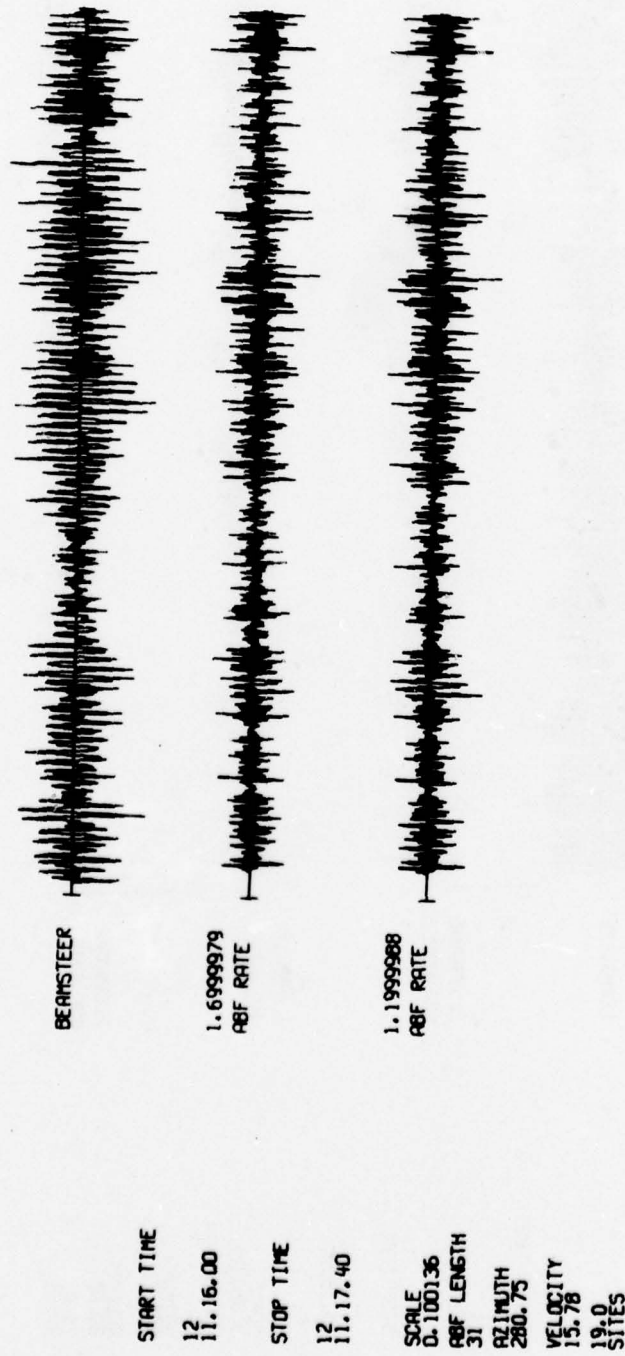
14 790111 5. 7.31.0 36.00N 22.00P 0 79.6 3.7



B-15

FIGURE B-14
PROCESSED TRACES FOR EVENT B-14

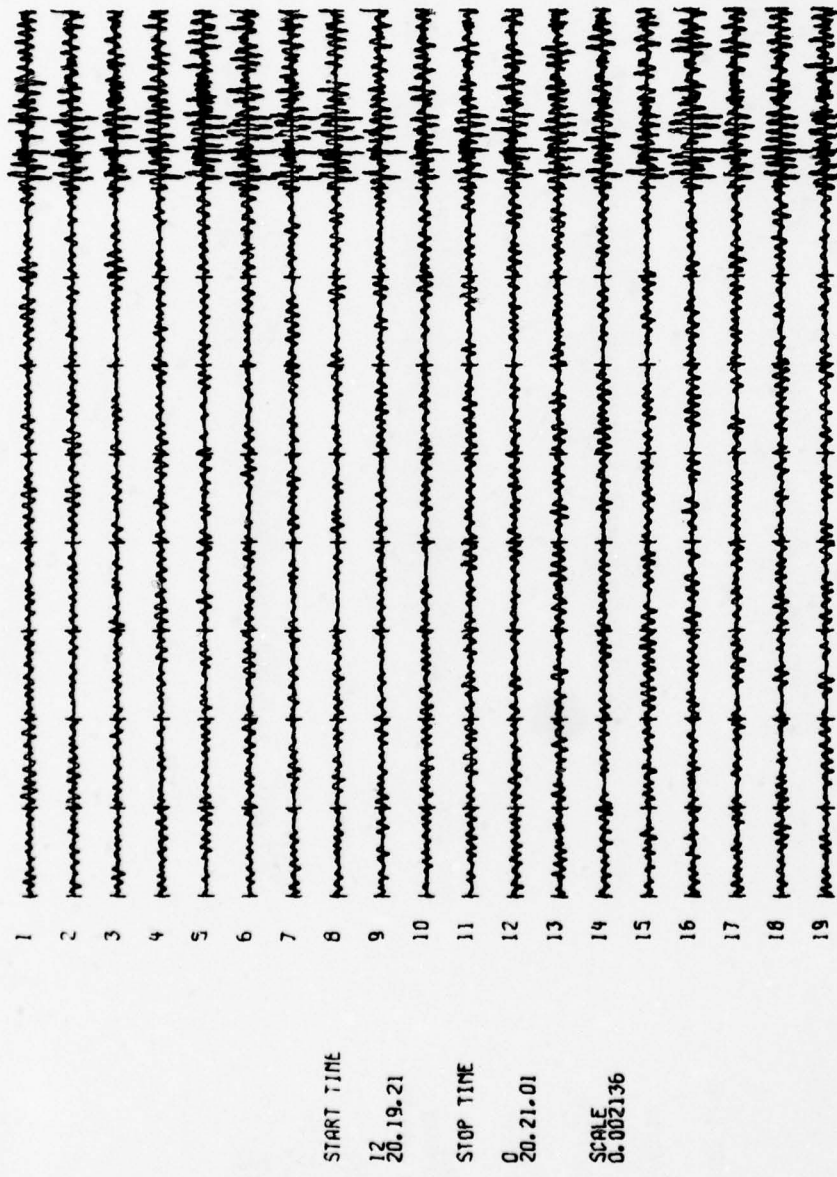
15 780112 11. 7.23.0 27.00N 60.00E 0 57.2 3.9



B-16

FIGURE B-15
PROCESSED TRACES FOR EVENT B-15

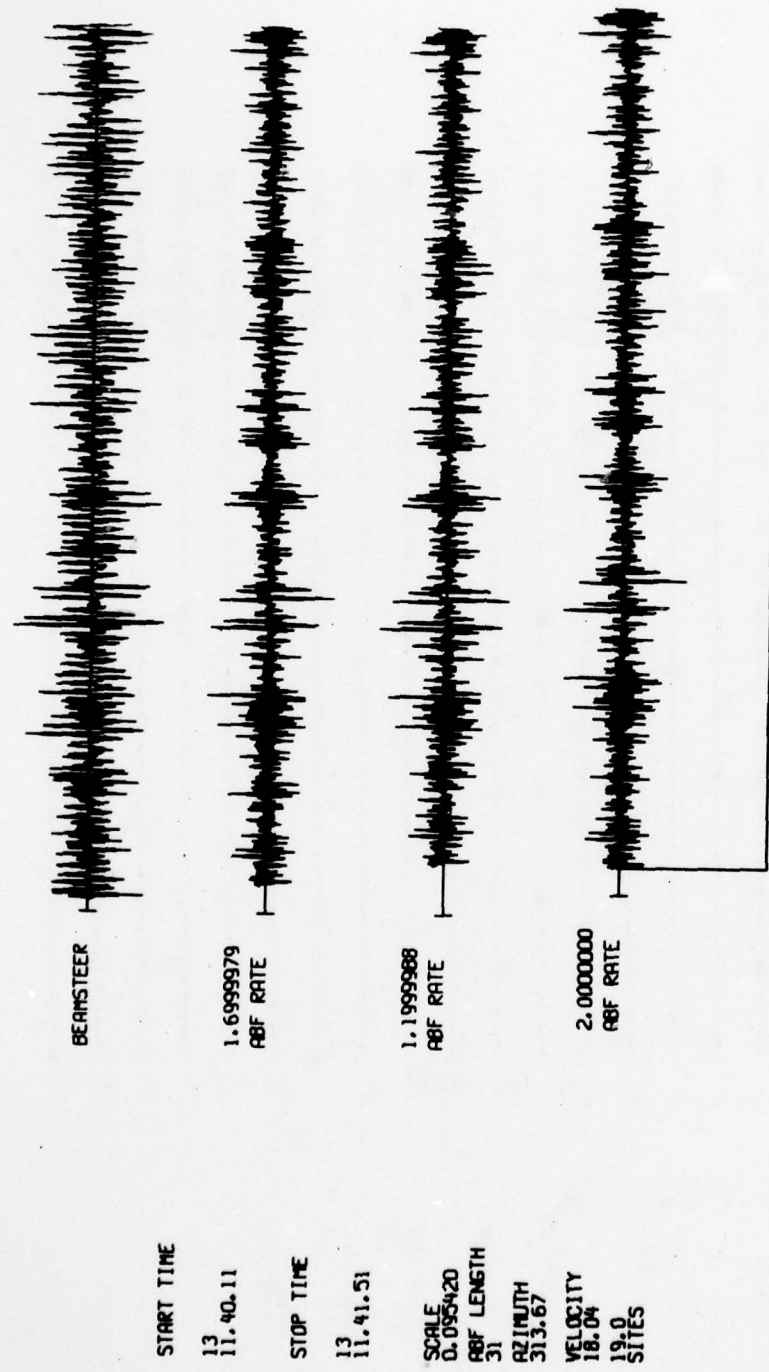
16 780112 20. 8.27.0 35.00N 24.00E 0 79.0 4.5 5.4



B-17

FIGURE B-16
PROCESSED TRACES FOR EVENT B-16

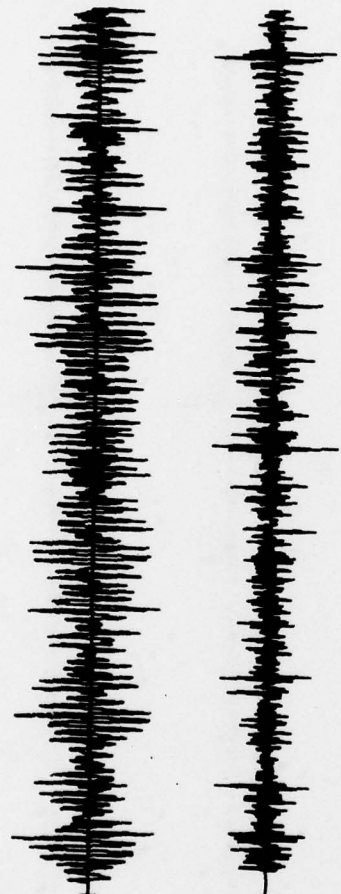
17 780113 11.30. 5.0 46.0CN 27.00P 0 70.6 3.6



B-18

FIGURE B-17
PROCESSED TRACES FOR EVENT B-17

19 780113 16. 1.55.0 35.00N 27.00E 077.0 4.3



START TIME

16.12.36

1.6999979
REF RATE

STOP TIME

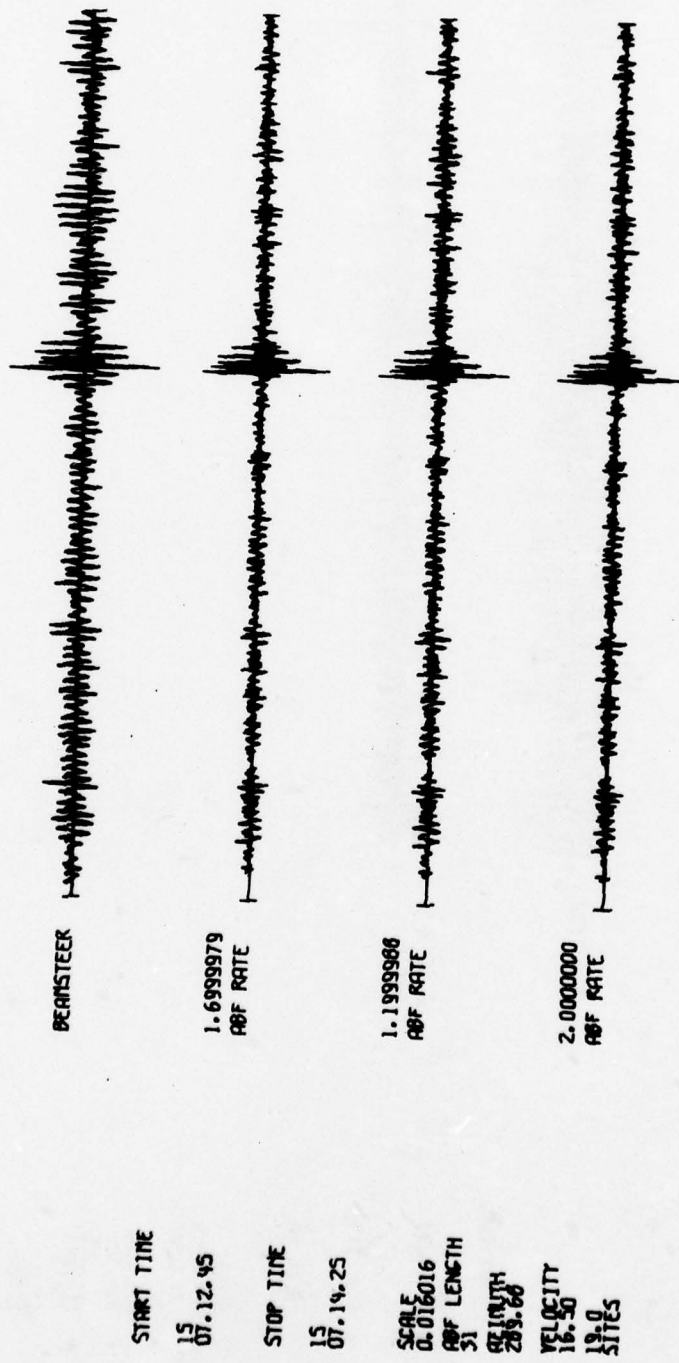
16.14.16

SCALE
0.198496
REF LENGTH
31
DEPTH
304.35
VELOCITY
18.43
19.0
SITES

B-19

FIGURE B-18
PROCESSED TRACES FOR EVENT B-18

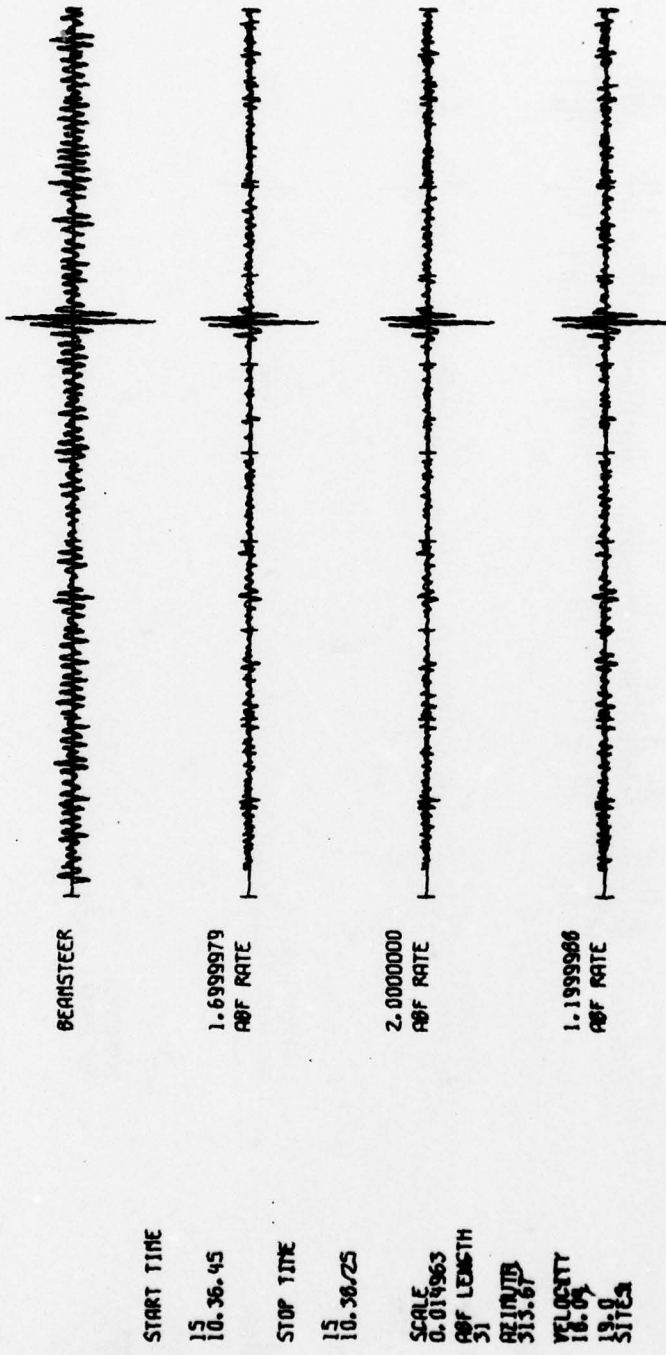
19 780115 7. 3.29.0 31.00W 50.00E 0 62.9 1.0 5.0 4.0



B-20

FIGURE B-19
PROCESSED TRACES FOR EVENT B-19

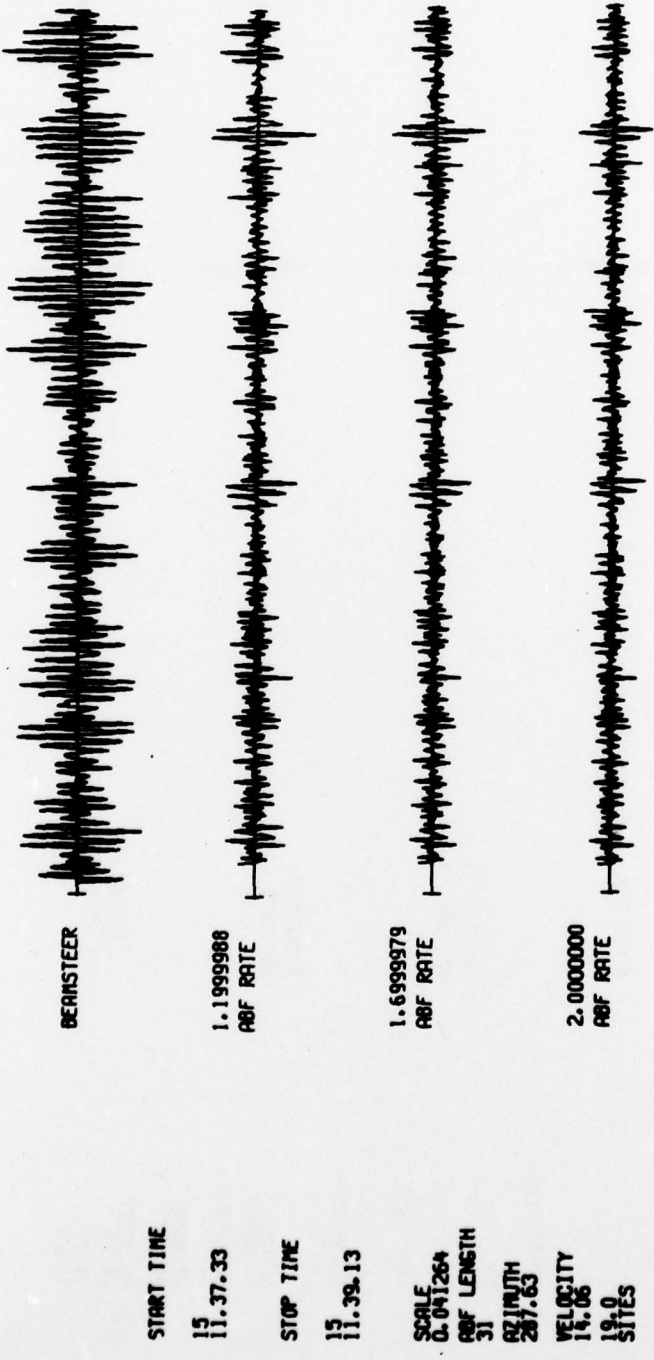
20 780115 10.26.39.0 46.0N 27.00E 3 70.6 4.1 5.1 4.9



B-21

FIGURE B-20
PROCESSED TRACES FOR EVENT B-20

21 780115 19.30.31.0 37.00N 71.00E 0 44.6 3.9 4.0



B-22

FIGURE B-21
PROCESSED TRACES FOR EVENT B-21

22 789121 1.21. 4.0 37.00N 71.00E 0 44.6 N. 4.2

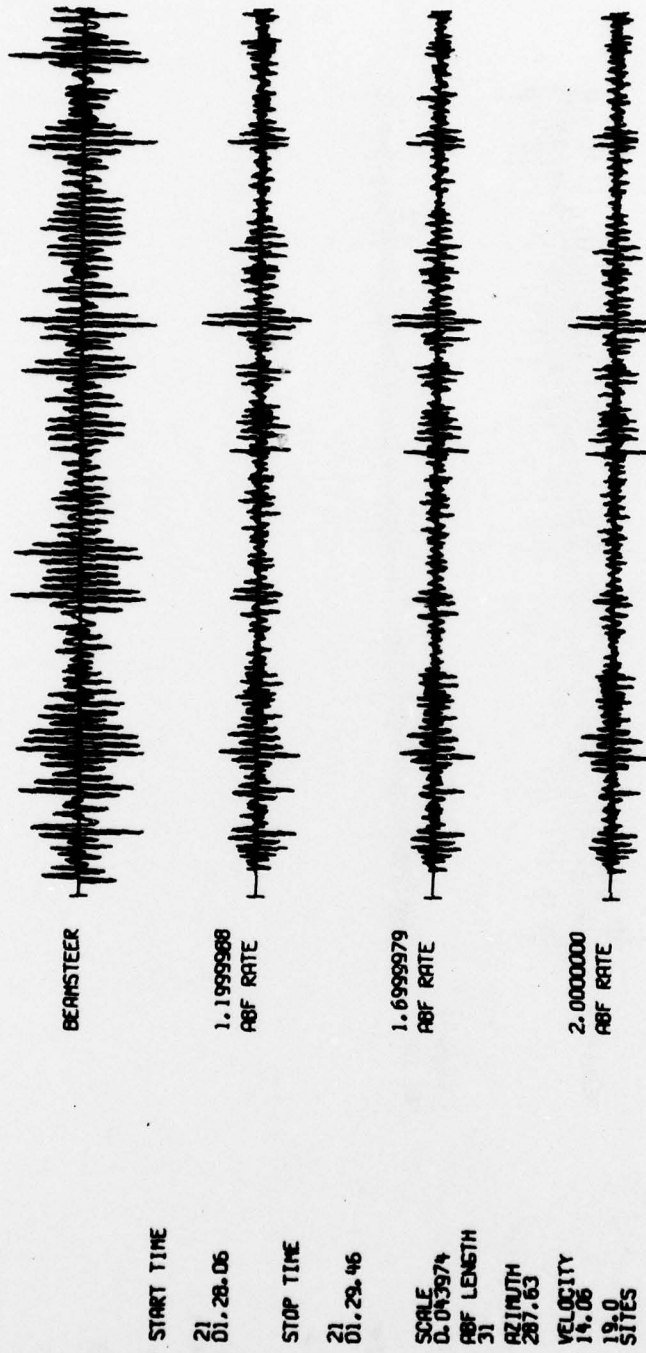
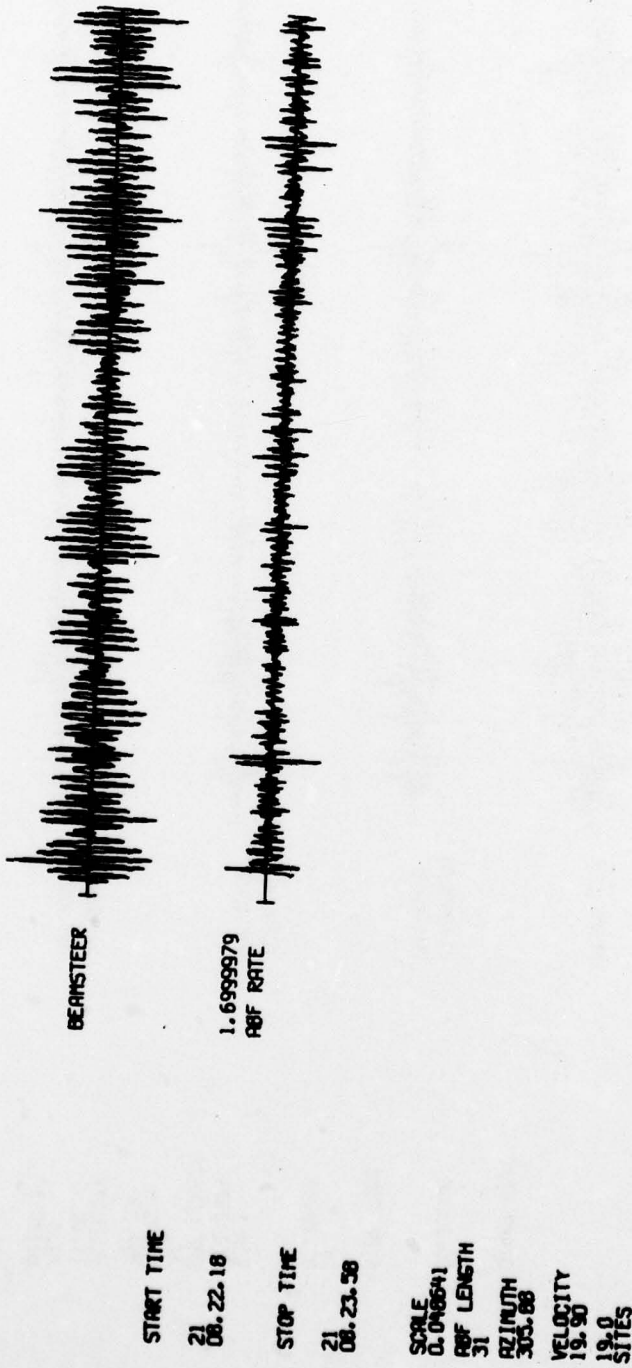


FIGURE B-22
PROCESSED TRACES FOR EVENT B-22

23 780121 8.11.24.0 35.00N 24.COP 0 79.0 4.0



B-24

FIGURE B-23
PROCESSED TRACES FOR EVENT B-23

24 780121 14.33.44.0 37.00N 71.00E 0 44.6 3.7 0.1

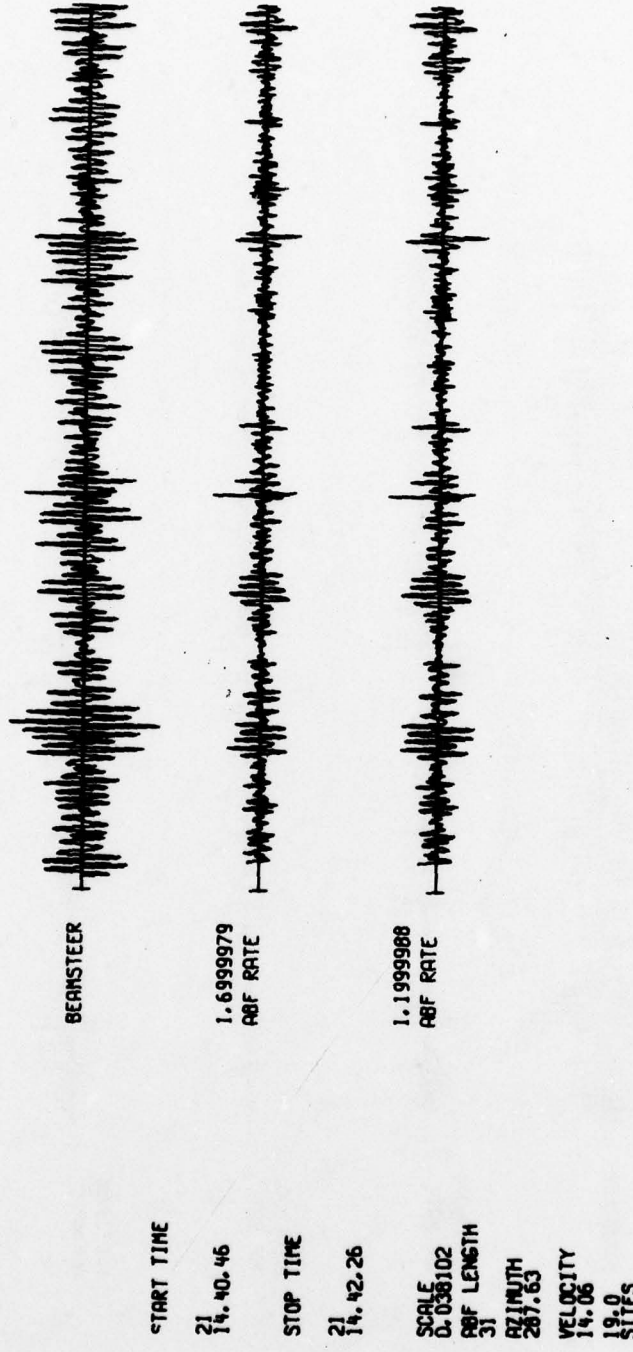


FIGURE B-24

PROCESSED TRACES FOR EVENT B-24

25 780124 10. 7. 8.0 35.00N 77.00E 0 40.7 4.5 4.2

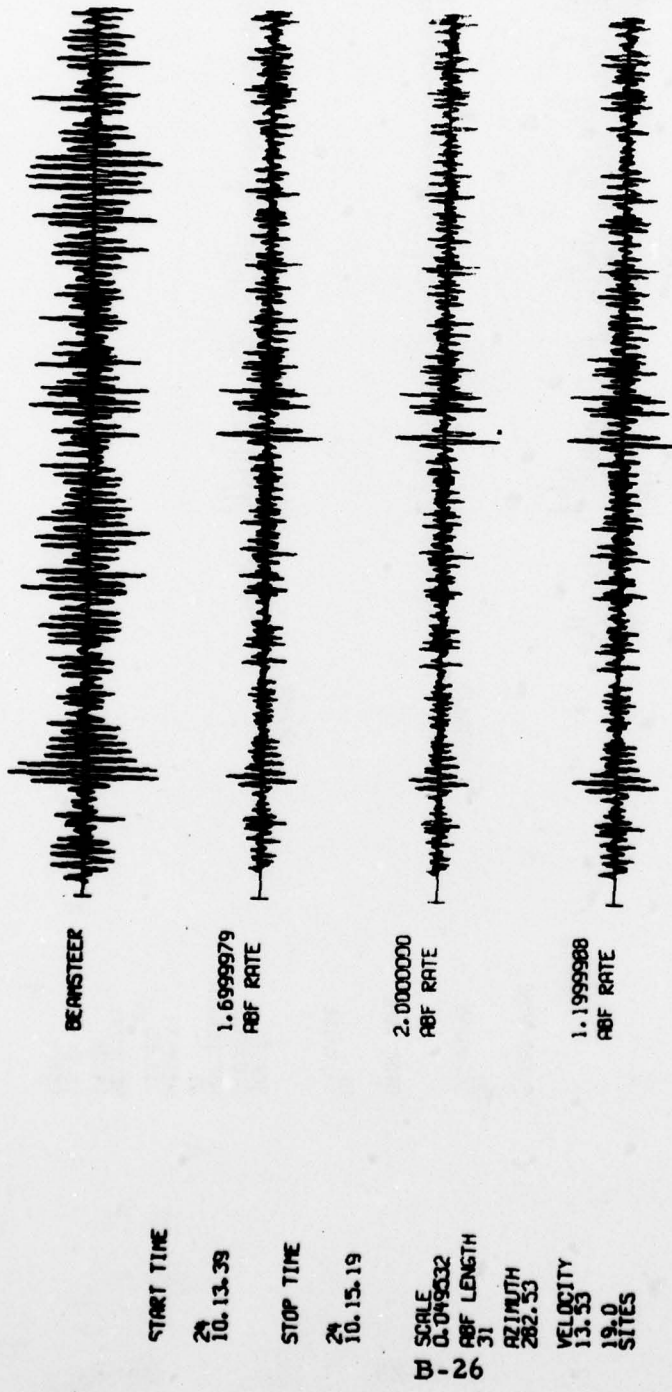
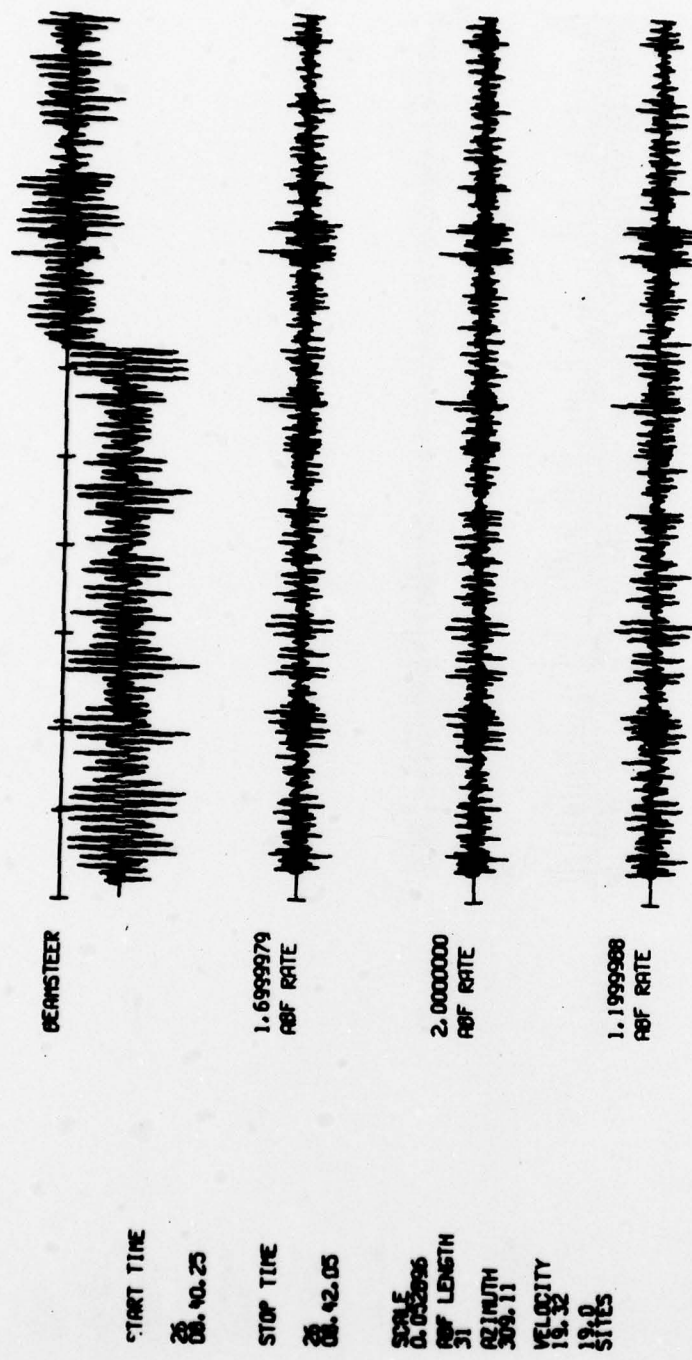


FIGURE B-25
PROCESSED TRACES FOR EVENT B-25

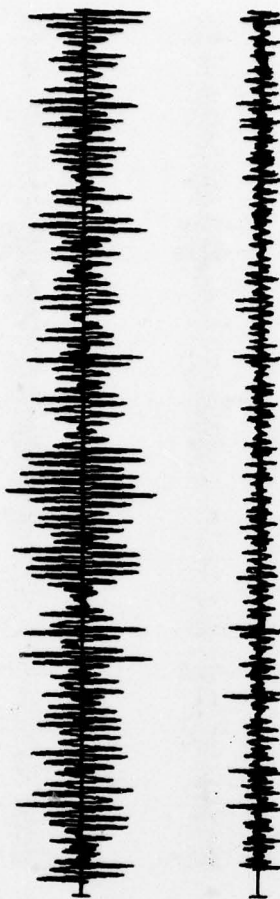
26 780126 8.29.45.0 39.00N 24.00E 076.5 3.7



B-27

FIGURE B-26
PROCESSED TRACES FOR EVENT B-26

27 780925 14.54.37.0 27.00N 60.00E 0 57.2 4.0



START TIME

26
13.03.14

1.6999979
REF RATE

STOP TIME

26
13.04.54

SCALE
0.049567
REF LENGTH
31
AZIMUTH
280.75
VELOCITY
15.78
19.0
SITES

FIGURE B-27

PROCESSED TRACES FOR EVENT B-27

28 780128 10.53.6.0 29.0CN 24.0CE 0 76.5 3.6

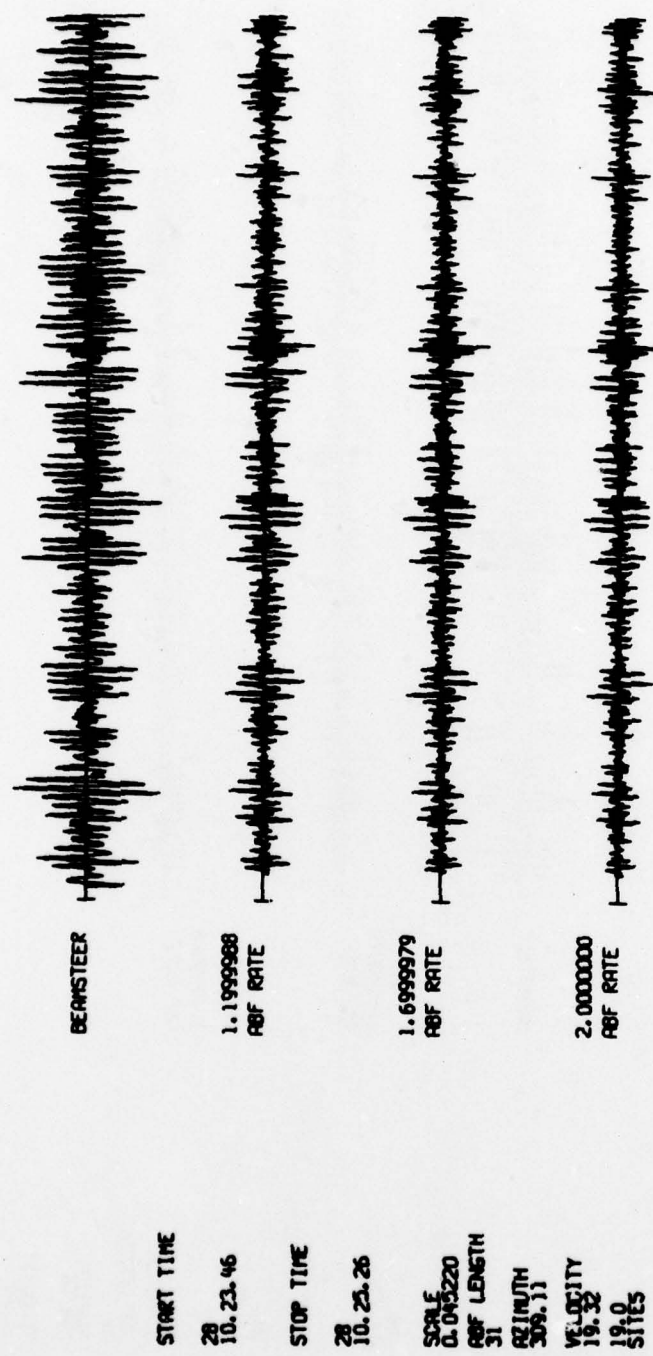


FIGURE B-28

PROCESSED TRACES FOR EVENT B-28

29 780128 14.19.17.0 34.00N 46.00E 0 64.4 4.1

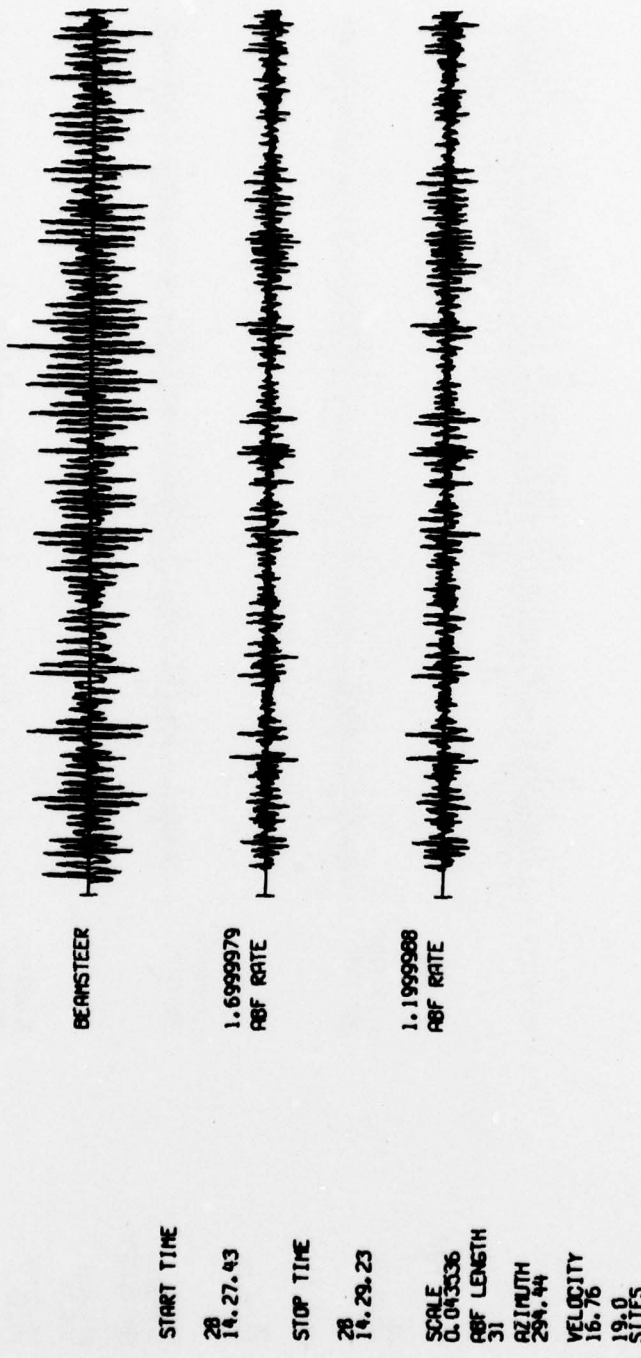
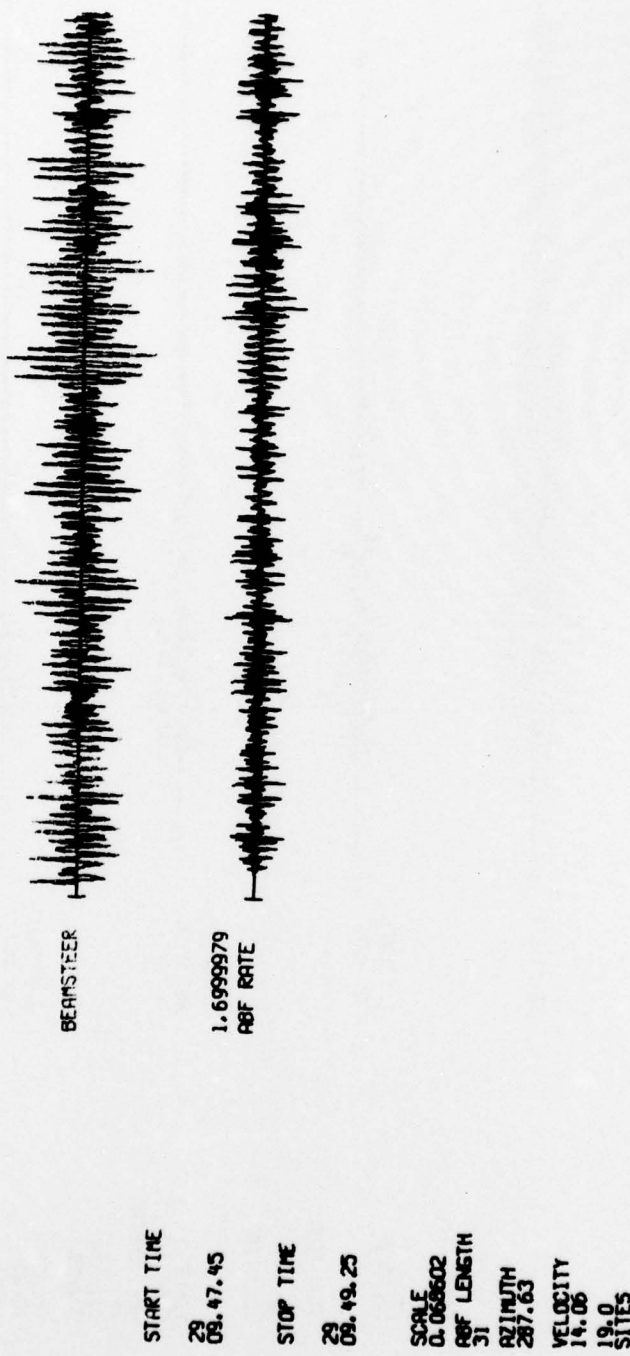


FIGURE B-29
PROCESSED TRACES FOR EVENT B-29

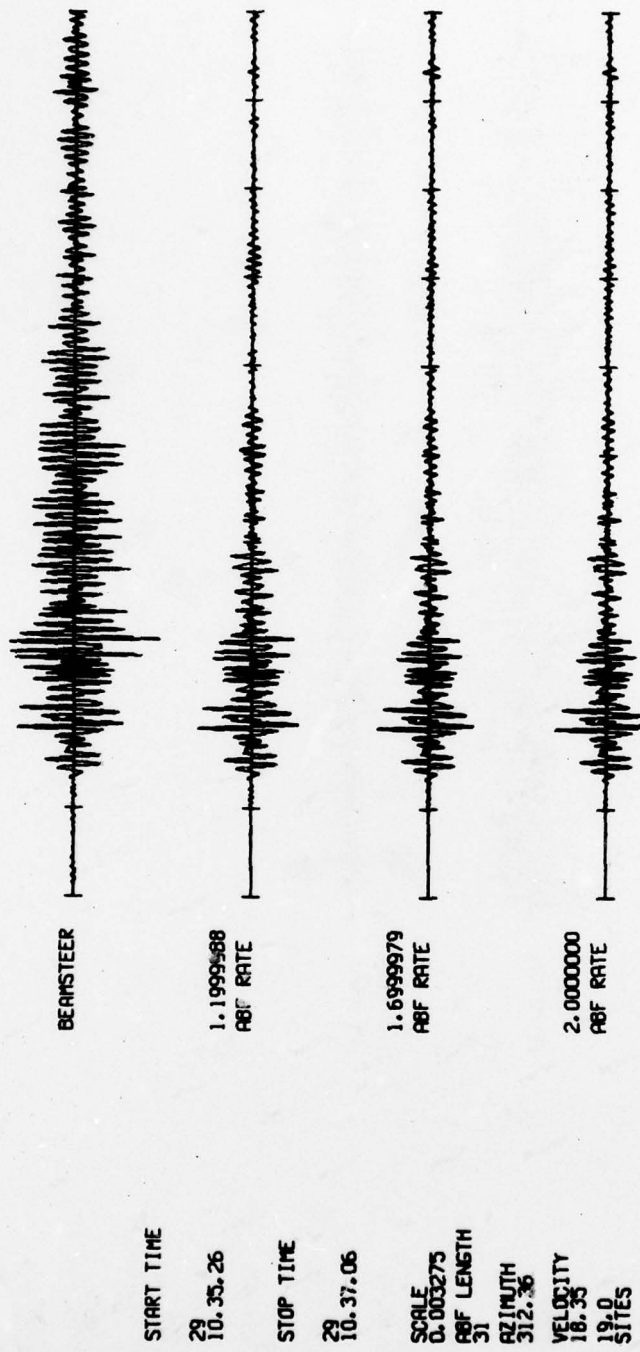
30 780129 9.40.43.0 37.00N 71.00E 0 44.6 3.9



B-31

FIGURE B-30
PROCESSED TRACES FOR EVENT B-30

31 780129 10.25.10.0 44.00N 26.00E 0 72.4 4.0 5.2 5.1



B-32

FIGURE B-31
PROCESSED TRACES FOR EVENT B-31

32 780129 17.32. 8.0 15.00N 56.00E 0 66.7 4.1

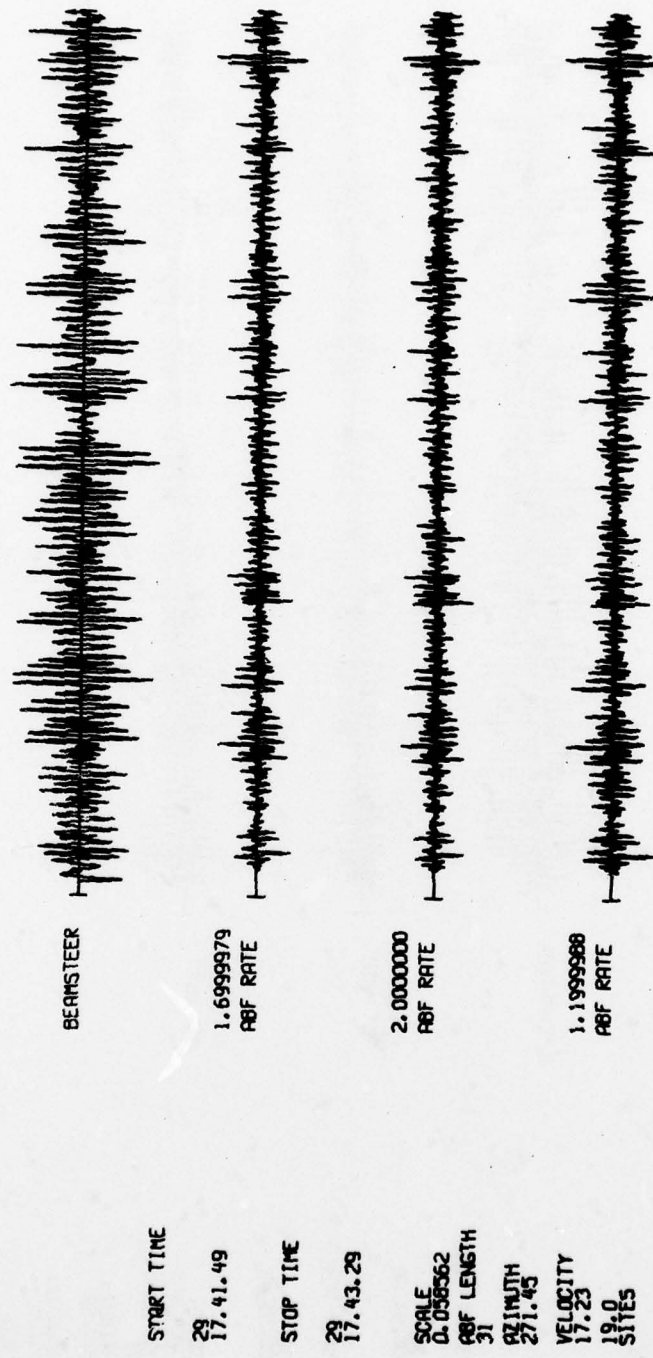


FIGURE B-32
PROCESSED TRACES FOR EVENT B-32

33 780130 7.53.14.0 35.00N 24.00E 0 79.0 3.9

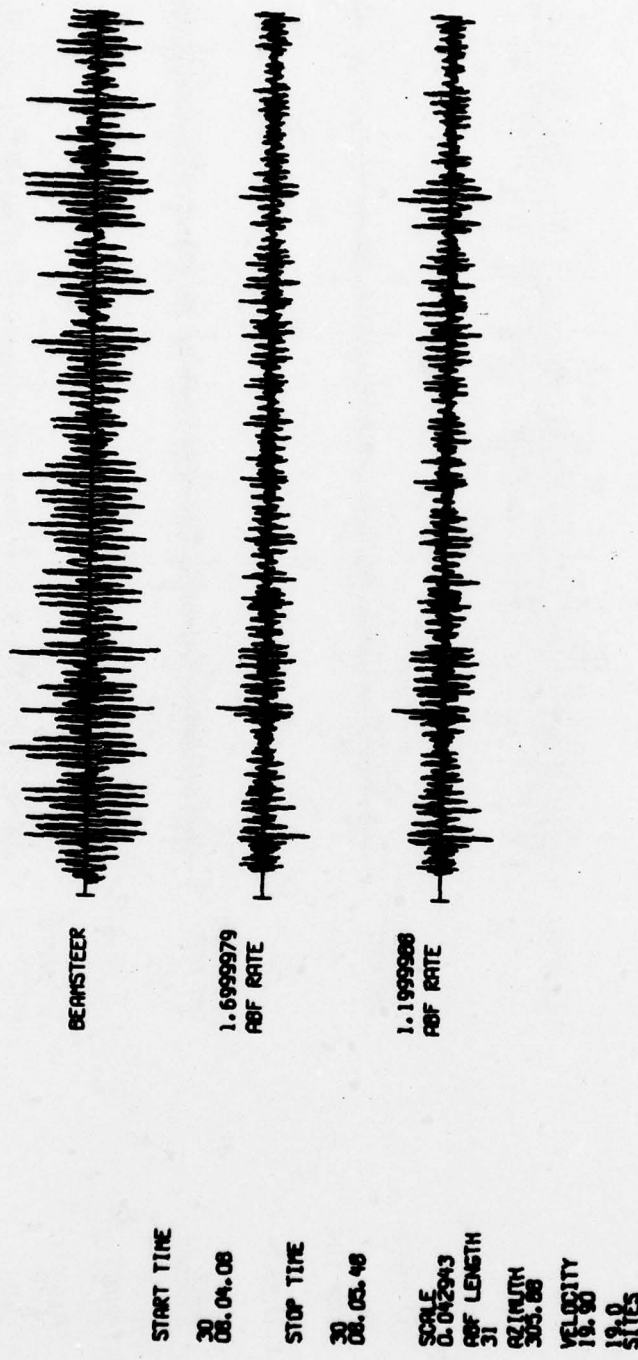
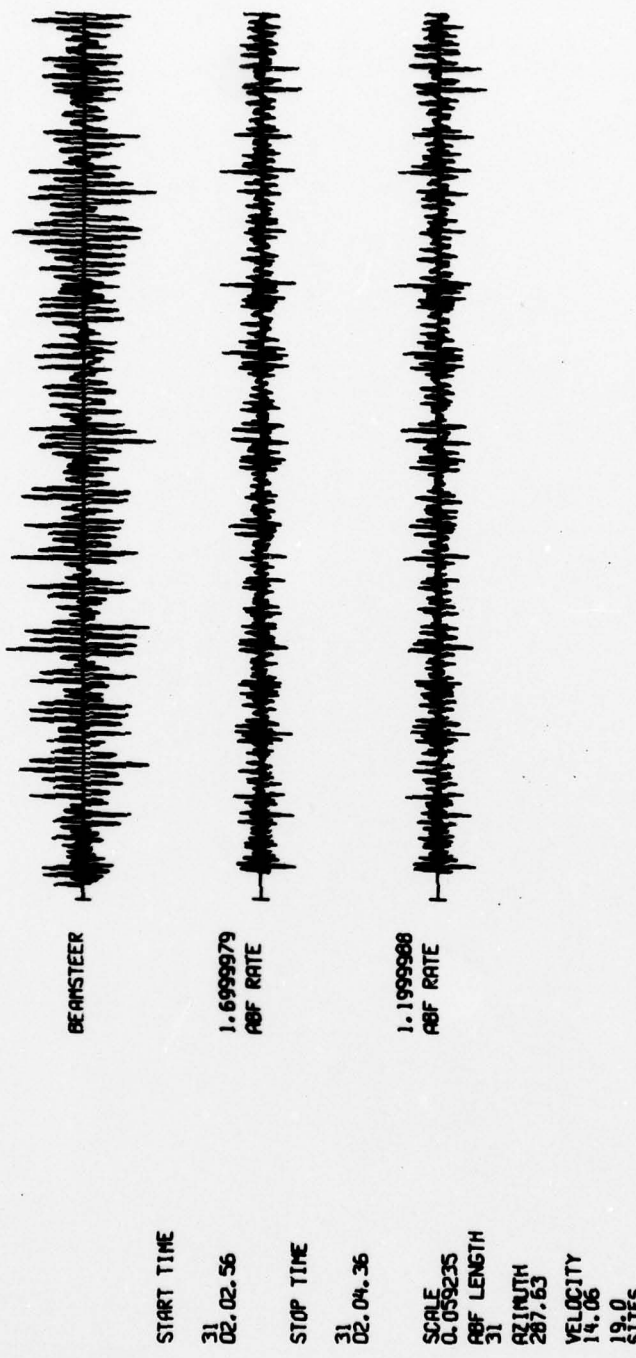


FIGURE B-33
PROCESSED TRACES FOR EVENT B-33

34 780131 1.55.54.0 37.00N 71.00E 0 44.6 4.1



B - 35

FIGURE B-34
PROCESSED TRACES FOR EVENT B-34